Imperial College London

Department: Medicine

Gene Control Mechanisms and Disease

Nadine Rothe

Gene regulation and epigenotype in Friedreich's ataxia

Supervised by:

Prof. Richard J. Festenstein

Submitted for the degree of Doctor of Philosophy

London 2008

Abstract

Friedreich's ataxia (FRDA) is known to be provoked by an abnormal GAA-repeat expansion located in the first intron of the *FXN* gene. As a result of the GAA expansion, patients exhibit low levels of *FXN* mRNA, leading to FRDA. Here, via chromatin immunoprecipitation (ChIP), the presence of a RNA pol II transcriptional pausing site at exon 1 of the *FXN* gene was demonstrated. At this site, FRDA EBV-cell lines exhibited elevated levels of the negative elongation factor NELF-E depending on the presence of a GAA repeat expansion compared to controls. This site may represent a rate-limiting step for *FXN* transcription and consequently provide a means to modify transcription levels in FRDA. Moreover, RNA pol II pausing site binding factors, such as NELF-E, were influenced by Nicotinamide treatment, a HDAC class III inhibitor. Therefore, factors sensitive to chromatin changes may influence the regulation of RNA pol II pausing and also balance otherwise positive chromatin changes. This new finding could explain the relatively minor effects of different drug approaches to up-regulate this gene. Furthermore, CTCF and the histone demethylase LSD1 were also found to be located at the *FXN* pausing site. Results suggest a function for LSD1 in demethylating H3K4me2 at the pausing site and potentially also in demethylating H3K9me3 in the case of frequently transcribed expanded GAA repeats. Therefore, LSD1 might play a crucial role in preventing heterochromatinisation of a euchromatic gene. Using primary transcript RNA-FISH, a delay in RNA pol II release from the pausing site and furthermore a dramatic loss of RNA pol II elongation in the presence of expanded GAA repeats was seen. The identified and characterised transcriptional pausing site at *FXN* is likely to play a repressive role and participates in the pathogenesis of FRDA.

Acknowledgements

Thank you to Prof. Richard Festenstein and Dr. Ana Pombo for helpful suggestions on this project.
Thank you for the corrections on this manuscript to: Richard Festenstein, Emily Ferenczi, Andrew Chapman, Nastassja Rothe, Susan Campbell, Sophia Lin and Anne Bygrave.

A special “Thank you” to Dr. Maria Mayan-Santos for not only a great time in the lab but hard work on this project.

Thank you to Cameron Osborne for teaching and helping me with the RNA-FISH *in situ* hybridisation.

A big “Thank you” for helpful advises and a good time in the lab goes to: Maria Mayan-Santos, Eleanor Tucker, Sophia Lin and Santiago Uribe Lewis.

Thank you to Ataxia UK for funding this work.

The biggest “Thank you” goes to my parents Karin and Burkhard Rothe, my sister Nastassja Rothe, and my as good as relatives Andrew Chapman and Carolina Nietzer for being always supportive and available.

Thank you to my examiners Prof. Paul Freemont and Prof. Veronica van Heyningen for taking the time to read this manuscript.

Contents

List of Figures

List of Tables

Introduction

Introduction

Friedreich's Ataxia

Friedreich's ataxia (FRDA) is the most common autosomal recessive neurodegenerative disease with an incidence of one in 50,000. The carrier frequency varies depending on the ethnic group from 1/60-1/100 (Pandolfo, 1998; Bidichandani et al., 1998). FRDA is well documented in Europe, the Middle East, South Asia (Indian subcontinent), and North Africa. To date, FRDA has not been recognised in Southeast Asia, in sub-Saharan Africa, or among Native Americans. Furthermore, a lower than average prevalence of FRDA is documented in Mexico (Gomez et al., 2004).

FRDA is caused primarily by an abnormal GAA repeat expansion located in the first intron of the *frataxin* gene (*FXN*) (Fig. 1) (Campuzano et al., 1996). The *FXN* gene consists of five alternatively spliced exons, which encode one of two open reading frames (Ensembl). Exons 1 - 5 produce the major transcript encoding the 210- amino acid mitochondrial protein, Frataxin. Most individuals suffering from FRDA are homozygous for large GAA trinucleotide repeat expansions of the polymorphic $(GAA)_n$ sequence in intron 1 (Campuzano et al 1996). The size associated with FRDA ranges from 66 to 1700 or more triplets (Campuzano et al 1996, Durr and Brice, 1996; Epplen et al 1997), although the majority of alleles contain 600 to 1200 repeats. This type of mutation is seen in 96 % of all *FXN* mutant alleles, only 4 % display point mutations inside the coding regions of *FXN*.

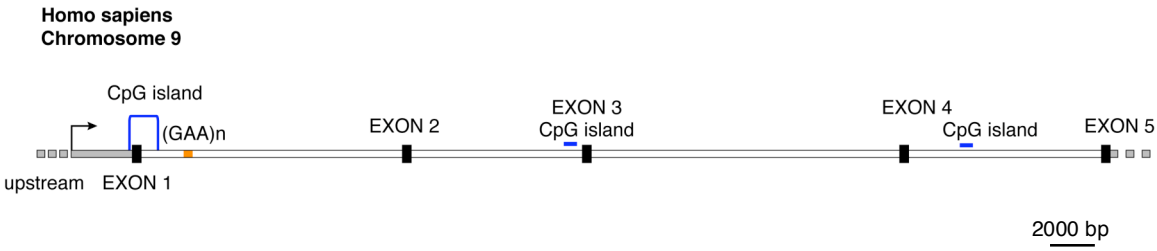

Figure 1: Location of GAA repeat is marked in orange, CpG- islands are marked in blue. *FXN* consists of 5 exons. The length of introns is displayed in correct proportion.

A normal $(GAA)_n$ repeat is situated at the centre of an Alu repeat element, showing a length polymorphism (Campuzano et al., 1996; Cossee et al., 1997; Montermini et al., 1997a). Furthermore, adjacent to the GAA triplet repeat a polymorphic mononucleotide tract of adenines (poly A tract) was identified (Monticelli et al., 2004). Unaffected individuals possess between 5 and 33 GAA repeats. Bimodal distribution exists among normal alleles in which 85 % have fewer than 12 GAA repeats (short normal) and the remainder comprise 12 - 33 repeats (long normal). Alleles longer than 27 GAA repeats are usually interrupted by a $(GAGGAA)_n$ sequence. However, the homopurine / homopyrimidine nature of the GAA tract is maintained in all individuals. A rare variation of a GAA triplet repeat was reported where two individuals were found carrying 65 tandem repeats of the GAAGGA hexanucleotide sequence instead of the normal GAA triplet repeat. This sequence seemed to be non-pathogenic (Ohshima et al., 1999).

The condition is characterised by progressive gait and limb ataxia, dysarthria, areflexia, loss of vibratory and position sense, and distal extremity weakness. Additional features include hypertrophic cardiomyopathy, scoliosis and diabetes. However, 25 % of patients carrying a *FXN* mutation do not fulfil all of these characteristics (Durr and Brice, 1996). Usually FRDA patients show a negative correlation between the size of the shorter allele expansion and the age of FRDA onset and the use of a wheelchair. A direct correlation is seen with disease severity, presence of cardiomyopathy, and optic atrophy (Durr and Brice, 1996; Filla et al., 1996; Schols et al., 1997).

Since there is no evidence *in vivo* for an effect on RNA processing in FRDA, the disease results directly from reduced *FXN* mRNA levels followed by reduced amounts of Frataxin protein (Bidichandani et al., 1998; Cossee et al., 1997; Ohshima et al., 1998). *FXN* mRNA is expressed mainly in tissues with a high metabolic rate, including liver, kidney, brown fat and heart. High levels of expression are also found in the spinal cord, whereas in the cerebellum lower levels of Frataxin predominate (Campuzano et al., 1997; Koutnikova et al., 1997). The GAA repeat expansion provokes a severe drop in *FXN* mRNA levels, 30 % below those of normal individuals, leading to the development of FRDA (Pianese et al., 2002). In line with this, FRDA patients show abnormalities in the spinocerebellar tracts, dorsal columns and to a lesser extent the cerebellum and medulla. Finally, 50 % of all fatal cases

occur because of heart failure and 75 % of all FRDA cases demonstrate evidence of cardiac dysfunction (Hewer, 1968), demonstrating the necessity for adequate Frataxin levels in the heart.

Despite a general genotype-phenotype correlation, it is not possible to predict the clinical outcome in an FRDA individual based on the genotype. Thus, it was suggested that the variability in FRDA severity is most likely caused by variations in individual genetic backgrounds (Montermini et al., 1997a; Montermini et al., 1997b). In general the size of the allele with the shorter GAA repeat expansion gives a better correlation with the rate of progression of FRDA (Filla et al., 1996; Monros et al., 1997; Richter et al., 1996). Notably, in 50 % of all FRDA cases the rate of disease progression also correlates with the age of onset (Montermini et al., 1997a; Bhidayasiri et al., 2005). The age of onset of FRDA ranges from the age of five to beyond 50 years, suggesting that additional factors are involved in the manifestation of the disease. Notwithstanding, a small pool of patients exists that exhibits a late onset of FRDA accompanied by only mild symptoms despite having a long GAA repeat expansion. This phenomenon will be discussed in more detail in the following paragraph.

FRDA types

Late onset patients can be divided into three subgroups, namely: late onset FRDA (LOFA), very late onset FRDA (VLOFA) and Acadians (Berciano et al., 2002; Bidichandani et al., 2000). Individuals with LOFA usually possess fewer than 500 GAA repeats in the shorter of both alleles (Durr et al., 1996, Filla et al., 1996, Montermini et al., 1997; Bhidayasiri et al., 2005). Individuals with VLOFA usually show fewer than 300 GAA repeats, at least in one of the expanded alleles (Berciano et al., 2002; Bidichandani et al., 2000). Nevertheless, an individual with VLOFA exhibiting expansions of greater than 800 repeats in each allele has been found (Bidichandani et al., 2000). This again emphasises the difficulty of predicting FRDA progression and also demonstrates the possibility of a beneficial genetic background. Therefore, additional factors might indeed influence the GAA expansion thus modifying the progression of the disease.

Further evidence for additional factors influencing *FXN* expression is given in Acadian FRDA patients. Acadian patients generally show a late onset, with a range of 18 to 44, with a mean of 27 years, accompanied by confinement to a wheelchair at a later stage and a much lower incidence of cardiomyopathy (Montermini et al., 1997). Despite these clinical differences, no significant differences were found in the size of the GAA expansions or in the coding region of *FXN* in this population. Acadians descend from a 17th- century French colony that settled in a region geographically separate from Quebec called Acadia. They developed and maintained their own culture for more than 400 years (Faragher, 2005). In this community one can hypothesise the existence of a more uniform genetic background, leading to an improvement in the case of an abnormal GAA repeat expansion in the first intron of the *FXN* gene.

Pathologic GAA repeat expansions

It has been suggested that the development of FRDA is caused by an abnormal GAA repeat expansion interfering with RNA pol II elongation. This is thought to lead to a severe deficiency of normally spliced *FXN* mRNA in individuals homozygous for the GAA expansion (Campuzano et al., 1997; Bidichandani et al., 1998).

Experiments conducted on *E. coli* and *S. cerevisiae* demonstrated *in vitro* and *in vivo* that the GAA triplet repeats constitute a length and orientation-dependent hindrance to elongation (Bidichandani et al., 1998, Grabczyk and Usdin, 2000; Ohshima et al., 1998). Sequences with more than 59 GAA triplet repeats form a structure called "sticky DNA", produced by the intermolecular association of two DNA triplexes (Sakamoto et al., 1999). A DNA triplex is formed upon binding of a pyrimidine or a purine single-stranded DNA to the major groove of a double helix, forming Hoogsten or reverse-Hoogsten hydrogen bonds between the purine strand and the duplex (Jain et al., 2002; Rajeev et al., 1997). Interruption in the purity of the GAA sequence for example by GGA, results in destabilization of sticky DNA accompanied by a lack of transcriptional inhibition (Ohshima et al., 1998, Sakamoto et al., 1999; Sakamoto et al., 2001a). Sticky DNA is detected by reduced mobility of DNA restriction fragments containing GAA•TTC repeats on gel electrophoreses and most likely arises from intra-molecular association of long GAA repeat triplexes. However, recent publications indicate that although the transcription through GAA repeats is

hampered, it is still possible (Krasilnikova et al., 2007). The following figure 2 extracted from review Mirkin S., (2007), illustrates schematically the triplex and sticky DNA configuration.

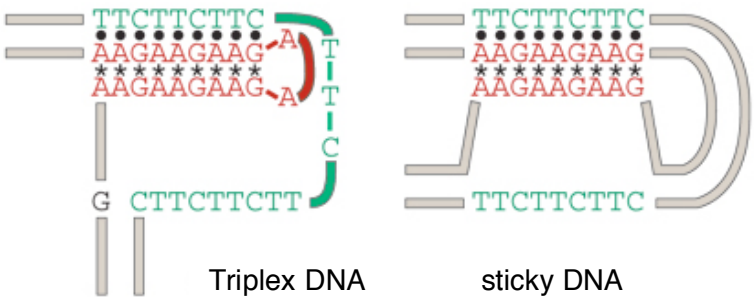

Figure 2: Sticky DNA structure can result from repetitive GAA- DNA. The structure-prone strand of the repetitive run is shown in red, its complementary strand in green and flanking DNA in beige. Triplex DNA and sticky DNA formed by the $(GAA)_n$·$(TTC)_n$ repeat. Figure 2 is extracted from review Mirkin S., Nature 447, 932-940, 2007.

Long GAA repeats can form triplexes containing 2 purine (R) GAA strands and 1 pyrimidine (Y) TTC stand, flanking a single-stranded pyrimidine region. The formation of a RRY triplex in plasmid DNA requires divalent metal ions and negative super-coiling. A high-resolution NMR structure of a GAA•TTC•GAA triplex has been presented and indeed a DNA triplex structure provoked by triplet repeats within the *FXN* gene was found (Mariappan et al., 1999). Using two different monoclonal antibodies against triplex DNA it has been shown that parts of the chromosomal DNA are naturally organised as triplex configurations, scattered among and within the chromosomes (Agazie et al., 1996; Burkholder et al., 1988; Ohno et al., 2002). Furthermore, these experiments showed cell type and cell cycle dependent staining patterns, indicating cell type specific arrangements of DNA in the nucleus (Agazie et al., 1996). Nuclei double stained with antibodies against centromeric- and triplex-$(GA/TC)_n$ tracts revealed a close spatial association of both signals, suggesting the possibility of chromatin organisation via DNA triplexes (Ohno et al., 2002).

On the other hand, Saveliev et al., (2003) showed that expanded GAA repeats introduced into the mouse genome induced position-effect variegation (PEV) of an adjacent reporter gene. This finding suggests that *frataxin* deficiency associated with expanded GAA repeats may also be mediated by an abnormal chromatin

organization. PEV occurs when a gene is located abnormally close to regions of heterochromatin. Silent heterochromatin is characterised by the presence of particular histone modifications for example, H3K9me3 and hypoacetylated histone tails. Further details of chromatin will be discussed in the second part of the Introduction. Of importance here is that mutagenesis studies have identified many genes, which have the potential to modify the extent of gene silencing in PEV *in vivo*.

Such genes encode factors which are either components of chromatin such as core histones or enzymes modifying chromatin, for example: histone acetyltransferases, deacetylases or methyltransferases (Reuter and Spierer, 1992). A key component of constitutive heterochromatin is Heterochromatin Protein 1 (HP1) (Eissenberg et al., 1992; Elgin, 1996). It has been shown that HP1, when over-expressed, is a powerful modifier of mammalian PEV which also increases GAA-repeat associated reporter gene silencing in transgenic mice (Festenstein et al., 1999; Saveliev et al., 2003). Therefore, one can hypothesise that an unusual non-B DNA structure, such as triplexes and/or the sticky DNA conformation adopted by GAA•TTC repeats, might initiate silencing of genes harbouring such repeats, as seen in the *FXN* locus of FRDA patients. Furthermore, proteins that recognise and bind these alternative DNA structures might initiate a cascade of events, leading to the recruitment of heterochromatic proteins and ultimately initiating gene silencing.

Pathology in Friedreich's ataxia results from deficiency of Frataxin and its function

Frataxin protein deficiency leads to a reduced antioxidant defence, deficient mitochondrial function and increased oxidative damage (Lodi et al., 2001c). Affected individuals show poor ATP production and cellular oxygenation in post-exercise skeletal muscle (Lodi et. al. 2001c; Seznec et al., 2005). Frataxin is required for the biogenesis of the iron-sulphur-cluster (ISC) and is therefore vital for the synthesis of the respiratory chain complexes I-III enzymes and the aconitases (Seznec et al., 2005). Since individuals suffering from FRDA show abnormal mitochondrial iron accumulation, Frataxin may also play a role in the regulation of mitochondrial iron content, however this could be a secondary manifestation (Bunse et al., 2003; Lodi et al., 2001a; Lodi et al., 2001b).

In mice, complete deficiency of *frataxin* (*Fxn*) leads to early embryonic lethality without evidence of iron accumulation (Cossee et al., 2000), indicating that *Fxn* is essential for early embryonic development and that iron accumulation is unlikely to be a primary pathophysiological event. A similar situation may occur in humans as to date no patient has been identified as having two alleles exhibiting Frataxin inactivating point mutations, implying homozygous lethality. Even more, during development homozygosity for very large GAA expansions still results in sufficient amounts of Frataxin (Pandolfo, 2006).

The development of tissue-specific conditional knockouts of mouse *Fxn* have resulted in models displaying specific features of the FRDA phenotype, such as neurodegeneration in the dorsal root ganglia, cardiomyopathy and diabetes mellitus (Puccio et al., 2001; Ristow et al., 2003; Seznec et al., 2004; Simon et al., 2004). Moreover, treatment with the anti-oxidant, Idebenone, which is discussed later on, delays the onset of cardiac pathology and even prolongs the life span of cardiac-specific *Fxn* knock-out mice (Seznec et al., 2004).

FXN promoter and potential regulatory factors

In order to develop compounds effective in increasing *FXN* levels, the identification of factors regulating its expression is required. These factors might include *cis*-acting DNA sequences and *trans*-acting proteins. Additionally, the influence of the chromatin structure at the *FXN* locus still needs to be assessed in normal versus FRDA individuals. An effort to search for *FXN* promoter elements identified a conserved initiator element and possible, so-called downstream promoter elements (DPE) (Sarsero et al., 2005). This work, which was achieved by using a reporter gene (EGFP) under the control of the proposed promoter site of *FXN* (FXN-EGFP cell line), also demonstrated that deletions downstream of the transcription initiation site had the most severe impact on reporter gene activity, reducing its expression by 60 %. Therefore, downstream elements may contribute significantly to *FXN* promoter activity (Greene et al., 2007; Sarsero et al., 2005).

Up-regulation of *frataxin* expression

Even though the regulation of *FXN* and specifically the down-regulation via GAA expansion remains unclear, a number of studies and screens have been conducted to identify compounds that increase the expression of *FXN*. As specified before, several ideas already exist as to how the GAA repeat expansion may negatively influence the transcription machinery. To date, several agents have been found to increase *frataxin* expression in cellular models such as hemin, butyric acid (Sarsero et al., 2005), and erythropoietin (Sturm et al., 2005). However, the mode of action for most of these agents and their efficiency in up-regulating *FXN* to adequate levels is unclear.

Therapies under investigation

As *frataxin* mRNA deficiency results in abnormal accumulation of intramitochondrial iron, defective mitochondrial respiration and overproduction of oxygen free radicals, antioxidant therapy initially appeared promising. Iron chelators were therefore proposed as a possible therapy for reducing the intra mitochondrial iron overload. Non-specific iron chelators such as desferrioxamine were used for the specific reduction of mitochondrial iron overload. Although *in vitro* studies using a mitochondrial-specific iron chelator (2-pyridylcarboxaldehyde) showed promising results (Richardson et al., 2001), a clinical trial was terminated because of lack of efficacy.

However, free radical captors such as coenzyme Q10, vitamin E, Idebenone (a short-chain analogue of coenzyme Q10), and more recently, mitochondrial-targeted Idebenone (MitoQ) are considered to be potential therapies for slowing the progression of FRDA (Lodi et al., 2001a).

Coenzyme Q10 and vitamin E

Following treatment with coenzyme Q10 and vitamin E over a period of three to six months, showed improved ATP production in the heart and skeletal muscle of individuals with FRDA. An open label trial of these drugs in ten individuals for 47 months resulted in sustained improvement in bioenergetics and improved cardiac

function as assessed by increased fractional shortening, implying improved left ventricle performance (Hart et al., 2005).

Idebenone

Early clinical trials with Idebenone showed a reduction of the left ventricular mass and wall thickness in some FRDA individuals with cardiac hypertrophy (Buyse et al., 2003; Mariotti et al., 2003; Rustin et al., 1999). However, the neurological condition of these patients continued to deteriorate slowly with Idebenone treatment (5mg/kg) over a seven-year follow-up. In addition, although cardiac hypertrophy decreased during this course, cardiac function did not improve (Ribai et al., 2007). Idebenone administered orally for one month at high doses of up to 75 mg/kg per day was well tolerated (Di Prospero et al., 2007). This finding led to a randomised placebo controlled trial using higher doses of up to 45mg/kg for six months. Again the higher-dose treatment was generally well tolerated and importantly was associated with an improvement in neurological function in FRDA patients, in a dose dependent manner. Indicating, that higher doses may be necessary to have a beneficial effect on neurological function (Di Prospero et al., 2007).

MitoQ and MitoVitE

In an effort to improve the delivery of Idebenone and vitamin E to mitochondria (Kelso et al., 2001; Smith et al., 1999), the compounds were linked to a lipophilic cation to produce MitoQ and MitoVitE, respectively. In a cell culture model using fibroblasts from affected individuals, Jauslin et al., (2003) showed that MitoQ was 800 times more active than Idebenone in protecting cells from endogenous oxidative stress. Although MitoVitE was less effective, it was still 20 times more effective than Idebenone. A trial of MitoQ in FRDA is planned to commence shortly. MitoQ taken orally accumulates in the heart and the brain of mice (Kelso et al., 2001), demonstrating its capacity to cross the blood brain barrier.

Gene therapy

The treatments proposed above have all improved the course of FRDA rather than cured the lack of Frataxin. Therefore, gene therapy would appear a desirable choice, addressing the cause rather than the consequences of FRDA. The first steps to supplement the loss of function of Frataxin via gene therapy have already been taken

(Fleming et al., 2005). Recombinant adeno-associated viral and lentiviral vectors expressing *FXN* cDNA were shown to partially correct sensitivity to oxidative stress in FRDA primary fibroblasts (Fleming et al., 2005). In both cellular and animal models it was shown that herpes simplex virus type 1 (HSV-1) amplicon vectors expressing either the entire FRDA genomic locus or *frataxin* cDNA were able to partially rescue the FRDA phenotype (Lim et al., 2007). Specifically, Gomez-Sebastian et al., (2007) found that FRDA primary fibroblasts harbouring HSV1:*FXN* exhibited a restored response to oxidative stress. In both studies a neurotropic herpes vector was used to correct the neurological degeneration found in FRDA. To this end, (Fleming et al., 2007) have shown that rota-rod test deficits in mice with localised *frataxin* reduction in the brainstem can be corrected by exposure to HSV-1:*FXN* cDNA. Still, a significant amount of basic research is required before gene therapy is feasible in a clinical setting.

Other gene based approaches

The results obtained for GAA•TTC repeats and their resulting DNA and chromatin structure led to the hypothesis that molecules interfering with triplex or sticky DNA formation and/or heterochromatin formation in the *FXN* gene would be beneficial. Promoting successful elongation through expanded GAA•TTC repeats might relieve the deficiency in *FXN* mRNA and protein in affected individuals (Grabczyk and Usdin, 2000; Saveliev et al., 2003; Vetcher et al., 2002). Furthermore, molecules that increase *FXN* promoter activity, either by acting on the DNA or the protein constituents of the transcription initiation or RNA chain elongation complexes, might also be therapeutic for FRDA (Sarsero et al., 2003).

Two groups focused on the identification of small DNA ligands to alleviate the proposed GAA•TTC repeat-mediated gene silencing. The first group performed a rational screen on small molecule DNA ligands to determine their effects on EGFP expression in the reporter cell lines described earlier (Grant et al., 2006). This study was based on the results of compound screening due to the ability to discriminate between different nucleic acid structures in a competition dialysis experiment. Here, compounds such as DAPI, diminazene Hoechst 33258, distamycin and pentamidine were found to increase EGFP expression of the *FXN*-EGFP cell line. The anti-infective pentamidine, used for the treatment of HIV-associated infections, was

shown to increase levels of Frataxin by 1.3 up to 2.2 fold in primary lymphocytes isolated from FRDA patients (Grant et al., 2006).

The second group demonstrated a promising potential treatment using linear β-linked polyamides. These pyrrol-imidazole polyamides can be designed to bind specifically homopurine DNA stretches (Dervan and Edelson, 2003; Janssen et al., 2000a; Janssen et al., 2000b; Urbach and Dervan, 2001). Given the very high affinity of polyamides for their target sites, these molecules should act as a thermodynamic sink and lock GAA-TTC repeats into double-stranded B-type DNA, preventing the transition to non-B DNA structures of long GAA•TTC (review Gottesfeld, 2007). Importantly, polyamides bound within coding regions of genes were shown to have no negative effect on transcription in mammalian cells. Finally, these molecules do not bind to RNA; therefore the RNA processing should be unaffected. Indeed in FRDA EBV-cell lines, an increase in RNA of ~ 2 fold was observable, however this effect was not preserved in non-dividing cells.

Animal models for FRDA

Koutnikova et al., (1997) cloned the complete coding region of mouse *Fxn* and studied its pattern of expression in developing and adult tissues. They found by *in situ* hybridisation analyses that *Fxn* expression correlated well with the main sites of neurodegeneration in FRDA. Nevertheless, the expression pattern of *Fxn* was broader than expected from the pathology of the disease. *Fxn* mRNA was predominantly expressed in tissues with a high metabolic rate, including liver, kidney, brown fat, and the heart. They also demonstrated that mouse and yeast *FXN* homologues contain a potential mitochondrial targeting sequence in their N-terminal domains and that disruption of the yeast (YFH1) gene results in mitochondrial dysfunction (Koutnikova et al., 1997).

Mice with tissue specific *Fxn* deficiency

Through a conditional gene targeting approach, Puccio et al., (2001) generated, in parallel, a striated muscle *Fxn* deficient mouse line and a neuron/cardiac muscle *frataxin* deficient line, which together reproduced important progressive pathophysiologic and biochemical features of human FRDA. These mice displayed

cardiac hypertrophy without skeletal muscle involvement, large sensory neuron dysfunction without alteration of the small sensory and motor neurons and deficient activity of complexes I-III of the mitochondrial respiratory chain and of aconitases. This model also demonstrated time-dependent intra-mitochondrial iron accumulation in a *frataxin* deficient manner, occurring after onset of the pathology and after the inactivation of the Fe-S-dependent enzymes. Therefore, these mice might represent the first mammalian models to evaluate possible treatment strategies for FRDA patients (Puccio et al., 2001).

Mice with $GAA_{(230)}$ repeat knock-in into *Fxn*

Miranda et al., (2002) generated transgenic mice with a GAA repeat expansion of 230 repeats introduced into the first intron of the mouse *Fxn* gene. However, the GAA repeat insertion is not comparable to the human location, as mice do not normally exhibit a GAA repeat in the first intron of *Fxn*. These mice showed reduced *frataxin* levels, but failed to exhibit a FRDA phenotype of motor deficits, iron overload, or meiotic/mitotic instability (Miranda et al., 2002).

Mice possessing the human *FXN* locus with a GAA expansion

Al-Mahdawi et al., (2006) generated two strains of human *FXN* YAC transgenic mice carrying pathogenic 190 or 190+90 GAA repeat expansions respectively in intron 1 of the human *FXN* gene. These mice, when crossed to rescue the $Fxn^{-/-}$ mice, showed decreased levels of human *frataxin* mRNA and protein expression in various tissues, including the brain, the heart and skeletal muscle, as well as increased levels of oxidised proteins. Phenotypically, these transgenic mice showed coordination deficits and a progressive decrease in motor activity from the age of 3 months, although none developed ataxia over a period of 2 years. Electrophysiological studies were suggestive of a mild, progressive peripheral neuropathy. Histology showed large vacuoles in dorsal root ganglia neurons and mild iron deposition in cardiomyocytes (Al-Mahdawi et al., 2006). However there is no control mouse with a normal GAA repeat at the *FXN* locus currently available. It is therefore difficult to prove that the observed phenomenon is based on the relatively short GAA expansion rather than on the construct itself.

Using the same mouse model, Clark et al., (2007) found that transgenic mice carrying expanded GAA repeats (190 or 82 triplets) in the human *FXN* gene showed tissue-specific and age-dependent somatic instability specifically in the cerebellum and dorsal root ganglia. The $GAA_{(190)}$ allele showed some instability at the age of 2 months and a significant expansion by 12 months, which was slightly greater than that of $GAA_{(82)}$, suggesting that somatic instability was also repeat-length dependent. There were lower levels of repeat expansion in proliferating tissues, indicating that DNA replication per se was unlikely to be a major cause of age-dependent expansion.

Mice with human *FXN* fused to EGFP

Sarsero and colleagues generated transgenic mice with a BAC genomic reporter construct consisting of an in-frame fusion between the human *FXN* and the gene encoding enhanced green fluorescent protein (EGFP). Since the expression of EGFP is under the control of the *FXN* gene regulatory elements, compounds which might up-regulate *FXN* transcription should be easily identified in these mice. However, the present construct contains only six GAA repeats and therefore only permits the identification of molecules acting in the wild type situation. Interestingly, this group identified hemin and butyric acid as positive enhancers of *frataxin* expression, even though an up-regulation of less than 20 % was seen (Sarsero et al., 2005)

As previously mentioned, the currently available treatment for FRDA patients is not satisfactory. This may in part be due to the approaches taken to date. In most cases the focus has been on overcoming the effects of lacking *frataxin* using other compounds. However, each affected tissue seems to suffer a specific problem caused by the lack of Frataxin. So far, it has proved difficult to treat FRDA with only one compound. Therefore, the ideal treatment may be a drug enhancing the reduced *frataxin* levels and possibly leading to an improvement in all affected organs.

Since mouse models exhibiting a GAA stretch linked to a reporter gene demonstrated sensitivity to epigenetic modifiers, these might be good candidates as potential drug targets (Festenstein et al., 1999; Saveliev et al., 2003). The second part of the Introduction will give a general overview of epigenetics and its factors, which might play a role in regulating *FXN* transcription.

Epigenetics

Overview of epigenetics

In the field of epigenetics the main focus of research lies on factors that allow cell specific processing of the genetic code, without changing the latter. Each cell of an organism contains the same genetic information but the expression pattern can differ drastically from cell type to cell type. Thus, mechanisms must be available firstly to allow a cell to develop a certain expression pattern and secondly to maintain this expression pattern during following cell divisions. There are three main mechanisms involved in the complex epigenetic gene regulation. The first one is the packaging of negatively charged DNA around basic histones (Luger et al., 1997). The resulting chromatin can then, depending on specific modifications of the histone tails, be loosened up or compacted further, resulting in a polymorphic accessibility to proteins such as transcription factors (see review Kouzarides, 2007). The second mechanism is the methylation of DNA, which stays in contact with specific histone modifications, setting a mark for the binding of proteins, which then can act in a chromatin repressive mode (Bird, 2001, 2002; Ng and Bird, 1999). The third mechanism involves non-coding RNAs (see review Kouzarides, 2007). They can act on the translational as well as on the transcriptional level. Importantly, the combination of all three mechanisms plays a crucial role in epigenetic regulation of the genome (see review Kouzarides, 2007).

This project focuses on the investigation of distinct histone modifications at the human *FXN* gene in FRDA patients. As discussed earlier, this GAA triplet repeat is known to form a non-B-triplex DNA structure possibly resulting in a more condensed chromatin structure. Here, the possibility of an abnormal histone code interfering with the otherwise open chromatin structure of the *FXN* locus caused by the GAA expansion will be investigated. Furthermore, the possibility of reversing the abnormally condensed structure via epigenetic modifiers will be tested.

Chromatin Structure

In eukaryotic cells, nuclear DNA is packaged into a higher ordered structure, known as chromatin. The basic repeating unit of chromatin is the nucleosome, consisting of a 147 bp DNA superhelix wrapped around a histone octamer complex consisting of 2

of each histone: H2A, H2B, H3 and H4 (Luger et al., 1997). An interaction between the DNA and histone molecules is established by electrostatic interaction between negative groups of the DNA and positive side chains of the histones (Ladik et al., 2007). The N-terminal tail of each core histone protein sticks out thereby providing an additional site for further modifications. These can affect the chromatin structure by disrupting or creating binding sites for certain chromatin associated proteins, ultimately leading to the activation or repression of transcription. Additionally, several histone variants such as H2A.Z and H3.3 exist although their exact functions remain elusive (see review Loyola and Almouzni, 2007).

Modifications of histones and their implication in chromatin structure

The development of the chromatin immunoprecipitation (ChIP) technique in the early 1990s allowed the investigation of proteins bound to particular DNA sequences *in vivo*. Thereby, living cells are cross-linked with formaldehyde, followed by cell lysis and sonication to release and break up the chromatin into smaller fragments. Using specific antibodies the DNA-protein complexes of interest can be immunoprecipitated. By reversing the cross-link and cleaning the remaining DNA, it is then possible to identify the protein-bound DNA sequences via the polymerase chain reaction (PCR) (Ebralidse et al., 1993; Orlando et al., 1997).

Most histone tail modifications were discovered or at least confirmed by mass spectrometry prior to the development of suitable antibodies. The majority of modifications occur at the amino- and carboxy- terminal part of the histone tails, with only a few being localised to the globular domain. The most common ones are acetylation (ac), methylation (me), phosphorylation (ph), ubiquitylation (ub) and sumoylation (SUMO). Every modification exhibits a unique charge and size therefore potentially exerting for each one a specific effect on the chromatin structure. Several target sites have been identified for these different modifications and their functions are only partly understood (see review Berger, 2007).

A crucial target site is the amino acid lysine, representing a key substrate for all the modifications mentioned above. The functional consequences of those modifications can be direct in causing structural changes or indirect through protein recruitment (see review Berger, 2007). For example, adding a small group, such as an acetyl or

methyl group produces a different effect on chromatin compared to the effects of a bulky ubiquitylation or sumoylation, which are nearly two-thirds of the mass of a histone molecule (Shahbazian et al., 2005). Moreover, methylation can occur in several steps from mono to tri-methylation, which can be placed symmetrically or asymmetrically. Again each type of methylation has its unique impact on the transcription of chromatin (see review Berger, 2007). Furthermore, modifications on lysine residues lead to opposing chromatin structures and functions depending on their position. For instance, the tri-methylation of H3K4 is associated with active chromatin (Bernstein et al., 2002; Ng et al., 2003; Pokholok et al., 2005; Santos-Rosa et al., 2002; Schneider et al., 2004; Schubeler et al., 2004), whereas the tri-methylation of H3K9 mediates epigenetic silencing (Fisher et al., 2006; Ringrose et al., 2004; Snowden et al., 2002; Wu et al., 2007). For maximal epigenetic complexity and flexibility most, if not all, histone modifications are dynamic and reversible (see review Berger, 2007). The most common post-translational histone-tail modifications and their transcriptional implications are summarised and displayed below (Fig. 3).

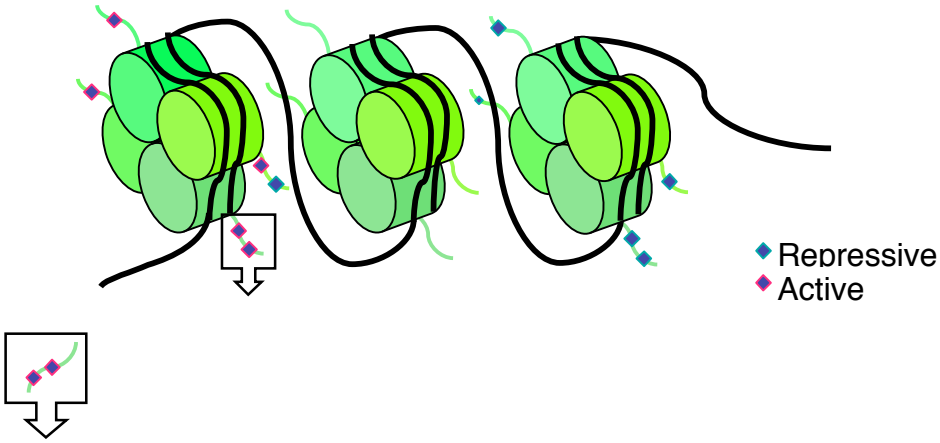

Histone post-translational modifications	Sites	Transcriptional Role
Acetylated lysine (**K**)	H3 (9, 14, 18, 56) H4 (5, 8, 13, 16) H2A, H2B	Activation
Phosphorylated serine/threonine (**S/T**)	H3 (3, 10, 28) H2A, H2B	Activation
Methylated arginine (**R**)	H3 (17, 23), H4 (3)	Activ. / Repression
Methylated lysine (**K**)	H3 (4, 36, 79)	Activation
	H3 (9, 27), H4 (20)	Repression
Ubiquitylated lysine (**K**)	H2B (120)	Activation
	H2A (119)	Repression

Sumoylation lysine	H2B (6/7), H2A (126)	Repression
Isomerised proline	H3 (30-38)	Activ. / Repression

Figure 3: Model of DNA wrapped around histone octamer consisting of pairs of H2A, H2B, H3 and H4. Each histone exhibits a flexible histone tail that can be dynamically modified. Shown here are histone sites with possible modifications and their implication for transcription.

So far, arginine residues appear to be strictly methylated and this is associated with active as well as repressive regulation of transcription (Kirmizis et al., 2007). Similarly, the phosphorylation of H3 occurs at loci of active transcription as well as during silenced mitotic chromosome condensation, demonstrating the importance of the genomic context when interpreting chromatin modifications (see review Berger, 2007). In the following part, selected histone tail modifications will be discussed in more detail.

H3K4 methylation

The methylation of H3K4 is associated with genes that are, or are destined to be, transcriptionally active and usually located in euchromatin (Litt et al., 2001). In line with this observation, H3K4me3 is primarily found at the 5' end of genes during the activation of transcription (Barski et al., 2007). This phenomenon, described in yeast, is most likely the result of recruitment of the Set1 histone lysine methyl transferase (HKMT) through phosphorylated Ser-5 of the carboxy-terminal domain CTD of the RNA polymerase (pol) II (Rossi et al., 2001). Ser-5 phosphorylation is known to release the RNA pol II from the initiation complex into an early elongating complex (Keogh et al., 2003). The following image (Fig. 4) illustrates the proposed mechanism and histone marks H3K4me2 and H3K36me3, which occur at the human *FXN* locus. Here, Set1 interacts with a RNA pol II associated factor (PAF complex), regulating different steps of RNA metabolism and also mediating the methylation of H3K4me2 (adapted from "Epigenetics" by Allis et al., 2007).

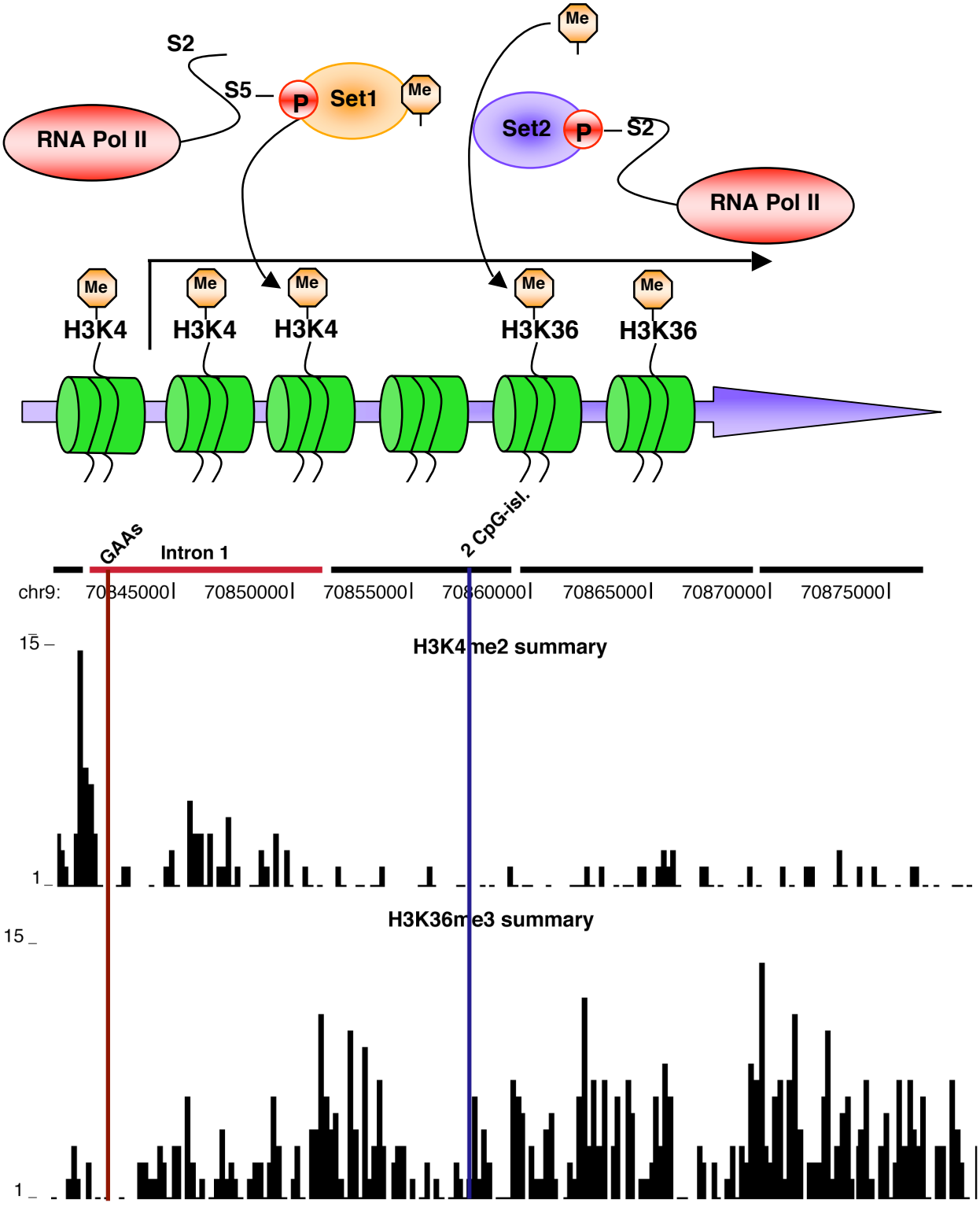

Figure 4: Proposed mechanism of H3K4 methylation by phosphorylated RNA pol II binding Set1 domain (adapted from "Epigenetics", Allis et al., 2007). *FXN* locus with location of GAA repeats (marked in red) and predicted second CpG-island (marked in blue) shown above ChIP results against H3K4me2 and H3K36me3. Histone modifications are extracted from database provided by Barski et al., 2007.

Mechanistically, the methylation of H3K4 can lead to the recruitment of specific factors such as the chromodomain helicase DNA binding protein 1 (CHD1) protein (an ATP-dependent helicase), which binds to H3K4me2 as well as me3 (Sims et al., 2005). CHD1 also binds to the nucleosome remodeling factor (NURF) complex and is known to mobilize nucleosomes at active genes in *Drosophila*. Likewise, evidence exists that the nucleosomal remodeling and histone deacetylase (NuRD) repressor complex can no longer bind to methylated H3K4 tails (Lee et al., 2005; Martin and Zhang, 2005). To further enhance the sphere of action, the methylation of H3K4 seems to communicate with other modifications. *In vitro* results have demonstrated that in the presence of H3K4me3 and H3S10ph, the binding of the suppressor of variegation 39 in human (SUV39H) to the inactive H3K9me3 mark was prevented (Dormann et al., 2006). As suggested by others, this might be an efficient way to avoid a repressive H3K9 modification on an actively transcribed gene (Dormann et al., 2006).

H3K36 methylation

In yeast, the methylation of H3K36 seems to be necessary for the efficient elongation of RNA pol II through coding regions and occurs predominantly towards the 3' end of active genes (Muller et al., 2007). The HKMT Set2, preferentially binding to the Ser-2 phosphorylated form of the RNA pol II is capable of methylating H3K36. Moreover, the recruitment of Set2 to active genes requires components of the aforementioned PAF complex, similar to the recruitment of Set1. Interestingly, in mammals H3K36me3 has been found at much lower levels around promoters of inducible genes (Zhang and Reinberg, 2001).

H3K9 methylation

The first HKMT identified was (SUV39H1) that methylates H3K9 (Rea et al., 2000). The *Drosophila* homolog, Su(var)3-9, was initially identified as a suppressor of variegation (SUV) indicating an involvement in the silencing mechanism of position effect variegation (PEV). This phenomenon involves the spreading of heterochromatin into adjacent euchromatic genes. The function of H3K9 methylation in pericentromeric heterochromatin formation is mainly defined through two factors, the SUV39H1 and its binding partner heterochromatin protein 1 (HP1) (Nakayama et

al., 2001). A model has been proposed whereby SUV39H1 methylates H3K9, thereby creating a binding site for HP1 via its chromodomain (Bannister et al., 2001; Lachner et al., 2001). Once HP1 binds, it is able to spread into adjacent nucelosomes via its association with SUV39H1, catalysing the H3K9me3 of neighbouring histones (Nakayama et al., 2001). Furthermore, via the chromoshadow domain, HP1 is able to self-associate thus facilitating the spread of heterochromatin.

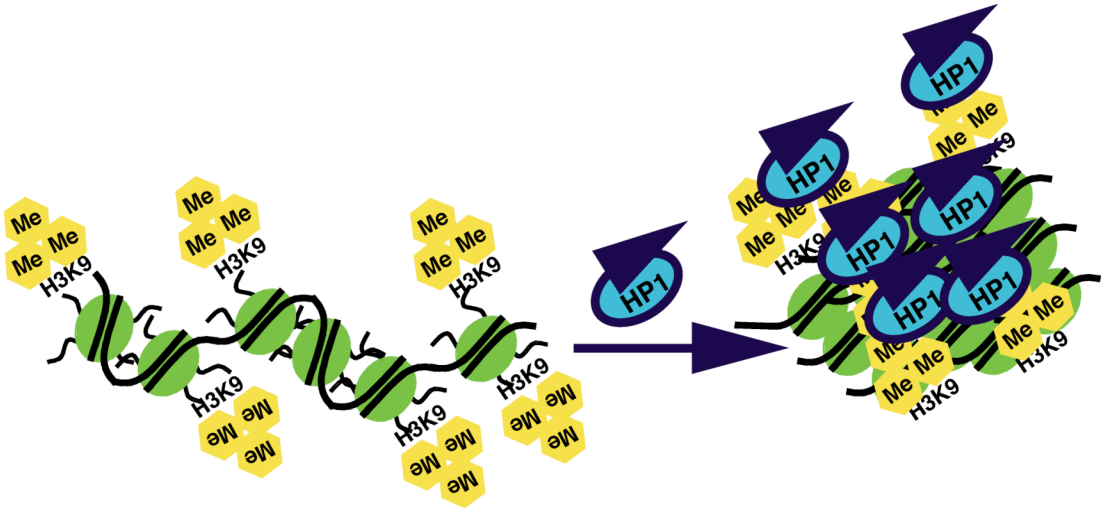

Figure 5: Heterochromatin establishment after methylation of H3K9me3 and HP1 recruitment. Adapted from "Epigenetics", Allis et al., 2007.

However, the model presented above seems to be valid only if a specific heterochromatin based recruitment for SUV39H1 exists. This previously missing link was demonstrated in fission yeast through the involvement of short interfering RNAs in heterochromatin formation (siRNAs) (Hall et al., 2002). These RNAs are transcribed from centromeric repeats bi-directionally and then processed into siRNAs by an enzyme called dicer. The siRNAs are subsequently packaged into a so-called RNAi effector complex RITS (**R**NA-induced **I**nitiation of **T**ranscriptional gene **S**ilencing), containing the chromodomain containing protein Chp1, which binds methylated H3K9. Thus, the initiation stage of heterochromatin formation is mediated via the targeting of the RITS complex to chromatin. In *S. pombe*, the spreading and maintenance of heterochromatin over a 20 kb region requires the methylation of H3K9 by the Clr4, a SUV39h homolog, and the binding of Swi6 (HP1 homolog) to H3K9 methylated chromatin (Martin and Zhang, 2005).

Since ChIP experiments revealed H3K9me3 at promoters of silenced mammalian genes, methylation of H3K9 might also be able to repress otherwise euchromatic

genes. This reasoning is of great interest for the identification of the molecular mechanism leading to severely reduced *FXN* levels. However, the mechanism leading to repression at euchromatic sites appears to be slightly different to that at heterochromatic regions. Here, the RB (retinoblastoma) protein recruits the histone lysine methyltransferase (HKMT) SUV39H1, which is followed by binding of HP1 to target genes. Unlike in heterochromatin, HP1 occupancy appears to be restricted to one or a few nucleosomes around the initiation site, even if H3K9 methylation occurs elsewhere at the promoter. The special restriction of HP1 on these euchromatic promoters and the prevention of spreading suggest a distinct mechanism of action for HP1 relative to its heterochromatic role (see "Epigenetics" by Allis et al., 2007). One possible explanation may be that HP1 acts as an anchor into heterochromatin-rich nuclear compartments (Obuse et al., 2004). Movements of gene loci within the interphase nucleus have been observed during the repression of euchromatic genes (Henikoff, 2001; Williams et al., 2006), which point toward the possibility that a silenced gene is displaced into a heterochromatic region. This movement appears to be dependent upon the gamma isoform of HP1 (Martin and Zhang, 2005).

Histone modifying enzymes

Histone modifications are of a dynamic and reversible nature allowing the epigenetic code to organise the DNA code. The dynamics of post-translational histone modifications are established via enzymes specific for each modification. Every modification has its own set of transferases and removing enzymes. Table 1 displays known histone residues and their specific histone methyltransferases (HMT) and demethylases present in humans. As an exception, arginine (R) methylation is altered by deaminases, converting it to citrulline (see review Bannister and Kouzarides, 2005).

Histone and residue	Methyltransferase	Demethylase/Deiminase	Function
H3R2	CARM1	-	Activator
	-	PADI4	Repressor
H3K4	SET7/Set9	-	Activator
	MLL	-	Activator
	Smyd3	-	Activator

		LSD1/BHC110	Repressor
		JARID1 family	Activator/Repressor
H3R8	PRMT5	-	Repressor
	-	PADI4	Repressor
H3K9	SUV39H1	-	Repressor, heterochromatin
	SUV39H2	-	DNA methylation, heterochromatin
	G9a		Imprinting, repressor
	Eu-HMTase1		Repressor
	SETDB1		Repressor, DNA methylation
	EZH2		Repressor
	-	JMJD2A/3A, JMJD2B, JMJD2C/GASC1, JMJD2D/2a/2b	Activator
H3R17	CARM1	-	Activator
	-	PADI4	Block to transcriptional activation
H3R26	CARM1	-	Activator
	-	PADI4	Block to transcriptional activation
H3K27	EZH2	-	Repressor
H3K36	NSD1		
	SMYD2		
	SET2		
		JHDM1a/b	
		JMJD2A/3A	Interacts with N-CoR and represses transcription
		JMJC2C/GASC1	
H3K79	DOT1L	-	Repressor, DNA damage
H4R3	PRMT1	-	Activator
	-	PADI4	Block to transcriptional activation
H4K20	Pr-SET7	-	Repressor
	SUV4-20H1/H2	-	Suppressor of variegation
	PR-Set7/8		Silent chromatin in euchromatic arm

Table 1: Human characterised enzymes responsible for the methylation and demethylation of histones. Source: Bannister & Kouzarides, doi:10.1038/nature04048.

Although a vast number of modifying enzymes are already known, it is most likely that more are waiting to be discovered. However, here the focus will be enzymes known to modify the histone residues H3K4 and H3K9. Following the earlier theme of dynamic epigenetic modifications, the methylation of H3K4 and H3K9 is also reversible. The next paragraph will examine the demethylation of lysine residues H3K4 and H3K9 in more detail.

Demethylation of Lysines

The recently discovered LSD1 (gene name: AOF2) (Shi et al., 2004), an enzyme removing methyl groups specifically from H3K4me2 and H3K4me1, changed the understanding of what was previously viewed as a very stable methyl group. LSD1 is present in a number of different repressor complexes. Some of them allow a more efficient demethylation of nucleosomal H3 lysines. However, the specificity of LSD1 can be modified via binding partners such as the androgen receptor (AR). This LSD1-AR complex is able to demethylate H3K9me1 and me2 rather than H3K4 and in this scenario acts as an activator (Metzger et al., 2005).

Additionally, five relatively new demethylases were identified (see review Takeuchi et al., 2006), all possessing a common catalytic structure called the Jumonji (JmjC)-domain, which is distinct from LSD1. These are found to demethylate distinct methyl states of H3K4, H3K9 and H3K36. The JmjC domain has been shown to demethylate histones in a $Fe2^{+}$ and α-ketoglutarate-dependent manner (see review Klose et al., 2006). One subclass contains a conserved N-terminal motif (JmjN domain). Comparison of the substrate preferences of JmjC and JmjN/JmjC-containing proteins has revealed that proteins with both a JmjN and JmjC domain prefer di- and trimethylated substrates whereas those with only a JmjC motif, demethylate mono- and dimethylated ones (Chen et al., 2006).

Mammalian cells encode four JmjN/JmjC proteins and are collectively referred to as the JARID1 family: JARID1a (Rbp2), JARID1b (Plu-1), JARID1c (SMCX) and JARID1d (SMCY). Unlike LSD1, which catalyses the removal of mono- and dimethylated histone H3K4 via an amino oxidase reaction, JARID1 proteins have a preference for H3K4me3 (Iwase et al., 2007; Klose and Zhang, 2007; Lee et al., 2007; Liang et al., 2007; Secombe and Eisenman, 2007). However, JARID1 activity

is not restricted to H3K4me3, as all four mammalian proteins are also able to efficiently demethylate H3K4me2 *in vivo* (Christensen et al., 2007; Iwase et al., 2007; Klose and Zhang, 2007; Lee et al., 2007), suggesting that JARID1 proteins of higher eukaryotes may have broader target specificity.

Because H3K4me3 surrounds the start site of transcriptionally active genes (Bernstein et al., 2002; Bernstein et al., 2005; Santos-Rosa et al., 2002; Schneider et al., 2004), the demethylase activity on H3K4me3 is thought to act as a transcriptional repressor. JARID1 and JARID1b are highly related (76 % identity, 90 % similarity) and each has been directly or indirectly linked to cellular transformation. Although JARID1b expression is normally largely restricted to the testis, it was originally isolated as a gene that was over-expressed in breast carcinomas (Barret et al., 2002; Lu et al., 1999).

Other enzymes modifying histone tails are the Ser/Thr phosphatases, which remove phosphate groups, ubiquitin proteases and mono-ubiquitin from H2B. Here, the focus lies on the methylation and acetylation status of *FXN* in the context of an abnormal GAA repeat expansion and the possibility of modifying the chromatin structure by histone deacetylase inhibitors (HDACi). Thus, only the histone sites of acetylation and their responsible enzymes will be discussed in the following section.

Histone acetylation

The steady-state acetylation level of histone proteins is achieved through the action of histone acetyltransferases (HATs) and histone deacetylases (HDACs) (see review Cheung et al., 2000; Narlikar et al., 2002). These modifications take place on the ε-amino group of lysine (K) residues using acetyl coenzyme A (Co A). Acetylation affects higher order folding of chromatin fibres, loosening the contacts between DNA and nucleosomes and/or histone-non-histone protein interactions (Carruthers and Hansen, 2000; Fischle et al., 2003; Shogren-Knaak et al., 2006; Tse et al., 1998; Wolffe, 2001). It is noteworthy that *in vitro* hyperacetylation of histone tails only seems to weaken histone tail-DNA binding (Mutskov et al., 1998), therefore they are unlikely to work as block against transcription factor access.

The first histone specific HAT, p55, isolated from *Tetrahymena* was shown to be the homologue of the yeast GCN5 (general control non-derepressible 5) (Brownell and Allis, 1996). Since then, many HATs have been identified (Tab. 2). They are divided into five families, including the GCN5-related N-acetyltransferases (HNATs); the MYST related HATs; p300/CREB-binding protein (CBP); the general transcription factor HATs; and the nuclear hormone-related HATs.

Histone tail modification	Enzyme acetylates	Function
H2A K5, H2B K 12, H2B K 15	CBP/p300	CREB-binding protein, DNA binding transcription factor
H3 K9	PCAF	Co-activator associated with p53
	GCN5L2	InterPro domain with PCAF
H3K14, H3K18	CBP/p300	CREB-binding protein, DNA binding transcription factor
	PCAF	Co-activator associated with p53
	GCN5L2	InterPro domain with PCAF
H4K5	CBP/p300	CREB-binding protein, DNA binding transcription factor
	MYST2	Synonyms: MOZ, YBF2/SAS3, SAS2 and TIP60 protein, histone acetyltransferase binding to ORC1
	HAT1	Histone acetyltransferase 1
H4K8	CBP/p300	CREB-binding protein, DNA binding transcription factor
H4K12	MYST2	Synonyms: MOZ, YBF2/SAS3, SAS2 and TIP60 protein, histone acetyltransferase binding to ORC1
	CBP/p300	CREB-binding protein, DNA binding transcription factor
H4K16	MYST3	Histone acetyltransferase (monocytic leukemia) 3
	TIP60	Transcriptional activation, catalytic site of the NuA4-complex

Table 2: Histone sites of acetylation and responsible acetylating enzymes and their functions. Adapted from review Yang, 2004.

Although a number of acetylating enzymes and their targets are known, this thesis will focus on the HATs acetylating H3K9 and H4K16, which are related to the GCN5 and MYST-family. Vertebrates additionally have a second gene encoding the

p300/CBP-associated factor (PCAF), which is about 73 % identical to GCN5 (Mizzen et al., 1996).

Many known nuclear HATs possess bromodomains, which recognise acetylated histone tails and thus participate in acetylation-dependent chromatin remodeling (Zeng and Zhou, 2002). The bromodomain is an approximately 110-amino-acid module with suggested roles in many different chromatin-related and independent functions (Nagy and Tora, 2007). Structural studies of both yeast Gcn5 and human PCAF bromodomains in complex with histone tail peptides revealed that GCN5 binds to histone H4 acetylated at K16 (Hudson et al., 2000; Owen et al., 2000), while PCAF seems to recognise H4 acetylated on K8 and also H3 acetylated on K14 (Dhalluin et al., 1999).

The MYST (**M**oz – now MYST3, **Y**BF2, **S**as2p, **T**ip) family is the largest but until recently one of the least studied families of histone acetyltransferases. TIP60 was originally identified in a screen for proteins interacting with the HIV tat gene product (Kamine et al., 1996). TIP60 seems to function as the catalytic subunit of the mammalian NuA4 complex (Thomas and Voss, 2007). The evolutionarily conserved multi-subunit complex, NuA4, is recruited by many factors to specific promoters, where it is thought to participate in histone acetylation and transcriptional activation.

TIP60 also has transcription independent roles in DNA damage responses and participates in the activation of kinases such as the ataxia-telangiectasia mutated (ATM) and the DNA-dependent protein kinase catalytic subunit (DNA-PKcs) following DNA double-strand breaks (DSB) (Squatrito et al., 2006). The first indication that TIP60 might have a role in DNA damage response (DDR) and/or DSB came from transfection experiments in HeLa cells, where over-expression of a dominant-negative allele of TIP60 reduced the efficiency of double strand break repair (Ikura and Ogryzko, 2003). New experiments imply that TIP60 may be involved in damage sensing, signaling and repair through several independent mechanisms (Squatrito et al., 2006).

The TIP60-NuA4 complex contains another protein kinase family member, called transformation-transactivation domain-associated protein (TRRAP), which is enzymatically inactive because of amino acid changes in its kinase domain. This

feature of TRRAP is conserved throughout evolution. The recruitment of TRRAP and Tip60 to DSBs was demonstrated by ChIP in mouse embryonic stem cells carrying a conditional knockout allele of TRRAP. Here the generation of a single DSB induced hyperacetylation of histone H4 in the surrounding chromatin. Deletion of TRRAP impaired Tip60 recruitment and H4 acetylation, as well as DSB repair by homologous recombination (Murr et al., 2006).

Histone Deacetylases (HDACs)

The enzymes removing acetyl-groups of histone tails are known as histone deacetylases (HDACs) and are presented by two distinct protein classes, the SIR2 family of NAD^+-dependent HDACs (class III) and the classical HDAC family. The latter consists of two different phylogenetic groups, namely class I and class II whose action is zinc dependent (Hernick and Fierke, 2005). The HDACs of class I are most closely related to the *S. cerevisiae* transcriptional regulator RPD3, whereas class II HDACs share homology with HDAC1, another yeast deacetylase (see review de Ruijter et al., 2003). In order to simplify the overwhelming number of HDACs, their functions and main targets are presented in the following table 3.

HDAC class	Name	Function
HDACs class I	HDAC1 and HDAC2	Complex dependent (found in Sin3, NuRD and Co-REST, can act directly on DNA-binding proteins (YY1, Rb binding protein 1 and Sp1, phosphorylation required for function
	HDAC3	SMRT and N-CoR are necessary for activity, is able to form oligomers with other HDACs like HDAC4, 5, but mostly it interacts with itself, may have role in cell cycle process
	HDAC8	Similar to HDAC3, probably very low abundance of expression
HDACs class II	HDAC6	Exhibits two catalytical domains in tandem, has signal for ubiquitination, probably particularly prone to degradation, functions as tubulin deacetylase but it is also found in the nucleus together with HDAC11
	HDAC10	Exists in two splice variants, interacts with HDAC1, 2, 3, 4, 5, 7
	HDAC4	Exhibit binding domains for CTBP, MEF2; show interaction with SMRT/N-CoR, BCoR and, the N-termini interact with MEF2 and
	HDAC5	

	HDAC7	blocks muscle cell differentiation. Suggested to by a link between DNA-binding recruiters and the HDAC3 containing complex
	HDAC9a, 9b, HDRP	Are splice variants, whereas HDRP lacks the catalytic domain, but is able to recruit HDAC3. All three interact with MEF2, indicating function in muscle differentiation.
HDAC11	HDAC11	More closely related to class I than to class II, not present in any known HDAC complex
HDACs class III **SIR2 family**[1]	SIRT1	Deacetylates histones (preference for H4K16), PCAF/MyoD, EP300, TAF168, HTATSF1, TP53, XRCC6, NKRF and forkhead proteins; Regulation of insulin and glucose homeostasis; Fat reduction, Neuron survival
	SIRT2	Predominantly cytoplasmic, deacetylates α-tubulin and histones, over expression delays mitosis, SIRT2 colocalises with chromatin during the G2/M transition, preference for H4K16 *in vitro*,
	SIRT3	Localised to mitochondrial matrix, *in vitro* deacetylates, multiple substrates including histones and tubulin, maybe important under conditions of energy limitation
	SIRT4	Localised to mitochondria and lacks detectable deacetylase activity but shows ADP-ribosyltransferase activity
	SIRT5	Localised to mitochondria with weak deacetylase activity and no apparent ADP-ribosyltransferase activity
	SIRT6	Nuclear protein, regulates DNA repair, role in aging
	SIRT7	Localised to nucleolus and promotes rRNA transcription, associated with RNA pol I, so far, no deacetylase activity measured, but activity NAD^+-dependent

Table 3: Histone deacetylase families (HDACs) and their known functions.

Table 3 demonstrates, that each HDAC owns its more or less specific sphere of action, making it a good target for inhibition. However, to date it has proven difficult to develop specific inhibitors against each individual HDAC rather than an entire class. Despite these hurdles, investigations are underway and the subsequent paragraph introduces the most common HDAC inhibitors (HDACi).

[1] Marcia C. Haigis and Leonard P. Guarente, Mammalian sirtuins – emerging roles in physiology, aging, and calorie restriction. Genes & Dev. 2006

Histone deacetylase inhibitors (HDACi)

HDAC inhibitors (HDACi) selectively alter gene transcription, in part through chromatin remodelling and through changes in the structure of proteins in transcription factor complexes (Gui et al., 2004). These non-histone protein targets are substrates such as hormone receptors, chaperon proteins and cytoskeleton proteins, which regulate cell proliferation and cell death. Table 4 gives a brief overview of areas and specific proteins influenced by HDACs.

Function	Proteins
DNA binding transcriptional factors	P53, c-Myc, AML1, BCL-6, E2F1, E2F2, E2F3, GATA-1, GATA-2, GATA-3, GATA-4, Ying yang 1 (YY1), NF-κB, MEF2, CREB, HIF-1a, BETA2, POP-1, IRF-2, IRF-7, SRY, EKLF
Steroid receptors	Androgen receptor, estrogen receptor a, glucocorticoid receptor
Transcription co-regulators	Rb, DEK, MSL-3, HMGI(Y)/HMGA1, CtBP2, PGC-1α
Signalling mediators	STAT3, Smad7, β-catenin, IRS-1
DNA repair enzymes	Ku70, WRN, TDG, NEIL2, FEN1
Nuclear import	Rch1, importin-α7
Chaperon protein	HSP90
Structural protein	α-tubulin
Inflammation mediator	HMGB1
Viral proteins	E1A, L-HDAg, S-HDAg, T-antigen, HIV Tat

Table 4: Areas and proteins targeted by histone deacetylases. Table adapted from review Bolden et al., 2006.

Despite the additional proteins targeted by HDACs, a large number of structurally diverse HDACi have been purified from natural sources or synthetically developed, and at least 13 have progressed to clinical development (see review Bolden et al., 2006). HDACi can be categorised by their chemical structure inhibiting the enzymatic activity of HDACs with different efficiency. HDACi treatments are considered valuable anti-cancer drugs, as HDACi selectively induce apoptosis in tumour cells. Clinical trials and preclinical animal experiments have shown potent anti-cancer activities at concentrations that are minimally toxic to the host (see review Bi and Jiang, 2006).

Common HDAC inhibitors [2]

Previous studies solving the structural details of HDAC-HDACi interaction have provided valuable insights into the mechanism of deacetylation of acetylated substrates (Finnin et al., 1999; Somoza et al., 2004; Vannini et al., 2004). The hydroxamic acid moiety of inhibitors directly interacts with the zinc ion at the base of the catalytic pocket (Xu et al., 2007). Most HDACi in clinical phase I and II are tested against several tumour types, such as acute myeloid leukaemia or cervical cancer. Nonetheless, the roles of HDACs and the effects of HDACi on an entire organism are still in early stages of discovery (WS Xu et al., 2007). The following table 5 gives a brief overview of different HDACi classes and their targets.

Class of HDACi	Compounds	HDAC target
Hydroxamate	SAHA, LBH589, PXD101, ITF-2357, PCI-24781	Class I, II
Cyclic peptide	FK228	HDAC1, 2
Benzamide	MS-275	HDAC1, 2, 3
	MGCD0103	Class I
	Sirtinol	Class III
Aliphatic acid	Phenylbutyrate, Valproic acid	Class I, II
	AN-9	Not known
	Baceca	Class I
	Savicol	Not known
Heterocyclic compound	Nicotinamide, Splitomicin	Class III

Table 5: Classes and names of common HDAC inhibitors and their targets. Adapted from review Xu et al., 2007.

Several studies using FRDA patient cell lines have suggested that common inhibitors targeting HDAC class I and II are generally not sufficient to reverse the down-regulation of *FXN*. Therefore, this thesis will focus on the possibility of treating FRDA patient cells with HDAC class III inhibitors such as Sirtinol, Splitomicin and Nicotinamide.

[2] WS Xu et al., 2007. Histone deacetylase inhibitors: molecular mechanisms of action. Oncogene 26, 5541-552.

HDAC class III inhibitors and targets

One of the main targets of HDAC class III inhibitors is the SIR2 family, which deacetylates other proteins as well as histones (see review Blander and Guarente, 2004**)**. The various targets and SIRT family members in mammals have already been described in table 3. This paragraph gives a more detailed view on the action of the SIR2-family. The yeast *SIR* protein complex has been implicated in transcriptional silencing and suppression of recombination. More specifically, it represses transcription at the telomeres, at the mating-type loci and at the ribosomal DNA. Unlike *Sir3* and *Sir4*, the *Sir2* gene is highly conserved in organisms ranging from archaea to humans. As mentioned previously, *Sir2* acts NAD^+ -dependently, a feature conserved from bacteria to higher eukaryotes. For each acetyl-lysine that is deacetylated by Sir2, one NAD^+ molecule is cleaved (Hoff et al., 2006; North and Verdin, 2004).

For silencing of the yeast rDNA locus only *SIR2* is required (Tanny et al., 1999). In mammals the deacetylation via Sir2 is involved in gene silencing, metabolic regulation and aging (Wood et al., 2004). In humans the majority of the SIR2 family members contain a motif of Cys-XX-Cys-$(X)_{15-20}$-Cys-XX-Cys in the conserved domain, binding to a Zn^+- ion (Sereno et al., 2006). However, in most cases the substrate specificity of the Sir2 enzyme remains elusive. In yeast, histone H4 at the rDNA sites is hypoacetylated in a Sir2-dependent manner (Zhao et al., 2004). Furthermore, a genome-wide array showed that a deletion of SIR2 leads to hyperacetylation of subtelomeric regions, the mating-type loci (*HML* and *HMR*), and the *rDNA* loci. The deletion of Sir2 caused an increase in H3 and H4 acetylation within the rDNA region. The largest increase in acetylation occurred on H3 (Kimura et al., 2002, Shia et al., 2006, Suka et al., 2004). In *Drosophila*, dSir2 is capable of deacetylating histone H4. In additional *in vivo* experiments, dSir2 was shown to be a requirement for heterochromatic silencing and a modest effect on position effect variegation was observed (Rosenberg and Parkhurst, 2002).

As described earlier the “histone code” interacts in some instances with DNA methylation i.e. particular histone modifications are physically associated with methylated DNA (Bird, 2001). The following section will give a brief introduction to the establishment of DNA methylation and its binding proteins.

DNA methylation

DNA can be covalently modified by methylation of the cytosine base in the dinucleotide sequence 5'CpG3' (Holliday and Pugh, 1975; Riggs, 1975). CpG is an abbreviation for cytosine and guanine separated by a phosphate. In mammals, DNA methylation patterns are established during embryonic development and later on maintained (Shen et al., 2002), however this does not have to be permanent. Changes in DNA methylation patterns can occur throughout life as part of a physiological response or secondary to environmental changes (Benett and Hasty, 2007). DNA methylation patterns are established via DNA methyltransferases (Dnmts). Four mammalian Dnmts are known, the so-called maintenance Dnmt1 and *de novo* Dnmt2, Dnmt3a and Dnmt3b (Bestor and Ingram, 1983; Li et al., 1992). Evidence exists that DNA methylation is beneficial for chromosomal stability, preventing in certain circumstances chromosome fusion, breakage and aneuploidy (Dodge et al., 2005; Ehrlich, 2003).

DNA from mammalian somatic tissues is methylated in 70 % of all CpG sites (Ehrlich et al., 1982). Mapping studies indicate that highly methylated sequences include satellite DNAs, repetitive elements including transposons, non-repetitive intergenic DNA and exons of genes. A key exception to this CpG methylation of the mammalian genome, are the CpG- islands. CpG- islands were detected as a fraction of vertebrate DNA that was cleaved unusually frequently by methylation-sensitive restriction enzymes (Cooper, 1983; Cooper et al., 1983). These GC-rich sequences are about 1 kb in length and usually nonmethylated (Bird et al., 1985). Most, if not all, CpG- islands mark promoters and 5' domains of genes. Approximately 60 % of human genes have CpG- island promoters (Shen et al., 2007).

The effect of DNA methylation in gene expression has been tested in several ways. One early example was the silencing of adenine phosphoribosyltransferase via CpG methylation, when transfected into cultured mammalian cells (Stein et al., 1982). The discovery of an inhibitor of DNA methylation called 5-azacytidine allowed further studies on the effects of CpG- methylation (Jones and Taylor, 1980). This nucleoside analogue is incorporated into DNA in place of cytidine and forms covalent adducts with DNA methyltransferases, thereby preventing further DNA methylation (Jones and Taylor, 1980).

The interference of DNA methylation with gene expression is most likely the result of established interference with potential CpG binding proteins. One prominent factor that binds exclusively to unmethylated CpG- islands is the CCCTC-binding factor (CTCF). CTCF is associated with transcriptional domain boundaries (Bell et al., 1999) and can insulate a promoter from the influence of remote enhancers (Felsenfeld et al., 2004; Jones et al., 2001). Another mechanism for repressing transcription via DNA methylation is the specific binding of proteins to methylated DNA. So far, the proteins of the methyl-CpG-binding domain (MBD) family (MBD1 to MBD4), the methyl-CpG-binding protein 2 (MeCP2) and the unrelated protein KAISO (Bird and Wolffe, 1999; Nan et al., 1997) have been identified. All of them seem to share the property of acting in a transcriptional repressive manner.

Hypothesis

The observations made so far suggest that in the first intron of *FXN* the formation of a triplex DNA structure is provoked by an expansion of GAA repeats in FRDA patients. This structure may activate an as yet unknown silencing mechanism resulting in variegation of expression. Therefore, a proportion of cells would express *FXN* and another proportion of cells would have a silenced *frataxin* gene. If variegation occured, it may be possible to elicit increase in expression level of the repressed *FXN* by inhibiting factors of PEV binding to GAA-triplexes.

Aim

In order to determine whether variegation of *FXN* expression occurs, EBV-transformed lymphocytes and primary lymphocytes from FRDA patients will be investigated at the single cell level. Furthermore, the chromatin structure of control versus FRDA individuals will be investigated via chromatin immunoprecipitation (ChIP). Also the binding of potential chromatin influencing proteins to the FRDA locus will be tested. Lastly, the effect of HDAC inhibitors on the pathogenic *FXN* locus will be investigated.

Results I

Results I

The following chapter will examine the *FXN* locus of unaffected and FRDA patients. The samples used are Epstein-Barr Virus (EBV) transformed cell lines and primary lymphocytes. All EBV-cell lines were chosen from unrelated patients and tested for correct karyotypes prior to investigations. Here the focus will lie on the transcription of *FXN* and its chromatin structure beginning from the 5' UTR up to the end of intron 1. The following figure 6 details the location of the primers used for the primary transcript RNA-FISH and ChIP experiments.

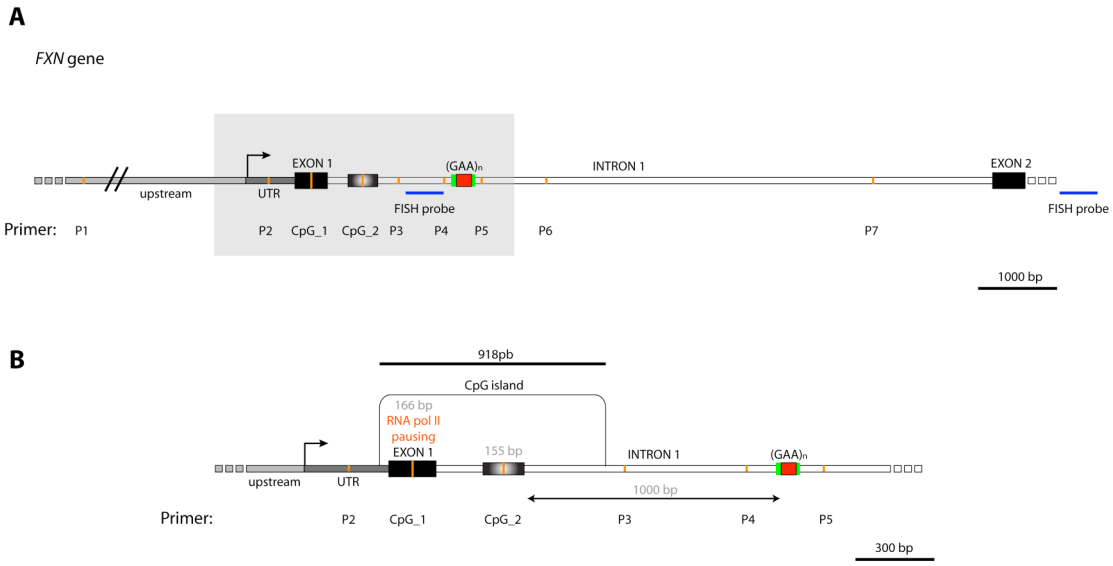

Figure 6: A) Location of primer pairs for ChIP experiment marked in orange and location of FISH probe 5' of the GAA expansion marked in blue. Bars marked in green are poly A sequences adjacent to the GAA repeat. Note that primer P1 lies 6000 bp 5' of the UTR and is not given in proportion. B) Displays a magnification of the area close to the first CpG- island predicted using the program at (http://cpgislands.usc.edu/) and the area adjacent to the GAA repeat.

Human cell lines and patient samples

Because the critical tissues affected in FRDA patients are very difficult to obtain, such as heart, dorsal root ganglia and cerebellum, the experiments were performed on lymphocytes, from patients and controls. FRDA lymphocytes show a reduced level of *FXN*; and therefore, provide a valid model for investigating the underlying molecular mechanism of *FXN* silencing in Friedreich's ataxia (Pianese et al., 2004). Since FRDA patients are relatively rare, most initial patient experiments were performed with two patient EBV-cell lines (GM15850, GM16234). For the negative control, a "normal" cell line GM14926 (GM14) was used throughout. Both patient cell

lines have the same GAA triplet repeat length but were derived from patients with different ages of FRDA disease onset. The GM15850 (GM15) patient had a normal childhood onset (~ 10 years) of FRDA, whereas the patient GM16234 (GM16) had a late onset where FRDA started at the age of ~ 20 years. Notably, the patient GM15 was 13 years old and the patient GM16 was 39 years old when the blood was taken to derive the EBV-cell line, therefore both cell lines display potentially different FRDA progression states. In order to partially control the experiments for age-related changes at the *FXN* locus, the healthy cell line GM14 was chosen from a control whose blood was taken at the age of 38. Primary lymphocytes were obtained from a homozygous individual being the son of the heterozygous father.

Genotyping of EBV-cell lines and primary cells

In order to distinguish between heterozygous and homozygous samples and to estimate the GAA expansion state of patients, a PCR with primers flanking the GAA expansion site was designed (see Materials and Methods p. 135). As this PCR was difficult to optimise and required a specific enzyme-mix it was important to verify that the multiple bands obtained (Fig. 7) were GAA containing products. Thus, half of the PCR product was digested with the enzyme *Mbo II* that specifically digests the GAA site (5'-GAAGA$(N)_8$^-3'). In healthy and heterozygous patients the band appearing at around ~ 380 bp is present, whereas it is missing in FRDA patients that exhibit a homozygous GAA expansion. Therefore, this PCR provides a good tool to distinguish between heterozygous and homozygous samples. Since the PCR does have limits in amplifying very long GAA repeats this technique has limitations in terms of measuring exact GAA expansion lengths and in discriminating between longer and shorter alleles.

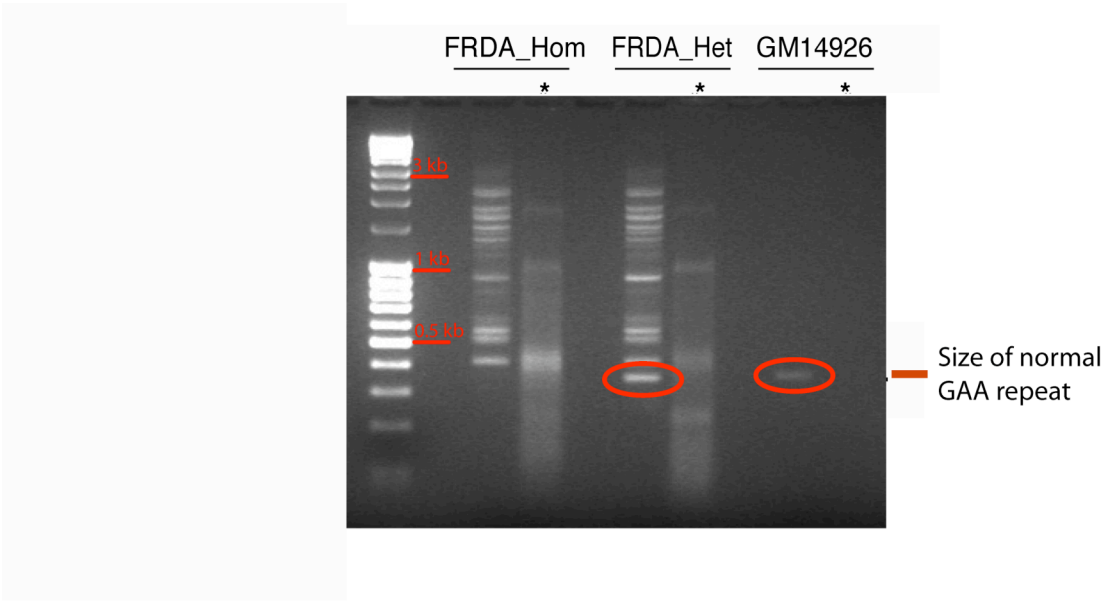

Figure 7: PCR amplified DNA fragments to confirm GAA repeat expansion in intron 1 of *FXN* gene. Results are shown from the control cell line, GM14 (6-34 GAA repeats), a heterozygous (FRDA_Het) and a homozygous (FRDA_Hom) individual. Lines marked with a star (*) exhibit the PCR product digested with *Mbo* II to test specificity of the GAA amplification. *Mbo* II cuts inside (GAA)n, digested fragments of the band containing the normal GAA repeat are too small to be detectable.

The first lane in each group exhibits the obtained PCR products, showing multiple bands of amplified GAA repeats. The second lane shows the PCR product digested with *Mbo II*, therefore PCR products containing GAA repeats have disappeared in this lane. The normal wild-type (*wt*) allele exhibits a short stretch of GAA repeats flanked by a stretch of unique sequences (380 bp), which is not detectable after the *Mbo II* digest.

FXN mRNA levels of cell lines

In order to verify *FXN* mRNA levels from all the EBV-cell lines, quantitative real-time reverse transcriptase Q- (RT) PCR measurements were performed. The RNA of a 1 ml cell culture was extracted using Trizol and the cDNA was obtained using the Invitrogen-kit as described in the Materials and Methods section (p. 130). For the real-time PCR experiment the Sybr-green Kit from Sigma was used. Each reaction was done in triplicate and three serial dilutions were measured per cDNA sample. In order to account for possible differences in reverse transcription efficiency or RNA amounts, the ct-values obtained for *FXN* were normalised to *beta-actin*. The mean value of each triplet was used for further calculations using the delta/delta-method

(p. 141). After normalisation to *beta-actin* mRNA levels, GM15 and GM16 were normalised to GM14 *FXN* mRNA levels, in order to detect the relative differences between the patient and the healthy cell lines.

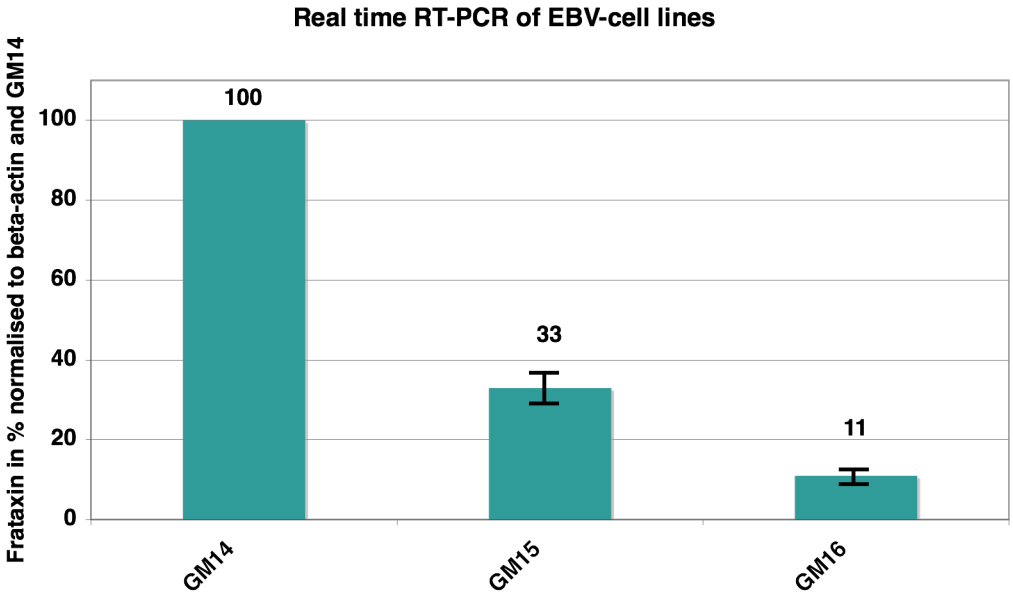

Figure 8: Q-real-time RT-PCR measurement of *FXN* mRNA from EBV-cell lines derived from a normal (GM14) and FRDA patients (GM15 and GM16). *FXN* was first normalised to *beta-actin*, and then using the delta/delta-method normalised to GM14 in order to verify the fold difference of *frataxin* expression. Each result shows the mean of 3 independent experiments. The error bars represent the standard deviation.

As shown in figure 8, while both patient FRDA EBV-cell lines exhibit a similar repeat length, they differ considerably in *FXN* expression. This is likely to be an effect of the different FRDA duration times, as the GM15 cell line, with a shorter progression of ~ 5 years, shows a significantly higher level of *FXN* (~ 33 %) than the GM16 EBV-cell line, from a patient who has been displaying signs of FRDA for 19 years (~ 11 %) (Materials and Methods p. 133). Indeed, it is somewhat unexpected that the *FXN* level of the GM15 cell line is still relatively high, as the supposed pathogenic expression level lies below 30 %. This could be a phenomenon of the EBV-transformation or a consequence of B-cell specific expression. B-cells are not known to be affected by FRDA (Jiralerspong et al., 1997; Puccio et al., 2001).

ChIP on three EBV-cell lines

For the purpose of assessing whether histone modifications and other factors might play a role in regulating *FXN* mRNA levels in FRDA, chromatin immunoprecipitation (ChIP) was used to investigate the EBV-cells described earlier. These were derived from 2 FRDA patients with different durations of FRDA but similar GAA repeat length and a healthy individual. As an internal control for the healthy cell line (GM14), ChIP was performed on primary cells from a healthy individual and on EBV-transformed cells from another healthy individual, in order to verify results from GM14. Chromatin was prepared as described in materials and methods (p. 139) and sonicated twice for a total of 1 h in intervals to reduce the chromatin size to a range between 150 and 400 bp (Fig. 9).

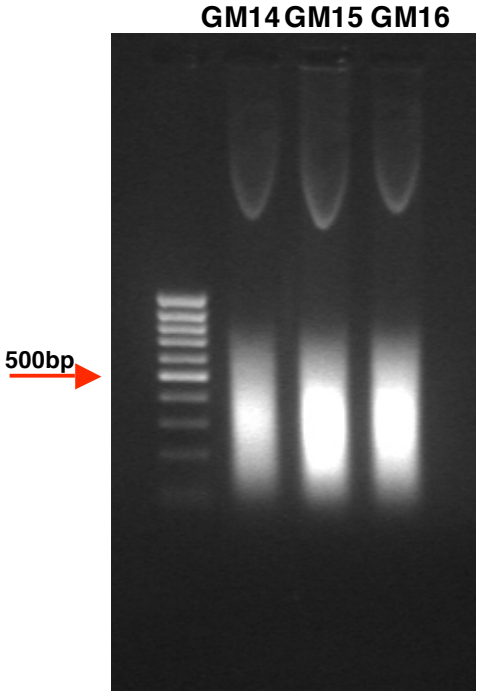

Figure 9: Picture of an agarose gel showing extracted and sheared chromatin from EBV-cell lines. 10 µl of 1 ml chromatin were loaded onto the gel after 1 hour of sonication. The resulting chromatin is between 150 and 400 bp in length.

To preserve its structure and modifications the chromatin was immediately snap-frozen and stored at -80°C. For the immunoprecipitation, 150 µl of chromatin were incubated with the antibody of choice at 4°C for 30 minutes in a sonicater water bath. In order to determine if the GAA expansion has a direct influence on chromatin

modification the *FXN* gene from the promoter region up to exon 2 was investigated in detail (Fig. 6).

In figure 10 the results of ChIP for all three EBV-cell lines are displayed following incubation with antibodies against RNA pol II, H3K4me2, H4K16ac and H3K9me3. RNA pol II was chosen in order to determine possible inhibitory effects of the GAA expansion to transcriptional elongation (Ohshima et al., 1998; Sakamoto et al., 2001b; Vetcher et al., 2002). The marker for open and recently transcribed chromatin H3K4me2 (Bernstein et al., 2002) was used in order to validate possible chromatin changes of active marks caused by abnormal GAA repeat expansions. Since the hypothesis states that by using an HDACi such as Nicotinamide the chromatin structure might be opened up, the target of Nicotinamide, H4K16ac, was also investigated. Lastly, in order to identify possible changes from euchromatin to heterochromatin in the presence of GAA repeat expansions H3K9me3, a marker for heterochromatin was tested.

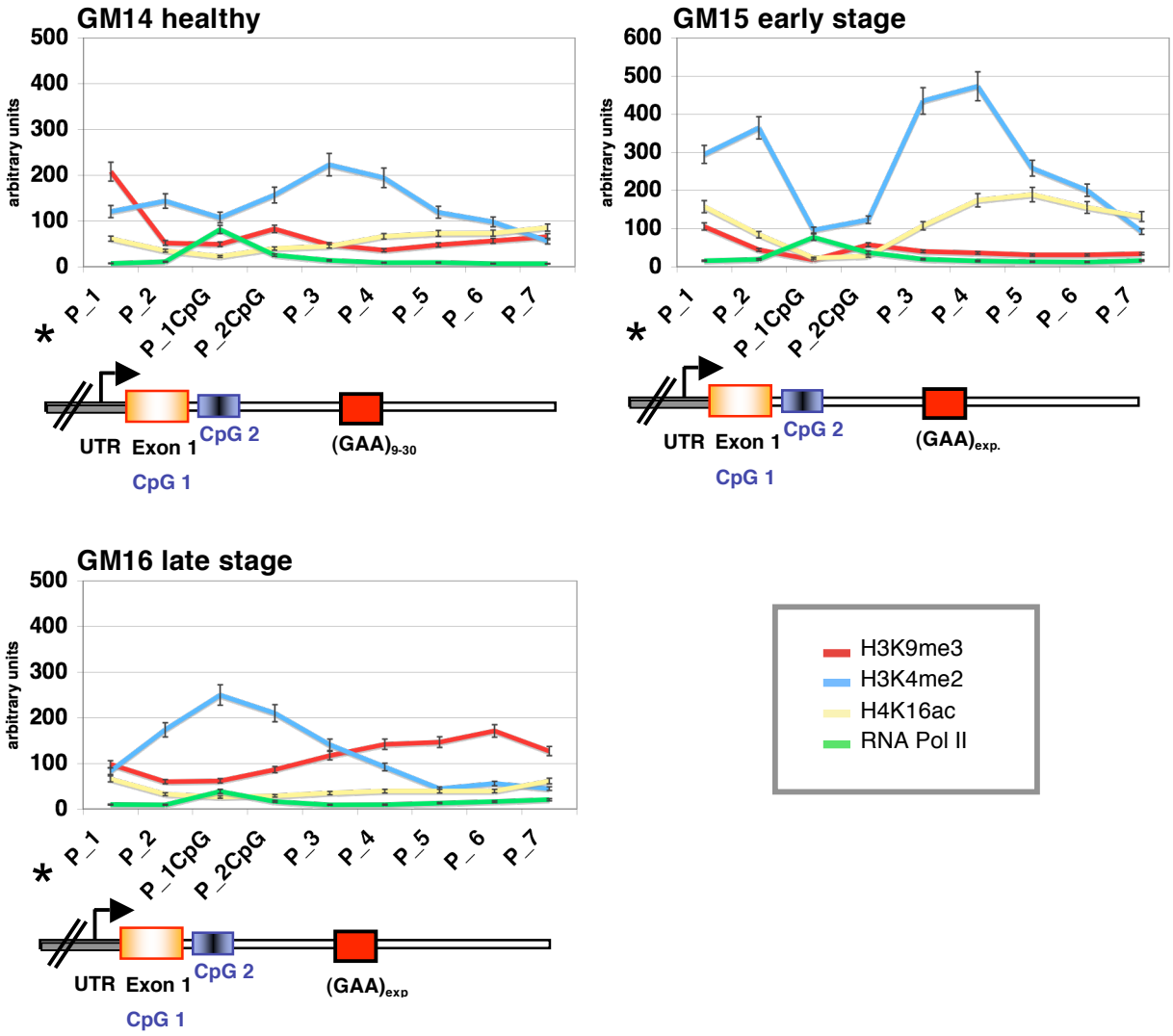

Figure 10: ChIP results from three EBV-cell lines against the antibodies H3K9me3, H3K4me2, H4K16ac and RNA pol II. A mini-map of the first part of the *FXN* locus is shown below. Note P1 is located 6000 bp upstream of *FXN* UTR. Each IP was performed at least twice and Q-real-time PCR measured three times in duplicate. Levels given are relative to H3 recovery. Presented is the mean of these experiments, the variation between experiments is usually +/- 5 % for each primer pair. GM15 and GM16 are normalised to levels obtained for GAPDH of GM14. The cell lines GM14 and GM15 display a RNA pol II pausing site inside exon 1. GM15 displays elevated levels of H4K16ac when compared to GM14 and GM16. GM16 alone displays elevated levels of H3K9me3. The exact primer locations are stated in Fig. 6 (p. 48).

I will first describe the results obtained from the GM14 cell line derived from a normal individual and then will go on to discuss the changes observed in the FRDA patient-derived cell lines GM15 and GM16. Each value is stated as the percentage of recovery when normalised to H3 (100%). As expected, in GM14, high levels were found for the “active” mark H3K4me2 as well as moderate levels for H4K16ac, and

except for a small peak at the beginning of intron 1, moderate levels of H3K9me3. Nevertheless, 6000 bp upstream of the *FXN* gene (*P1), high levels of H3K9me3 were detected. In keeping with the known low level of transcription for this gene, RNA pol II showed rather low levels (~ 18 %) across the *FXN* gene, comparable with RNA pol II levels detected at the inactive *beta-globin* gene (~13 %), and in contrast to the active *GAPDH* gene, where levels of ~ 60 % were found (data not shown). Unexpectedly, high levels of RNA pol II (~ 80%) were detected inside exon 1 (P1_CpG) (Fig. 10). This region is part of a mostly unmethylated CpG- island covering 918 bp (Fig. 6).

A similar phenomenon of, so-called "RNA pol II pausing", close to promoter regions inside exon or intron 1 of several genes has been described in the regulation of transcription (Coppola et al., 1983; Fivaz et al., 2000; Krumm et al., 1995; Li et al., 1999; Muse et al., 2007). Such "RNA pol II pausing" is thought to play a crucial role in the correct regulation of the *c-myc*, *c-fos*, *hsp70* and *p21* genes. Given that the mechanism of regulation of *FXN* transcription is little understood, this new finding may point towards an important level at which this gene is regulated. The region around exon 1 displaying high RNA pol II levels shows, in contrast, reduced levels of the histone marks H3K4me2 and H4K16ac (Fig. 10), whereas H3K9me3 peaks slightly at the end of the CpG-island. Since all modifications were normalised to the unmodified histone H3 ChIP results (Fig. 11), the possibility that the missing/reduced histone modifications are based on the absence of nucleosomes at this site can be excluded.

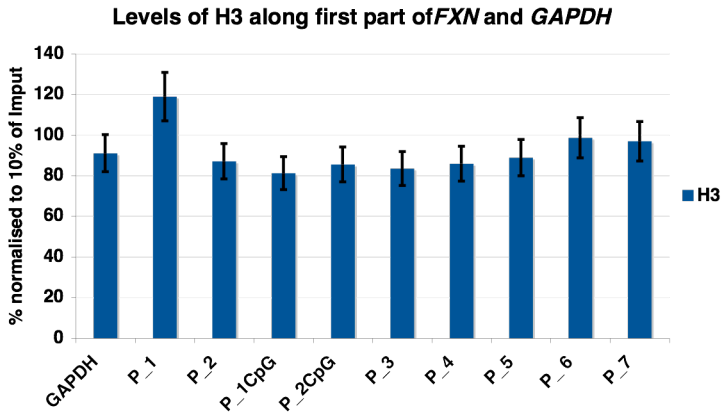

Figure 11: IP with anti-H3 antibody against chromatin of GM14 EBV-cells. Histone H3 levels are normalised to 10% of the Input and shown for each primer pair used. Each IP has been Q-real-time PCR measured three times and in duplicate. Error bars indicate standard deviation.

Although variations of H3 levels occur across the investigated area, no major differences are seen.

Unexpectedly, the early onset GM15 FRDA cell line exhibits significantly elevated levels of the so called “active marks” H3K4me2 and H4K16ac, and shows even less H3K9me3 compared to the normal GM14 cell line (Fig. 10). The dramatic increase of H3K4me2 in the presence of an abnormal GAA repeat expansion might be explicable by the former observation that a DNA GAA-triplex structure slows down the elongation process of the RNA pol II (Mariappan et al., 1999; Sakamoto et al., 1996). This might increase the probability of methylation of histone H3K4, as the HMTase Set1, that methylates H3K4 is bound to the early elongating RNA pol II (Krogan et al., 2003). However, this simple explanation cannot account for the increased H3K4 levels seen 5’ of the GAA repeat expansion. Strikingly, the levels of H3K4me2 and H4K16ac were decreased inside the CpG- island however the pronounced peak of RNA pol II was similar (~ 80 %) to the one in GM14.

Analysis of the late stage FRDA GM16 cells revealed a very low *FXN* mRNA expression and a markedly different chromatin set-up (Fig. 10). Here, H3K4me2 was increased 5’ of the GAA expansion, peaking inside the mostly un-methylated CpG-island (Fig. 32 Results II) and showing a reduced level 3’ of the GAA expansion. Moreover, the inactive mark H3K9me3 showed generally higher levels 5’ and 3’ of the GAA expansion, compared to GM14, possibly indicating heterochromatinisation (Lachner et al., 2001). A similar reduction of active marks in inactive genes was found in genes such as *beta-globin* (Kanduri et al., 2006). In addition, the histone modification for open chromatin, H4K16ac, showed slightly lower levels than the normal cell line. Although, RNA pol II still peaked inside exon 1 it was to a lesser extent than the other two cell lines (~ 40 %).

ChIP against DNA binding proteins

The ChIP method was further employed to investigate potential transcriptional regulating factors of the *FXN* gene. The following results will focus only on proteins tested and found to bind along the area of interest. The negative elongation factor E (NELF-E) was tested as a potential candidate to maintain the observed putative RNA pol II pausing site. In *in vitro* systems, the 5,6-dichloro-1β-ribofuranosylbenzimidazol (DRB) sensitivity-inducing factor (DSIF) and NELF can

arrest elongation of transcripts by RNA pol II soon after transcriptional initiation. NELF consists of 4 subunits all of which are required for NELF to function as a negative elongation factor (Ping and Rana, 2001; Wu et al., 2003; Yamaguchi et al., 1999; Zhang et al., 2007). Another important factor is PTEF-b, a cyclin-dependent kinase, allowing transition into productive elongation (Price, 2000). When the CTD of RNA pol II is phosphorylated by PTEF-b, negative regulation by DSIF-NELF is overcome and elongation resumes (Ping and Rana, 2001; Wu et al., 2003; Yamaguchi et al., 1999; Zhang et al., 2007). This mechanism, established for *in vitro* transcription, is reminiscent of transcriptional regulation involving a block to elongation in eukaryotic cells (Fujita et al., 2007). Additionally an interaction between NELF-E and nascent RNA has been suggested (Johansson et al., 2007), however the actual mechanism still needs to be addressed.

MeCP2 was tested as a possible silencing factor (Drewell et al., 2002; Fuks et al., 2003; Kimura and Shiota, 2003; Nan et al., 1998), as the online CpG-island finder (http://cpgislands.usc.edu/) predicted two CpG- islands at the *FXN* gene, one of them covering the area of the putative pausing site. All three isoforms of HP1 (CBX1, 3, 5) were tested in order to investigate potential heterochromatinisation mediated by the GAA repeat expansion (Fig. 12).

A striking co-localisation of HP1-γ (CBX3) with the previously observed peak of RNA pol II inside exon 1 was detected in all three lines (Fig. 12). HP1γ was not detected elsewhere in the locus. HP1-β, HP1-α did not exhibit any significant binding to the *FXN* locus although there is a paucity of data in the literature showing effective ChIP with the available antibodies for these isoforms (Fuks t al., 2003).

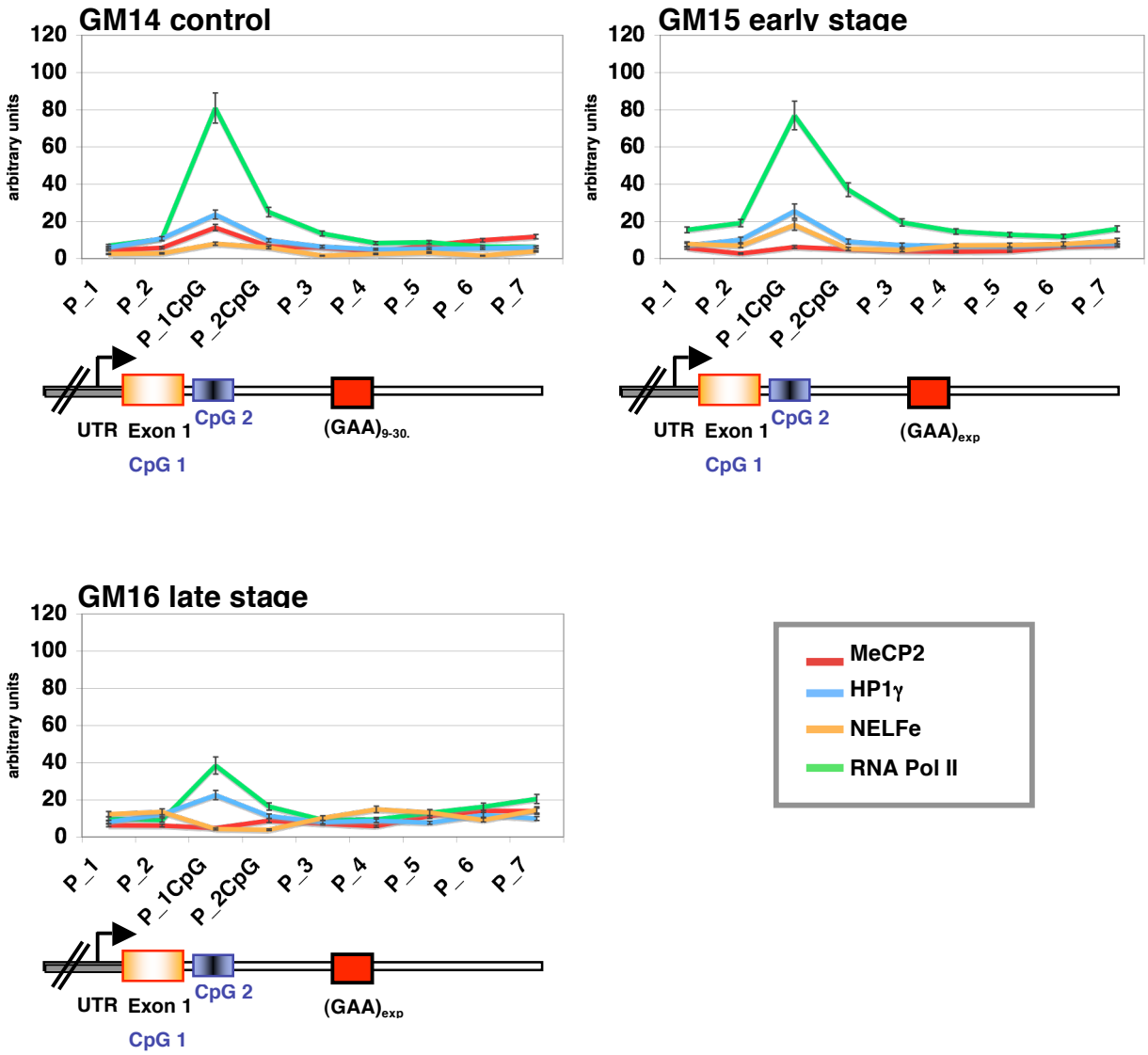

Figure 12: **ChIP results on all EBV-cell lines with antibodies against MeCP2, HP1γ, NELF-E and RNA pol II. Again a mini-map of the first part of the *FXN* locus is given below. Note P1 is located 6000 bp upstream of *FXN* UTR. Each IP was performed at least twice and Q-real-time PCR measured three times in duplicate. Levels given are relative to the recovery of H3. Each value of GM15 and GM16 is subsequently normalised to GM14 via GAPDH. Presented is the mean of these experiments, the variation between experiments is usually +/- 5 % for each primer pair. Only GM14 displays a peak of MeCP2 over the putative pausing site. HP1γ is found in all three cell lines at similar levels over the putative RNA pol II pausing site. NELF-E shows increased binding over the pausing site in GM15 compared to the control GM14 cell line. GM16 lacks a peak of NELF-E over the pausing site and shows binding further along *FXN*.**

It is thought that gene repression in mammals can be provoked via DNA methylation which is then stably maintained by the action of methyl-CpG binding proteins such as MeCP2 (Kimura and Shiota, 2003; Fuks et al., 2003). In order to assess whether MeCP2 might have an effect in reducing the *FXN* mRNA level in the case of an

abnormal GAA expansion, ChIP was performed (Fig. 12). As displayed, the normal cell line, GM14, showed MeCP2 binding inside exon 1. This was also where the highest level of CpG- methylation was found, as will be presented in the following chapter (Fig. 32). In contrast, and somewhat counter-intuitively, the patient cell lines expressing subnormal levels of *FXN* showed the least DNA methylation. In accordance with this, these low-expressing cell lines also showed the lowest MeCP2 binding. Following the idea of a possible silencing mechanism through DNA methylation, provoked by the GAA expansion, one would have expected more CpG- methylation and MeCP2 in patient cell lines. As this was not the case, one might argue that MeCP2 binding and DNA methylation at this site may not play an important role in the down-regulation of the *FXN* gene in FRDA patient cell lines.

The negative elongation factor NELF-E is known to promote RNA pol II arrest together with DSIF (Aida et al., 2006; Wu et al., 2003; Yamaguchi et al., 1999). Even though the exact regulatory mechanisms of DSIF and NELF in promoting the RNA pol II arrest are not well understood, it has been proposed that DSIF and NELF act in concert to induce polymerase arrest via their direct interaction with the nascent transcript (Aida et al., 2006; Wu et al., 2003; Yamaguchi et al., 1999). Intriguingly, the ChIP experiments of the patient GM15 cell line possess a slightly higher degree of NELF-E binding (~ 17 %) at the RNA pol II-pausing area (Fig. 12) than the normal cell line (~14 %). Since neither for the sample lacking the NELF-E antibody (data not shown) nor for the GM16 cell line binding for NELF-E was detectable the here obtained results and minor changes between cell lines are most likely highly significant. Consistent with hypotheses for other genes, NELF-E might also play an important role in the RNA pol II pausing and regulation of the *FXN* locus. In the patient GM16 cell line, NELF-E is detected at a higher level close to the expanded GAA repeats but hardly inside the CpG- island, NELF-Es proposed site of action (Fig. 12). This cell line also exhibits an abnormal chromatin pattern, a lower RNA pol II peak and a very low *FXN* expression. Interestingly, an inverse correlation between NELF-E binding and the RNA pol II peak and histone mark H3K4me2 was found (Fig. 10 and 12).

FXN real-time measurement of UTR versus Exon 4

The unexpected presence of an RNA pol II pausing site at the *FXN* locus made it

necessary to assess the possibility of prolonged pausing provoked by the GAA expansion. In such a case, one might expect different levels of the 5' UTR transcript for each of the cell lines, as the release of the RNA pol II from the pausing site may also influence subsequent processing of the primary transcript RNA containing the UTR (Krogan et al., 2003). Moreover, in patient cell lines, an increase in the relative proportion of the 5' UTR compared to the exon 4 transcripts would be expected because of the known inhibitory effect of the GAA expansion (Bidichandani et al., 1998; Grabczyk and Usdin, 2000; Krasilnikova et al., 2007). To test this hypothesis, real time measurements of RNA levels of the 5' UTR versus exon 4 in EBV-cell lines were performed. For detection of primary transcripts of exon 4 rather than total mRNA, the primer for exon 4 lies inside intron 3 (see Material and Methods).

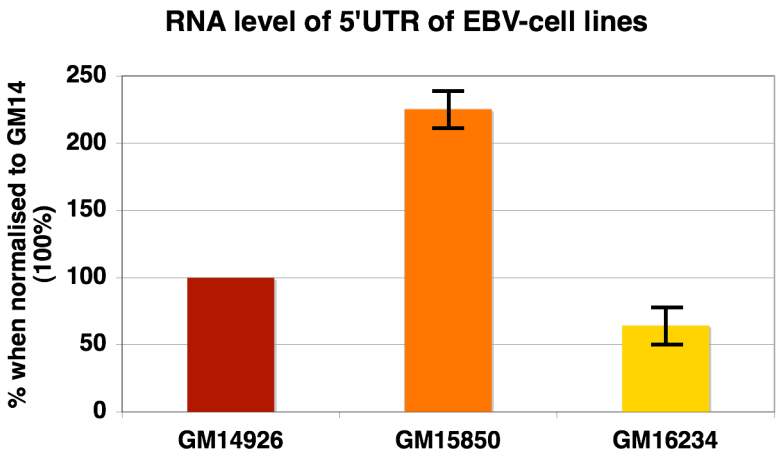

Figure 13: Analysis of *FXN* primary 5' UTR transcripts by RT-PCR. All *FXN* ct-values were normalised to *beta-actin*. The data of GM15 and GM16 are expressed relative to the normal GM14 cell line. Each RT- measurement was performed twice and in triplicate. The error bars display the standard deviation of two independent experiments.

On normalising the *FXN* 5' UTR levels to the control GM14 cell line, the "early stage" GM15 cell line displayed ~ 2.2 times more 5' UTR-RNA than the healthy cell line (Fig. 13). It is tempting to speculate that the increase in 5' UTR is related to the increased binding of the negative elongation factor NELF-E, which may delay the release of the RNA pol II pausing and thereby increase the stability of the transcript. However, further studies are needed to explore this. Nevertheless, the GM16 cell line, which hardly expresses any *FXN,* displayed only 60 % of the measured GM14 UTR transcript, in accordance with the disturbed RNA pol II pausing found earlier

(Fig. 10). One possible explanation is less efficient transcriptional initiation of GM16 compared to the other lines, thereby limiting the amount of RNA pol II available to accumulate at the pausing site.

The measured RNA levels of exon4 were normalised to the UTR of the respective cell line. Figure 14 shows that, in the case of the healthy cell line the level of primary RNA transcript of exon 4 is similar to that of the 5' UTR. As both primer pairs exhibit different efficiencies, this is not an absolute measurement of the real distribution but acts as a comparator for the transcriptional situation in the FRDA patient.

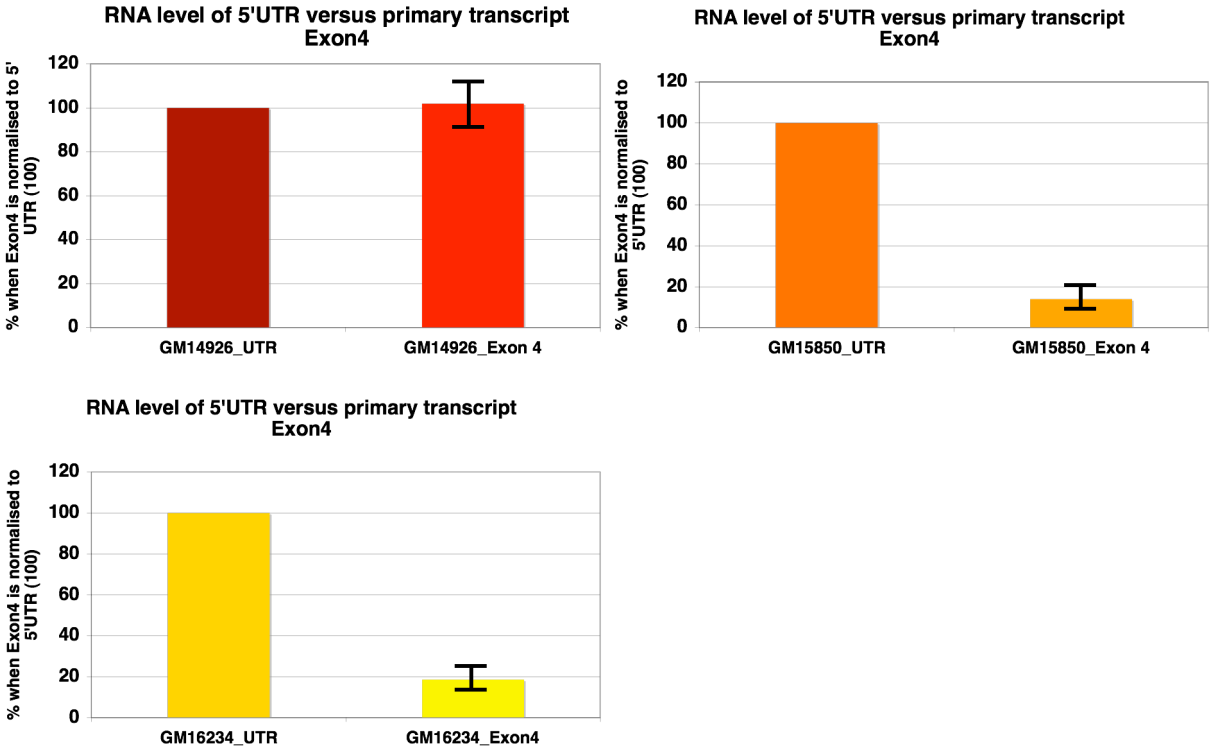

Figure 14: Primary transcript levels of Exon 4 relative to 5' UTR of three EBV-cell lines. Each *FXN* value has been normalised to *beta-actin*. Each RT-PCR measurement was done twice and in triplicate. The error bars indicate the standard deviation of two experiments.

The exon 4 primary transcript RNA level of the FRDA EBV-cell lines was significantly reduced relative to the 5' UTR level in the presence of a GAA expansion (Fig. 13). Note that each value of exon 4 is normalised to its respective 5' UTR value. Considering the 2.2 fold increase of the GM15 5' UTR, the exon 4 levels is actually ~ 32 % of GM14 and for the GM16 cell line, the level is ~ 11.4 % of GM14. This roughly matches the previously measured total mRNA levels (Fig. 8). Without

consideration of the starting 5' UTR levels, the amount of exon 4 RNA seems to be similar in both patient lines, providing evidence for similar elongation efficiency in both patient cell lines, which indeed exhibit the same repeat length.

Summarising the above, this experiment provides evidence for a two-step mechanism whereby the GAA expansion contributes to the dramatic reduction of *FXN* transcription. First, one may propose that the RNA pol II pausing release is delayed as the level of 5' UTR product for the GM15 FRDA cell line was double that of the normal cell line. A similar finding was found by Gu and colleagues where RNA pol II pausing protected the primary transcript from nuclease activity 5' of the pausing site (Gu et al., 1996). Secondly, the elongation through the GAA expansion is hampered. In the context of a disrupted RNA pol II pausing site, as seen for GM16, it seems that initiation of *FXN* is disordered and less 5' UTR is initially present. The experiment suggests that the combination of a GAA dependent hampered release of the RNA pol II from its pausing site and the additionally hampered elongation through the GAA repeat might lead to a substantial and pathogenic decrease in *FXN* levels.

FXN mRNA levels in primary lymphocytes

In order to verify the experiments conducted on EBV-cell lines, the initial experiments were repeated on primary lymphocytes obtained from FRDA patients. To control for differing genetic backgrounds, *FXN* mRNA levels from homozygous as well as from heterozygous relative patients were measured by real-time RT-PCR and compared to levels of unaffected individuals. To ensure the validity of the normalisation process, each sample type was initially normalised to *beta-actin, 18S rRNA* and *GAPDH*.

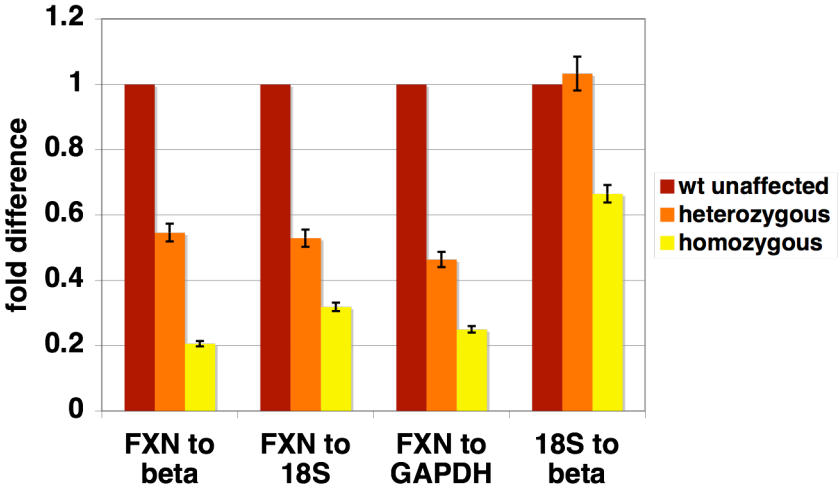

	FXN to beta	FXN to 18S	FXN to GAPDH	18S to beta
Control_wt	1	1	1	1
Father_het	0.546	0.529	0.463	1.032
Son_hom	**0.206**	0.319	**0.250**	0.665

Figure 15: Real-time RT-PCR measurement of primary cells obtained from a normal, a heterozygous and a homozygous individual. All three samples were normalised to *beta-actin*, *18S* and *GAPDH*. RNA was extracted using Trizol. Using the SuperScript-Kit (Invitrogen) according to supplier's instructions, cDNA was produced. The heterozygous patient exhibits ~ 51 % and the homozygous patient ~ 26 % *FXN* mRNA levels of the normal individual.

In figure 15 each column displays the three different genotype samples normalised to *beta-actin*, *18S* and *GAPDH*, followed by a further normalisation of the heterozygous sample to the unaffected one. The mean of the heterozygous sample is ~ 51 % of *FXN* mRNA level whereas the homozygous sample has ~ 26 % of the normal individual. To explain the discrepancy occurring in the homozygous sample when normalised to *18S*, ct-values of *18S* were further normalised to *beta-actin*. This revealed a significantly lower level of *18S* in the homozygous patient sample. It was therefore decided to normalise all further RNA level measurements to *beta-actin*.

Primary transcript RNA-FISH on primary cells

In order to determine whether a mechanism similar to position effect variegation (PEV) occurs in FRDA patients, rather than a down-regulation of *FXN* in all cells, primary transcript RNA-fluorescence *in situ* hybridisation (FISH) was performed on primary lymphocytes. Intronic probes (Fig. 6) were used to estimate the proportion of

cells currently transcribing *FXN* rather than measuring the steady state level of mRNA. This is because the detected intronic sequences should reflect an actual elongation event as these are rapidly spliced from the primary transcript and degraded (Gribnau et al., 1998). Two different probes were used against *FXN*, to detect transcriptional changes occurring 5' and 3' of the GAA expansion. The exact location of the FISH probes is displayed in figure 6.

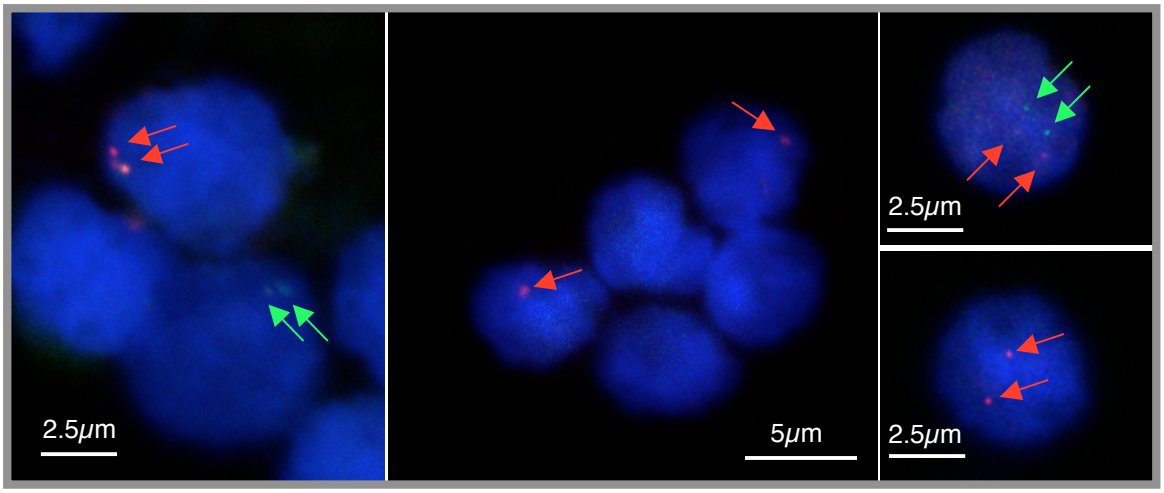

Figure 16: Primary transcript RNA-FISH on primary lymphocytes from FRDA patients. Displayed are images of primary lymphocytes hybridised with a probe recognising *FXN* primary transcript RNA 5' of the GAA probe (red) and the control gene CD19 (green). Usually, *FXN* and CD19 signals do not appear in the same plane. The signal intensity does not differ between controls and FRDA patients, provided a signal for *FXN* is seen. Arrows indicate signal.

Lymphocytes from a control group, a heterozygous and a homozygous individual for expanded GAA repeats were probed 5' of the repeats and *FXN* signals were counted (Fig. 16). Three slides per probe for each affected individual were prepared and 60 cells were counted on each slide. The control group consisted of three healthy individuals and for each, 2 slides were examined. The results (Fig. 17) display the average of two slides counted as percentage. The error bars shown for the control group indicate the standard deviation between healthy individuals. In order to minimise the potential effect of genetic background differences, the chosen heterozygous individual is the father of an affected homozygous son. To avoid false positive results through DNA hybridisation a negative control was conducted. Therefore, control slides were treated with RNase prior to hybridisation and no signals for *FXN* were detectable. As internal control for the RNA hybridisation, a probe for the B-cell marker CD19 was designed. The control probe consists of parts

of CD19 intron 4 - 5 and intron 7 – 8 (see Material and Methods) that is expressed bi-allelically and therefore is a suitable internal control (Fig. 16).

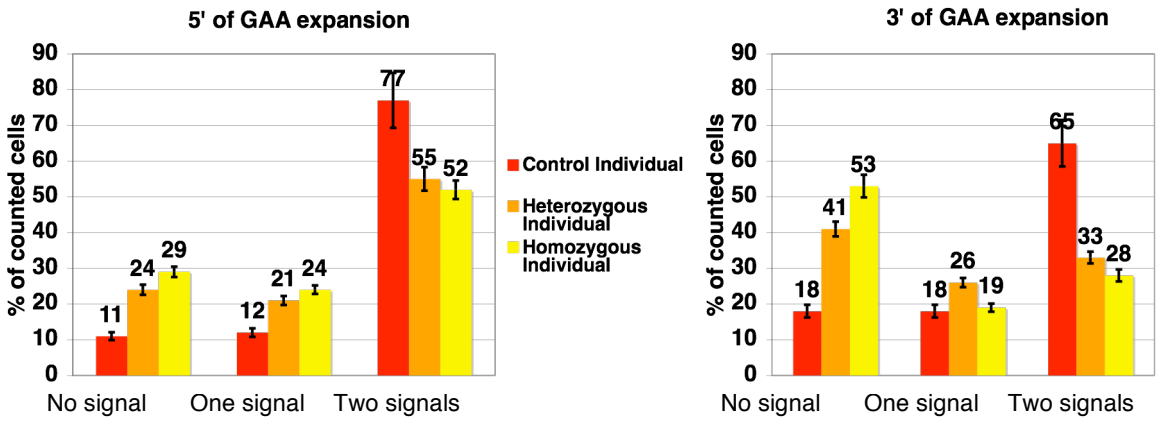

Figure 17: Primary transcript RNA-FISH on primary cells obtained from a normal (red), a heterozygous (orange) and a homozygous (yellow) FRDA patient. The left diagram shows the results obtained using the probe 5' of the GAA repeat. The right diagram shows the results obtained with the probe recognising intron 3 and 4. Each bar represents the result of three independent experiments where three slides (60 cells / slide) per individual were counted. The error bar represents the standard deviation of the results of three independent experiments.

The control cells hybridised with the probe 5' of the GAA repeat expansion showed that *FXN* is mainly bi-allelically expressed, as 77 % of cells showed two *FXN* signals. Cells from the heterozygous individual with a repeat length of ($GAA^{\sim 1000}$/$GAA^{\sim 25}$) showed two signals for *FXN* in only 55 % of counted cells. Cells from the homozygous individual with a repeat length of ($GAA^{\sim 1000}$/$GAA^{\sim 500}$), expressed *FXN* in 52 % of counted cells 5' of the GAA repeat also bi-allelically (Fig. 17). However, the proportion of non-expressing cells of the heterozygous (24 %) and the homozygous (29 %) individual was approximately twice and three times, respectively, that of the control group (11 %).

In comparison to the 5' probe, hybridising the cells with the probe 3' of the GAA repeats, the proportion of non-expressing cells from the control increased only slightly to 18 %. In contrast, the heterozygous and homozygous individual revealed a substantial increase in the proportion of non-expressing cells to 41 % and 53 % respectively (Fig. 17). In line with this, the proportion of bi-allelically expressing cells 3' of the GAA repeats decreased considerably. Whereas 65 % of control lymphocytes

showed bi-allelic expression, this was detectable only in 33 % of heterozygous and 28 % of homozygous cells. The proportion of mono-allelically expressing cells increased just for the control and the heterozygous lymphocytes. The proportion from the homozygous individual decreased to 19 %, indicating a further decrease of *FXN* transcription by the allele exhibiting the shorter GAA expansion, when compared to the wild type allele.

Compared to controls, both the heterozygous and the homozygous individual showed a reduction in *FXN* expressing cells. Furthermore, this experiment shows that a proportion of cells are still able to express *FXN* bi-allelically even in the presence of a long GAA expansion.

ChIP on primary cells of unaffected individual

In order to investigate certain histone modifications at the *FXN* locus in fresh lymphocytes, blood samples were taken from a healthy individual, the lymphocytes were isolated and the chromatin extracted (see Material and Methods section). The amount of chromatin was limited, therefore initially only three antibodies (H3K9me3, H3K4me3 and RNA pol II) were used for ChIP.

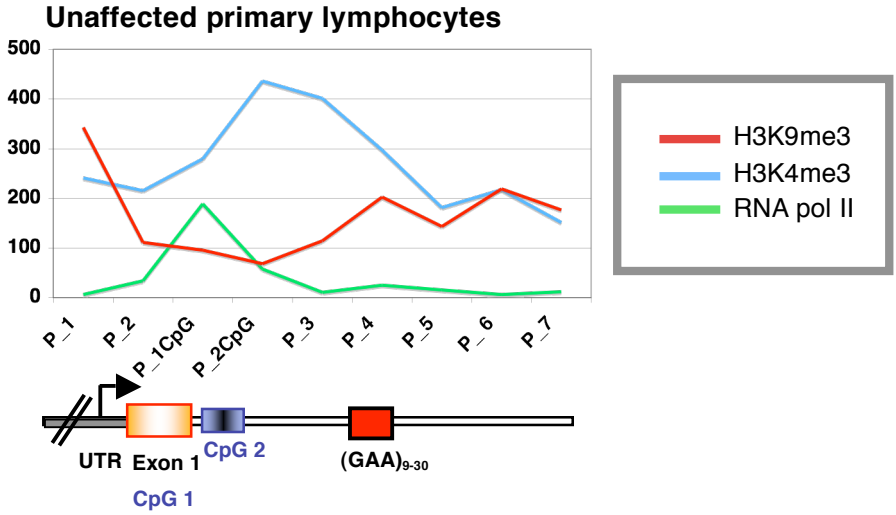

Figure 18: ChIP on primary lymphocytes from an unaffected individual. Displayed are H3K9me3, H3K4me3 and RNA pol II. Presented is the mean of two independent IPs, each Q-real-time measured in duplicate. The variation between experiments is usually +/- 5 % for each primer pair. Again a peak of RNA pol II over the putative pausing site (P_1CpG) is seen. The active H3K4me3 histone mark gives a similar pattern seen for H3K4me2 in GM14. The H3K9me3 modification, an indicator for silenced genes, is comparatively low compared to the signal seen 6000 bp upstream (P1) of *FXN*.

Similar to the ChIP results obtained from EBV-cell lines presented earlier (Fig. 10 + 12), the RNA pol II exhibits a peak inside exon 1, resembling a typical feature of known RNA pol II pausing sites (Fivaz et al., 2000; Krumm et al., 1995). These experiments show that the RNA pol II is present at a relatively low level (~ 18 %) across the *FXN* gene, compared to GAPDH (~ 45 %) (Data not shown). The active mark H3K4me3 shows a peak after the pausing site, decreasing 3' of the normal GAA repeat expansion. A similar pattern was observed for H3K4me2 in the control GM14 and patient GM15 EBV-cell line presented before (Fig. 10). H3K9me3, the hallmark of heterochromatin, shows a moderate level across the pausing site. However, a slight increase 5' of the GAA repeat is followed by a slight decrease followed by another slight increase. Unexpectedly, the overall H3K9me3 level in these primary "normal' lymphocytes is comparable to the level measured in the barely expressing GM16 EBV-cell line, whereas GM14 and GM15 exhibit lower H3K9me3 levels (Fig. 10). However, in contrast to the barely expressing cell line GM16, which lacks H3K4me2 3' of the pausing site, the normal primary lymphocytes possess a high level of H3K4me3. The observed H3K9me3 level discrepancies between control primary and EBV-cell lines might also be due to cell type differences,

as the primary cell chromatin extract consists of a mixed cell population of T- and B-cells.

ChIP on primary cells from heterozygous and homozygous FRDA individual

As mentioned before, the material obtained for ChIP experiments from fresh patient blood was limited; therefore initially only antibodies against RNA pol II and H3K4me3 were tested. Results demonstrate a high level of the 'open' chromatin mark H3K4me3 in the presence of the GAA repeat, consistent with the high level of H3K4me2 seen in the patient EBV-cell line GM15. Furthermore, the RNA pol II pattern for both the GAA-repeat homozygous and the heterozygous individual revealed a much lower peak at the RNA pol II pausing site than the control (Fig. 19).

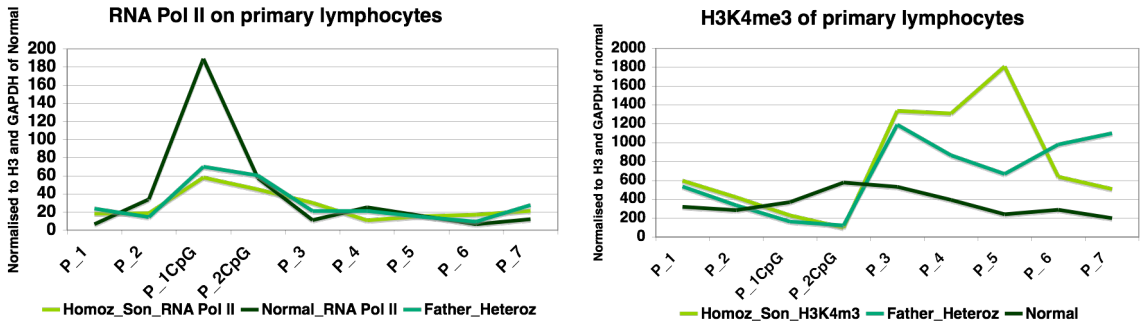

Figure 19: ChIP on primary cells with anti-RNA pol II and anti-H3K4me3 antibodies. Displayed are results of a healthy, a heterozygous (father) and a homozygous individual (his son). Presented is the mean of one IP measured three times in duplicate. The variation between experiments is usually +/- 5 % for each primer pair. Both the father and the son display a decreased peak of RNA pol II over the pausing site, when compared to the unrelated control. The active H3K4me3 mark is increased in the father and the son, although in the son to a higher extent when compared to the control.

Unexpectedly, the RNA pol II pattern of the heterozygous and homozygous individual is similar to the one obtained for the barely expressing patient GM16 EBV-cell line (Fig. 10). In contrast, the pattern for the active H3K4me3 mark is increased in both, the father and the son, when compared to the unrelated control, resembling a similar feature seen in the GM15 FRDA EBV-cell line (Fig. 10). As mentioned earlier, the investigated homozygous individual was severely affected by FRDA and suffered from the disease for over 10 years. Therefore it is possible, that the patient

represents an intermediate between the two extreme EBV-cell lines GM15 and GM16. The GAA repeat expansion is similar and the lines mainly differ in the FRDA duration time, apparently leading to a substantial difference in *FXN* expression and RNA pol II pausing pattern.

It is also surprising that the heterozygous individual shows similar ChIP results for RNA pol II and H3K4me3 to the homozygote. If the expanded GAA repeat were simply inhibiting the RNA pol II elongation of *FXN,* an unaffected unexpanded allele would be expected to display normal RNA pol II pausing. Therefore, a peak at least half the size observed for a normal individual should be present. These results are consistent with those of the primary transcript RNA FISH (Fig. 17), which were also unexpected, demonstrating a similar quantitative reduction of primary transcript 5' of the GAA repeat in heterozygous and homozygous individuals.

Interestingly, a patient (indicated as woman HOM) possessing shorter GAA repeats (~300/100) displayed a similar disrupted RNA pol II pausing signal, but lower H3K4me3 levels than the patient with the long repeats.

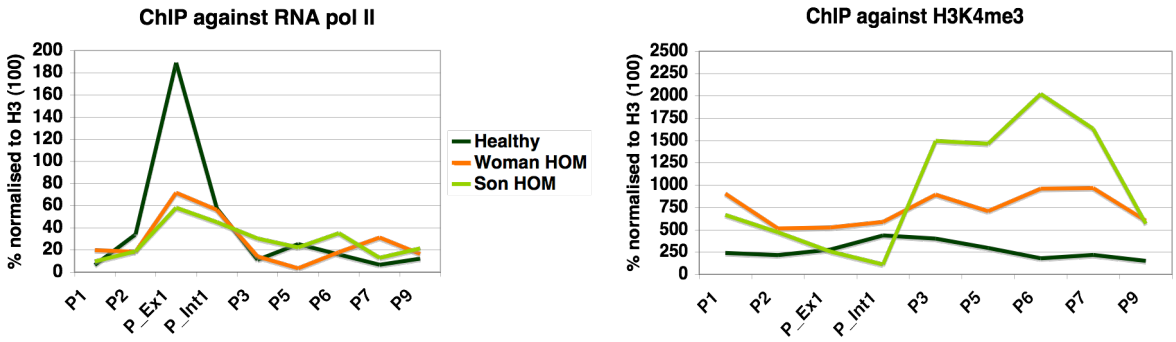

Figure 20: ChIP against RNA pol II and H3K4me3 on primary lymphocytes from two homozygous FRDA individuals. Both patients have a different length of GAA expansions, the "Woman" (~ 300/~ 100) and the "Son" (~ 1000 / ~ 500). Here, the pattern of RNA pol II is also changed when compared to the control. The level of the H3K4me3 pattern seems to depend on the length of the GAA repeat. Each IP was subject to Q- real-time measurement for 3 times and in duplicate. Presented is the mean of these experiments, the variation between experiments is usually +/- 5 % for each primer pair.

These observations on primary lymphocytes indicate that the lack of proper establishment of the RNA pol II pausing site might precede the change of histone modifications to a silenced chromatin state. The disrupted RNA pol II pausing site

might even be a requirement for the eventual change of histone modifications at the *FXN* locus, rather than the recruitment of heterochromatic factors by the GAA repeat itself. It is difficult to interpret ChIP results from the heterozygous individual, as the healthy allele cannot be discriminated from the expanded allele. However, as H3K4me3 modification levels are intermediate between the healthy heterozygous and the FRDA homozygous individual, the RNA pol II result is likely to be true. This confirms the RNA-FISH results obtained earlier where inhibition of transcription at the healthy allele was seen. The remarkable increase of H3K4me3 seems to be a feature provoked by the GAA repeat and dependent on its length, as the homozygous son has a much larger GAA expansion than the homozygous woman, with a correspondingly higher H3K4me3 pattern (Fig. 19 + 20).

Data from genome-wide high resolution histone-methylation profiling[3]

Advanced laboratory techniques and bioinformatics allow genome-wide high-resolution screenings suitable for the investigation of various interests, although at high costs. Due to this fast and efficient development it was possible to extract data on histone methylation marks present at the *FXN* locus of a normal individual from the following data base http://dir.nhlbi.nih.gov/papers/lmi/epigenomes/hgtcall.html.

The performed ChIP experiments presented in figure 10 are in accordance with the results displayed in this article. Therefore, the displayed antibodies in the following figures provide as additional valuable information. In figure 21, a magnification of the area of the *FXN* UTR up to the first half of intron 1 is shown, including the chromatin histone modifications H3K4me3, me2, me1 and RNA pol II. The location of the normal GAA repeat is indicated at the top of the figure. Each H3K4me mark seems to have its own unique pattern in this area. H3K4me2 is hardly present around the UTR, displays a peak shortly after the start of intron 1 and decreases soon after. On the contrary, H3K4me1 shows elevated levels at the beginning of the UTR followed by a gap around exon 1, increasing as soon H3K4me2 decreases. H3K4me3 seems to fill in the gap between H3K4me2 and H3K4me1, with a peak at the beginning of intron 1, sloping down to where H3K4me1 starts. The peak of RNA pol II, resembling

[3] Cell Resource, Barski et al., Cell 129, 823-837, May18, 2007, Link: http://dir.nhlbi.nih.gov/papers/lmi/epigenomes/hgtcall.html

the RNA pol II pausing site, coincides with the lower levels of H3K4me3, me2 and me1 around exon 1 beginning of intron 1.

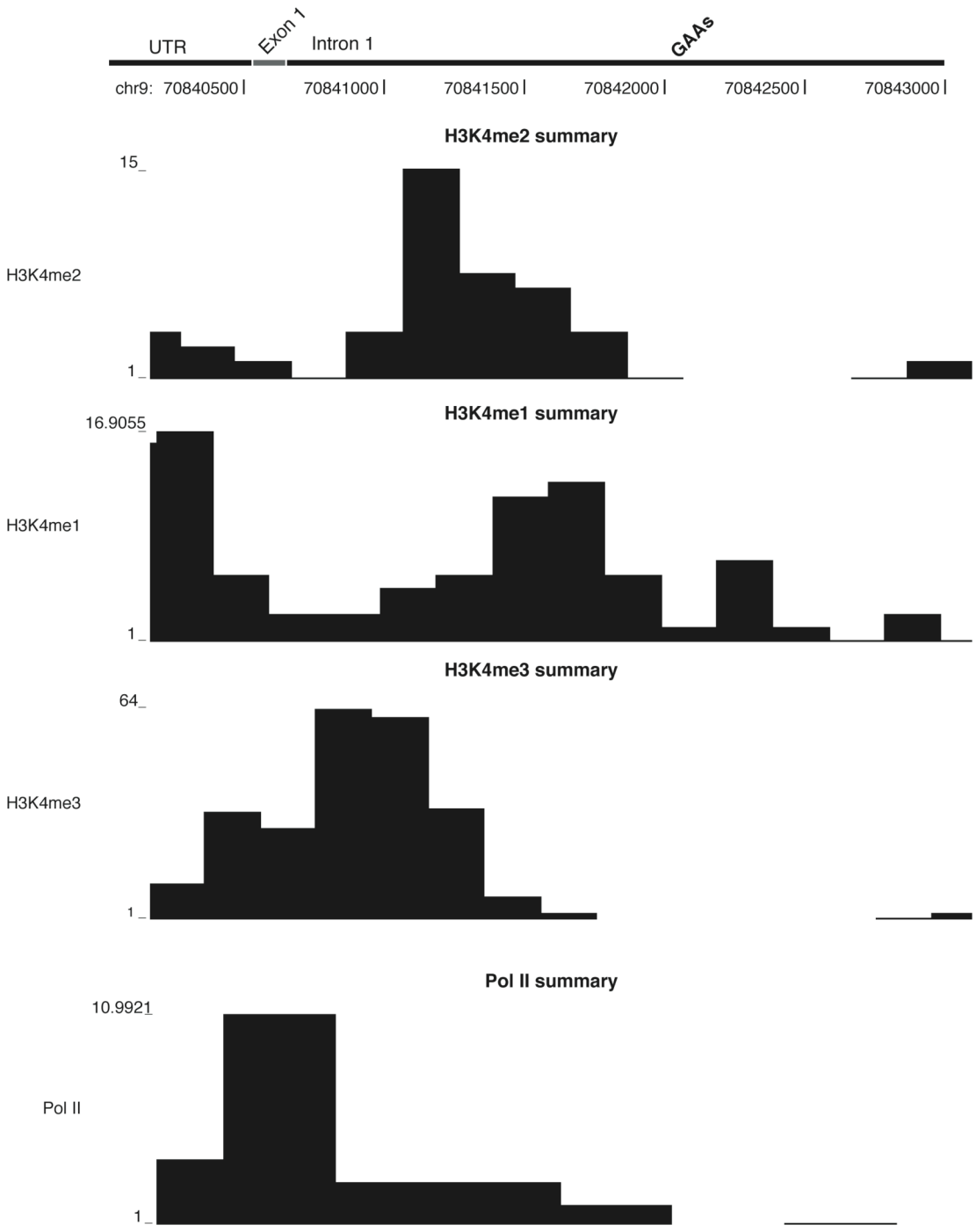

Figure 21: Chromatin modifications by genome wide ChIP analysis at the human *FXN* loci. Histone modifications displayed for H3K4me2, me1, me3 and the RNA pol II are from resting T-cells. The black bars indicate the amount of chromatin immunoprecipitated by the respective antibody. No bar at all indicates data is missing for that stretch of the genome. Data were analysed by direct sequencing analysis of ChIP DNA samples using Solexa 1G genome analyser. For each antibody the highest value at the area of interest is represented by the number at the far left, resembling relative IP efficiency (results extracted from databank provided by Barski et al., 2007).

Figure 22 displays results obtained for the antibodies against RNA pol II, CTCF and H2A.Z along the entire *FXN* gene. Here, H2A.Z, known to locate around functional regulatory elements, is also found around the putative RNA pol II pausing site. Also CTCF was found at high levels around this regulatory site. This is well in accordance with previous reports that CTCF occurs around CpG-islands, also present at this element in the *FXN* gene. A recent publication performing genome-wide screening indicates that this set-up is indeed specific for RNA pol II pausing (Bao et al., 2007). Further evidence for this specificity is that the second CpG-island in intron 2 does not show any of the features found at the RNA pol II pausing site, as neither CTCF nor MeCP2 (own results) binding occurred.

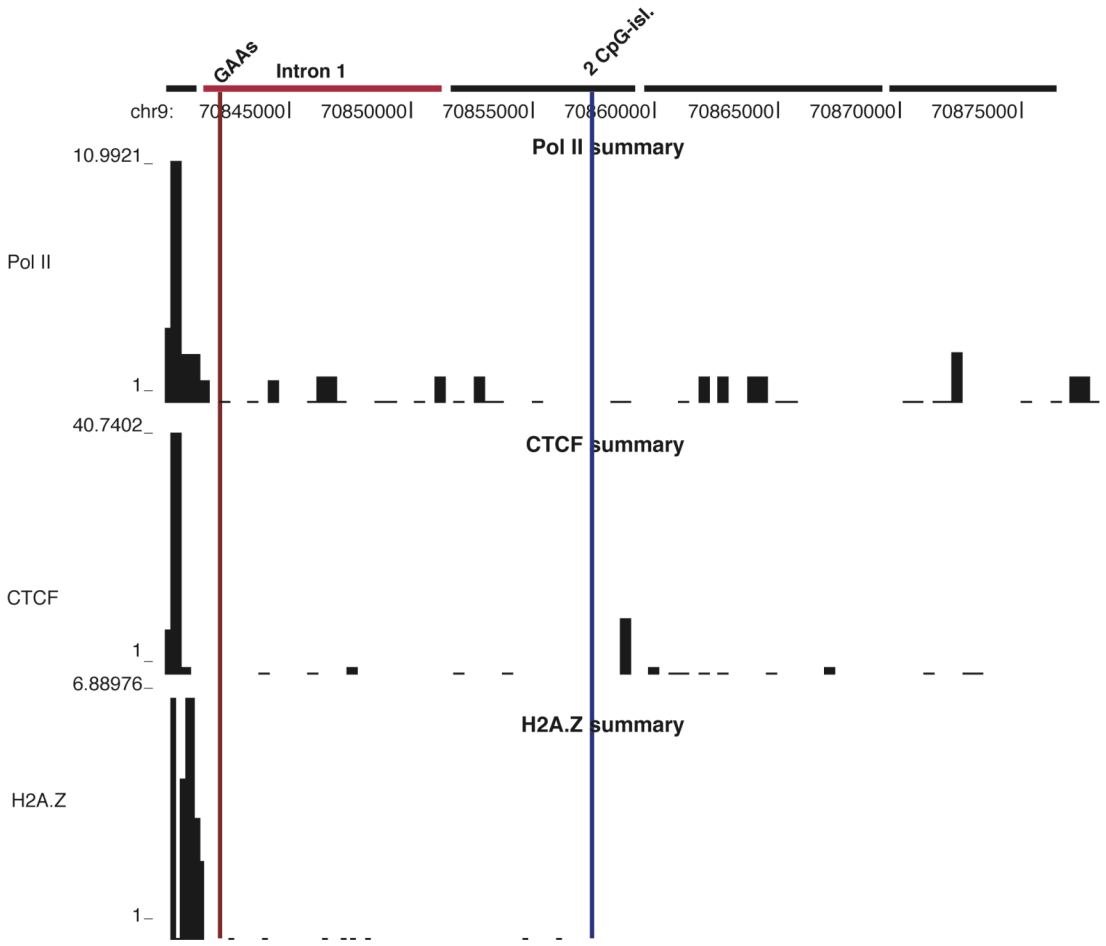

<u>Figure 22:</u> Entire *FXN* locus, ChIP results are from RNA pol II, CTCF and H2A.Z. Black bars indicate IP results from the beginning of the *FXN* 5' UTR, no bars indicate missing data sets. Location of GAA repeat is indicated as a red line, location of second CpG- island is indicated with a blue line. Data were analysed by a direct sequencing analysis of ChIP DNA samples using Solexa 1G genome analyser. For each antibody the highest value at the area of interest is given as a number far left, resembling relative IP efficiency (results extracted from databank provided by Barski et al., 2007).

Figure 23 displays again the active histone marks H3K4me2, me1 and me3, over the entire *FXN* gene. Clearly, the most pronounced mark is H3K4me3 at the very beginning of the gene, whereas H3K4me2 displays a gap at this point. H3K4me2 shows moderate levels where H3K4me3 is present, and seems to increase where H3K4me3 is present at low levels. H3K4me1 is the only mark to display a high peak at the very beginning of the gene. Only moderate levels of H3K4me1 are present where H3K4me2 occurs, however there is an additional peak in the middle of intron 1. This peak is quite distant from the GAA repeat as well as from the second CpG- island and its role might be worth investigating, especially as this feature is not present anywhere else at this locus. The rest of the *FXN* gene does not seem to show any additional interesting features of these active histone marks.

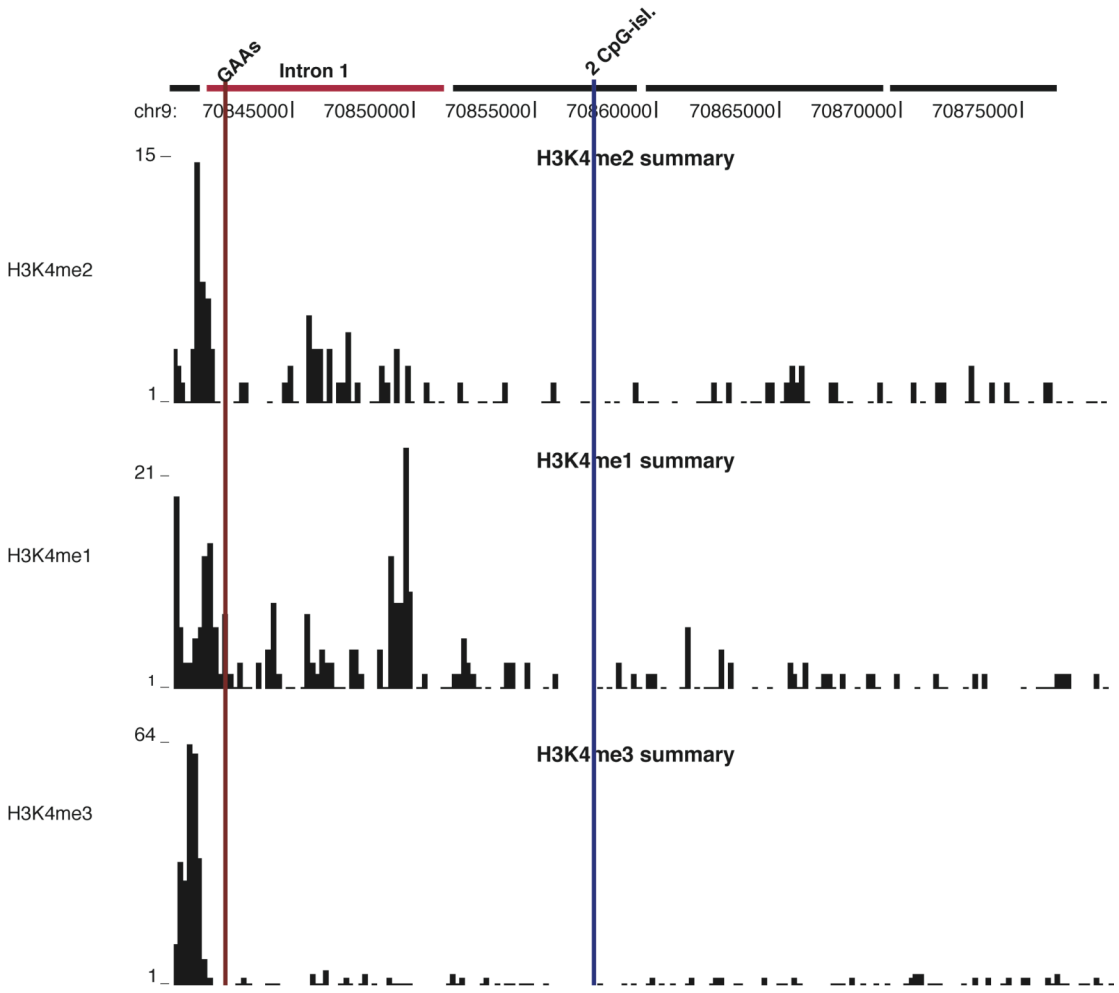

Figure 23: Entire *FXN* locus with ChIP results of H3K4me2, me1 and me3. Location of GAA repeat is depicted with a red line; location of second CpG- island is indicated with a blue line. Black bars indicate result of IP with respective antibody. Data were analysed by direct sequencing analysis of ChIP DNA samples using Solexa 1G genome analyser. For each

antibody the highest value at the area of interest is given as a number at the far left, resembling relative IP efficiency (results extracted from databank provided by Barski et al., 2007).

Figure 24 displays modifications correlating with the expression status of genes, such as H3K27me1, H3K36me3, H4K20me1 H2BK5me1 and H3K9me1. These are well represented at the *FXN* locus, indicating a constant level of activity despite low expression levels. Interestingly, H3K36me3, a mark for recently transcribed chromatin, is present more towards the 3' end of the gene and exhibits a significantly lower signal around the pausing site. This might indicate constant RNA pol II presence at this particular part of the gene, whereas delayed transcription occurs after the pausing site. This observation corresponds with the finding that *FXN* is expressed at very low levels in lymphocytes exhibiting a RNA pol II pausing site.

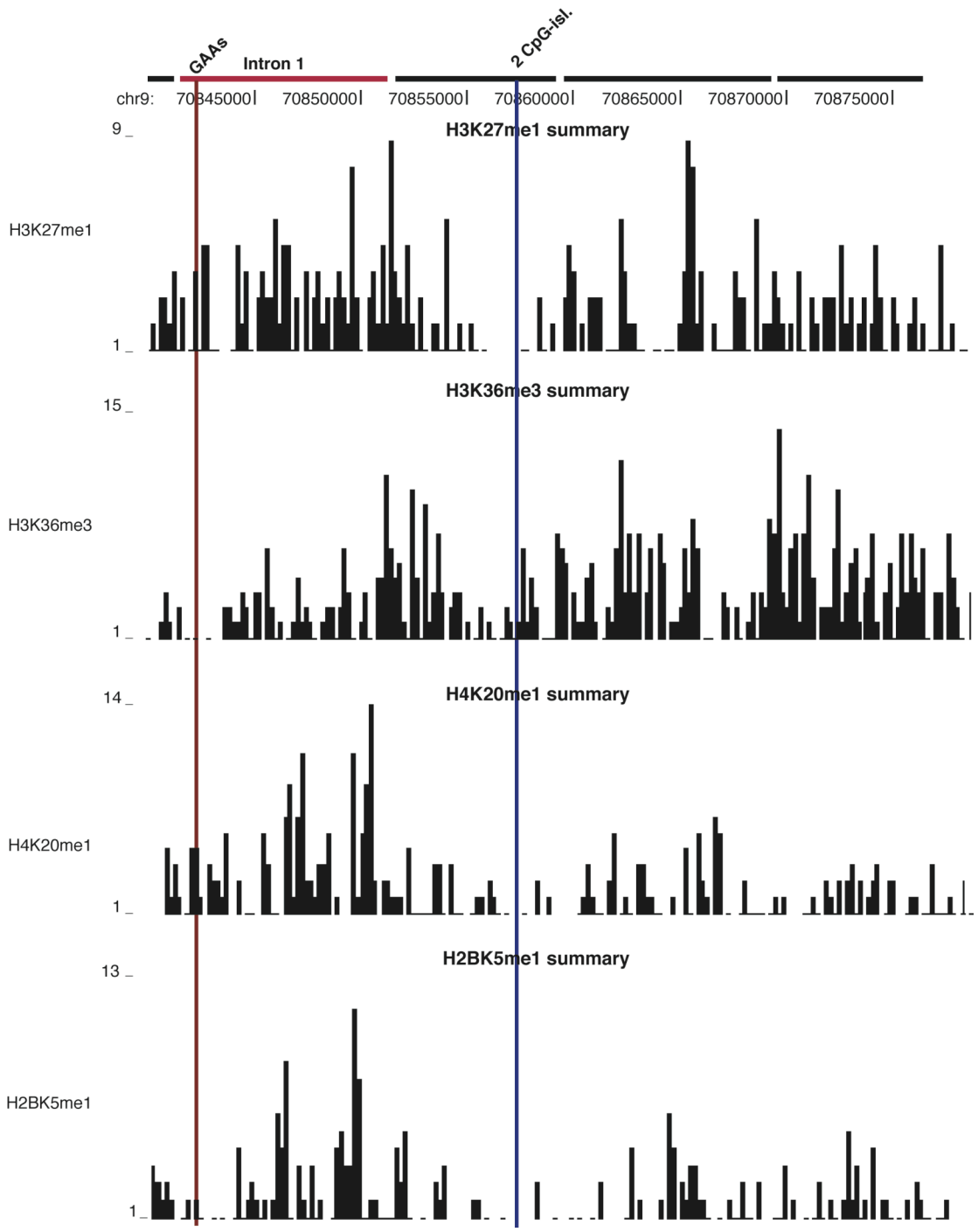

Figure 24: Entire *FXN* locus with ChIPs of H3K27me1, H3K36me3, H3K20me1 and H2BK5me1. Location of GAA repeat is depicted with a red line; location of second CpG- island is indicated with a blue line. Black bars indicate amount of IP, no line at all indicates missing data set. Data were analysed by direct sequencing analysis of ChIP DNA samples using Solexa 1G genome analyser. For each antibody the highest value at the area of interest is given as a number on the far left, resembling relative IP efficiency (results extracted from databank provided by Barski et al., 2007).

Concerning the regulation of *FXN,* the recently identified H2BK5me1 mark may provide evidence for the role of the RNA pol II pausing site. H2BK5me1 is a histone

mark correlated with expression (Barski et al., 2007) and exhibits elevated levels shortly 3' of the pausing site. These seem to decrease following the end of intron 1, suggesting a regulatory role for intron 1 as a feedback mechanism for *FXN* regulation. So far, little is known about this particular modification, but it is interesting that the elevated level occurs 3' of the pausing site and decreases again at the beginning of exon 2.

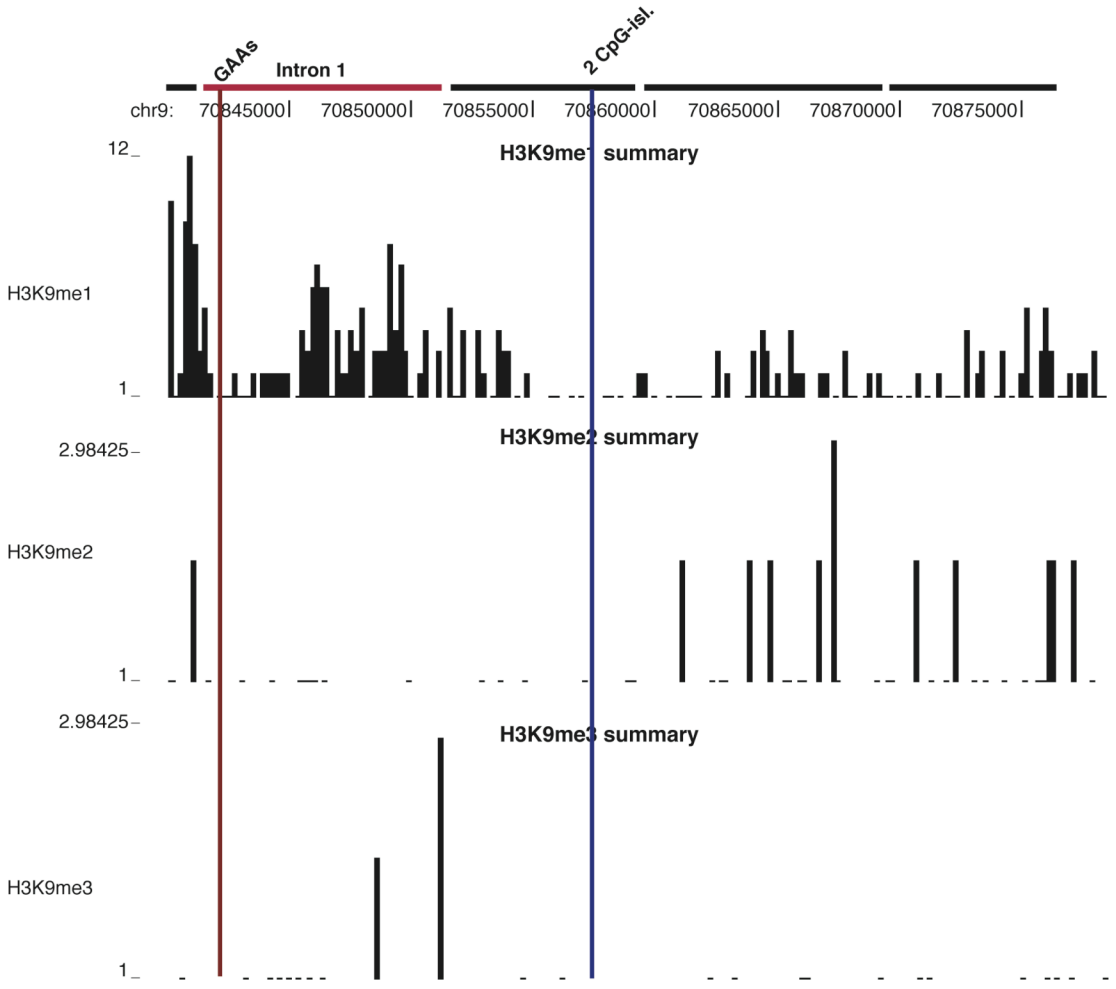

Figure 25: Histone modifications H3K9me1, me2 and me3 along the entire *FXN* locus. Location of GAA repeat is depicted with a red line; location of second CpG-island is indicated with a blue line. Black bars indicate amount of IP, absence of a line indicates a missing data set (Barski et al., 2007).

As presented in figure 25, the histone marks H3K9me2 and me3, known to mediate silencing, are absent or only present at negligible levels at the normal *FXN* locus, whereas the active mark H3K9me1 is well presented. The inactive marks H3K79me1, me2 and me3 are also absent (not displayed).

Results II

Results II

The following chapter will examine the effect of chromatin modifiers such as HDAC inhibitors on the chromatin structure *FXN* locus and its expression. Experiments were conducted primarily on the three EBV-cell lines GM14, GM15 and GM16 previously described using the primers described in Results I (Fig. 6).

Drug treatment of EBV-cell lines

It is now well established that the chromatin state of DNA can influence gene expression. As stated in the Introduction, chromatin is a dynamic protein-DNA-structure that can be modified by, amongst others, histone-acetyl-transferases (HATs) and histone-deacetylases (HDACs). Therefore, exposure of patient cells to HDAC inhibitors (HDACi) may change the chromatin structure into a more "open" arrangement, which might facilitate *FXN* mRNA expression. Thus, HDAC inhibitors are good candidates for positively influencing *FXN* gene expression in FRDA patients. Herman et al. were able to show that a new HDAC inhibitor increased *FXN* mRNA levels in primary resting lymphocytes as well as in EBV-cell lines derived from FRDA patients (Brunett et al., 2006; Herman et al., 2006). Notably, a number of commonly used HDAC class I and II inhibitors were not effective in reversing *FXN* silencing, indicating the specificity of this new inhibitor.

Treatment of EBV-cell lines with potential drugs

Since commonly used HDAC class I and II inhibitors are not effective in enhancing *FXN* transcription, the HDAC class III inhibitors Sirtinol and Splitomicin were tested here. These are known to inhibit members of the SIR2 (silent information regulator)-like family (Bitterman et al., 2002; Grozinger et al., 2001). These enzymes, also known as sirtuins, have multiple targets, act NAD^+-dependently and are implicated in telomeric and rDNA silencing in humans (Grozinger et al., 2001). Three out of seven known sirtuin members are located in the nucleus (SIRT1, SIRT6 and SIRT7) whereas SIRT2 shuttles between the cytoplasm and the nucleus (see review Haigis and Guarente, 2006). Most HDAC inhibitors (HDACi) as well as the mammalian sirtuins have a number of different targets, one of them being histones. Here, the focus will lie on the activity of sirtuins on histones, since opening up the chromatin structure via acetylation of *FXN* might facilitate its expression. However, an influence

on *FXN* expression provoked by one of the other HDACi targets presented in table 4, can never be fully excluded. So far, the most characterised histone target of sirtuins is the deacetylation of the H4K16ac modification. In *Drosophila* it was shown that this modification correlates best with processes thought to “open” chromatin structure (Taiplae and Akhtar, 2005). Thus, it seemed reasonable to treat EBV-cell lines with sirtuin inhibitors, despite their diverse functions, to determine whether simply “opening up” the *FXN* locus would be sufficient to relieve the hampered *FXN* transcription in FRDA patients.

Each previously described EBV-cell line was treated for 72 hours with Splitomicin (100 μM), Sirtinol (100 μM) and HDAC_4b (1 mM and 2 mM).

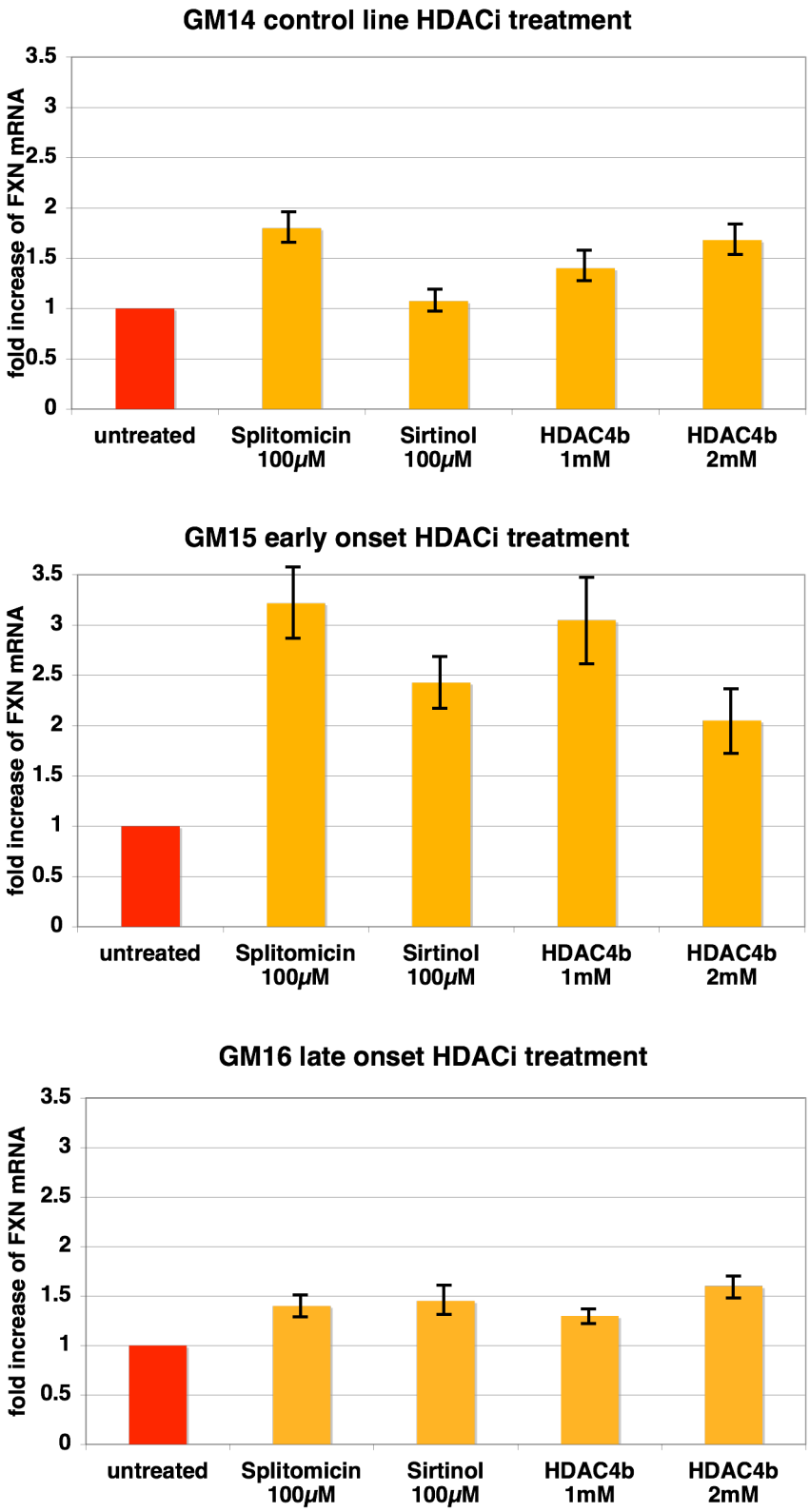

Figure 26: HDACi treatment of EBV-cell lines. All three EBV-transformed cell lines were treated with HDAC class III inhibitors and HDAC_4b. Displayed is the fold increase in *FXN* mRNA expression levels following HDACi treatment, measured by Q- (RT) PCR. Each result displayed is the mean of three independent experiments. Each sample was normalised to *beta-actin*. The values are expressed as a ratio to the corresponding untreated sample. The error bars indicate the standard deviation, after normalisation to the untreated sample.

The early stage FRDA GM15 cell line exhibits the best response to all drug treatments, whereas the later stage GM16 cell line responded in a similar manner to the control GM14 cell line (~ 1.5 fold). The published HDAC class I or II, HDAC_4b inhibitor (1 mM and 2 mM) treatment produced an expected increase of ~ 2 to 3 fold on the GM15 cell line. However, the EBV-cell line GM16 and the control GM14 cell line hardly responded to this treatment at all (~ 1.3 to 1.8 fold). The fact that the GM15 cell line behaved in accordance with previous reports validates the reliability of this technique. On treatment with the HDAC class III inhibitor Splitomicin (100 μM), the early stage FRDA cell line, GM15, showed a similar ~ 2 to 3 fold increase of *FXN* mRNA as had been observed following HDAC_4b treatment. The effect on *FXN* expression in the late stage FRDA GM16 cell line was less (~ 1.4 fold) than for the control GM14 cell line (~ 1.7 fold). Sirtinol (100 μM), the second HDAC class III inhibitor tested, increased *FXN* mRNA expression with reasonable efficiency (~ 2.3 fold) in the early stage GM15 cell line, whereas no major increase was obtained for the later stage GM16 (~ 1.3 fold) or the control cell line GM14 (~ 1.1 fold).

These results suggest that at early stages of FRDA (GM15), an HDAC inhibitor may lead to a GAA repeat expansion-dependent-increase of the *FXN* mRNA. However, if the disease has progressed further and the *FXN* mRNA level is already very low (~ 10 %), the treatment is unlikely to be effective in reviving its expression. After culturing these EBV-cell lines through ~ 20 passages, all three cell lines lost the ability to respond to the HDACi treatment, then only displaying an increase of ~ 1.3 fold (see also Fig. 27). A trivial explanation for this would have been that the HDAC inhibitor was sensitive to storage or specific cell culture conditions, however, fresh stocks of inhibitors did not restore the previously seen effects, which were similar to those presented for Nicotinamide (Fig. 27). Consistent with this, Gottesfeld and colleagues observed a similar finding, that later passages of these cells lost their sensitivity to the HDAC_4b inhibitor, (personal communication, Gottesfeld). In further experiments it was decided to switch to another HDAC inhibitor, Nicotinamide, which is thought to be more stable under cell culture conditions than Splitomicin or Sirtinol (Posakony et al., 2004).

Nicotinamide treatment of EBV-cell lines and *FXN* mRNA levels

As Sirtuins act NAD^+-dependently, Nicotinamide can also inhibit the deacetylation of H4K16ac, a product of the SIRT- mediated deacetylation reaction. Here, Nicotinamide directly competes with NAD^+ for binding to the pocket of the Sir2- family catalytic domain (Landry et al., 2000a; Landry et al., 2000b).

FXN mRNA levels were determined by quantitative real-time reverse transcriptase PCR Q- (RT) PCR and normalised to the control cell line. This measurement revealed a *FXN* mRNA level of ~ 33 % for the early-stage EBV-cell line (GM15), whereas the cell line from a patient at a later stage (GM16) exhibited ~ 10 % of the normal *FXN* level (Fig. 27). No difference was observed for the control *beta-actin* mRNA between the three cell lines.

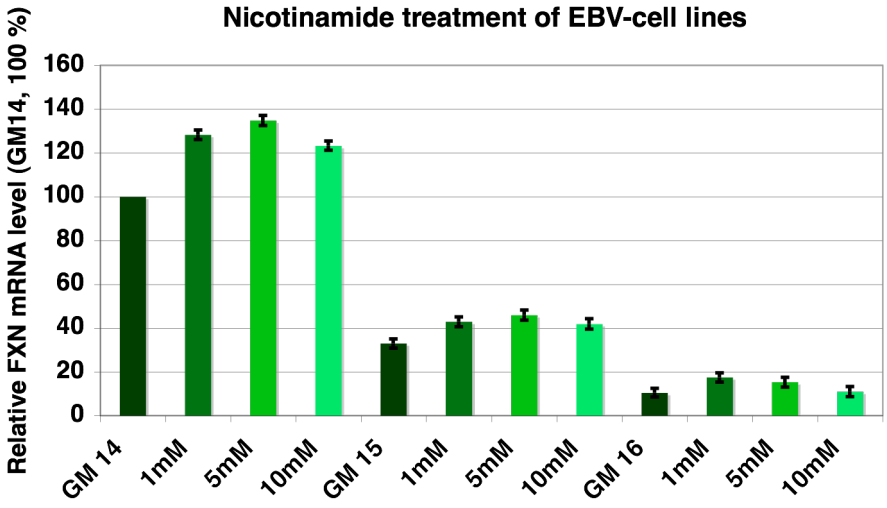

Figure 27: Nicotinamide treatment of control and FRDA EBV-cell lines followed by quantitative real-time PCR measurement of *FXN* mRNA expression. Nicotinamide treatment for 72 h increased *FXN* mRNA in all cell lines. All values are normalised to *beta-actin* mRNA levels, which were unaffected by Nicotinamide. The fold changes in *FXN* mRNA compared to untreated control cells are approximately 1.2 - 1.4 in each cell line. Treatment of cell lines was repeated three times. Extracted RNA from each treatment was measured three times in serial dilutions and duplicate. The error bars indicate the standard deviation between results of three independent experiments.

On treatment of the EBV-cell lines with the HDAC class III inhibitor, Nicotinamide; the actual *FXN* mRNA level increased only by ~ 1.2 - 1.4 fold in each cell line, similar to the levels seen after ~ 20 passages with various other HDAC inhibitors such as

Sirtinol, Splitomicin and HDAC_4b (not shown). An increase in *FXN* mRNA levels occurred with Nicotinamide treatment at doses of up to 5 mM whereas at 10 mM this declined and higher doses were toxic.

Histone mark changes after Nicotinamide treatment - RNA pol II pausing is stable

In order to investigate whether an HDAC class III inhibitor modifies the chromatin structure of the *FXN* locus, ChIP on treated cells was performed using the antibodies presented in Results I (Fig. 28). All three cell lines were treated for 72 hours with 10 mM Nicotinamide. The histone profiles from untreated cells that were presented in Results I are displayed again for comparison.

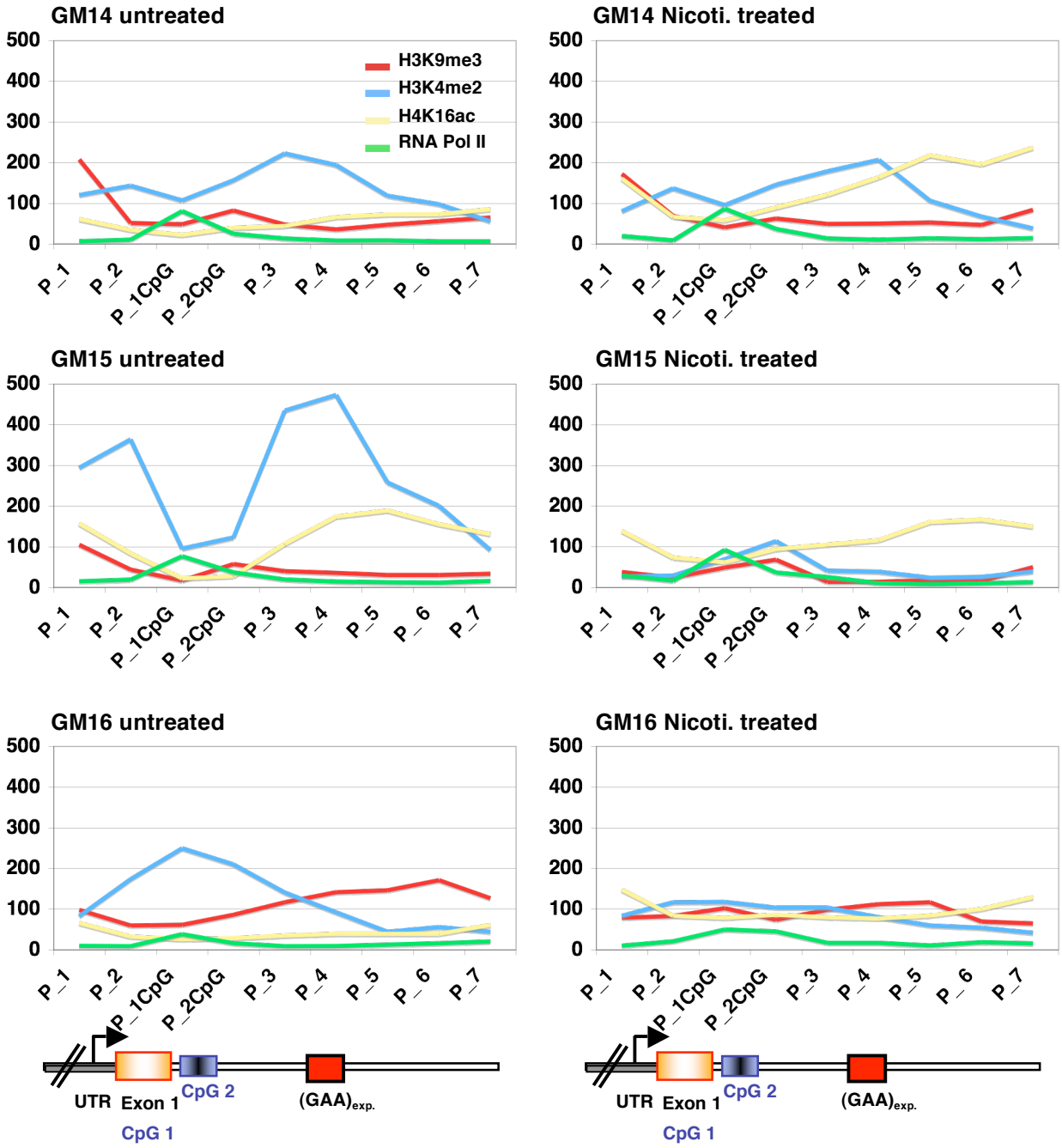

Figure 28: Histone modifications detected at the *FXN* gene of untreated and Nicotinamide-treated cell lines. The amount of *FXN* DNA immunoprecipitated by H3K9me3, H3K4me2, H4K16ac and RNA pol II antibodies was quantified by real-time PCR as described in Materials and Methods. Primer pair location is indicated below each figure, except P_1, which is 6000 bp upstream of *FXN*. Data displayed are an average of two independent immunoprecipitations; each immunoprecipitation was quantified in duplicate.

As expected, the H4K16 acetylation as a target of HDAC class III (Wiren et al., 2005) increased in all three cell lines studied, notably to different extents (Fig. 28). Here, the control GM14 cell line showed the highest increase of H4K16ac (~ 2 fold after the

putative RNA pol II pausing site) compared to the untreated sample, whereas in the early stage GM15 cell line this effect was not seen. However, the untreated GM15 sample initially exhibited a high baseline level of H4K16ac, maybe indicating a level of H4K16ac saturation (Fig. 28). The late stage GM16 cell line also showed an increase in H4K16ac but the pattern was different. Surprisingly, H3K4me2 levels decreased drastically in cells derived from FRDA patients but not in the control line, indicating that this mark was particularly sensitive to the combination of Nicotinamide and an abnormal GAA repeat expansion. The histone modification H3K9me3 showed a slight decrease in all three cell lines compared to the untreated samples. The amount of RNA pol II bound at the pausing site was unchanged in the GM14 and GM15 cell lines. In GM16 the already reduced RNA pol II peak was broader after the Nicotinamide treatment.

Nicotinamide treatment changes binding of factors possibly influencing the pausing of RNA pol II

The novel finding, presented in this thesis, that RNA pol II accumulates in exon 1 of the *FXN* locus suggests that this gene might require tight regulation, mediated via the RNA pol II pausing site and its binding factors. In pursuit of the hypothesis of a 'tight-regulation' of the *FXN* locus via the RNA pol II pausing site, it was important to investigate the binding of factors influencing the RNA pol II pausing site. It was therefore investigated whether the opening of the chromatin structure via an increased acetylation of H4K16 would change the binding pattern of the RNA pol II regulating factor NELF-E.

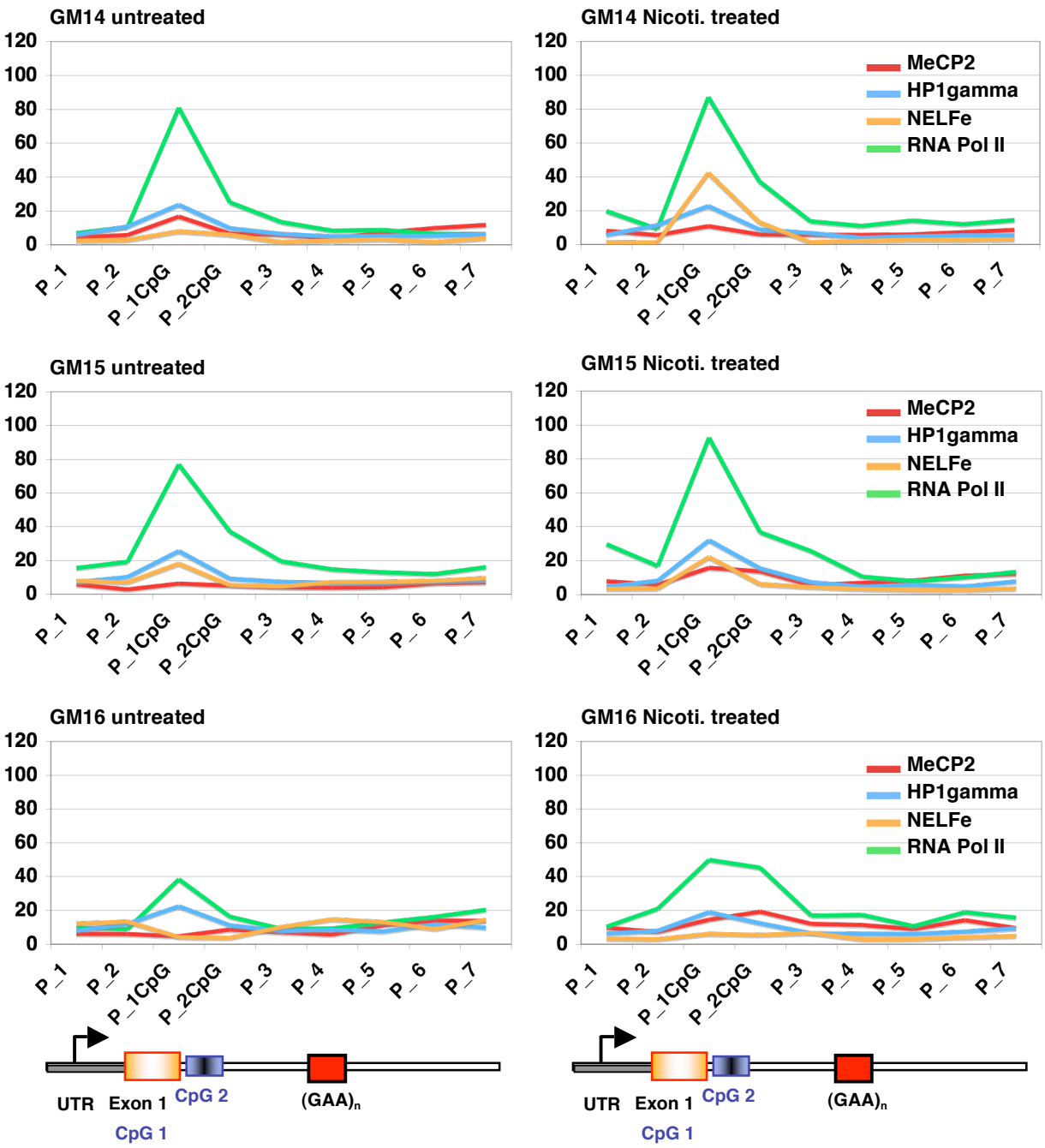

Figure 29: ChIP against DNA-binding proteins on three EBV-cell lines. In order to assess the changes induced by Nicotinamide treatment the ChIP results presented in Results I are displayed again. ChIP was performed on normal and FRDA cell lines using antibodies against human MECP2, RNA Pol II, HP1γ and NELF-E. IP samples were subject to quantitative real-time PCR measurements. Each sample was measured at least twice in triplicate. Following Nicotinamide treatment the control cell line GM14 shows increased NELF-E binding at the RNA pol II pausing site, whereas GM15 and GM16 do not seem to change. Following Nicotinamide treatment only GM16 displays a change of RNA pol II pattern over the pausing site. The binding of HP1γ is unaffected in all three EBV-cell lines.

As displayed in figure 29, Nicotinamide treatment might have provoked a slight increase of RNA pol II inside the CpG- island in the cell lines GM14 and GM15

compared to the untreated samples. Moreover, after Nicotinamide treatment the cell line GM16 exhibited an expanded RNA pol II peak along the entire CpG- island. A slight increase of MeCP2 binding was found towards the end of the CpG- island in the FRDA patient cell lines. Although borderline, these results correlate well with the ChIP-chop results showing corresponding de/increases in methylation levels, which will be discussed shortly (Fig. 32). Moreover, the observed decreased binding of MeCP2 in the control GM14 cell line correlates well with the observed decreased degree of methylation after Nicotinamide treatment. The control cell line GM14 displayed an increase in NELF-E binding, which correlates with high increase in H4K16ac in this line (Fig. 28). Accordingly, the early-stage FRDA cell line GM15, which did not display a change in H4K16ac levels, did also not show an increase in NELF-E binding over the *FXN* putative pausing site. Furthermore, the late stage GM16 cell line exhibited a reverse NELF-E binding pattern following Nicotinamide treatment compared to the untreated sample. In short, these results suggest a correlation between NELF-E and RNA pol II levels inside the CpG- island, since the peak of NELF-E coincides with the peak of the RNA pol II. This suggests that the interplay between chromatin structure, NELF-E and RNA pol II binding levels might be an important feature in regulating the amount of *FXN* mRNA.

LSD1 and JARID1

The question of how Nicotinamide treatment of FRDA patient EBV transformed cells leads to a dramatic decrease in H3K4me2 and me3 remains elusive. Furthermore, the observed H3K4 methylation and demethylation seems to require the presence of an abnormal GAA repeat expansion. Recently, an increasing number of lysine demethylating enzymes have been discovered displaying potential candidates for demethylating H3K4 (Iwase et al., 2007). The lysine-specific demethylase 1 (LSD1) was the first enzyme discovered and is also referred to as BHC110 or p110b. LSD1 was found to demethylate the specific lysine H3K4me1 and H3K4me2 using an amine oxidase reaction (Lawrence et al., 2004). However, LSD1 lacks the ability to demethylate H3K4me3. Enzymes of the JARID1-family encoding a JmjC-domain are able to demethylate H3K4me3 to di- and mono- forms but no further. Interestingly, the JARID1 family also binds to H3K9me3 indicating a cross talk between H3K9me3 and H3K4me3 in transcriptional repression (Iwase et al., 2007).

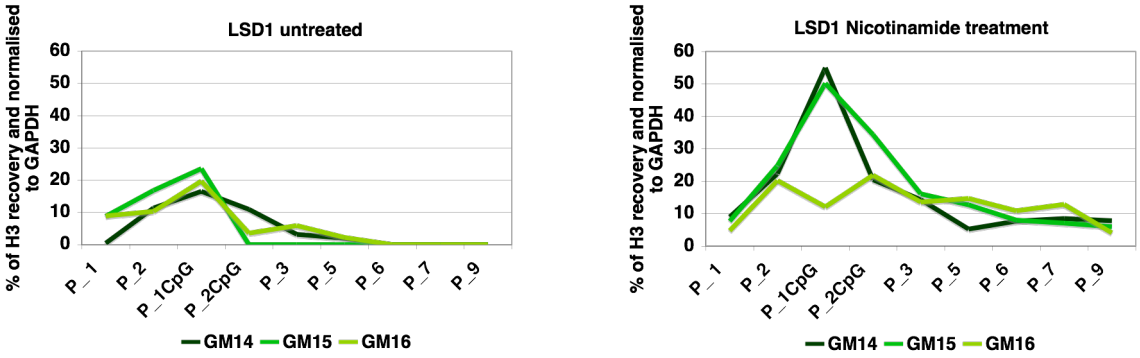

Figure 30: ChIP against LSD1 on Nicotinamide treated and untreated EBV-cell lines. Each IP was done twice and each resulting DNA sample was quantitative real-time PCR measured in triplicate. Results display a dramatic increase of LSD1 over the putative RNA pol II pausing site for GM14 and GM15 following Nicotinamide treatment.

Figure 30 shows the results of all three cell lines investigated for LSD1 binding, on the left untreated and on the right following Nicotinamide treatment (Fig. 30). In untreated all three cell lines, similar LSD1 levels are present around the RNA pol II pausing site, although the patient GM15 line exhibits an additional peak 5' of the GAA expansion. Following Nicotinamide treatment, the control GM14 cell line as well as the patient GM15 cell line displayed an increase in LSD1 at the pausing site of more than 2 fold. In contrast the GM16 cell line exhibited a decrease of LSD1 around the pausing site post-Nicotinamide treatment, which was accompanied by a broader peak for RNA pol II (Fig. 29). In summary, following Nicotinamide treatment, an increase of LSD1 is seen at the pausing site independent of the GAA expansion, if the RNA pol II pausing site is undisturbed. In the presence of a disturbed RNA pol II pausing set-up, as seen for GM16, this recruitment is missing. Since the rise in LSD1 levels are similar around the pausing site of GM14 and GM15, it seems unlikely that the loss of H3K4me2 in the patient cell lines is provoked by LSD1.

The second potential candidate possessing demethylase activity was JARID1b with its ability to demethylate H3K4me3 as well as H3K4me2. Surprisingly, the untreated sample of GM16 displayed a peak of JARID1b, whereas the control GM14 cell line and the patient GM15 cell line did not display any signals for JARID1 at the *FXN* locus (Fig. 31).

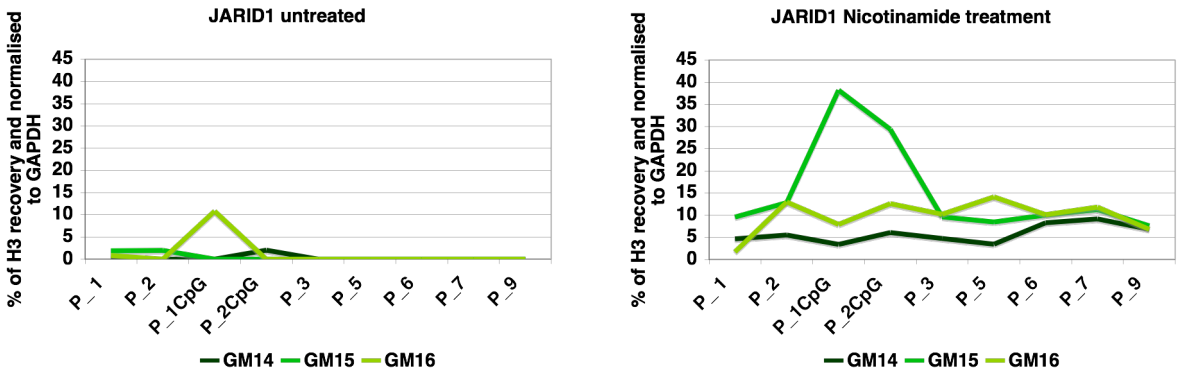

Figure 31: ChIP against JARID1b of Nicotinamide and untreated EBV-cell lines. Results display in untreated samples only for GM16 a peak of JARID1b over the pausing site. Following Nicotinamide treatment GM15 displays a peak for JARID1b that was not detected in the untreated sample, whereas GM16 and GM14 do not show this feature. Each IP was done twice, each independent IP was quantitative real-time PCR measured in triplicate.

However, following Nicotinamide treatment this situation was altered. Although the control GM14 cell line displayed negligible levels of JARID1b, the patient GM15 cell line now displayed a significant peak of JARID1b around the RNA pol II pausing site. In contrast, the patient GM16 cell line showed the reverse, with a reduction in the former peak over the RNA pol II pausing site. However both patient cell lines showed elevated levels 3' of the pausing site. This finding might explain the H3K4me2 demethylation of an active gene after Nictoinamide treatment, however the underlying mechanism has not yet been elucidated.

ChIP-chop assay

The 'ChIP-chop' technique (see Materials and Methods) was used to determine the degree of CpG-methylation (Preuss et al., 2007) at the predicted 918 bp CpG- island. In brief, the predicted island is not heavily methylated. Interestingly the GM15 patient cell line showed particularly low levels of DNA methylation (Fig. 32). GAPDH (exon 4) was used as a negative control and the second CpG-island inside intron 2 of the *FXN* gene, which exhibits a high degree of methylation, was used as a positive control (Fig. 32).

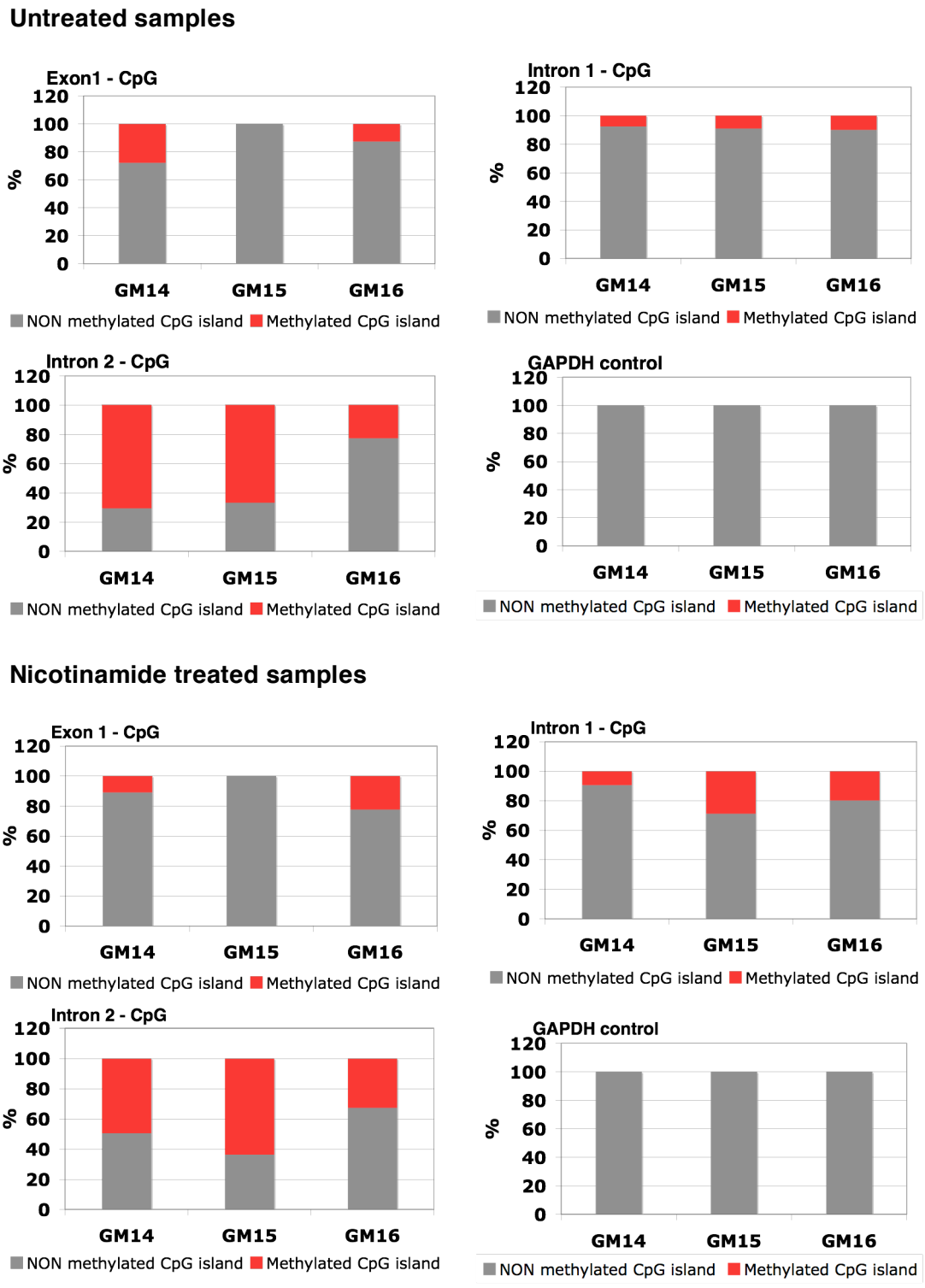

Figure 32: **DNA-methylation at the *FXN* locus in FRDA and control EBV-cell lines. ChIP-chop assay of untreated and Nicotinamide treated EBV-cell lines. ChIP experiments were performed against histone H3. DNA of immunoprecipitate was incubated with the methylation-specific nuclease McrBC. Undigested DNA was quantified by Q- (RT) PCR as described in Materials and Methods. Graphs show the degree of DNA methylation in red. As a methylation negative control, *GAPDH* (exon 4) was used, and as a methylation positive control the CpG-island localized in**

intron 2 of the *FXN* gene was used (all primers shown in Material and Methods). Results represent the average of two ChIP-chop experiments; each resulting DNA sample was measured in triplicate.

Unlike the first CpG- island covering exon 1 and the first part of intron 1 the second predicted CpG- island is ~ 65 % methylated in the control cell line and in the early stage FRDA patient cell lines (GM15). The later stage FRDA patient (GM16), exhibits ~ 20 % of methylation at this island. Intron 1, however, seems to be consistently un-methylated in untreated samples. Unexpectedly, after Nicotinamide treatment, intron 1 gained a certain degree of DNA- methylation, which was dependent on the abnormal GAA expansion. Furthermore, the control cell line seemed to lose DNA methylation in exon 1 as well as in the second CpG- island. This was not observed in the FRDA patient cell lines. Although these changes are rather minor, they are consistent with the changes in the amount of bound MeCP2 (Fig. 29). The GAPDH control locus was unaffected by the Nicotinamide treatment.

In summary, the chromatin modifications of the *FXN* locus change dramatically after Nicotinamide treatment. Furthermore, the DNA methylation pattern, as seen in the ChIP-chop assay (Fig. 32), was also modified. As the level of *beta-actin* mRNA validated by Q- (RT) PCRs was unchanged by the Nicotinamide treatment all *FXN* mRNA measurements were normalised to *beta-actin* mRNA. However, on measuring actual *FXN* mRNA levels by Q- (RT) PCR, an increase of only 1.2 - 1.4 fold per cell line was observed (Fig. 27). From the obtained ChIP and Q- (RT) PCR results one can conclude that the chromatin structure influences the level of *FXN* gene transcription only to a certain degree. However, the putative RNA pol II pausing site was not sufficiently influenced by Nicotinamide, to enhance transcription enough to restore or raise the *FXN* mRNA to control cell line levels. Understanding the regulation of *FXN* is pivotal for developing rational approaches to stimulate a therapeutic increase in the expression of *FXN* at the pathogenic *FXN* locus.

Treatment of patient primary lymphocytes with Nicotinamide

In order to test the efficiency of Nicotinamide treatment in primary lymphocytes of FRDA patients, freshly extracted lymphocytes were cultured for 3 days in RPMI 1640 Medium containing 10 mM Nicotinamide. This was important, as the published

HDAC_4b inhibitor (Herman et al., 2006) had been claimed to work in primary cells more reliably than in EBV-transformed cell lines (personal communication Gottesfeld J., Scripps). It was necessary to determine whether a similar phenomenon was true for the HDAC class III inhibitors. For this treatment, blood from a heterozygous father and his homozygous son was taken; the lymphocytes were extracted and then treated as stated. This blood sample was taken 18 months after that for the mRNA measurements presented in Results I. Interestingly, a further decrease in *FXN* levels was seen in the severely affected son. Whereas the son had previously displayed ~ 39 % of the fathers *FXN* level, it now had dropped to ~ 21 %.

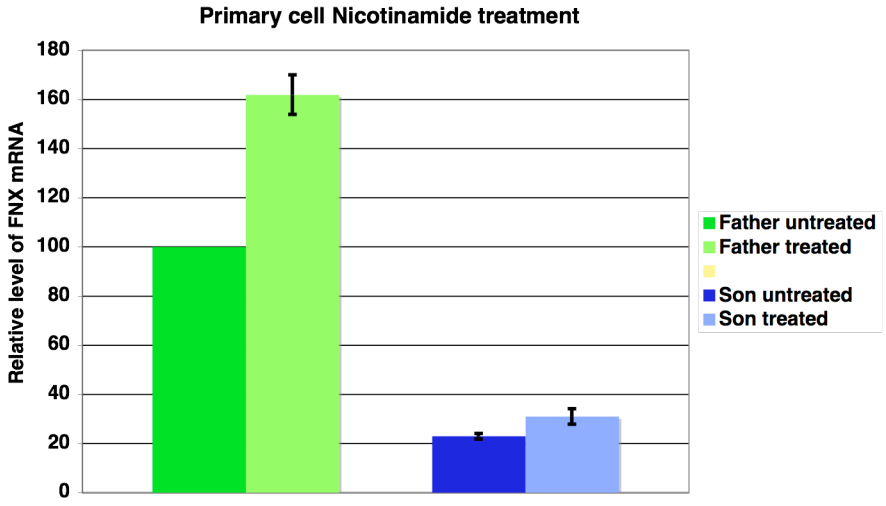

Figure 33: ***FXN*** **mRNA levels from primary lymphocytes, extracted from a heterozygous (Father) and a homozygous (Son) individual for the GAA expansion. Displayed are the values before and after a 3 day 10 mM Nicotinamide treatment. Each Q-RT-PCR measurement was done twice in triplicate.**

As shown in figure 33, Nicotinamide treatment did increase the *FXN* level in the heterozygous individual ~ 1.6 fold and in the homozygous individual ~ 1.4 fold. It is not surprising that the increase in the heterozygous individual is higher than in the homozygous one. By simply “opening-up” the chromatin structure, the RNA pol II elongation will still be hampered to a greater extend in the presence of two alleles with an abnormal GAA expansion. In this situation the HDACi treatment is unlikely to be able to restore the FRDA patient *FXN* level to non-pathogenic levels (30 % of normal). The son, untreated displaying ~ 10% of normal *FXN* levels, would experience an increase of only ~ 14 % .

Treatment of EBV-cell lines with 5-aza-2-deoxycytidine

In order to test for possible positive effects on *FXN* expression, assays with different concentrations of a DNA methylation inhibitor, 5-aza-2-deoxycytidine, were performed. EBV-cells were treated with different concentrations of 5-aza-2-deoxycytidine for 48 hours and RNA was extracted with Trizol.

As shown in figure 34, the 5-aza-2-deoxycytidine treatment was counterproductive. When normalised to *beta-actin* a decrease of ~ 40 % in *FXN* expression occurred in all cell lines tested. This could be due to many factors. One possibility is that this drug influences other genes that regulate *FXN* levels. Furthermore, the observed methylation in the second CpG- island may be important for the correct transcription of *FXN* so a methylation change of the CpG- islands might negatively influence *FXN* expression.

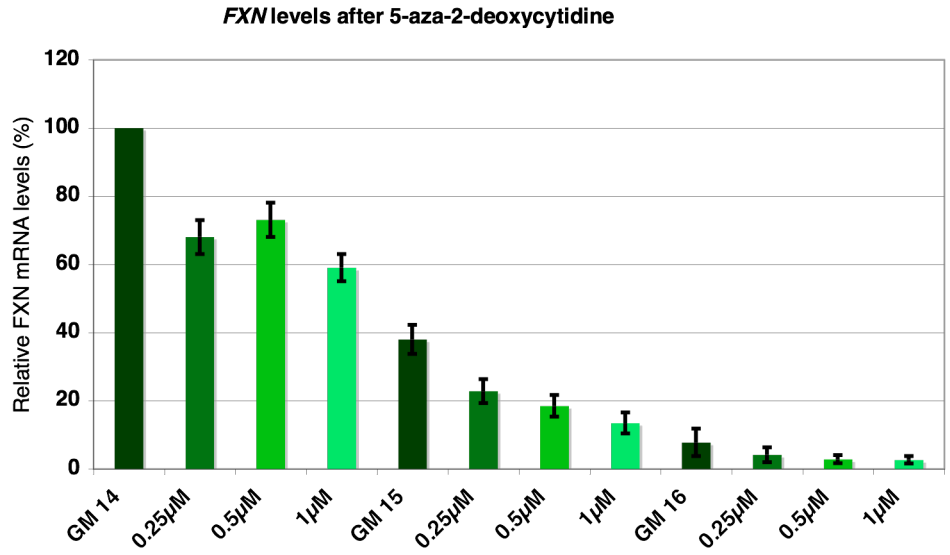

Figure 34: ***FXN*** **levels following a 5-aza-2-deoxycytidine treatment of EBV-cell lines. EBV-cell line treatment was performed for 48 hours with different concentrations. Extracted RNA was measured with quantitative real-time PCR twice and each in triplicate. Error bars give the standard deviation between the means of two independent measurements. Each value for treated GM14 and all values for GM15 and GM16 were normalised to the untreated GM14 sample (set 100%). No increase in** ***FXN*** **expression was observable but a dramatic decrease was seen in normal cells as well as in FRDA patient cells.**

Results III

Results III

The following chapter describes experiments performed to reveal possible differences of the regulatory *FXN* pausing mechanism in the presence of a normal and an abnormal GAA expansion.

Further testing of the RNA pol II pausing site with DRB

In order to investigate the pausing mechanism of the RNA pol II pausing site in more detail a 5,6-dichloro-1β-ribofuranosylbenzimidazol (DRB) treatment was performed. DRB is known to inhibit the phosphorylation activity of the positive transcription elongation factor b (PTEF-b) on the RNA pol II CTD-S2 as well as NELF-E, thereby preventing the elongation of RNA pol II (Marshall et al., 1996; Chodosh, 1998). DRB treatment allows us to test the consequences of disrupting the phosphorylation activity of PTEF-b at the *FXN* locus. Moreover, the negative elongation factor (NELF) was previously found to be necessary for the negative function of DSIF (Yamaguchi et al, 1999). Although neither factor had any effect alone, the combination of DSIF and NELF slowed the elongation of RNA pol II. Importantly, this effect was eliminated by PTEF-b (Yamaguchi et al., 1999).

All EBV-cell lines were treated with 50 μM of DRB for 5 h followed by chromatin and RNA extraction. Firstly ChIP results against various antibodies are presented of untreated and DRB treated samples. Following these results, the effect on *FXN* mRNA levels will be discussed.

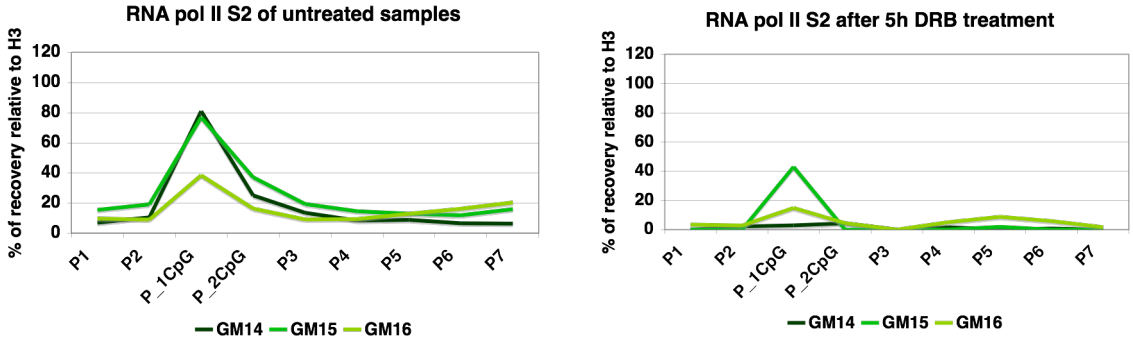

Figure 35: ChIP result of DRB treated and untreated EBV-cells against RNA pol II S2. Displayed are the control (GM14) and FRDA EBV-cell lines (GM15 and GM16) untreated and for 5 hour DRB treated. Presented is the mean of two independent experiments, the variation between experiments is usually +/- 5 % for each primer pair. Following DRB treatment a severe decrease in RNA pol II S2 levels was seen all three lines, however for the control GM14 cell line no signal was detectable.

As mentioned previously, S2-phosphorylated RNA pol II accumulates at the pausing site. Here, the control GM14 and FRDA patient GM15 exhibit similarly high levels of ~ 80 units, whereas the EBV-cell line GM16, with low levels of *FXN* expression, displays approximately half of this RNA pol II S2 accumulation. After a 5 h DRB treatment, the phosphorylation of RNA pol II CTD-S2 and NELF-E is impeded and productive transcriptional elongation should no longer be possible. As expected, the control GM14 cell line does not exhibit any signs of S2-phosphorylated RNA pol II at the pausing site. This is not true for the FRDA patient cell lines GM15 and GM16. Both still exhibit roughly half of the previously detected amount of S2-phosphorylated RNA pol II in untreated cells. From this result two things become clear. Firstly, in ChIP experiments the antibody used against S2-phosphorylated RNA pol II appears reasonably specific, as the healthy cell line loses the signal when the phosphorylation activity of PTEF-b is prevented. Secondly, a simple explanation for the significant amount of S2-phosphorylated RNA pol II at the pausing site in FRDA patient cell lines is the retention of phosphorylated RNA pol II S2 at the pausing site, which has not been utilised during the course of a 5 h DRB treatment. This result supports the hypothesis that a delayed release of RNA pol II pausing seems to occur in the presence of a pathogenic GAA expansion in FRDA patient cells.

In order to verify the ChIP experimental conditions it was necessary to perform an additional experiment using an antibody against RNA pol II S5. The S5 modification is established by CDK7 (mammals) and known to occur at promoters, initiating the promoter escape by RNA pol II and displaying the phase of early elongation (Krishnamurthy et al., 2004). Therefore, as CDK7 is not a target of DRB it should have no direct effect on levels of RNA pol II S5. However it is important to note that for different antibodies the absolute recovery can vary significantly and therefore it is not possible to directly compare RNA pol II S5 levels to the results obtained for RNA pol II S2.

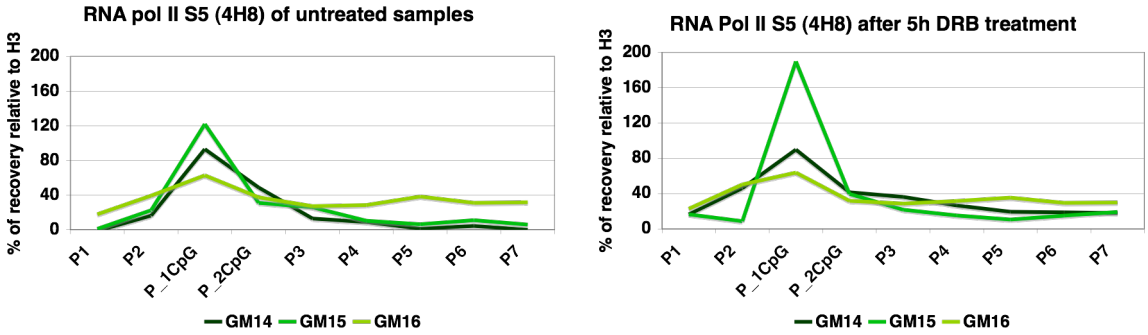

Figure 36: ChIP against RNA pol II S5 of DRB treated and untreated EBV-cell lines. Presented is the mean of two independent experiments, the variation between experiments is usually +/- 5 % for each primer pair. Results of untreated control (GM14) and FRDA EBV-cell lines (GM15, GM16) show a peak for RNA pol II S5 over the pausing site. Following DRB treatment a significant increase for RNA pol II S5 levels is seen for the FRDA GM15 cell line.

The untreated samples GM14 and GM16 exhibit similar distributions of RNA pol II S5 and RNA pol II S2. However, GM15 shows a slightly higher level for RNA pol II S5 at the pausing site compared to GM14, which differs from the results obtained for RNA pol II S2, where GM14 and GM15 display similar levels. After DRB treatment the levels of RNA pol II S5 for GM14 and GM16 were similar, although, for GM14 a slightly higher level was found after the pausing site. Unexpectedly, the FRDA patient cell line GM15 exhibited a significant increase of RNA pol II S5, accompanied by a slight drop after the pausing site compared to the untreated sample. Reviewing the ChIP results of both RNA pol II modifications suggests that the presence of a GAA repeat expansion (in GM15) favours not only the accumulation of RNA pol II S5 at the pausing site but also hampers the escape of RNA pol II S2. To take the investigation

further the behaviour of NELF-E, also a phosphorylation target of the DRB sensitive PTEF-b was investigated.

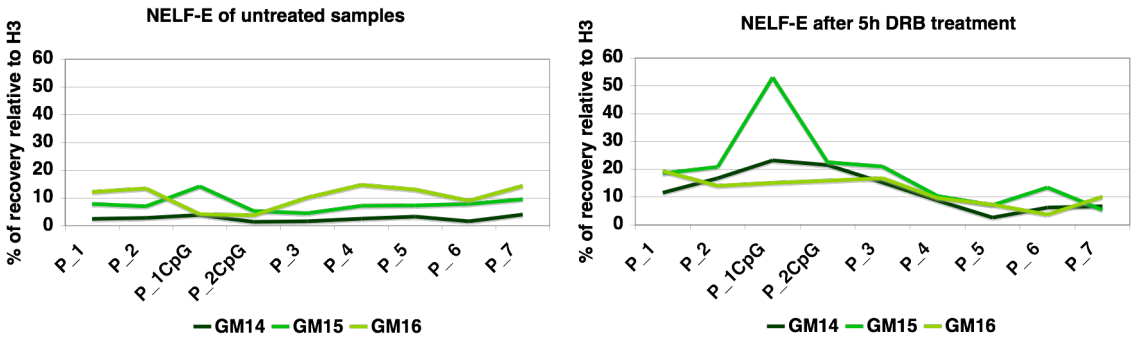

Figure 37: ChIP against NELF-E of untreated and 5 h DRB treated EBV-cell lines. Presented is the mean of two independent experiments, the variation between experiments is usually +/- 5 % for each primer pair. Following DRB treatment in all three EBV-cell lines an increase of NELF-E was seen over the *FXN* locus, however GM15 displayed the most significant increase in NELF-E levels over the pausing site.

Untreated samples from the GM15 cell line, which express ~ 30 % *FXN* mRNA levels compared to controls, exhibit a higher peak of NELF-E compared to the healthy GM14 cell line. In GM16, the NELF-E peak at the pausing site is even less pronounced than in the control line. Furthermore, the FRDA GM16 cell line, which expresses low levels of *FXN*, displays an unusual chromatin composition that is accompanied by less binding of RNA pol II to the pausing site (Fig. 29).

One of the functions of PTEF-b is the phosphorylation of NELF-E, which then gets released from the RNA pol II pausing site, thereby contributing to the pausing escape and proper elongation. This is supported by the observation that following DRB treatment all three cell lines generally display higher NELF-E levels indicating that the release of RNA pol II from the pausing site seems to be prevented. Interestingly, the effect of DRB on the FRDA patient cell line GM15 is significantly higher than on the control GM14 or the low level *FXN* expressing GM16 line. This result suggests that the presence of a GAA repeat expansion (GM15) can cause the recruitment of abnormal NELF-E levels to the transcribed *FXN*, thereby impeding the pausing escape of RNA pol II S2, thus ultimately leading to an accumulation of both RNA pol II phosphorylated forms S5 and S2 at the pausing site.

In order to further investigate this hypothesis the chromatin mark for “active” or recently transcribed DNA, H3K4me2, was also tested.

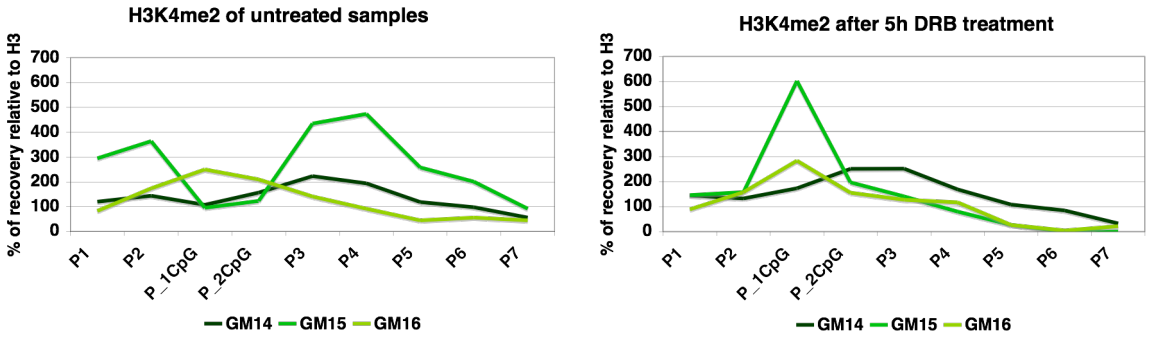

Figure 38: ChIP against H3K4me2 of untreated and 5 h DRB treated EBV-cell lines. Presented is the mean of two independent experiments, the variation between experiments is usually +/- 5 % for each primer pair. Following treatment no major change for GM14 and GM16 was seen, but again GM15 displayed a significant change. Now a peak of H3K4me2 over the pausing site and a loss of H3K4me2 3’ of the pausing site was identified.

As described in chapter 1, the “dip” of H3K4me2 around the RNA pol II pausing site appears more pronounced in the FRDA patient cell line GM15 and in primary cells of FRDA patients, than is seen in control cells. Interestingly, the increase of the H3K4me2 found around the GAA repeat seems to increase with the size of the GAA expansion, if *FXN* mRNA levels around 30 % are seen. The GM16 cell line that expresses extremely low levels of *FXN,* exhibits the reverse pattern, showing a peak of H3K4me2 at the pausing site, which is then followed by low levels. This feature has not yet been detected in primary cells from FRDA patients. Following a 5 h DRB treatment the control GM14 cell line exhibits a slight increase of H3K4me2 around the RNA pol II pausing site, although the overall pattern is comparable to the untreated sample. This result is similar for the GM16 cell line where no significant changes occur in levels of H3K4me2. Strikingly, the patient cell line GM15 showed a dramatic change. The former “dip” was transformed into a considerable peak over the RNA pol II pausing site and moreover the previously high levels of H3K4me2 around the GAA expansion disappeared (Fig. 38). This observation will be discussed later on in the Discussion in more detail (see p. 113).

Since the active mark H3K4me2 after DRB treatment seemed to be diminished 3' of the pausing site it was interesting to investigate whether this had an effect on the "inactive" chromatin mark H3K9me3.

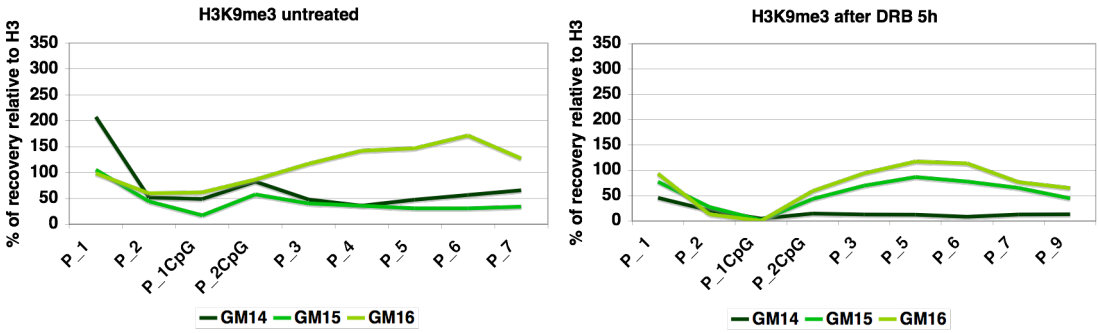

Figure 39: ChIP against H3K9me3 of untreated and 5 h DRB treated EBV-cell lines. Presented is the mean of two independent experiments, the variation between experiments is usually +/- 5 % for each primer pair. Following DRB treatment H3K9me3 levels increased 3' of the RNA pol II pausing site for GM15, whereas for GM14 and GM16 only a slight decrease was detectable.

Indeed in the GM15 cell line, following 5 h DRB treatment there was a ~ 2 fold increase in H3K9me3 levels 3' of the pausing site. On the contrary the control GM14 and FRDA GM16 cell line displayed a slight decrease. This mark is low in GM15 as long as elongation occurs. Thus the lack of sufficient elongation might be crucial whether heterochromatic marks, such as H3K9me3, are established at the *FXN* locus in FRDA patients.

As the boundary factor CTCF was also found at RNA pol II pausing sites, its binding at the *FXN* locus was investigated, following a 5 h DRB treatment.

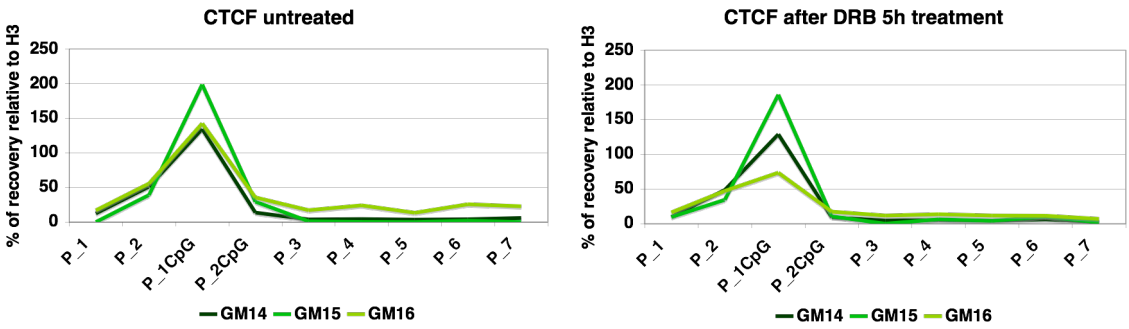

Figure 40: ChIP against CTCF of untreated and 5 h DRB treated EBV-cell lines. Presented is the mean of these experiments, the variation between experiments is usually +/- 5 % for each primer pair. Following DRB treatment GM14 and GM15 were more or less unchanged, however the FRDA GM16 cell line displayed a decrease over the pausing site.

All untreated EBV-cell lines exhibit a pronounced peak for the CTCF DNA binding factor around the pausing site. GM15 exhibits ~ 40 % more binding than the other two lines. However, following a 5 h DRB treatment the GM16 cell line loses ~ half the amount of CTCF which was present previously, whereas the other two cell lines do not.

Because the patient cell lines displayed a significant change in the levels of H3K4me2 following DRB treatment, the binding of the histone lysine demethylase LSD1 was also investigated.

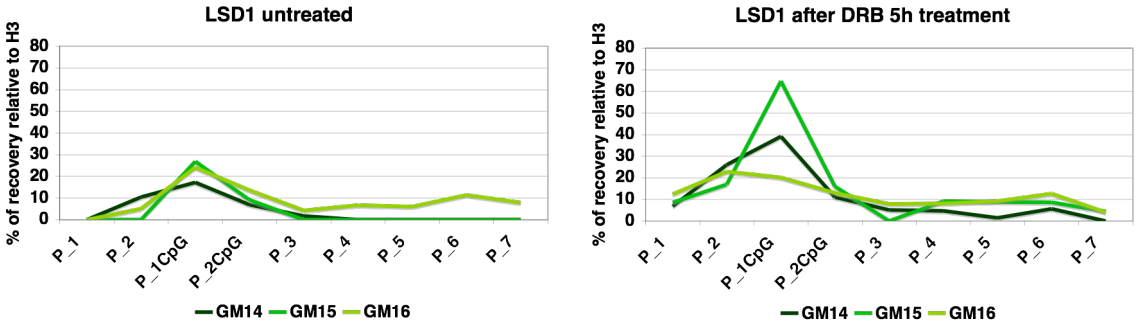

Figure 41: Levels of LSD1 measured via ChIP of untreated and 5 h DRB treated EBV-cell lines. Presented is the mean of two independent experiments, the variation between experiments is usually +/- 5 % for each primer pair. Following DRB treatment LSD1 increased over the pausing site of GM14 and GM15, whereas GM16 displays a shift of LSD1 towards the 5' end of *FXN*.

Both untreated patient cell lines displayed similar levels of LSD1 around the pausing site, whereas the control cell line exhibits slightly less. Interestingly, inhibiting S2-phosphorylation of the RNA pol II CTD during the 5 h DRB treatment changed the recruitment of LSD1 to *FXN*. GM15 exhibits a nearly 3 fold and GM14 an ~ 2.5 fold increase of LSD1 at the pausing site. In the case of GM15 this occurs in parallel with a substantial increase of H3K4me2 at the pausing site (Fig. 38). Therefore, it is possible that an abnormal increase of H3K4me2 triggers an additional recruitment of LSD1 to the RNA pol II pausing site. Interestingly, the control GM14 cell line, although showing an increase of LSD1, displayed only a minor increase in H3K4me2 levels at this site. It is possible that, in the case of a normal GAA repeat length the accumulation of H3K4me2 might be simply compensated by additional LSD1, whereas the presence of an abnormal GAA repeat expansion hampers this mechanism. Untreated cells show in the case of extremely low expression of *FXN* (GM16) an additional increase around the promoter region. Strikingly, this correlates with the level of H3K4me2 detected and will be discussed further in the Discussion.

In order to investigate these observations further it is necessary to account for the actual *FXN* mRNA changes after a 5 h DRB treatment.

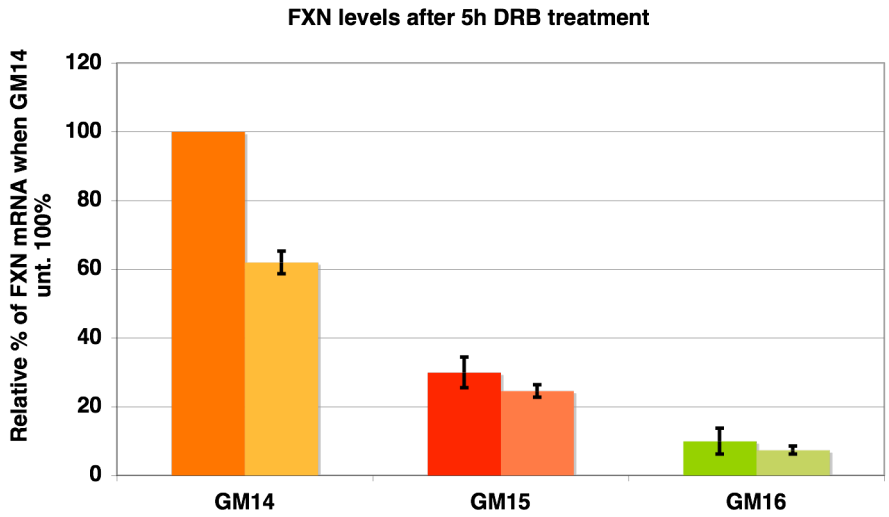

Figure 42: *FXN* mRNA levels of untreated and 5 h DRB treated EBV-cell lines. Displayed are relative *FXN* mRNA levels, normalised to untreated GM14 (dark orange). Untreated samples are displayed in dark colour, DRB treated in the corresponding lighter version. Each *FXN* ct-value has been normalised to *beta-actin*. RNA was Q-real-time measured twice in triplicate and serial dilutions. The error-bars indicate the standard deviation of two independent experiments. The most decrease of *FXN* levels is seen in the control GM14 cell line.

As displayed in figure 42, following DRB treatment for 5 h, the largest effect on *FXN* mRNA levels is seen in the control GM14 cell line, which shows a decrease of 40 %. This might be explained by the observation that the available RNA pol II S2 at the pausing site was fully used at some point during the 5 hours and further elongation was then no longer possible. In order to address more precisely when this scenario occurred, further time point experiments will be necessary. Considering that the H3K4me2 pattern hardly changed (Fig. 38) (indicating previously transcribed chromatin), it is possible that the final usage of S2 phosporylated RNA pol II had occurred earlier rather than later. In contrast, even after DRB treatment the patient cell line GM15 exhibits RNA pol II S2 at the pausing site (Fig. 35). Although elongation competent S2-phosphorylated RNA pol II is still available, this cell line exhibits only a slight reduction in *FXN* mRNA (minus ~ 18 %) in response to DRB treatment. Furthermore the large increase of the negative elongation factor NELF-E, seen occurring predominantly in the GM15 cell line might hamper the release of the RNA pol II S2 (Fig. 35 + 37). To further address these possibilities the H3K4me2 levels obtained can be considered. Following a 5 h DRB treatment GM15 lost its active H3K4me2 mark over the GAA repeat and additionally displayed a significant peak of H3K4me2 at the pausing site, resembling a similar pattern to that obtained for the untreated GM16 cell line that expresses *FXN* at a very low level. In yeast, H3K4 is methylated by the Set1 domain, which targets the S5 phosphorylation of RNA pol II (Peters and Schubeler, 2005) By analogy, as GM15 exhibited an increase

in RNA pol II S5 phosphorylation at the pausing site, the pronounced H3K4me2 peak might be due to the recruitment of a SET-domain K4 methylase. Moreover, these results might also partly explain the H3K4me2 pattern observed in the presence of very little *FXN* mRNA as is seen in GM16. Here, the lack of sufficient RNA pol II S2 escape from the pausing site might facilitate the increased H3K4me2 signal over the pausing site by a similar mechanism (Fig. 38). Noteworthy, that so far a peak of H3K4me2 over the pausing site was not detected in any primary cells of FRDA patients, potentially indicating a very late event in the evolution of the FRDA disease. Still, surprisingly, both FRDA patient samples seemed to be less affected by a 5 h DRB treatment than the control cell line. One explanation might be that after a 5 h period the lack of elongation does not affect the patient cell line as much as the control cells, since the RNA pol II S2 escape occurs to a lesser extent to begin with, when compared to the control cell line. Therefore, in the control cell line the hampered elongation occurring due to additional recruitment of NELF-E, or missing elongation, is more distinct. In summary, this experiment gave further evidence for a hampered escape of RNA pol II from the pausing site in the presence of an abnormal GAA repeat expansion.

LSD1 inhibitor Tranylcypromine

The detection of LSD1 accompanied by the intriguing “dip” of the active H3K4me2 chromatin mark at the pausing site led to the idea that LSD1 might be part of the mechanism regulating the RNA pol II pausing and its release. In order to test this possibility EBV-cell lines were treated with Tranylcypromine to inhibit the demethylase activity of LSD1. Tranylcypromine is a non-hydrazine monoamine oxidase inhibitor (Yang et al., 2007). For this experiment the EBV-cell lines were treated for 24 h in order to account for possible chromatin changes occurring after mitosis and replication. The treatment was then followed by chromatin extraction and immunoprecipitation. Firstly, the RNA pol II S5 ChIP results will be discussed.

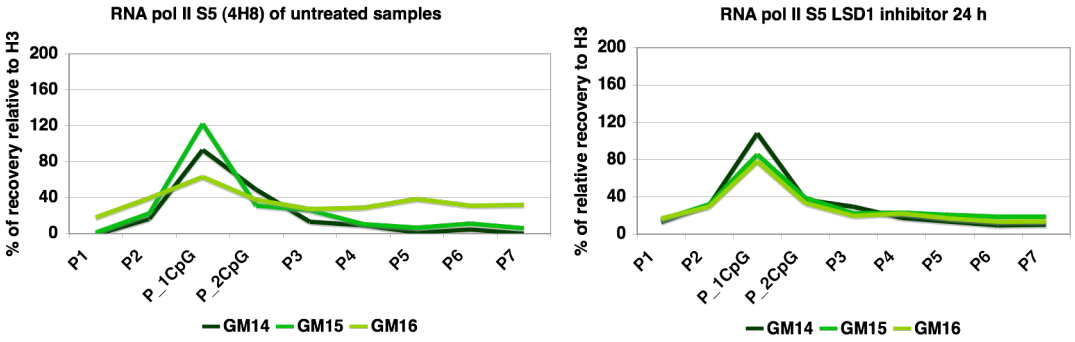

Figure 43: ChIP against RNA pol II S5 of EBV-cell lines treated with LSD1 inhibitor Tranylcypromine for 24 h. Presented is the mean of two experiments, the variation between experiments is usually +/- 5 % for each primer pair After this treatment the control GM14 cell line displays unchanged RNA pol II S5 levels, however GM15 displays a significant decrease and GM16 an increase.

Again, the untreated samples display a pronounced peak of RNA pol II S5 at the pausing site and the highest peak is seen for the patient GM15 cell line. Following a 24 h Tranylcypromine treatment this situation is altered. The control cell line displays a slightly higher peak for RNA pol II S5 compared to the untreated sample, whereas for the patient GM15 cell line a decrease at the pausing site is detectable (minus 40 %). Interestingly, the patient GM16 cell line now exhibits a sharper and also slightly increased peak at the pausing site. Furthermore, a drop in overall RNA pol II S5 levels is seen only in the patient GM16 cell line, whereas the control GM14 cell line demonstrates a slight increase after the pausing site.

Performing ChIP against the active chromatin H3K4me2 mark also revealed an interesting change after the Tranylcypromine treatment.

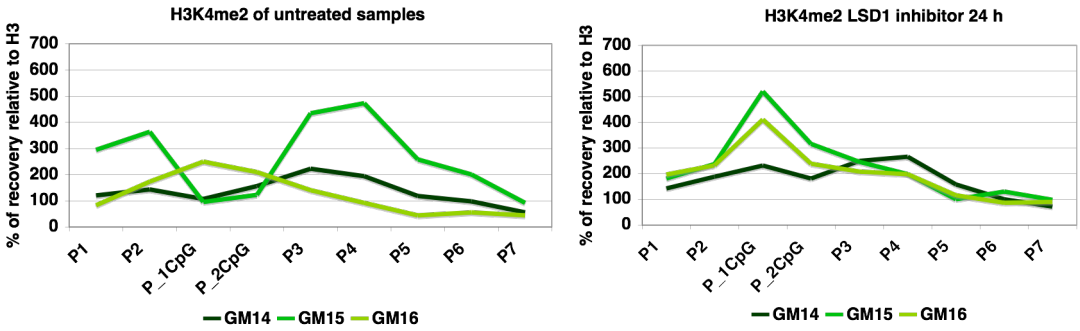

Figure 44: ChIP against H3K4me2 after 24h Tranylcypromine treatment of three EBV-cell lines. Presented is the mean of two IP experiments, the variation between experiments is usually +/- 5 % for each primer pair Now GM14 displays a sight peak over the pausing site, although the H3K4me2 pattern 3' of the pausing site is more or less unchanged. The FRDA GM15 and GM16 EBV-cell lines both display a significant increase in H3K4me2 levels over the pausing site. In case of GM15 this is also accompanied by a dramatic decrease of H3K4me2 levels 3' of the pausing site.

Untreated EBV-cell lines display a peak of H3K4me2 only in the patient GM16 cell line at the RNA pol II pausing site, whereas this is lacking in the control GM14 and the patient GM15 cell line. Notably, after a 24 h Tranylcypromine treatment this pattern changed remarkably in the patient GM15 cells, which carry a GAA repeat expansion. GM15 not only displays a dramatic increase in H3K4me2 over the pausing site, but in addition there is a marked drop in H3K4me2 3' of this site. This might be indicative of reduced transcriptional elongation, and similar to the observation made after DRB treatment (Fig. 38). No dramatic change following Tranylcypromine treatment was detected in the GM16 cell line, which unlike GM15 did not initially exhibit a pronounced H3K4me2 pattern after the pausing site. Additionally, for GM16 a further increase of H3K4me2 levels was seen over the pausing site. Interestingly, the control GM14 cell line displays only a minor increase of H3K4me2 at the pausing site, however relative to the overall H3K4me2 level this might still be significant. Again, the overall H3K4me2 pattern of the GM14 cell line, similar to the result obtained for the DRB treatment, does not seem to change significantly. This is consistent with transcriptional elongation occurring despite the inhibition of LSD1 activity.

The binding of the negative elongation factor NELF-E was also investigated, because the GM15 cell line seemed to lack sufficient RNA pol II elongation, indicated by reduced levels of H3K4me2, despite the accumulation of RNA pol II at the pausing site.

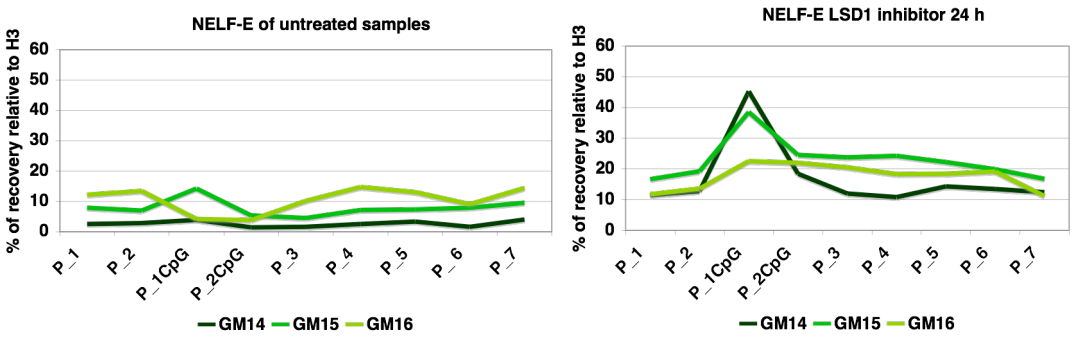

Figure 45: ChIP against NELF-E of three EBV-cell lines with and without 24 hour Tranylcypromine treatment. Presented is the mean of two experiments, the variation between experiments is usually +/- 5 % for each primer pair. Following the treatment, all three EBV-cell lines display an increase of NELF-E over the pausing site.

In the case of LSD1 inhibition a marked increase of NELF-E was detected at the pausing site, especially in the control GM14 line. Interestingly, this increase of up to ~ 40 units is as pronounced as that seen after the Nicotinamide treatment (Fig. 12). Similar to the Nicotinamide treatment the patient GM15 cell line again shows an increase of NELF-E over the pausing site but the change is not as pronounced as that seen for GM14. For the patient GM16 cell line the NELF-E pattern differs slightly from that seen following Nicotinamide or DRB treatment (Fig. 12 + 37). Here, the NELF-E seems to be located predominantly at the pausing site rather than further along the *FXN* gene.

Interestingly, recent publications (Metzger et al., 2005) indicate that under certain circumstances LSD1 is able to demethylate H3K9me3/2. In order to test this possibility ChIP was performed against H3K9me3.

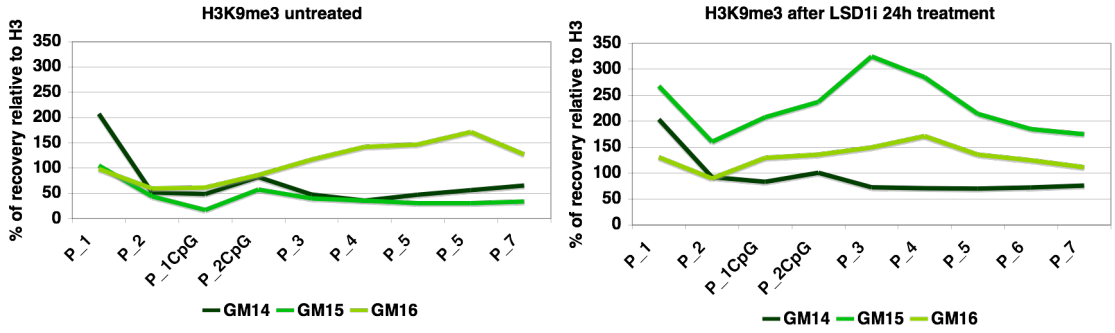

Figure 46: ChIP against H3K9me3 of untreated and 24 h Tranylcypromine treated EBV-cell lines. Presented is the mean of two experiments, the variation between experiments is usually +/- 5 % for each primer pair. Following treatment, a dramatic increase in H3K9me3 levels was seen in the FRDA cell line GM15 only. GM14 and GM16 displayed more or less similar pattern for H3K9me3.

As discussed before, the inactive H3K9me3 histone mark is only pronounced in the patient GM16 cell line that also shows a very low expression of *FXN*. Although the control and the patient GM15 cell line show a slight peak of H3K9me3 immediately after the pausing site, no significant H3K9me3 level was observed around the GAA repeat expansion. Following a 24 h treatment with the LSD1 inhibitor Tranylcypromine, this situation changed significantly for the patient GM15 cell line. In line with the observed decrease of H3K4me2 after the pausing site, H3K9me3 increased considerably after the inhibition of LSD1. Notably, the inactive mark H3K9me3 did not change after Nicotinamide treatment (Fig. 28), despite the severe decrease of H3K4me2 after the pausing site. In this scenario the LSD1 activity would be expected to be unaffected by the Nicotinamide treatment and therefore, despite the lack of H3K4me2, the establishment of H3K9me3 might have been prevented by LSD1. However, since the DRB treatment also increased H3K9me3 levels, although to a lesser extent, it might be that simply the lack of RNA pol II release and elongation provoked the establishment of heterochromatic marks such as H3K9me3. As during Nicotinamide treatment the elongation should be slightly enhanced since *FXN* mRNA levels increased, heterochromatinisation could have been prevented simply through transcription without the involvement of LSD1. However, since the H3K9me3 levels after Tranylcypromine treatment seem to be more pronounced than following DRB treatment it is possible that LSD1 also plays a role in preventing heterochromatisation at the abnormal expanded GAA repeat through its potential demethylating activity on H3K9. LSD1 present at the *FXN* locus would then not only

demethylate H3K4me2 around the pausing site but also H3K9me2/3 around the GAA repeat and its possible expansions, thereby opposing heterochromatisation of *FXN*.

However, in the control cell line GM14 and the low expressing GM16 cell line the absence of LSD1 activity caused only a slight increase of H3K9me3 levels around the GAA repeat, again demonstrating that a GAA repeat expansion is in theory able to acquire heterochromatic marks. Thus, in the particular case of *FXN,* this phenomenon might be prevented either via active transcription or/and by the presence of LSD1. Considering, the initially pronounced H3K9me3 levels of the low *FXN* expressing patient GM16 cell line, it is possible that no further increase was seen after LSD1 inhibition. In order to obtain a better idea of the changes observed after Tranylcypromine treatment, it was important to verify whether the inhibition of LSD1 activity had any effect on the actual LSD1 distribution along the *FXN* locus.

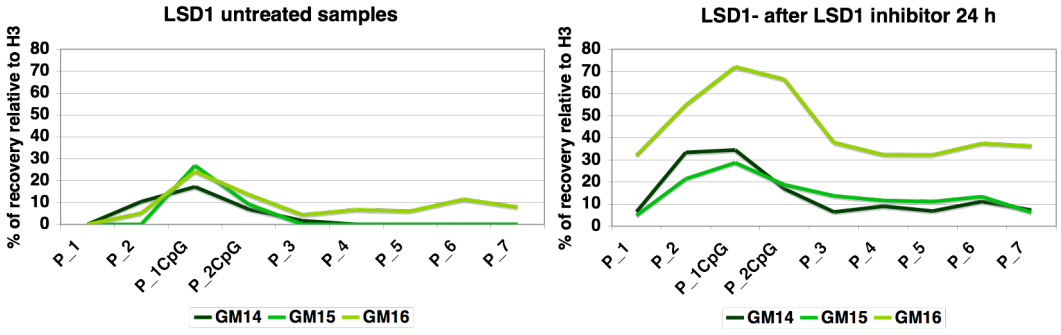

Figure 47: ChIP against LSD1 before and after 24 h Tranylcypromine treatment of three EBV-cell lines. Presented is the mean of two experiments, the variation between experiments is usually +/- 5 % for each primer pair. Following treatment, GM14 and GM15 displayed a slight change in LSD1 levels, only GM16 displayed a ~ 3 fold increase in LSD1 levels over the *FXN* locus.

In general, following a 24 h Tranylcypromine treatment the amount of detectable LSD1 increased especially at the promoter (P_2) and around the pausing site. Interestingly, the patient GM15 cell line displayed the lowest increase, whereas the normal GM14 cell line showed ~ double the amount of LSD1 binding. Surprisingly, the patient GM16 cell line showed a ~ threefold increase across the *FXN* locus. This phenomenon might also explain the minor increase of H3K9me3 as more LSD1 is bound to *FXN*, and therefore even in the presence of an inhibitor a certain activity might be present. After inhibition of the demethylase activity, increased LSD1 binding is surprising, however, one way of balancing the lack of activity might be to compensate by recruiting additional enzymes. Nevertheless, the differences

observed in the amount of LSD1 present, in each cell line, are neither expected nor obvious.

Finally it was decided to investigate the levels of CTCF after Tranylcypromine treatment, as this protein was also found to bind at the RNA pol II pausing site.

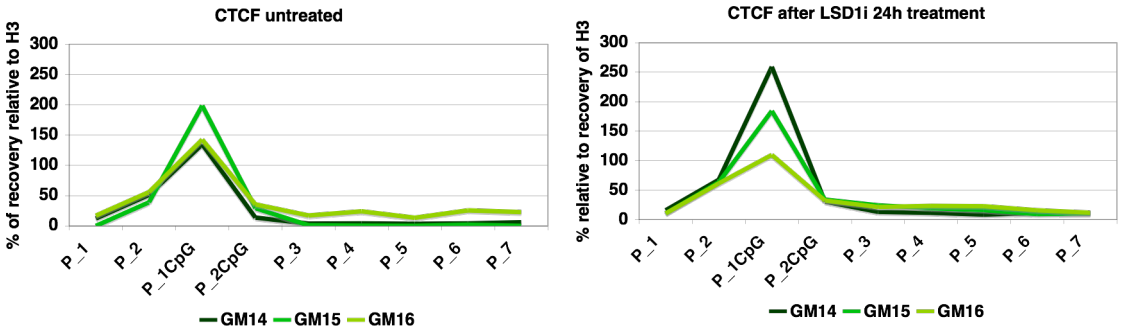

Figure 48: ChIP against CTCF before and after a 24 h Tranylcypromine treatment of EBV-cell lines. Presented is the mean of two experiments, the variation between experiments is usually +/- 5 % for each primer pair. Following treatment the control GM14 cell line displayed an increase of CTCF over the pausing site, whereas CTCF levels of the FRDA GM15 cell line seemed to be unchanged. In contrast, GM16 displayed a decrease of CTCF at this site.

Interestingly, when investigating untreated samples, CTCF seems to be more pronounced at the RNA pol II pausing site in the presence of a GAA repeat expansion, when the cell line expresses *FXN* reasonably (GM15). Then again, the control GM14 and the patient GM16 cell line exhibit similar CTCF levels over the pausing site. However, after a 24 h Tranylcypromine treatment this pattern changes. The healthy GM14 cell line now shows an increase of ~ 50 % CTCF binding over the pausing site, whereas both patient cell lines exhibit a decrease of ~ 25 %. This phenomenon might be explained by the fact that both patient cell lines show a dramatic change in the H3K4me2 pattern over the RNA pol II pausing site (Fig. 44), which might hamper CTCF binding, whereas the control GM14 cell line exhibited a more or less unchanged H3K4me2 pattern over the pausing site. As CTCF is known to function as an insulator element and GM14 also showed the highest increase of NELF-E, CTCF might also play a crucial part in the regulation of *FXN* mRNA levels. Possible roles of CTCF at the pausing site will be explored further in the Discussion.

In order to fully explain the observed chromatin and DNA binding protein changes at the *FXN* locus it was necessary to measure the actual changes in *FXN* mRNA levels following a 24 h Tranylcypromine treatment.

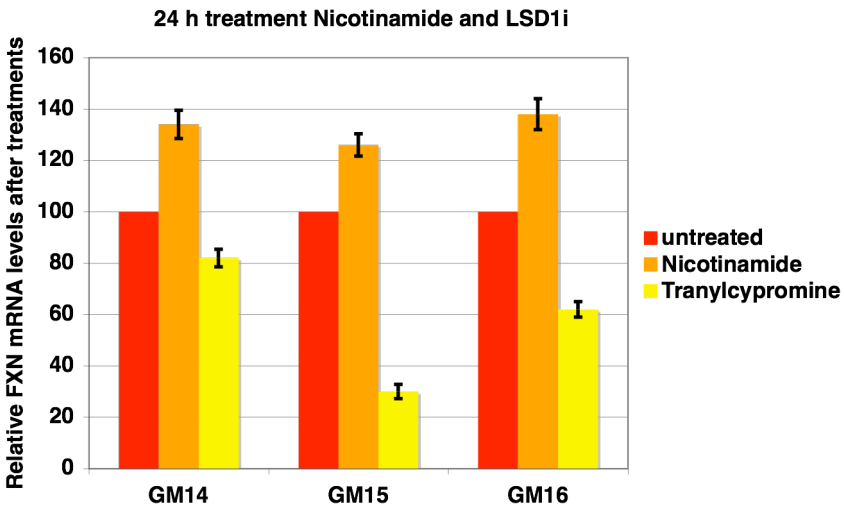

Figure 49: ***FXN*** **mRNA levels after a 24 h Nicotinamide and Tranylcypromine treatment of three EBV-cell lines. Displayed are relative** ***FXN*** **mRNA levels, each treatment of each cell line has been normalised to its respective untreated level and set 100 % (red). Nicotinamide treated samples are displayed in orange, Tranylcypromine treated samples in yellow. Each** ***FXN*** **ct-value has been normalised to** ***beta-actin*****. RNA was Q-real-time measured twice in triplicate and serial dilutions. The error-bars indicate the standard deviation of two independent experiments. Tranylcypromine treatment had the most severe effect on** ***FXN*** **levels of the FRDA GM15 EBV-cell line and a severe effect on GM16. The control GM14 EBV-cell-line showed only a minor decrease of ~20 % on** ***FXN*** **mRNA levels.**

An additional Nicotinamide treatment was performed in order to control the mRNA measurement. Nicotinamide treatment for 24 h showed the expected results with an ~ 1.3 fold increase, therefore the assay was verified. The control GM14 cell line responded with a relatively minor decrease of ~ 20 %. However, the greatest effect, with a decrease in *FXN* mRNA of ~ 70 % was seen in the relatively well expressing patient GM15 cell line. This is also in complete contrast to the levels detected after a 5 h DRB treatment, where the biggest effect was seen in the control GM14 cell line, whereas the FRDA GM15 cell line seemed hardly affected (Fig. 42). Interestingly, after 24 h of Tranylcypromine treatment GM16 shows also a more pronounced decrease of *FXN* mRNA levels (minus ~ 40 %).

In summary, the *FXN* mRNA levels measured are well in accordance with the observed H3K4me2 and H3K9me3 levels. The least affected GM14 cell line still exhibits similar levels of H3K4me2 and H3K9me3 when compared to the untreated sample. However, the negative elongation factor NELF-E and the insulator factor CTCF are more pronounced at the pausing site, probably accounting for a slight delay in releasing the elongating RNA pol II, which leads to a reduction in *FXN* mRNA levels. After the inhibition of LSD1, the patient GM15 cell line, showed a dramatic drop in the active mark H3K4me2 as well as a marked increase in the inactive H3K9me3 histone mark, which corresponds well with the decrease of *FXN* mRNA levels. Furthermore, in the case of an abnormal GAA repeat expansion a putative role for LSD1 in maintaining the open chromatin structure was suggested, by preventing heterochromatisation via the demethylation activity on H3K9me3. Moreover the additional amount of NELF-E at the pausing site might further hamper RNA pol II elongation, finally resulting in the ~ 80 % decrease of *FXN* mRNA. Interestingly, in this scenario the boundary factor, CTCF, decreased by ~ 25 %. Similar to the DRB treatment, the patient GM16 cell line does not exhibit a marked change in the pattern of H3K4me2 although an increase was observed at the pausing site. Moreover, the inactive H3K9me3 mark did not seem to change considerably, possibly because of the additional significant LSD1 recruitment and its extremely low initial level of *FXN* expression. Nevertheless after a 24 h Tranylcypromine treatment, the level of NELF-E increased and may possibly hamper the RNA pol II release additionally, resulting in a final decrease of ~ 40 % in *FXN* mRNA levels. In that scenario the patient GM15 cell line also showed decreased binding of the boundary factor CTCF (~ 25 %) to the RNA pol II pausing site. The differences observed in the decrease of *FXN* mRNA levels between the two patient cell lines might be caused by the existence of different rates of release from RNA pol II pausing. When untreated samples are compared, GM15 shows in contrast to GM16 a higher level of H3K4me2 indicating a higher rate of RNA pol II elongation. Therefore, after a period of 24 h Tranylcypromine treatment, the effect of additional NELF-E on *FXN* expression might be more severe in the low expressing GM15 cell line than in the very low expressing GM16 cell line.

Discussion

Discussion

Following the identification of an abnormal GAA repeat expansion as the cause of FRDA, many studies have focused on the properties of GAA repeat expansions. Although experiments showed the potential inhibitory effect of GAA repeat expansions on RNA elongation and chromatin structure (Bidichandani et al., 1998; Grabczyk et al., 2007; Grabczyk and Usdin et al., 2007; Krasilnikova et al., 2007; Krasilnikova and Mirkin, 2004), one has to bear in mind that most of these studies were conducted on plasmids and reporter genes. These artificial conditions may not reflect the actual cell response to an abnormal DNA/chromatin structure occurring at the *FXN* locus in humans. Since the GAA repeat is flanked by poly AAA sequences that are conserved in the chimpanzee and the human, it is possible that this sequence might have evolved a specific function in the human *FXN* (Fig. 6).

To date, in human no general promoter elements of *FXN* have been found (Greene et al., 2005), and surprisingly few studies have looked in detail at the regulatory elements of this locus. It is possible that the normal GAA repeat expansion has a function in regulating the human *FXN* gene. Furthermore, elements lying ~1000 bp 5' of the GAA repeat were recently proposed to contribute to the down-regulation of *FXN* (Greene et al., 2007). In this thesis it was demonstrated via ChIP and quantitative real-time PCR that *FXN* mRNA levels are relatively low (Fig. 10). Moreover, an over-expression of Frataxin was suggested to be toxic (Fleming et al., 2005). One can speculate that *FXN* transcription may be subject to tight regulation to ensure low levels of Frataxin. However, the progressive nature of FRDA and the mechanism underlying the severe down regulation of *FX*N transcription is still unclear.

In this thesis ChIP experiments revealed a RNA pol II transcriptional pausing site within a scarcely methylated CpG- island at exon 1 of the human *FXN* locus (Fig. 10). Gene regulation via RNA pol II pausing has been observed for a number of genes that are tightly regulated such as *c-myc*, *HSP70, MKP-1* and *HIV* (Fivaz et al., 2000; Krumm et al., 1995; Li et al., 1996; Palangat et al., 1998; Schneider et al., 1999). Thereby, the access and initiation of the basal transcription machinery is permitted, but further RNA pol II elongation is subject to negative regulation by factors that are

still mostly unknown (Svetlov et al., 2007). Therefore, this element may be a key regulatory feature of the *FXN* locus. Interestingly, genes regulated via pausing of the RNA pol II, such as *c-myc*, possess a triplex forming repeat structure downstream of this regulatory element (Belotserkovskii et al., 2007), suggesting a possible role for the triplex-forming GAA repeat in the function of the RNA pol II pausing site at the human *FXN* locus.

Each gene bearing an RNA pol II pausing site seems to possess a specific regulatory mechanism which may be triggered by hormones, heat-shock or specific transcription factors (Li et al., 1996; Mooney and Landick, 2003; Schneider et al., 1999; Wu et al., 2003), making it difficult to predict the factors involved in fine-tuning the regulation of the *FXN* gene. For example, Frataxin is thought to protect against cytotoxic stress that might also contribute to the fine-tuning of *FXN* gene regulation (Jiralerspong et al., 2001). In addition, NELF-E and CTCF previously identified on other RNA pol II pausing sites (Bao et al., 2007; Chernukhin et al., 2007; Wu et al., 2003; Yamaguchi et al., 1999; Zhang et al., 2007) were also found at the *FXN* pausing site and are therefore likely to play a regulatory role (Fig. 12 + 40). Notably, a regulatory response has been seen at the RNA pol II pausing site following treatment with the HDACi, Nicotinamide (Fig. 28). The *FXN* chromatin structure of the control GM14 cell line was modified as expected by increased levels of H4K16ac (Fig. 28), However, the ensuing effects on transcription may have been antagonised by the concomitant recruitment of NELF-E to the RNA pol II pausing site (Fig. 12). Furthermore, the treatment with increased concentrations of Nicotinamide (1 - 10 mM) showed a linear but only minor increase of *FXN* mRNA levels (up to 1.4 fold) (Fig. 27). Notably the other chromatin modifications tested were more or less unaffected (Fig. 10).

Given that NELF-E possesses an RNA-recognition-motif (Rao et al., 2006; Zhang et al., 2007) one can speculate that the RNA pol II pausing site may act in concert with the first intronic primary transcript of *FXN*. This RNA may also include the normal range of GAA repeats. The results from Nicotinamide treatment suggest two plausible regulatory mechanisms for *FXN*. The first mechanism could be due to the, increased transcription rate, which is facilitated by the enhanced open chromatin structure, leading to higher levels of RNA (primary intron 1). This in turn may feedback on NELF-E, leading ultimately to enhanced NELF-E levels at the pausing site, subsequently delaying the release of RNA pol II, and thereby antagonising

excessive *FXN* transcription (Fig. 30). The second mechanism is exclusively based on the chromatin structure change. Here, elevated levels of H4 acetylation and the resulting chromatin conformational change may trigger the additional recruitment of NELF-E to the pausing site. Interestingly, a recent study on *HIV* demonstrated an increase of transcription and replication of the virus after the depletion of NELF-E (Zhang et al., 2007), demonstrating a role for NELF-E in transcriptional regulation. Moreover, after NELF-E depletion elevated levels of acetylated H4 were observed, suggesting coupling of transcription elongation and chromatin remodeling (Zhang et al., 2007).

To date, the role of CTCF at the pausing site is not very well understood but it has been shown that CTCF is a component of the RNA pol II protein complex interacting directly with the RNA pol II (Chernukhin et al., 2007). Furthermore, CTCF shows different binding kinetics to each of the diverse RNA pol II phosphorylation states depending on its own phosphorylation status (Chernukhin et al., 2007). A stronger interaction was seen between CTCF and the unphosphorylated RNA pol II when compared to the hyperphosphorylated form of RNA pol II (Chernukhin et al., 2007). The fact that CTCF can be phosphorylated on multiple sites opens various possibilities for the influence of CTCF on the RNA pol II and its arrest or release (Chernukhin Igor et al., 2007). However, the lack of appropriate antibodies against the diverse phosphorylation states of CTCF, make it difficult at present to investigate these potential mechanisms in detail. Nevertheless, the potential role for CTCF as an activator was demonstrated in experiments where a single CTCF target site was sufficient to activate the transcription from a promoter-less reporter gene (Chernukhin Igor et al., 2007).

Considering the presented ChIP results on control cells and information from publications to date (Barski et al., 2007), one can envisage a new model for the transcriptional regulation of *FXN* in the case of a normal GAA repeat length. The presence of H3K4me2/me3 around the transcriptional initiation site and H3K27me1, H3K36me3, H4K20me1 and H2BK5me1 further downstream would be consistent with an open chromatin structure in the regions flanking the pausing site (Fig. 24). Furthermore, inactive marks are missing, such as H3K9me2/me3, H3K79me1, me2 and me3, potentially allowing access to the transcriptional machinery (Fig. 25). Assuming tight regulation of *FXN* is necessary, the identified factors NELF-E, CTCF

and LSD1 (Fig. 12 + 40 + 30) may play a role in the regulation of *FXN*. Moreover, at the pausing site a specific chromatin structure predominates allowing potential regulatory factors to bind (Fig. 10). The presence of both S5 and S2 phosphorylated forms of RNA pol II (Fig. 35 + 36) suggest an area where a switch from "initiated" to "sufficient" elongation may occur, probably partly regulated via the previously mentioned factors.

This new model seems consistent with the finding that following the inhibition of the kinase p-TEFb via DRB, the RNA pol II S2 phosphorylated form is no longer present and an ~ 40 % reduction of *FXN* mRNA levels occurs (Fig. 42). Considering that during a period of 5 h there was little change to the H3K4me2 pattern (indicating previously transcribed chromatin), it is possible that the final usage of S2 phosphorylated RNA pol II occurred towards the end of the 5 h treatment. It is noteworthy that, the levels of RNA pol II S5 did not change, showing the important function of p-TEFb, performing the switch from initiated to the efficient elongation form of RNA pol II S2 at the pausing site (Fig. 35 + 36). Therefore the almost unchanged H3K4me2 pattern may be explained via previously available RNA pol II S2 at the pausing site. Although at some point no efficient elongation was possible, the H3K4me2 pattern is still detectable, indicating a rather recent event. In order to address more precisely at which point this scenario occurred, further time point experiments will be necessary. NELF-E is also affected by the inhibition of DRB demonstrated by an increase of NELF-E at the pausing site (Fig. 37), which may lead to a delay in RNA pol II S2 release. This in turn may subsequently contribute to the 40 % decrease in overall *FXN* levels observed when compared to the untreated samples (Fig. 42).

The intriguing presence of the demethylase LSD1 at the pausing site led to the hypothesis that the demethylation of H3K4me2 may be an essential requirement for the establishment of the RNA pol II pausing site. Therefore, a Tranylcypromine treatment, which inhibits LSD1 demethylase activity, was performed for 24 h (Yang et al., 2007). Interestingly, the control GM14 cell line responded with a relatively minor decrease in *FXN* mRNA levels of ~ 20 % (Fig. 49), despite a slight increase of H3K4me2 (Fig. 44) and LSD1 levels around the pausing site (Fig. 46). The overall pattern of H3K4me2 and H3K9me3 was more or less unchanged (Fig. 44 + 46). However, the negative elongation factor NELF-E and the boundary factor CTCF

seemed to be more pronounced at the pausing site, the former probably accounting for a slight delay in releasing the productive-elongating RNA pol II, contributing to the observed reduction in *FXN* mRNA levels (Fig. 49). Despite an increase in H3K4me2 levels, the establishment of the RNA pol II S5 pausing at exon 1 was not disturbed by Tranylcypromine treatment, therefore it is unlikely that the activity of LSD1 alone is responsible for the set-up of the *FXN* pausing site. However, a minor negative effect on the *FXN* transcription rate was seen, accompanied by increased CTCF, NELF-E and LSD1 levels. This again suggests a change in the balance of factors at the RNA pol II pausing site, associated with the interruption of the usual configuration of an RNA pol II pausing site. It is tempting to speculate that the physiological role of the pausing site may strictly limit the level of *FXN* mRNA and up regulation may only occur in response to appropriate signals. The type of effects seen here following pharmacological manipulations and the effects of the GAA repeat expansion suggest that feedback mechanisms exist to impose limits on the level of Frataxin. Such mechanisms are likely to involve both the pausing element and the chromatin structure and will need to be considered when attempting to increase *FXN* levels via drug treatments that act on chromatin or influence RNA pol II pausing.

By using the primary transcript RNA FISH method it was evident that *FXN* expression although bi-allelic was not constant (Fig. 17). Here, the "5' probe" recognised the RNA 5' of the GAA repeat directly downstream of the RNA pol II pausing site (Fig. 6). Although ChIP experiments showed a clear presence of RNA pol II at exon 1, suggesting that this is true for most cells, not every cell displayed a primary transcript signal. In primary cells from a control individual, 77 % of cells displayed two signals for *FXN* expression, indicating a bi-allelic expression (Fig. 17). The remaining cells displayed either zero or one signal, possibly reflecting the paused RNA pol II in these cells, or a phenomenon similar to PEV (Fig. 17). Interestingly, further downstream, covering intron 3 and intron 4, less cells (65 %) displayed bi-allelic expression, indicating a loss in efficient expression along the *FXN* gene even in the presence of a normal repeat length (Fig. 17).

Taken together, it seems likely that the RNA pol II pausing site is partly regulated via factors such as NELF-E, CTCF and LSD1 and may interact with the primary transcript RNA levels produced as well as with the chromatin state of the *FXN* locus. Since NELF-E has already been suggested to act as a transcriptional attenuator

being important for controlling the duration and magnitude of transcriptional responses (Aida et al., 2006; Ping and Rana, 2001; Yamaguchi et al., 1999) this regulation is likely to occur at the *FXN* locus. Furthermore, the finding that several different drug approaches increased *FXN* mRNA only slightly by up to ~2 fold (Burnett et al., 2006; Gottesfeld, 2007; Herman et al., 2006) could be explained by the existing tight regulatory mechanism responding to changes either in chromatin structure or amounts of primary transcript RNA.

HP1-γ was detected at the RNA pol II pausing site. This occurred independently of the GAA repeat length, transcription or chromatin state (Fig. 12). HP1-γ has been shown to bind to some euchromatic regions (Lomberk et al., 2006) and growing evidence exists that the evolutionary conserved HP1's are involved in gene-specific regulation within both heterochromatin and euchromatin as activator and/or repressor molecules. Additionally, it was suggested that HP1γ acts as an anchor between heterochromatic and euchromatic regions of the nucleus (Lomberk et al., 2006). The presence of HP1-γ at the pausing site is intriguing and certainly warrants further investigation.

Chromatin structure of patients

Unexpectedly, the FRDA GM15 cell line derived from a patient with early stage FRDA demonstrated higher levels of open chromatin marks (H3K4me2 and H4K16ac) than the control GM14 cell line (Fig. 10), and possessed even less CpG- island methylation (Fig. 32). The finding that primary cells from FRDA patients also showed higher levels of H3K4me2/3 than controls (Fig. 19 + 20), questions the original hypothesis that a certain number of cells would attract heterochromatin via the GAA repeat expansions, resulting in a PEV similar phenomenon. Hereby, only a proportion of cells would still be able to fully transcribe *FXN,* ultimately leading to the severe decrease in *FXN* levels demonstrated in FRDA patient cells. However, the pattern found in the EBV-cell line GM16 demonstrates the potential of heterochromatin formation over the gene in case of a GAA expansion (Fig. 10). In this case, only a proportion of cells might be able to fully transcribe *FXN*, ultimately leading to the severe decrease in *FXN* levels. Such differences between patients may reflect different stages in the evolution of the disease and/or different extents of variegation.

The elevated levels of H4K16ac detected in cases with an abnormal GAA repeat expansion may occur as a physiological response to overcome the triplex structure provoked by the expanded GAA repeats (Jain et al., 2002; Mariappan et al., 1999). As previously discussed in the introduction, chromatin can be severely modified by the neutralization of the lysine charge through acetylation, thereby alleviating chromatin decondensation by increasing the accessibility to the nucleosomal DNA (Annunziato and Hansen, 2000; Kouzarides, 2000). In contrast to H3 acetylation, ensuring the proper control of gene expression, the acetylation of H4K16 seems to be more important for the chromatin structure and the regulation of the DNA topology (Chiani et al., 2006; Shogren-Knaak et al., 2006; Vaquero et al., 2007). Additionally, H4K16ac antagonizes certain residues connected to inactive chromatin marks, such as H3K9me3 (O'Neill et al., 2006; Vaquero et al., 2004).

Moreover, H4K16 acetylation has also been linked to DNA repair. DNA double strand breaks (DSB) can be repaired via homologous recombination and non-homologous end joining (Kruszewski and Szumiel, 2005; Murr et al., 2006; Pollard et al., 2007). Importantly, following DNA damage, acetylation occurs at specific residues of histone H4 such as K16 (Murr et al., 2006). In spite of this, these modifications are not involved in the repair process per se, but instead facilitate DNA repair by globally relaxing the chromatin, thereby allowing improved access to the repair machinery (Vaquero et al., 2007). Since GAA repeats and DNA triplexes have been reported to be prone to recombination events (Panyutin and Neumann, 1994; Panyutin et al., 2005; Ziemba et al., 2001), and triplet-repeat instability has been shown to be dependent on DNA repair pathways (Collins et al., 2007; Pollard et al., 2007), one can speculate that the "DNA damage response machinery" may be recruited to the *FXN* locus in FRDA patients. Furthermore, recent experiments in *E. coli* showed the involvement of RecA-dependent pathways in ensuring the integrity of expanded GAA repeats (Pollard et al., 2007). RecA is responsible for the post-replicative DNA repair (Spies and Kowalczykowski, 2006). Consequently, to secure further mitosis events the acetylation of H4K16 at the *FXN* locus of FRDA patients may be triggered in order to allow access for DNA repair and/or protection for the unusual chromatin structure (Pollard et al., 2007).

In contrast to the early-stage GM15 cell line, the late-stage FRDA patient GM16 cell

line lacked elevated H4K16ac marks, even with similar GAA repeat length (Fig. 10). Despite the similarity in repeat length, the chromatin situation may be different due to the low rate of expression occurring at the *FXN* locus. The phenomenon of heterochromatin at satellite repetitive DNAs may explain the difference between these two cell lines. Satellite repeats are usually predominantly heterochromatic, rarely transcribed and potentially prone to homologous recombination and non-homologous end-joining events (Warburton et al., 1993). These threats to DNA integrity are thought to be prevented by the establishment of heterochromatin (Yunis and Yasmineh, 1971). Since the GM16 cell line also displays a disturbed RNA pol II pausing site, this may lead to a lack of sufficient transcription and subsequently allow the formation of heterochromatin indicated by elevated H3K9me3 levels over the expanded GAA repeat, thereby possibly preventing further DNA damage at the *FXN* locus (Fig. 10).

Consequently, the DNA damage response machinery would target a GAA repeat expansion only if *FXN* is frequently transcribed. As this does not seem to be the case for GM16, this specific DNA protection mechanism would not be recruited and the second protective mechanism “heterochromatinisation” would take precedence in order to assure DNA integrity (Fig. 10). This model may also explain the phenomenon observed by Saveliev et al., (2003). Their repeat expansion was located downstream of the human CD2 transgene, and since these repeats were probably not transcribed they were therefore able to initiate heterochromatin formation (Saveliev et al., 2003).

It is noteworthy that in primary cells of FRDA patients a lack of H3K4me2 levels downstream of the pausing site has not been detected to date (Fig. 19). This may indicate a very late event rather than a predisposition for the FRDA onset or severity of the disease (Fig. 10). Since a transcription coupled repair mechanism was previously shown (Andressoo and Hoeijmakers, 2005), it seems possible that the RNA pol II itself serves as a tool for recognising DNA damage. Interestingly, the inhibition of elongation via DRB and Tranylcypromine treatment in the FRDA GM15 patient cell line (Fig. 39 + 46) induced an increase of H3K9me3 levels. Again this suggests that the activation of the DNA damage response machinery at *FXN* largely depends on the elongation activity of the RNA pol II. If this crucial factor is missing at the *FXN* locus, a GAA expansion has the potential to establish inactive chromatin

marks such as H3K9me3 (Fig. 10), possibly in order to prevent further DNA damage. However, this scenario seems to be an upstream event depending on the missing elongation rather than the prevention of RNA pol II elongation because of existing heterochromatin.

Notably, the levels of H3K4me2 and me3 observed at the beginning of *FXN* correspond to the length of GAA repeats (Fig. 20). Therefore, it is possible that a certain number of factors belonging to the DNA damage response machinery are recruited to the *FXN* locus, equivalent to the length of the GAA repeat. This in turn would lead, depending on the length of the GAA repeat, to a slowing down of the RNA pol II elongation. This may increase the probability of the methylation of H3K4 through Set1 (Santos-Rosa et al., 2002), leading to the observed repeat dependent increase of H3K4me2 levels (Fig. 20). Interestingly, a persistently stalled RNA pol II can result in either arrest of the cell cycle or pre-programmed cell death (Laine and Egly, 2006; van den Boom et al., 2002). This phenomenon may be one explanation for the progressive duration of FRDA, since in certain cell types, the problem of stalled RNA pol II at the GAA repeat may eventually lead to cell death, resembling the typical symptoms and features of ataxia (McLeod, 1971).

The proven increase of DNA methylation (Greene et al., 2007) at certain *FXN* areas of FRDA patients may be a further measurement of DNA protection to prevent mis-segregation or recombination events at GAA repeat expansions. The treatment of EBV-cell lines with the DNA methylation inhibitor 5-aza-2-deoxycytidine resulted typically in a decrease of ~ 40 % of *FXN* mRNA levels, and this may indicate the importance of certain amounts of DNA methylation at specific sites (Fig. 34). However, since 5-aza-2-deoxycytidine acts genome-wide (Ballestar et al., 2006) the detected down-regulation may also be secondary and be provoked by other factors influencing the regulation of *FXN*.

In addition to the differences seen in the chromatin structure around the expansion of GAA repeats the early stage FRDA GM15 patient cell line also displayed increased NELF-E, CTCF and LSD1 levels compared to the control GM14 cell line at the RNA pol II pausing site (Fig. 12 + 30 + 40). The increase of NELF-E may be caused, as explained earlier, either by an additional amount of *FXN* intronic RNA which may or may not include the abnormal GAA repeat expansion, or may simply be due to the

presence of acetylated H4 due to the GAA repeat expansion. However, to fully explain the presence of LSD1 at the pausing site (Fig. 30) in EBV-cell lines, one has to consider the results obtained following the 24 h Tranylcypromine treatment.

Here, the most dramatic effect of Tranylcypromine treatment on *FXN* mRNA levels was seen in the FRDA GM15 cell line (minus ~ 80 %) compared to the control GM14 (minus ~ 20 %) and the FRDA GM16 cell line (minus ~ 40 %) (Fig. 49). Furthermore, a severe increase in NELF-E levels over the pausing site was shown in all three EBV-cell lines (Fig. 45). Noteworthy is that the control GM14 cell line showed the highest increase despite the smallest effect seen on the mRNA level (Fig. 49). Since the elongation of the control GM14 cell line did not seem to be drastically affected, the NELF-E binding may partly depend on the transcribed *FXN* RNA. Here, again, in the case of lacking LSD1 activity a balancing mechanism was seen via the additional recruitment of NELF-E to the pausing site (Fig. 45).

Importantly, the inhibition of LSD1 led to a severe increase of H3K9me3 levels around the GAA repeat expansion in GM15 that was not seen in the control GM14 or the FRDA GM16 cell line (Fig. 46). However, the actual mechanism leading to this phenomenon is not easy to analyse. Two possibilities seem fitting. Firstly, the missing LSD1 activity at the pausing site may lead, to a disruption of the RNA pol II release, depending on the GAA repeat expansion. Thereby the missing RNA pol II elongation promotes the establishment of heterochromatic marks at the GAA repeat expansion in order to prevent possible DNA damage. However, this scenario seems not entirely convincing considering that the elongation of the control GM14 cell line was hardly affected by LSD1 inhibition, despite the increase of H3K4me2 at the pausing site. Here, a reasonable, although slightly delayed elongation was detected by the measurement of *FXN* mRNA levels (- 20 %) (Fig. 49) possibly via increased NELF-E levels. Therefore the second possibility gains more weight, where the inhibition of LSD1 may lead to the inactivation of its second crucial task, the demethylation of H3K9 at the expanded GAA repeat (Fig. 10). This may occur during RNA pol II elongation in order to allow the establishment of chromatin relaxing histone marks such as H4K16ac (Fig. 10).

Noteworthy is that following DRB treatment the amount of RNA pol II S5 at the pausing site of GM15 was slightly increased following the establishment of

heterochromatin when compared to the control GM14 (Fig. 36). This may additionally indicate a delay or disturbance of the switch from initiated (S5) to efficient elongation (S2 phosphorylation) of RNA pol II in case of present heterochromatic marks. Therefore, the unusual chromatin structure may prevent the escape from the pausing site and its efficient elongation as seen in the FRDA GM16 cell line by preventing this crucial step at the pausing site (Fig. 10).

Moreover, the FRDA GM16 cell line displays elevated LSD1 levels around the site where H3K9Kme3 occurs, however, for some reason the potential demethylation is not sufficient, and may also depend on the transcriptional rate. Unexpectedly, following Tranylcypromine treatment the amount of LSD1 increased in all three EBV-cell lines at the *FXN* locus, however the FRDA GM16 cell line shows an approximate threefold increase whereas the other two show roughly double the amount (Fig. 47). This raises the question whether LSD1 is fully functional in this cell line and the noted chromatin modifications of GM16 may be due to deregulation or dysfunction of LSD1. Furthermore, only GM16 displays an additional peak for the demethylase JARID1b at the pausing site (Fig. 39) that may be triggered through a missing demethylase LSD1 activity in this cell line (Fig. 47). However, another possibility for elevated levels of H3K4me2 at the pausing site of GM16 may occur in order to recruit more RNA pol II to overcome the present heterochromatic state (Fig. 10).

By measuring the levels of transcribed 5' UTR of *FXN*, it was shown that the FRDA patient GM15 cell line displayed ~ 2.2 fold of the control GM14. Since this method measures mRNA as well as primary transcript this result is surprising since *FXN* mRNA level of GM15 are considerably lower (Fig. 13). Therefore, this may be due to the more severe RNA pol II pausing or its delayed release from exon 1. This also indicates some sort of protection for the 5' UTR-RNA in the case of the paused RNA pol II (Fig. 10). Interestingly, the very low expressing GM16 cell line showed only 60 % of the 5' UTR levels present in the control GM14 cell line, suggesting two things. Firstly, the disrupted RNA pol II pausing site (Fig. 10) leads ultimately to less initiation of RNA pol II demonstrated via decreased levels of 5' UTR-RNA. Secondly, the 5' UTR present at the cytoplasmic mRNA may not be as stable or long-lived as the primary transcript 5' UTR present in the nucleus, since GM16 displays merely 10 % of the mRNA level that GM14 does, but still exhibits nearly 60 % of the measured 5' UTR (Fig. 13).

A delay in the release of the RNA pol II pausing site in the presence of a GAA repeat was also demonstrated via primary transcript RNA-FISH (Fig. 17). Since primary transcript RNA-FISH represents a snapshot of the actual transcription at a certain point in time, the observed differences between the control individual and the FRDA heterozygous and homozygous individuals are helpful (Fig. 17). Here, RNA-FISH experiment were performed on cells of a heterozygous and homozygous carrier for a GAA expansion, hybridized with a probe that recognises primary transcripts 3' of the pausing site. Both types showed a bi-allelic expression and roughly the same amount of cells displaying two signals (50 %) (Fig. 17). Since both types display different amounts of *FXN* mRNA levels (Fig. 33) this suggests that although the RNA pol II release may be affected in both cases, the elongation through the expanded GAA repeat is a crucial impediment to the ultimate amount of cytoplasmic mRNA.

A similar finding was observed for the RNA pol II ChIP experiment were both individuals presented an equally disturbed pattern over the pausing site (Fig. 19). However, 3' of the GAA repeat expansion the situation changed again, and as expected, the heterozygous individual showed less cells that did not express *FXN* (41 % versus 51 %) and had a higher percentage of cells possessing one or two signals (Fig. 17). This possibly accounts for the undisturbed elongation through the unexpanded allele following the delayed release of the RNA pol II pausing site.

Furthermore, the DRB treatment performed substantiates the idea of a delay of RNA pol II pausing release depending on the GAA repeat expansion (Fig. 35 to 42). Here, the largest effect on *FXN* mRNA levels is seen in the control GM14 cell line (minus 40 %) (Fig. 42) whereas the FRDA GM15 cell line merely displayed a decrease of 18 %. Unexpectedly, after a 5 h inhibition of RNA pol II S2 phosphorylation, the patient cell line GM15 still exhibits a reasonable amount of RNA pol II S2 (Fig. 35). The obvious explanation may be that after a 5 h period the lack of elongation is not as dramatic in the patient cell line when compared to the control GM14 cell line, since the RNA pol II S2 escape occurs to a lesser extent to begin with. Moreover, in contrast to the control GM14 line (Fig. 35), the pool of elongation competent S2-phosphorylated RNA pol II is still available and no adequate H3K4me2 levels are detectable, which would indicate elongation 3' of the pausing site. This may however be explained by the severe increase in the negative elongation factor NELF-E seen occurring predominantly in the GM15 cell line

(Fig. 37), thereby possibly hampering the release of the RNA pol II S2 (Fig. 35). Since GM15 also shows an increase in levels of RNA pol II S5 at the pausing site (Fig. 36), the pronounced H3K4me2 peak (Fig. 38) might occur through the additional targeting of Set1-like enzymes to the pausing site. These observations may also partly explain the observed H3K4me2 pattern in the presence of very little *FXN* mRNA as seen in GM16 (Fig. 8), where a redirection of Set1 methylation to the pausing site seems possible (Fig. 4).

Apparently, the *FXN* regulatory element is able to counteract chromatin or expression changes via various factors to balance these at the *FXN* locus. This was also seen following Nicotinamide treatment (Fig. 30). Here, the FRDA cell lines showed not only a slight increase in RNA pol II and *FXN* mRNA levels but also increased levels of NELF-E, MECP2 and LSD1 at the pausing site (Fig. 28 + 30). As discussed earlier one possibility is that NELF-E responds sensitively to increased H4 acetylation. Therefore, the relatively minor increase observed in NELF-E levels following Nicotinamide treatment may be due to the little changed H4K16ac state (Fig. 28). More surprising, the FRDA GM15 cell line lost the pronounced H3K4me2 mark 3' of the pausing site, accompanied by a binding of the demethylase JARID1 within the pausing site (Fig. 31). This indicates that the *FXN* locus possessing expanded GAA repeats is particularly sensitive to increased transcription rate or additional chromatin change mediated via a sirtuin inhibitor such as Nicotinamide. In this case an additional factor such as JARID1b is recruited (Fig. 31) and potential positive effects may get cleared. This result might also explain the rather poor increase in *FXN* levels after exposing EBV and primary cells to HDAC inhibitors in general (Gottesfeld, 2007; Grant et al., 2006; Hebert and Whittom, 2007; Sarsero et al., 2003).

Summary

It seems likely that in the case of an abnormal GAA repeat expansion occurring in FRDA patients, two events influence the transcription of *FXN*. Firstly, in the presence of a correctly functioning RNA pol II pausing site with a relatively frequent transcription rate, an open chromatin structure is established (Fig. 10). Thereby, access for the binding of proteins belonging to the DNA damage response machinery may be allowed in order to secure the integrity of the GAA expansion. This in turn

potentially slows down the RNA pol II elongation, however H4K16ac seems to be a sign of successful DNA repair (Murr et al., 2006), assuring the integrity of the DNA and allowing RNA pol II elongation even if at a slower speed. Secondly, the regulatory element represented by the RNA pol II pausing site seems to be additionally negatively influenced by the presence of a GAA repeat expansion. This may be triggered either via the abnormal chromatin structure and/or the occurring primary RNA transcript bearing the expanded GAA repeats. Therefore, initially a severe delay in RNA pol II release from the pausing site and subsequently an additional slowing down of the RNA pol II occurs through the expanded GAA repeats. These two events together lead to the observed severe drop in *FXN* mRNA levels (Fig. 8). Therefore, the RNA pol II pausing site may be a more suitable target for possible treatments for FRDA since the chromatin of the repeat probably should not be changed and furthermore the chromatin structure and/or the RNA of the GAA repeat itself might influence this regulatory element.

Identifying the factors and components, such as NELF-E and parts of the primary transcript RNA, playing a part in the orchestration of RNA pol II pausing and its release, may reveal a suitable and more specific drug target. Perhaps bypassing the inhibitory signal triggered by the GAA expansion to the RNA pol II release may lead to a more sufficient and stable increase in *FXN* levels. FRDA Acadian patients may be a valuable source in identifying these potential targets. This group of patients has a late onset with a much milder FRDA phenotype, despite long GAA repeats. Acadian FRDA patients may possess a disturbed feedback function on the pausing and release mechanism, which may allow more efficient transcription despite an expansion of the GAA repeat. That the sequence of the GAA repeat may indeed be important in regulating the RNA pol II pausing site is further suggested by the observation that expanded repeats bearing an interruption of $(GAGGAA)_{65}$ did not reveal any signs of FRDA (Cossee et al., 1997).

Future

Having identified the possibly crucial regulatory element of *FXN*, in the future it will be necessary to purify the protein complex mediating the RNA pol II pausing, thereby additional drug targets may be identified to allow a more specific drug design in order to enhance *FXN* transcription.

However, it will be important to clarify whether proteins belonging to the DNA damage response machinery, such as TIP60 or TRRAP, actually mediate the integrity of expanded GAA repeats. Furthermore, it will be essential to investigate whether stalling of the RNA pol II at the GAA repeat expansion indeed triggers apoptosis under certain circumstances. This scenario may be true for specific cell-types or certain transcription rates of *FXN*, and has to be investigated in detail in order to identify whether this phenomenon can be prevented in any way. This is a crucial point since apoptosis of the cell would be triggered because of the GAA repeat expansion, even if the lack of *FXN* would be supplemented e.g. via viruses possessing *FXN*.

Materials and Methods

Materials and Methods

General techniques

Deionised water (18.2 MΩ) was used to prepare all stock solutions and reactions. The only exceptions were fluorescence *in situ* hybridisation and RNA experiments where RNase-free sterile distilled water was used (BDH). All reagents were purchased from Sigma and all solutions and reactions were made up in water unless otherwise stated. All small volume centrifugation steps were carried out at room temperature using a desktop centrifuge (Eppendorf) and at 4°C in a refrigerated centrifuge (Beckman). A refrigerated centrifuge (Heraeus 1.0R) was used for larger universal and falcon tubes. DNA containing solutions were stored at -20°C in the short term and at -80°C in the long term. Solutions containing RNA were generally snap frozen and stored at -80°C. Mouse tissues were stored at -80°C. All antibodies were stored for short term at 4°C and long term at -20°C - if necessary in the dark. Oligonucleotide primers were obtained from SigmaGenosys, and stock solutions (100 µM) and aliquots (10 µM) were stored at -20°C. Commonly used solutions and buffers are shown below

5x TBE	450 mM Trisborate, 10 mM EDTA
10x TAE	400 mM Trisacetate, 10 mM EDTA
20x SSC	3 M NaCl, 0.3 M sodium citrate
10x TE	100 mM Tris-HCl, 10 mM EDTA
100x Denhardt's solution	2% (w/v) BSA, 2% (w/v) Ficoll 400, 2% (w/v) polyvinylpyrrolidone
Phenol:chloroform:isoamylalcohol pH 7.5	25:24:1 equilibrated with 10 mM Tris-HCl,
PBS (phosphate buffered saline)	171 mM NaCl, 3.3 M KCl, 10.1 mM Na_2PO4, 1.8 mM KH_2PO_4

Lysis solution	100 mM Tris-HCl pH 5.5, 5 mM EDTA, 200 mM NaCl, 0.2 % (w/v) SDS
LB-broth	1 % (w/v) bactotryptone, 0.5 % (w/v) bactoyeast extract, 1 % (w/v) NaCl
LB-agar	L-broth with 1.5 % (w/v) bactoagar
ChIP IP- buffer	150 mM NaCl, 50 mM Tris-HCl (pH 7.5), 5 mM EDTA, NP-40 (0.5 % vol/vol), Triton X-100 (1.0 % vol/vol). If necessary, add freshly prepared 0.5 μl 0.1 M PMSF in isopropanol and 1:1000 protease inhibitor cocktail (Sigma) per ml IP-buffer.
ChIP-beads	Protein-G-Agarose / Salmon Sperm DNA 50 % slurry from Upstate

Gel electrophoresis of DNA

Agarose gel electrophoresis was used to separate 50 bp - 10 kb DNA fragments. Electrophoresis was carried out using a horizontal gel electrophoresis apparatus (Gibco BRL), connected to a power supply (Biorad Powerpac 300). Agarose gels were usually made from 0.7 - 1.2 % agarose melted in 1x TAE buffer. After the agarose was cooled down to ~ 60°C, 0.5 µg/ml of ethidium bromide solution was added and mixed well. The agarose was cast in a horizontal gel tray and wells were formed with a suitable comb. The electrophoresis buffer consisted of 1x TAE. DNA solutions were re-suspended in 1x loading buffer (0.125 % w/v orange G; 1x TAE; 30 % glycine), prior to loading into the wells for the gel. Electrophoresis was carried out at 60 V. DNA size markers (DNA Ladder, Low Range or High Range and MBI Fermentas) were run simultaneously with the samples. DNA was visualised with a GelDoc 2000 (Biorad) system using Quantity One software linked to an Apple Macintosh G4 computer.

DNA digestion with restriction endonucleases

DNA was digested with restriction enzymes using the manufacturers' supplied 10x restriction buffers and digestion temperatures (Boehringer Mannheim or New England Biolabs). Plasmid DNA was digested for one to two hours at the appropriate temperature, with 1x restriction buffer and 1x BSA if necessary. Generally 3 units of enzyme were used for each µg DNA with the volume of restriction enzyme not exceeding one tenth of the reaction volume.

Phenol: chloroform extraction of DNA from proteins

Proteins were removed from aqueous solutions of DNA by extraction with equal volumes of phenol: chloroform: isoamylalcohol (25 : 24 : 1). Centrifugation at 12,000 g for 15 minutes at room temperature separated the phases. The aqueous (upper) phase was retrieved, avoiding contamination with any protein at the interface between the organic and aqueous phases. A further equal volume phenol : chloroform : isoamylalcohol 25 : 24 : 1 extraction was performed and again the aqueous phase retrieved. Finally the solution was extracted with equal volumes of chloroform to remove traces of phenol and the DNA was recovered by ethanol precipitation. For genotyping transgenic mice by PCR no precipitation was performed. One µl of the aqueous phase was used per reaction following the first phenol : chloroform : isoamylalcohol extraction.

Precipitation of DNA

DNA was precipitated from low salt solutions by mixing with one tenth of the volume with 3 M of sodium acetate (NaOAc) at a pH of 5.0 and precipitated by mixing it with two volumes of 100 % ethanol. Occasionally when DNA was precipitated from a large volume, one volume of 100 % isopropanol was substituted for absolute ethanol. The remainder of the procedure was identical. DNA yield was determined by spectrophotometry with NanoDrop (ND- 1000).

Measurement of DNA concentration

The concentration of DNA in an aqueous solution was determined by the absorption of ultra violet light (UV- light) at 260 nm. As the fraction of the absorbed UV radiation

is directly proportional to the concentration of DNA, an optical density value (OD_{260}) of 1 equals a concentration of 50 µg/ml. The purity of the solution is given by the ratio of $A_{260/280}$. This ratio should be around 1.8.

Purification of DNA from agarose gels

DNA fragments from 120 bp to 10 kb were isolated from TAE agarose gels using the Qiagen-kit following the manufacturers' instructions. The gel slice was weighed and dissolved at 50°C in an appropriate volume of dissolving buffer (provided with the kit). The DNA/agarose solution was loaded onto a microfuge spin column and spun for 1 min at 13,000 rpm. DNA adsorbed to the column and was washed with 750 µl of the provided washing buffer. The DNA was eluted by adding 30 µl of water onto the column and incubated for 1 min at room temperature before centrifugation at 13,000 rpm for 1 min.

Transformation of bacteria and purification of recombinant DNA

Chemically competent E. coli DH5α (Invitrogen) cells were routinely used. 50 µg/ml of ampicillin was used in agar plates and bacterial growth media to select for the pCR®4-TOPO (4.0 kb) plasmid.

2 µl of the ligation reaction were mixed with 25 µl of competent cells (Invitrogen) and kept on ice for 30 minutes. The cells were heat shocked at 42°C for 30 seconds, followed by the addition of 250 µl of SOC-medium and incubated at 37°C for 1 hour. Cells were plated onto LB-agar plates containing ampicillin and incubated at 37°C overnight. Single colonies were picked, inoculated into 3 ml of LB-broth containing ampicillin and again cultured overnight at 37°C.

Extraction of total RNA with Trizol (Invitrogen)

Total RNA was extracted from human lymphocytes and mouse tissues using Trizol. ~10^6 cells were washed in PBS by centrifugation at 1,300 rpm for 7 minutes at 4 °C. The cell pellet was gently loosened and resuspun in 1 ml of Trizol. Lymphocytes were homogenised by pipetting up and down, mouse tissues were homogenised by using the ultra-thorax. Samples were then incubated for 5 minutes at room temperature. 200 µl Chloroform per 1 ml Trizol was then added and samples were

vigorously shaken for at least 15 seconds and incubated for further 2 to 3 minutes at room temperature. Samples were centrifuged at 12.000 g for 15 minutes at 4°C. The upper aqueous phase was then transferred into a fresh tube and 500 µl Isopropyl alcohol (per 1 ml Trizol) was added. Samples were incubated at room temperature for 10 minutes and again centrifuged at full speed for 10 minutes at 4°C. The RNA-pellet was washed once with 1 ml of 75 %-ethanol (DEPC-water) and centrifuged at 7.500 g for 5 minutes. The RNA pellet was briefly dried for 5 to 10 minutes and re-spun in DEPC-water. Samples were stored at -80°C.

Complementary DNA (cDNA) amplification (RT-PCR)

For the reverse transcription reaction, ~5 µg of RNA were mixed with 1 µl of random primers (hexamers), 1 µl dNTP and water to obtain a final volume of 12 µl. The mix was heated up to 65°C for 5 minutes and immediately chilled on ice. Afterwards, 8 µl of well vortexed 4 µl 5x first strand buffer, 2 µl DTT and 1 µl RNasin were added. The mixture was then incubated for 2 minutes at 25°C. To start the reaction 1 µl of ThermoScript II (Invitrogen) was added and incubated for 10 minutes at 25°C, followed by 1 hour at 50°C. To neutralise the remaining RNA, 2 µl of RNase H (10 units) was added followed by an incubation at 37°C for 30 minutes. To inactivate RNase H the samples were incubated for 5 minutes at 85 °C and then kept at -20 °C.

EBV-transformed cell lines

Lymphoblastoid cell lines were obtained from Coriell Cell Repositories[4] that had been established by Epstein-Barr virus transformation of peripheral blood mononuclear cells using phytohemaglutinin as a mitogen. The basic culture conditions for lymphoblasts were 15 ml of RPMI 1640 Medium (plus 2 mM of L-glutamine, 15 % heat inactivated fetal calf serum (FCS), and 100 µg/ml of Penicillin/Streptomycin (GIBCO) in T25 tissue culture flasks.

GM14926: healthy individual, male, 38, Caucasian.
GM15850: early onset not specified, blood sample taken at the age of 13, GAA repeats (650/1030), male, Caucasian.

[4] http://locus.umdnj.edu/nigms/nigms_cgi/quick.cgi

GM16234: onset at 20 years, blood sample taken at the age of 39, GAA repeats (580/1030), female, Caucasian. All stated repeat lengths are published by Coriell, and were determined by southern-blot analysis.

EBV transformation of blood

The patients' blood was diluted 1:1 with RPMI (+ 20 % heat inactivated FCS) and carefully layered over 15 ml of Ficoll-paque in a 50 ml universal tube (ethical approval is in place). The blood was then continuously centrifuged at 2,000 rpm for 20 minutes. The lymphocyte layer was carefully removed with a sterile plastic pipette. The lymphocytes obtained were washed twice with RPMI (+10 % FCS), first at 1,800 rpm for 4 minutes and a second time at 1,200 rpm for 4 minutes. After the 2nd centrifugation the lymphocytes were counted and re-spun with an aliquot of EBV-virus. The suspension was incubated for 1 hour at 37°C in a water bath. The cells were then distributed between the wells of a 24-well plate at approximately 2x 10^6 cells/well in a volume of 1.5 ml/well with 10 μg/ml of PHA (1 % of the final concentration of a previously prepared 1mg/ml stock). The cells were cultured and split as required. Usually it took at least 8 weeks till enough cells were grown in order to store them in liquid nitrogen for future experiments.

Preparation of EBV-virus suspension

A vial of B95-8 marmoset cell line was thawed in a 37°C water bath and transferred to a 15 ml test tube. 10 ml of medium RPMI (+ 20 % FCS) was added a drop at a time. The cells were then centrifuged at 800 rpm for 5 minutes, the supernatant was removed and the cells washed again. Afterwards the cells were re-spun in 50 ml of medium (+10% FCS) and transferred into a 75 cm^2 flask. The cells were then grown to a high density and the medium was changed within 2 days. Finally the flask was cultured for 7 days until the medium was bright yellow. The cells were then centrifuged at 1,200 rpm for 5 minutes and the supernatant was filtered through a 0.22 μm filter into freezing vials. The vials were frozen in liquid nitrogen and the cells were frozen separately in 10^7 cells/vial according to the cell freezing protocol.

Freezing cells

For the freezing of cells, 1.5 ml of 10 % DMSO in RPMI and 30 % FCS were added drop wise with constant agitation to the re-spun cell pellet (25 cm^2 flask). The cell suspension was dispensed into labelled freezer vials and placed into “Mr. Frost”. Cells were stored for at least 3 days at -80°C and then transferred into liquid nitrogen.

FICOLL for lymphocyte extraction of human blood

To separate lymphocytes from human blood, 15 ml of Ficoll was placed in a 50 ml Falcon tube and topped up with 30 ml of whole blood/PBS suspension. The suspension was spun at 1,500 rpm for 20 minutes at room temperature. The top layer was discarded and the inter-phase containing the lymphocyte layer were transferred into a 15 ml Falcon tube containing 5 ml of pre-warmed PBS/10% FCS and centrifuged at 1,200 rpm for 5 minutes. The lymphocyte pellet was washed twice in 10 ml 1x PBS at 4°C. Finally the cells were suspended in 1 ml PBS and immediately spotted onto poly-L-coated slides.

GAA-genotype human

In order to differentiate between heterozygous and homozygous samples a PCR reaction with the Expand High fidelity Kit (Roche) was performed. All steps were done on ice. First Mix1 was set-up containing 1 μl NTP’s, 1 μl Primer Left, 1 μl Primer Right, 0.8 μl DNA and 22.2 μl H_2O, per reaction. Mix1 was vortexed briefly and the Mix2 was prepared to contain 19.25 μl H2O, 5 μl Buffer and 0.75 μl enzyme. After slight vortexing Mix2 was added onto Mix1 and again mixed. The program was performed as followed: 94°C for 2 min; 10 cycles of 94°C for 15 sec, 53 °C for 30 sec, 68°C for 4 min; 20 cycles of 94°C for 15 sec, 58°C for 30 sec, 72°C for 4 min; 72°C for 7 min; 12°C indefinitely. Primer Left: ACTTTGGGAGGCCTAGGAAG
Primer Right: TCCAGAGATGCTGGGAAATC

Primary transcript RNA FISH *in situ* hybridisation

Fixation of cells for RNA *in situ* hybridisation

Two small spots (~ 15 µl) of a single cell suspension were immediately pipetted onto poly-L-coated slides. The cells were allowed to settle for 90 seconds and carefully transferred into fixative.

The fixation-tray (22.5 cm x 40 cm) was filled with 500 ml of Fixation solution (4 %-formaldehyde, 5 % acetic-acid in normal saline).

After 17 minutes fixation, slides were washed three times in 3 different Coplin jars in 1x PBS for 5 minutes each. After washing, slides were dehydrated for 5 minutes in 70 % ethanol (DEPC) and stored in 70 % ethanol at -20°C.

Protocol for preparation of single-stranded DIG-labelled DNA probes for RNA-FISH

300 µg of plasmid DNA was linearised in a volume of 300 µl containing 100 units of the appropriate restriction enzyme for 2.5 hours at 37°C. The digest was analysed on an agarose gel and the DNA extracted with the Qiagen Extraction-Kit according to manufacturer's instructions. The DNA was re-spun in 100 µl RNase-free water.

For the *in vitro* transcription, 10 µg DNA, 10 µl of rNTP's (100 mM), 29 µl water, 20 µl 5x T7 buffer, 1 µl RNasin and 10 µl of either T3 or T7 polymerase were mixed and incubated at 37°C for 4 hours. After incubation 2 µl of DNase I (20 units) were added and incubated for 20 minutes at 37°C. To extract the RNA, 40 µl of 6.6M NH_4Ac and 140 µl phenol/chloroform (pH 4.5) were added. The mixture was carefully vortexed and centrifuged at full speed for 10 minutes. After centrifugation most of the soluble phase was removed and the remaining back-extracted with an additional 30 µl of water. The 'back extract' and the soluble phase were combined and chloroform extraction performed. To precipitate the RNA 425 µl ice cold ethanol was added to the soluble phase and incubated overnight at –20°C. After incubation the RNA was spun at 13,000 rpm (4°C) and the pellet washed once with 70 % ethanol (DEPC-water), the pellet was briefly air-dried and dissolved in 100 µl DEPC-water. An aliquot was run on an agarose gel to ensure the RNA was intact and the OD was measured to check purity and concentration.

Reverse transcription reaction

For the reverse transcription reaction ~5 µg of RNA was mixed with 0.5 – 1.5 µl of random primers (hexamers) and 7.3 µl dNTP-dDIG (or later dUTP-FITC, dUTP-Tetramethylrhodamine) Water was added to obtain a 12 µl final volume. The mix was heated up to 65°C for 5 minutes and immediately chilled on ice. Afterwards, 4 µl of well vortexed 5x first strand buffer, 2 µl DTT and 1 µl RNasin were added. The mixture was then incubated for 2 minutes at 25°C. To start the reaction 1 µl of ThermoScript II (Invitrogen) was added and incubated for 10 minutes at 25°C, followed by 1 hour at 50°C. To neutralise the remaining RNA, 2 µl of RNase H (10 units) was added followed by incubation at 37°C for 30 minutes. If the cDNA was labelled for an RNA-FISH probe, the probe was purified using the Qiaquick Nucleotide Removal Kit and eluted into 50 µl ddH_2O.

Prehybridisation treatment

Slides were equilibrated for 5 minutes in 70 % ethanol followed by 5 minutes equilibration in 0.1 M Tris-HCl (pH 7.5), 0.15 M NaCl (TS) at RT. To access the nuclei a 0.01 % pepsin digest was performed in 0.01 M HCl for 5 minutes at 37°C. Slides were rinsed briefly in distilled, DEPC-treated H_2O, to neutralise most of the pepsin and fixed for 5 minutes in 3.7 % formaldehyde/PBS at RT. After fixation, slides were washed in PBS for 5 minutes at RT and stepwise dehydrated in 70 %, 90 % and 100 % ethanol (3 minutes each) and air-dried.

Negative control

To test if the protocol recognised RNA only, separated slides were incubated with 100 µg/ml RNase (Roche, DNase free) in 1x PBS for 25 minutes at 37°C prior to hybridisation, followed by three washes of 5 minutes each and a stepwise dehydration as described before.

Hybridisation

The hybridisation mix contained 1-5 ng/µl of a single stranded DNA probe. With slides lying flat, the hybridisation mix with the denatured probe was applied immediately, adjacent to the spot of cells (40 µl). The slides were gently covered with cover slips and incubated in a humidified chamber (2x SSC plus 25 % formamide) at

37°C over night. After incubation cover slips were removed by dipping the slides briefly in 2x SSC. The slides were then washed three times for 10 minutes in pre-warmed 2x SSC at 37°C. One additional wash was performed for 5 minutes in 0.1 M Tris-HCl, pH 7.5, 0.15 M NaCl, 0.05 % TWEEN 20 (TST) at RT.

Depending on the labelling of the probe, slides were blocked pre-incubation in 0.1 M Tris-HCl, pH 7.5, 0.15 M NaCl, containing blocking reagent from Roche[5] (TSB). 100 µl of TSB was applied directly onto the slide while lying flat and covered with 24 x 60 mm cover slips. Slides were incubated for 30 minutes in a humidified chamber (TS soaked paper) at room temperature. After removing the cover slip and the excess blocking solution the first primary antibody diluted in 100 µl of TSB was applied, covered with a cover slip and incubated in a humidified chamber for 30 minutes at room temperature. After incubation, slides were washed twice for 5 minutes in TST at room temperature, followed by application of the secondary antibody diluted in 100 µl of TSB and covered with cover slips and incubated in a humidified chamber for 30 minutes at room temperature. After applying and incubating all necessary antibodies, slides were washed twice for 5 minutes in TST at room temperature followed by 10 minutes DAPI-staining in TST- solution. Slides were again washed for 5 minutes in TST and washed for 5 minutes in TS at room temperature. Finally the slides were stepwise dehydrated in 70 %, 90 %, 100 % ethanol (3 minutes each) and air-dried. Mounting media was applied and sealed-in with a coverslip.
Slides were analysed with a Delta-vision microscope set-up from Olympus and images were processed with SoftWorX software. Slides were stored at 4°C for up to 6 months.

Chi-square test

A very quick and simple statistical test to determine the probability of the obtained results by chance, under a specific hypothesis, is the chi-square test. In this case the chi-square test is ideal to evaluate the statistically significant differences between proportions of two or more groups in a data set. For this purpose the normal individual is used as the standard, and the heterozygous and homozygous patient present the samples tested.

[5] Blocking Reagent number 1 112 589

$$\chi 2 = \frac{(\text{Sample} - \text{Standard})^2}{\text{Standard}}$$

By adding the obtained $\chi 2$ values for each different signal distribution reveal differences between groups when compared to the normal standard.

Chromatin Immuno-Precipitation

Preparation of *in vivo* cross-linked chromatin (Joel D Nelson et al., 2006)

Recipes for the buffer used in the preparation and immuno-precipitation of chromatin are found on page 130. Cells were fixed *in vivo* by the addition of 40 µl of 37 % formaldehyde per ml RPMI-medium and incubation for 15 min at room temperature. The cross-linking reaction was quenched by the addition of 125 mM of glycine and incubated for 5 minutes. Fixed cells were then pelleted by centrifugation at 1,200 rpm for 8 minutes and washed twice with ice cold PBS. Cells were lysed by adding 1 ml of IP-buffer containing protease inhibitors, resuspending the pellet and pipetting up and down several times in a micro-centrifuge tube. Nuclei were then centrifuged at 12,000 g for 1 min at 4°C and then supernatant aspirated. The nuclear pellet was washed again with 1 ml IP-buffer (+ inhibitors). To shear the chromatin, the washed pellet was re-suspended in 1 ml IP-buffer (+ inhibitors) per 10 million cells and sonicated for 30 minutes at a high level for 15 sec with a pause of 25 sec in ice water. The lysate was cleared by centrifugation at 12,000 g for 10 min at 4°C. The supernatant was distributed into new tubes, snap frozen and stored at -80°C. One vial was used for isolate all the DNA, to determine shearing efficiency and as a control for the amount of input DNA used in precipitation.

For immunoprecipitation the antibody of choice with the recommended concentration was added to the chromatin and incubated in an ultrasonic water bath for 30 minutes at 4°C. Afterwards chromatin was spun at 12,000 g for 10 min at 4°C. Protein-G-Agarose beads (20 µl per IP sample) which had been washed three times, were added to new tubes and ~ 90 % of cleared IP-chromatin was added and incubated for at least 2 hours on a rotating wheel (20 to 30 rotations per min) at 4°C. As a control for unspecific binding, chromatin with no added antibody was added to the same amount of beads. Following incubation samples where washed five times with 1 ml of IP-buffer (without inhibitors).

DNA was isolated by adding 100 µl of 10 % Chelex-100 slurry to washed IP-samples. Samples were briefly vortexed and boiled for 10 minutes. The boiled suspension was centrifuged for 1 min at 12,000 g at 4°C and 80 µl of the supernatant were transferred into a new tube. Afterwards 120 µl of water (NANOpure) was added to the beads, vortexed for 10 s and again centrifuged. This supernatant was then pooled with the previous one and used for further real-time PCR analysis. The purified DNA can be used in PCR at up to 25 % of the reaction volume.

ChIP-chop assay

The ChIP-chop assay published by Sasha Preuss and Craig Pikaard (2007) was slightly modified and performed as the figure below describes.

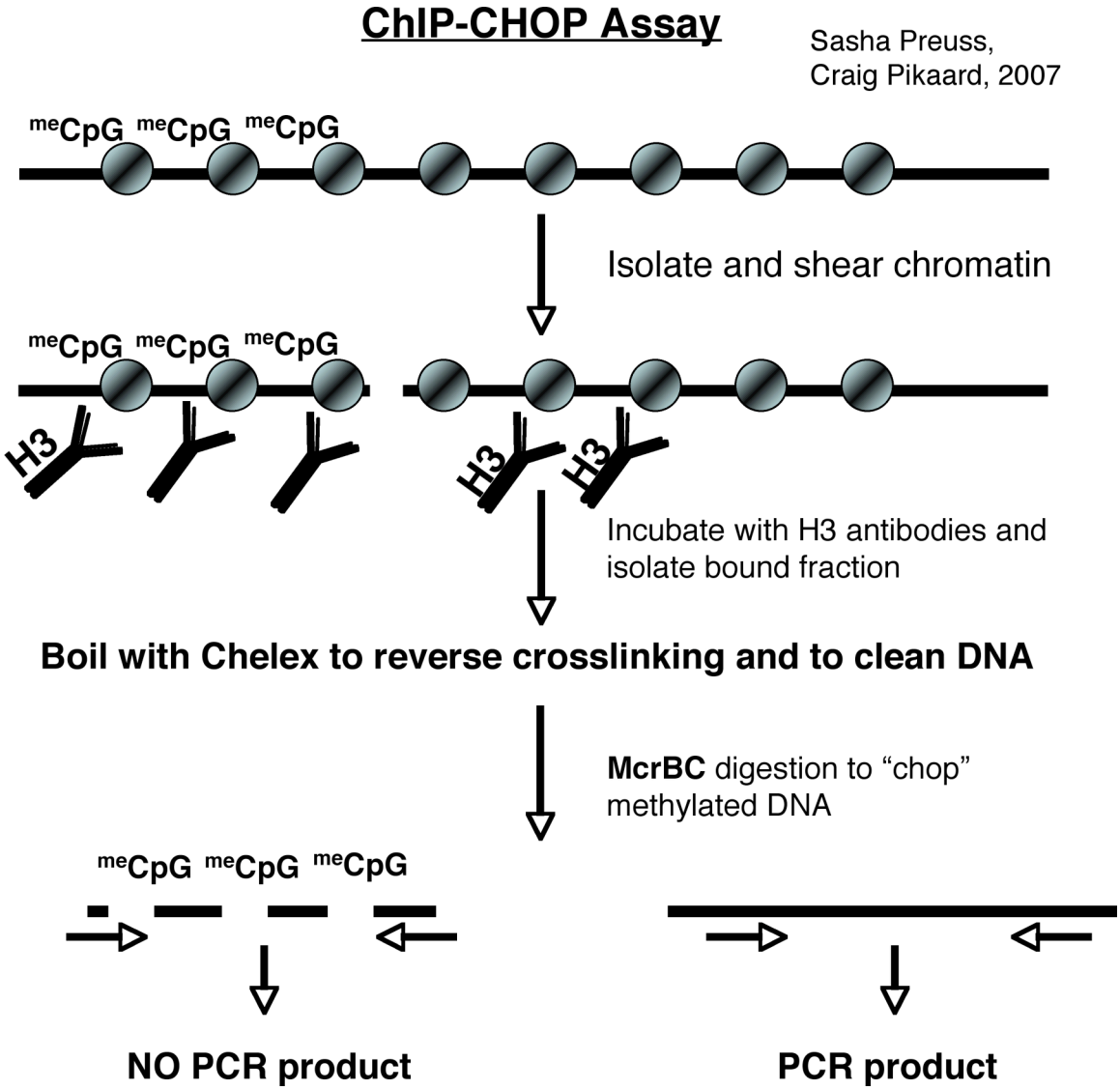

Figure 50: Visualisation of ChIP-chop technique. For each reaction, 100 µl post-IP chromatin was used. Adapted from Preuss et al., 2007.

Real-time PCR analysis

Recovered DNA was quantified by real-time PCR amplification using the Jumpstart SYBR Green Pre-mix kit (Sigma) and the standard curve method. A 20 µl reaction was set up containing 10 µl pre-mix and 100 to 200 nM primers. Standard curves (7 points of 2- fold serial dilutions) and samples for each primer pair were set up in duplicate and analysed on a Chromo4 DNA engine (MRJ), running the appropriate Opticon acquisition and analysis software. A typical PCR program was 94°C for 2 minutes followed by 39 cycles of 94°C for 40 seconds, 59°C for 40 seconds, 72°C for 40 seconds, plate read, 75°C for 1 second, plate read, 80°C for 1 second, plate

read, 82°C for 1 second and plate read. This program was followed by a melting curve analysis (74°C to 96°C, plate read every 0.2°C, 1 second hold at each temperature) to ensure the absence of primer dimmers and that the plate was read at an adequate temperature for each primer pair. The cycle threshold was arbitrarily set on an intersection with the linear range of the amplification curves observed on a logarithmic scale. The Delta-Delta C_T method was used to obtain an approximate change in values for control versus target samples. As this method assumes that the reference (*beta-actin* for mRNA levels and *GAPDH* for ChIP) and target gene (*FXN*) have similar efficiencies, each designed primer pair was tested to meet this criteria. In case of validating mRNA levels, measurements were performed in three serial dilutions order to ensure accuracy. In case of validating ChIP experiments each C_T per tested antibody was normalised against the C_T of histone H3. In order to validate the ChIP efficiency H3 was normalised to 10 % of the Input. Furthermore, to account for cell line differences each patient EBV-cell line was normalised to the control GM14 cell line. All analysis of real-time PCR values was performed using Microsoft Excel software.

Primers

PCR primer design

Oligonucleotides for use in PCRs were all designed using Primer3 software (http://frodo.wi.mit.edu/cgi-bin/primer3/primer3_www.cgi) (Rozen and Skaletsky, 2000).

Primers for human FISH probes

Primer name	Sequence	Product length
FXN probe 5' GAA repeat Left	TTCCTGGAACGAGGTGAAAC	560 bp
FXN probe 5' GAA repeat Right	CTCCGGAGAGCAACACAAAT	
In4Probe2L	TGGCAACCCGATAGCAGTA	504 bp
In4Probe2R	GGGCTAGTTCATCCACCTCA	
In3Probe3L	GTGGCCACTGTCTGTGCTAA	942 bp
In3Probe3R	TGATGTCTCTCCTGCCTCCCT	
In4Probe4L	CTGGGCGACAGAGTGAGACT	863 bp
In4Probe4R	CTGGAGTGCAGTGGTGTGAT	
In2Probe6L	CAACAAGAAGCCACCGGTAT	555 bp
In2Probe6R	CGTAGGAGAGGCTGGTTGAC	
In1Probe7L	GATGGTACCTGGTGGCTGTT	372 bp
In1Probe7R	GTAGATGCAAGGGGTGGAGA	
In3newLeft	GAAGCGTGCATTTTGGATTC	680 bp
In3newRight	AACCAAACGCAGCTGCTAGA	

CD19 primer for RNA FISH on human

Primer name	Sequence	Product length
CD19 In4/5 L	CTGCAATTCACAAACCCAAC	315 bp
CD19 In4/5 R	CAGACTCAAAGTCCCAAGCTG	
CD19 In7/8 L	CACTCTCCTCATCCCTCCAA	360 bp
CD19 In7/8 R	GAGAGGGGCATTGTAAGACG	
CD19 cDNA L	AGAACCAGTACGGGAACGTG	741 bp
CD19 cDNA R	AACATTGCTCCAGAGGTTGG	
CD19In4-5(2)L	GGGCATCCTTCTTTTTCCTC	749 bp
CD19In4-5(2)r	TCTCAAGGAACCGCAAGTCT	
CD19In5-6(2)L	GGCCAGTCTGACAACCATCT	393 bp
CD19In5-6(2)R	GTGCCTGTAATCCAGCACT	

Human Primers for genotyping GAA repeats

Primer name	Sequence	Product length
GAA-PrLeft	ACTTTGGGAGGCCTAGGAAG	~250+ GAA
GAA-PrRight	TCCAGAGATGCTGGGAAATC	
Pr5ChIP_2trL	GCTGCGTCTTTAACGTTTCC	247 bp
Pr5ChIP_2trR	CACACTCAGCCCCTTACCAT	

Human Primers for real time RNA *FXN* levels

Primer name	Sequence	Product length
UTR and Exon 1 Left	AGCAGCATGTGGACTCTC	157 bp
UTR and Exon 1 Right	CAGGTCGCATCGATGTCG	
Exon 4 to Exon 5 Left	ATCCAGTGGGGACCTAAGC	132 bp
Exon 4 to Exon 5 Right	AAGGAAGACAAGTCCAG	
Exon 1 to Exon 5 Left	GACATCGATGCGACCTG	376 bp
Exon 1 to Exon 5 Right	CAGTCCAGTCATAACGC	
Exon 2 to Exon 5 Left	GAACCAACGTGGCCTCA	338 bp
Exon 2 to Exon 5 Right	CAGTCCAGTCATAACGC	
Beta-actin RT Left	GCGGGAAATCGTGCGTGACATT	220 bp
Beta-actin RT Right	GATGGAGTTGAAGGTAGTTTCGTG	

Human Primers for ChIP

Primer name	Sequence	Product length
P1 upstream FXN 6114bp Left	GGGATTTCTTTTCCCCAGAG	190 bp
P1 upstream FXN 6114bp Right	ACCTTGCAGGACACCAAAAC	
P2 upstream FXN 1735bp Left	CCCCACATACCCAACTGCTG	127 bp
P2 upstream FXN 1735bp Right	GCCCGCCGCTTCTAAAATTC	
CpG_1 FXN Exon 1 1322bp Left	GGAGCAGCATGTGGACTCTC	189 bp
CpG_1 FXN Exon 1 1322bp Right	CGGCGCGGATACTTACTG	
CpG_2 FXN Intron 1 1006bp Left	CTCCCGGTTGCATTTACACT	155 bp
CpG_2 FXN Intron 1 1006bp Right	GTGACAAGCATGGAGACAGC	
P3 FXN Intron 1 633bp Left	CTGACCCGACCTTTCTTCCA	123 bp
P3 FXN Intron 1 633bp Right	TGGGCGTCACCTTTATCTTC	
P4 FXN Intron 1 383bp Left	GAAACCCAAAGAATGGCTGTG	116 bp
P4 FXN Intron 1 383bp Right	TTCCCTCCTCGTGAAACACC	
P5 FXN Intron 1 241bp 3' G Left	CTGGAAAAATAGGCAAGTGTGG	117 bp
P5 FXN Intron 1 241bp 3' G Right	CAGGGGTGGAAGCCCAATAC	
P6 FXN Intron 1 878bp 3' G Left	CCCTTGCACATCTTGGGTAT	177 bp
P6 FXN Intron 1 878bp 3' G Right	GAGAAAAGGGTGGGGAAGAG	
P7 FXN Intron 1 5494bp 3' G Left	AGCCCCACATTCTCAGACAC	172 bp
P7 FXN Intron 1 5494bp 3' G Right	ACGCACCAAAGGGTAACTTG	
CpG_In2 FXN Intron 2 Left	ACCGTGTTATCTGCCTGC	176 bp
CpG_In2 FXN Intron 2 Right	CTGGTCTGAACTCGTGAC	
Beta-globin Exon 2 Left	GCTGGTGGTCTACCCTTGGA	150 bp
Beta-globin Exon 2 Right	AGGTTGTCCAGGTGAGCCAG	
GAPDH gene Exon 4 Left	CACCGTCAAGGCTGAGAACG	134 bp
GAPDH gene Exon 4 Right	ATACCCAAGGGAGCCACACC	

Antibodies

Antibody	Company	Dilution used
RAT anti- Dinitrophenyl hapten	Serotec, MCA 1212	1.25 : 1000
FITC-donkey – anti- GOAT	Jackson ImmunoResearch Number: 705-096-147	1:50 – 1:200
FITC-goat - anti RAT	Jackson ImmunoResearch Number: 112-096-068	1:50 – 1:200
Sheep anti- Digoxigenin	Roche, 1333089	1:800
Rhodamine Red-X-conjugated anti- SHEEP	Jackson ImmunoResearch Number: 713-295-003	1:500

Antibodies for Chromatin Immunoprecipitation

Antibody	Company	Concentration	Amount used
H3 K9 tri methyl, rabbit polyclonal	Abcam, ab8898	400 µg/ml	2-4 µg per IP
Anti-HP1α, mouse monoclonal IgG_1	Upstate, Cat. 05-689, Lot 30223	0.57 µg/µl	2-4 µg per IP (5 µl)
Anti-HP1γ, mouse monoclonal IgG_1	Upstate, Cat. 05-690, Lot 0608038477	2 µg/µl	2-4 µg per IP (3 µl)
Anti-H3, rabbit polyclonal IgG	Upstate, Cat. 06-755	0.9 µg/µl	2-4 µg per IP (3 µl)
Anti-H3 K4 di-methyl, rabbit polyclonal IgG	Abcam, ab7766	0.5 µg/µl	2-4 µg per IP
Anti-H3 K4 tri-methyl, rabbit polyclonal	Abcam, ab8580	Concentration varies	2-4 µg per IP
Anti-H3 K9 di methyl, rabbit polyclonal IgG	Abcam, ab7312	Concentration varies	2-4 µg per IP
Anti-H3 K9 acetyl, rabbit polyclonal IgG	Upstate, Cat. 06-942	2 µg/µl	2-4 µg per IP
Anti-H3 K9 acetyl, rabbit polyclonal ChIP grade	Abcam, ab4441	1 µg/µl	2-4 µg per IP
Anti-H3 S10 phospho, mouse monoclonal	Upstate, Cat. 05-598, Lot 26436	2 µg/µl	2-4 µg per IP
Anti-H3 K14 acetyl, rabbit polyclonal IgG	Upstate, Cat. 06-911,	2 µg/µl	2-4 µg per IP
Anti-H3 acetyl	Upstate, Cat. 06-599, Lot 29505	1 µg/µl	2-4 µg per IP
Anti-H4 K16 acetyl, rabbit antiserum	Upstate, Cat. 07-329, Lot 26818	2 µg/µl	2-4 µg per IP
Anti-H4 K20 tri methyl rabbit polyclonal IgG	Abcam, ab9053	500 µg/ml	2-4 µg per IP
Anti-UBF	Santa Cruz, SC-13125, Lot K0805	0.2 µg/ml	2 µg per IP
Anti-MeCP2, rabbit polyclonal	Upstate, Cat. 07-013	2 µg/µl	2-4 µg per IP
Anti-H3, rabbit polyclonal	Abcam, ab1791	Concentration varies	2 µg per IP
Anti-RNA polymerase II CTD repeat YSPTSPS (phospho S2)	Abcam, ab5095	Concentration varies	5 µg per IP
Anti-RNA polymerase II CTD	Abcam, ab5131	Concentration	5 µg per IP

repeat YSPTSPS (phospho S5)		varies	
Anti-SUV39H1, mouse monoclonal, ChIP grade	Abcam, ab12405	2.3 μg/μl	5-10 μg per IP
Anti-NELFe, sheep polyclonal	Abcam, ab28038	Whole antiserum	5-10 μl per IP
Anti-CTCF, rabbit polyclonal	Abcam, ab10571	0.3 μg/μl	15 μl per IP
Anti-LSD1, rabbit polyclonal	Abcam, ab17721	1 μg/μl	5 μg per IP

Abbreviations

Abbreviations

A	adenine
ac	acetylated
AR	androgen receptor
ATP	adenosine 5’-triphosphate
BAC	bacterial artificial chromosome
bp	base pair
BSA	bovine serum albumin
C	cytosine
cDNA	complementary deoxyribonucleic acid
CHD1	chromodomain helicase DNA binding protein 1
ChIP	chromatin immunoprecipitation
Co A	coenzyme A
CO_2	carbon dioxide
CpG	cytosine-phospho-guanine
CTCF	CCCTC-binding factor
CTD	C-terminal domain
DAPI	4',6-diamidino-2-phenylindole
ddH_2O	double distilled water
DDR	deoxyribonucleic acid damage response
DIG	digoxigenin
DNA	deoxyribonucleic acid
DNase	deoxyribonuclease
Dnmt	deoxyribonucleic acid methyl transferase
DPE	downstream promoter element
DRB	5,6-dichloro-1β-ribofuranosylbenzimidazol
DSB	deoxyribonucleic acid double strand break
dsDNA	double-stranded DNA
DSIF	DRB sensitivity-inducing factor
dUTP	2’-deoxyuridine 5’-triphosphate
E. coli	*Escherichia coli*
EDTA	ethylendiamintetraacetatic acid
ES	embryonic stem
e. g.	for example

EGFP	enhanced green fluorescence protein
et al.	et alii
EtOH	ethanol
FCS	fetal calf serum
Fig.	Figure
FISH	fluorescence *in situ* hybridisation
FITC	fluorescein isothiocyanate
FRDA	Friedreich's ataxia
FXN	human frataxin locus
Fxn	mouse frataxin locus
G	guanine
GCN5	general control non-derepressible 5
H	histone
h	hour
HAT	histone acetyl transferase
HDAC	histone deacetylase
HDACi	histone deacetylase inhibitor
Het	heterozygous
HIV	human immunodeficiency virus
HKMT	histone lysine methyltransferase
HMT	histone methyl transferase
Hom	homozygous
HP1	heterochromatin protein 1
HSV-1	herpes simplex virus 1
i.e.	that is
ISC	iron sulfur cluster
Jmj	Jumanji
K	lysine
kb	kilobase pairs
kg	kilo gram
l	litre
M	molar
M&M	materials and methods
MDa	mega Dalton
MBD	methyl CpG binding domain

me	methylated
mg	milligram
min	minutes
MitoQ	mitochondrial targeted Idebenone
ml	millilitre
mM	millimolar
mRNA	messenger RNA
N	adenine / cytosine / guanine / thymine
NELF	negative elongation factor
ng	nano gram
NMR	nuclear magnetic resonance
NP	neural progenitor
NTP	nucleotide triphosphate
NuRD	nucleosomal remodelling and histone deacetylase
NURF	nucleosomal remodelling factor complex
OD_x	optical density at a wavelength of x nm
PAF	polymerase associated factor
PBS	phosphate buffered saline
PCR	polymerase chain reaction
PEV	position effect variegation
pH	pH value
ph	phosphorylated
PK	protein kinase
pol	polymerase
p-TEFb	positive transcription elongation factor b
H_xR_x	$histone_x$ at $arginine_x$
R	purine
RB	retinoblastoma
RNase	ribonuclease
RNA	ribonucleic acid
rpm	rounds per minute
RT	room temperature
SDS	sodiumdodecylsulfate
sec	second(s)
Ser	serine

SIR	silent information regulator
SSC	sodium chloride / sodium citrate
ssDNA	single stranded DNA
S/T	serine/threonine
SUMO	sumoylated
T	thymine
Tab.	Table
TAE	tris-acetate-EDTA-buffer
TE	tris-EDTA-buffer
Tris	tris (hydroxymethyl)-aminomethane
ub	ubiquitinylated
UTR	untranslated region
UV	ultra violet
Vol	volume(s)
Wt	wild type
Y	pyrimidine
YAC	yeast artificial chromosome
YFH1	yeast frataxin homolog
%	percent
°C	degree Celsius
%w/v	weight/volume
%v/v	volume/volume

Appendix

Appendix

Experiments on transgenic mice

Friedreich's ataxia is a tissue specific disease where the main pathogenic sites are the heart, the cerebellum, the dorsal root ganglion and the spinal cord (McLeod, 1971). Evidently, it is difficult to obtain these affected tissues from patients. Therefore, a mouse model should be the ideal source to overcome this problem. As stated in the introduction, several mouse models are already available with each holding advantages and disadvantages in studying Friedreich's ataxia. During the course of this project the results of a murine chromatin modification genome-wide mapping approach became available (Mikkelsen et al., 2007), and to complete the picture, the murine *frataxin* locus will be investigated in the following paragraph.

Chromatin modifications genome wide map approach[6]

In Mikkelsens et al. article, the application of single-molecule-based sequencing technology for high-throughput profiling of histone modifications in mammalian cells was the central theme. Chromatin marks such as H3K4me3, H3K9me3, H3K27me3, H3K36me3 and H4K20me3 were investigated on different cell types, like ES-cells, neural progenitor (NP) cells and embryonic fibroblasts (MEF). As a basic principal it was found that H3K4 and H3K27 trimethylation effectively discriminate genes that are expressed, poised for expression, or stably repressed, and therefore reflect cell state and lineage potential. The trimethylation of lysine 9 and lysine 20 was detected at satellite, telomeric and active long terminal repeats, being able to spread into proximal unique sequences. Imprinted regions were found to hold lysine 4 and lysine 9 tri-methylation marks. Finally, they were able to show that the chromatin state can be read in an allele-specific manner by using single nucleotide polymorphisms.

Chromatin modifications at the *Fxn* locus

The transcription of the murine *frataxin* starts from the opposite strand of the DNA and the most pronounced signal of histone marks available is the H3K4me3 at the

[6]Nature articles: doi:10.1038/nature06008: genome wide maps of chromatin state in pluripotent and lineage-committed cells, TS Mikkelsen et al., 2007

beginning of the gene, indicating active transcription (Bernstein et al., 2002). Since there are no data available for the promoter or the untranslated region, it was not possible to investigate this region in detail. Nevertheless, chromatin data sets for three different cell types of *Fxn* are available, showing a minor difference between all three cell types for the H3K4me3 mark. The signal in the more specialised NP cell although not as broad is equally high as in the ES cell. The H3K36me3 modification indicates recently transcribed chromatin (Barski et al., 2007), increases towards the end of the gene and does vary between all three cell lines. The H3K27me3, H3K9me3 and H4K20me3 modifications, indicating inactive chromatin (Barski et al., 2007), show minor peaks throughout the gene and no significant differences between the three cell types. The IP data for the RNA pol II at the *Fxn* locus was not available.

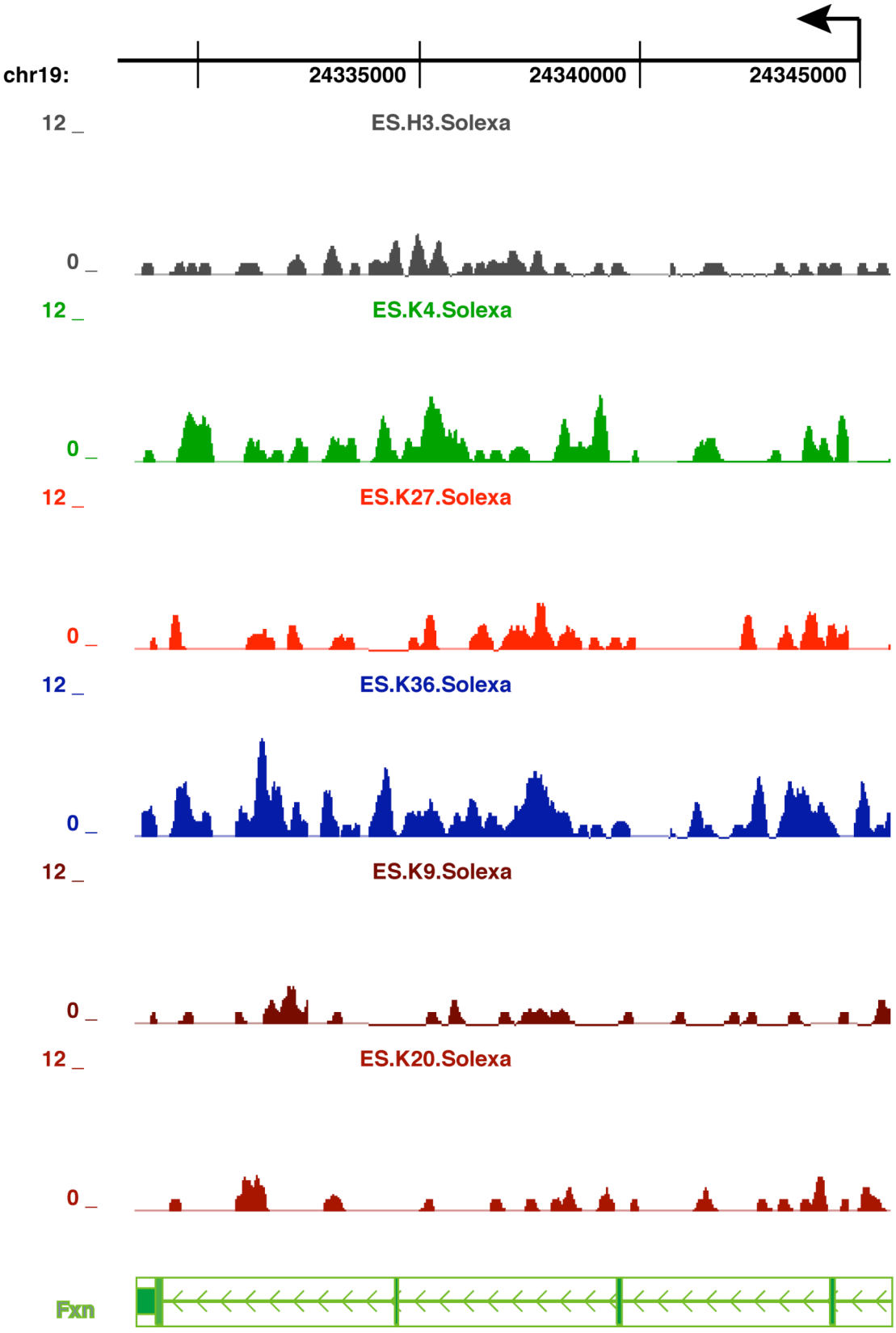

Figure 51: **Displayed are H3K4me3 (K4), H3K27me3 (K27), H3K36me3 (K36), H4K20me3 (K20) at the murine *Fxn* in embryonic stem cells. In general the active marks predominate versus the inactive ones. Position of exons is indicated in green bars, the arrows indicate direction of transcription. Exact position of *Fxn* at chromosome 19 is given in top scale.**

The following figure 52 shows the histone modifications detected at the *Fxn* in neural progenitor cells. In general no obvious major change is detectable between these two cell types.

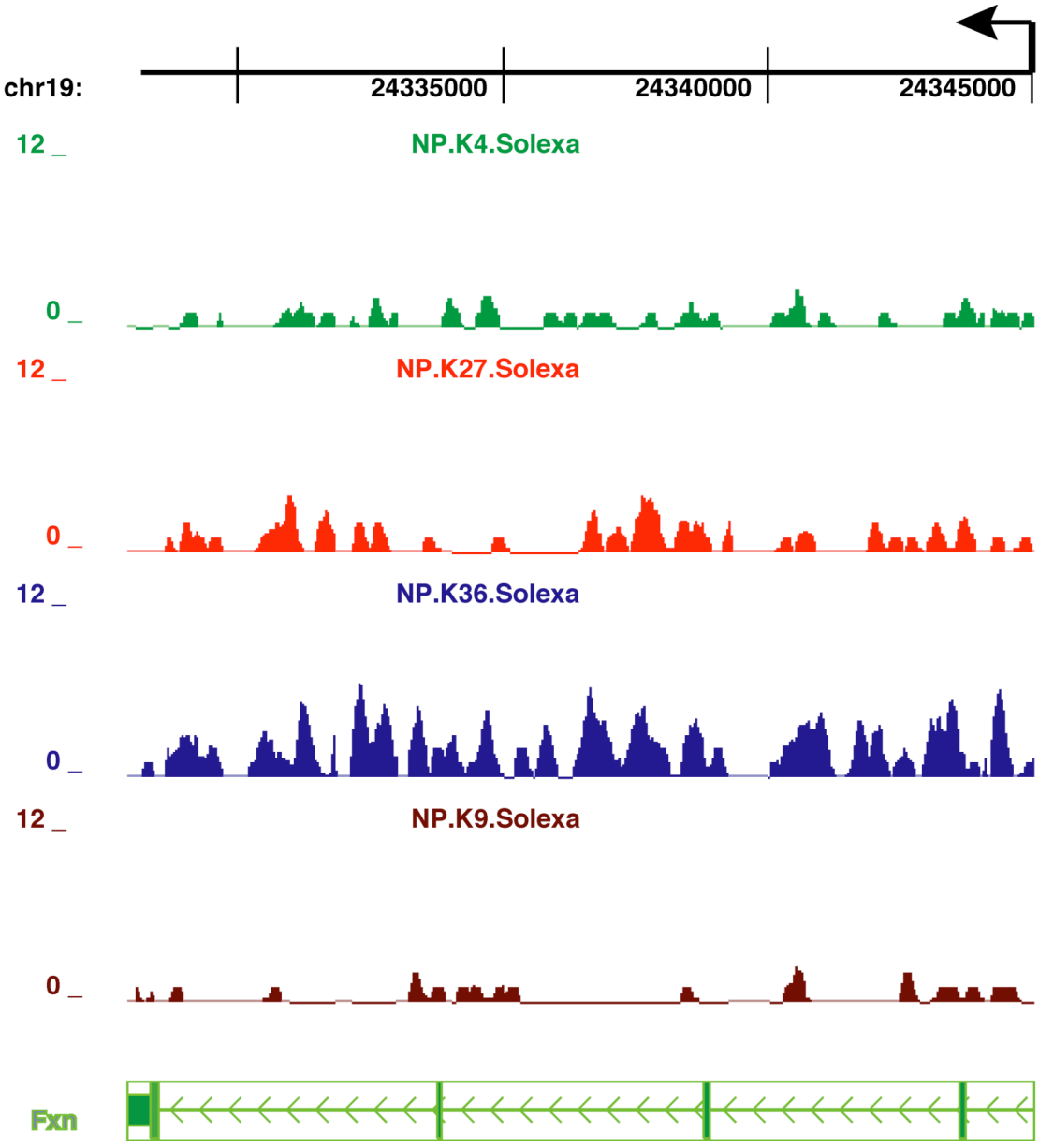

Figure 52: Displayed are H3K4me3 (K4), H3K27me3 (K27), H3K36me3 (K36) and H3K9me3 (K9) of NP-cells. Again the active mark H3K36me3 predominates along *Fxn*. Position of gene is given in top scale, exact position of exons is given in corresponding green bars below histone diagrams.

The following figure 53 illustrates the same histone marks for MEF- cells. Here an increase in the active H3K36me3 mark is seen. However, the other available modifications show similar pattern to the ES and the NP cells.

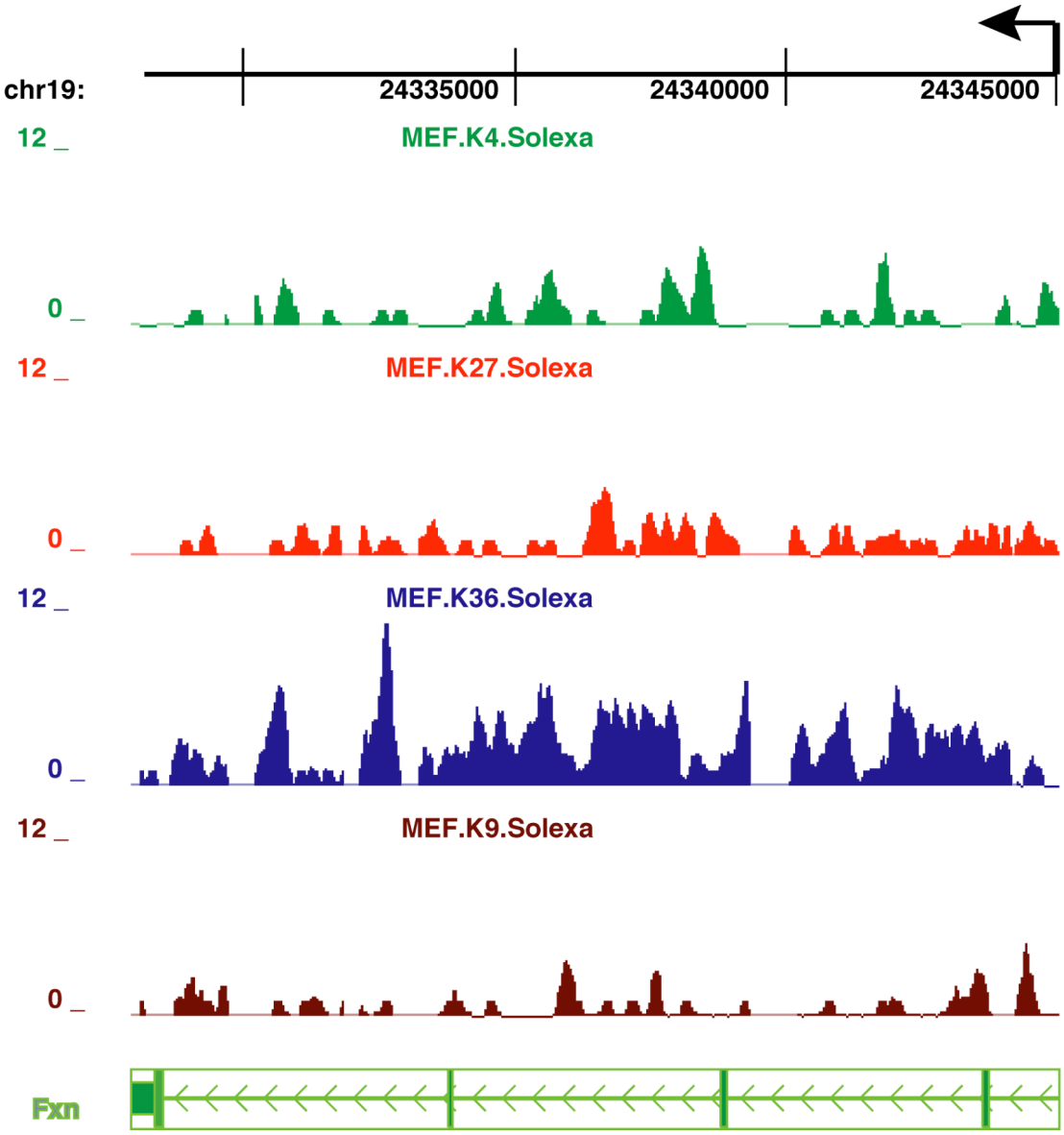

Figure 53: Displayed are H3K4me3 (K4), H3K27me3 (K27), H3K36me3 (K36) and H3K9me3 (K9). Only the active H3K36me3 mark displays slightly higher levels compared to the cell types introduced earlier. Again position of gene is given in top black scale, exact position of *Fxn* exons is given in green bars below.

To summarise, the murine *Fxn* displays similar to the human, mainly active chromatin marks. These do vary between certain tissues to a certain extend suggesting that these histone modifications might play a part, or reflect, tissue-specific transcriptional regulation of the *Fxn* gene. The next section will discuss the tissue specific expression of *Fxn* in more detail.

Murine *frataxin* expression levels in different tissue types[7]

The database introduced in this article, also provides information on mRNA expression levels obtained from the GNF expression atlas 2 (GNF1M Mouse Chip). For the murine *frataxin* mRNA the following levels were obtained and stated in the table below. *Fxn* mRNA levels are categorised into relatively high expressed (on the website marked in light red), moderately expressed (marked in dark red), and weakly expressed (marked in green). Tissues where there was no data available are marked in black.

Relatively high expressed	Moderately expressed	Weakly expressed	No data available
Thymus	Spleen	Frontal cortex	Cerebellum
B-cells	Bone marrow	Substantia nigra	Hippocampus
$CD8^+$-T-cells	Heart	Amygdala	Preoptic
Bone	$CD4^+$-T-cells	Hypothalamus	Olfactory bulb
Skeletal muscle	Thyroid	Dorsal stratium	Upper Spinal cord
Vomeronasal organ	Large intestine	Eye	Trigeminal
Placenta	Snout epidermis	Lower spinal cord	Adrenal gland
Embryo at day 6.5	Tongue	Dorsal root ganglia	Pituitary
	Embryo at day 9.5	Lymph node	Salivary gland
	Embryo at day 10.5	Mammary gland	Pancreas
		Prostate	Kidney
		Adipose tissue	Liver
		Brown fat	Trachea
		Bladder	Digits
		Uterus	Embryo at day 7.5
		Stomach	Embryo at day 8.5
		Small intestine	
		Lung	
		Epidermis	
		Testis	
		Oocyte	
		Fertilised egg	
		Blastocysts	

Table 6: Diverse mouse tissues show certain *Fxn* expression level. Data was obtained from GNF expression atlas 2 (GNF1M Mouse Chip) provided Mikkelsens et al.

Additional information is given for developmental stage-specific expression. Here, the investigation of embryonic day 14.5, revealed weak expression in the spinal cord, the medulla oblongata, the dorsal root ganglia and the lung. At post-natal (P) day 14, the

[7] **Nature articles: doi:10.1038/nature06008**

Fxn expression in the dorsal root ganglia is restricted to the cortical region where the sensory neuron cell bodies are located. In non-neural tissues, a strong expression was seen in the developing liver from day E10.5 onwards. Moreover, murine *frataxin* expression was detected in the heart and the cortex of the developing kidney from day E12.5 onwards. High expression was observed in the brown adipose tissue in small islands around the neck and back at day E14.5, then highly abundant during days E16.5 and E18.5 but disappeared from the brown adipose tissue from day P14 onwards. On day E14.5 until post-natal life, expression was also seen in the thymus and the developing gut. Prominent *Fxn* expression was found on day P14 in the spleen whereas in the thymus this was restricted to the proliferating cells in the cortical zone.

From this analysis, most affected tissues in human Friedreich's ataxia, like spinal cord and dorsal root ganglia, are naturally low expressed in mice. However, one cannot assume that the same situation is true for the human but parallels could still exist. For this reason the following scenarios are thinkable. The inhibiting effect of the expanded GAA repeat might be more severe in the case of tissues expressing at low levels. One can speculate that the cell should have a self-regulating ability; thus, it might be able to up-regulate *frataxin* expression in response to low protein levels. However, following the idea presented in the result section I and II that humans might possess a strict regulatory mechanism of *FXN,* it seems that in human this regulatory mechanism is not controlled by the amount of *frataxin* protein levels. A simple and very efficient regulation for the cell would therefore be a regulation controlled via the produced primary transcript RNA, possibly implicating the normal GAA repeat expansion. Consequently, an abnormal GAA expansion would greatly disturb this in low expressing tissues even tighter regulated mechanism, primarily affecting tissues with a tight *frataxin* regulation such as the spinal cord where only low levels naturally occur. Since the mouse does not exhibit a GAA repeat naturally, it seems unlikely that this part of the DNA or RNA plays a role in the tight regulation the normal *Fxn* regulation. Therefore in mice, although a lack of sufficient *Fxn* might lead to a similar phenotype, the underlying mechanism leading to the dramatic decrease in low expressing tissues might be different.

Homology mouse and man

Considering the argument above, there might be an additional explanation why a mouse model using the murine *frataxin* fails to present a phenotype. Even though a homology on the mRNA level of ~ 85 % occurs between mouse and man, the first exon along with the intron does not seem to have any homology at all. Demonstrated in Results I and II before, the human *FXN* exon 1 has a rather crucial function in regulating gene expression as no common promoter was identified so far. Moreover, the GAA repeat is flanked by special sequences already implicated in the RNA pol II pausing. This structure along with the GAA repeat is highly conserved in primates but absent from mice.

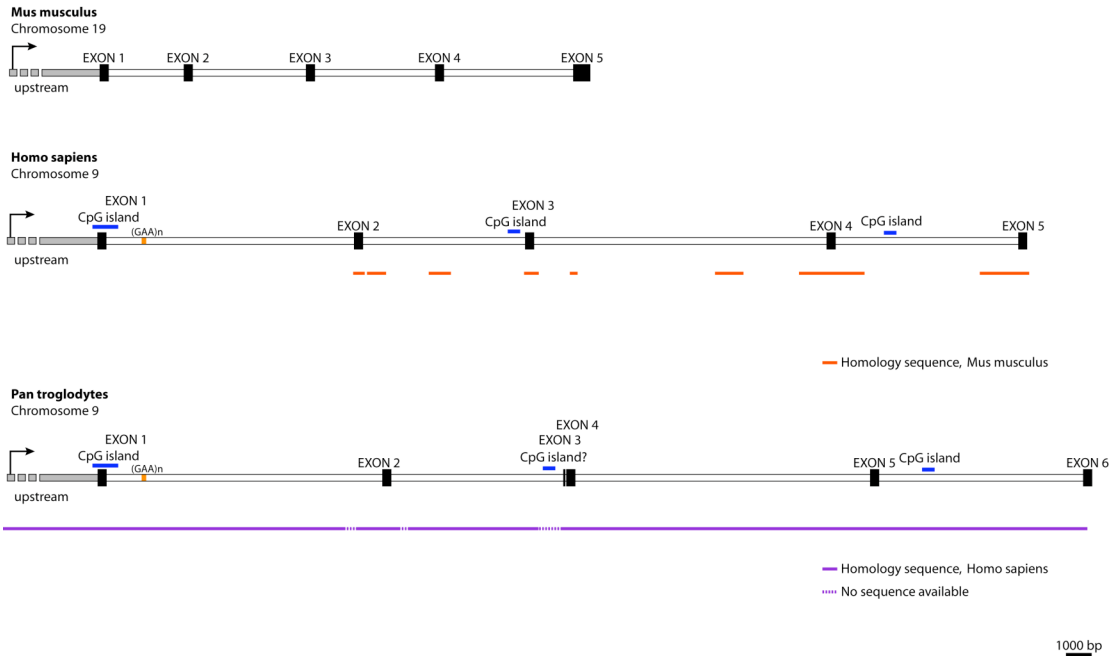

Figure 54: Homology between mouse and man is marked with red bars. Exons and introns are depicted only schematic not in proportion. Exon 1 and intron 1 show no homology between mouse and man. Homology between chimpanzee and human is marked in purple.

This could indicate a different *frataxin* regulatory mechanism between mouse and man. If the normal sized GAA repeat did play a role in the human *frataxin* regulation, the mouse model might not show the same severe effects in tissues normally affected in FRDA patients, as the GAA repeat does not naturally contribute to the regulation of the murine *Fxn*. The observed down regulation of the murine *frataxin* would therefore purely demonstrate a hampered transcription of *frataxin* because of the introduced GAA repeat. However, this itself might not be sufficient to create a FRDA phenotype in mice as the additional severe reduction in humans provoked by

the in human occurring RNA pol II pausing possibly involving the GAA repeat site is missing.

YAC transgenic mice with human *frataxin*

Considering the earlier findings, it was decided that a transgenic mouse carrying the human *frataxin* gene with its appropriate surrounding genomic DNA sequences should be a good working model. These mice were obtained by introducing a GAA expansion into a 370 kb human genomic YAC clone, 37FA12 (Al-Mahdawi et al., 2004) possessing the entire *FXN* gene with 9 GAA repeats. The human wt YAC was able to rescue the lethal phenotype of *Fxn*$^{-/-}$ in mice. Homologous recombination between a plasmid containing a $GAA_{(230)}$ expansion and a retrofitted YAC 37FA12 resulted in a final modified YAC that contained $GAA_{(190)}$ repeats (Al-Mahdawi et al. 2004). After microinjection, Al-Mahdawi et al. obtained a mouse having one YAC, including one $GAA_{(190)}$ expansion, called YG22. To ensure a phenotype, these mice should ideally be crossed with mice exhibiting a homozygous knock-out for the murine *Fxn* (Hall et al., 2002). However, RT-PCR and western blot analysis of tissues from both transgenic lines detected relatively high levels of human *FXN* mRNA and protein expression in all tissues studied. The following figure is exctracted from Al-Mahdawi et al., 2004 and slightly modified (Fig. 55).

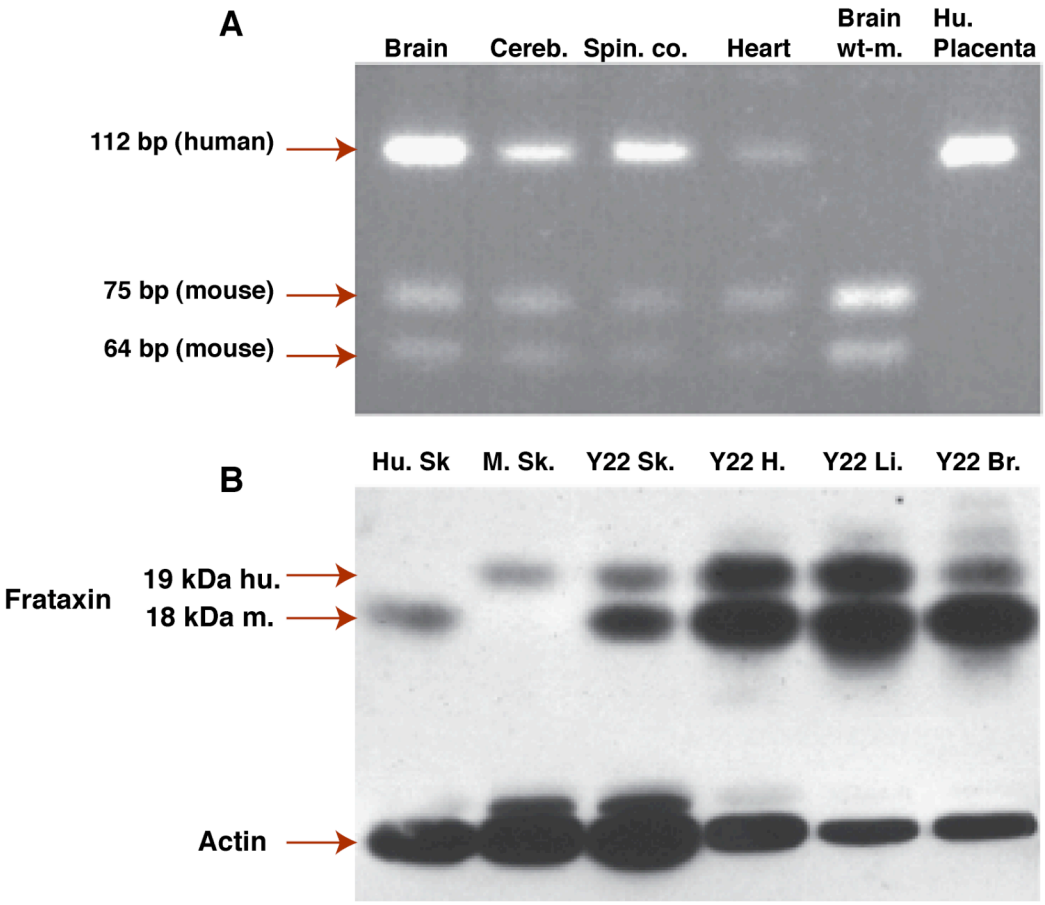

Figure 55: ***Frataxin*** **levels of human, non-transgenic and Y22 transgenic mice. (A) Displayed are mouse and human** ***frataxin*** **mRNA levels. Mouse** ***frataxin*** **product has been digested in order to differentiate human from mouse. (B) Western blot of human and mice** ***frataxin*** **(Extracted from Al-Mahdawi et al., 2004).**

ChIP against histone antibodies

In order to examine the human *frataxin* locus in affected tissues, chromatin immunoprecipitation (ChIP) was performed on formaldehyde fixed thymus, heart, liver and cerebellum. Liver was included as reports from collaborators (personal communication M. Pandolfo) mentioned liver as a tissue that expresses *frataxin* at a high level.

As only limited chromatin material was available, the three histone marks H3K9me2, H3K4me2 and H4K16ac were investigated. Each diagram shows the results of one histone modification of all tissues investigated. Chromatin was extracted from tissues

of two mice. Each IP was measured in triplicate. Every value displayed was firstly normalised to H3 and then to GAPDH in order to avoid tissue specific differences. For better comparison, each corresponding antibody result of the human lymphocyte cell line GM15 is displayed in green.

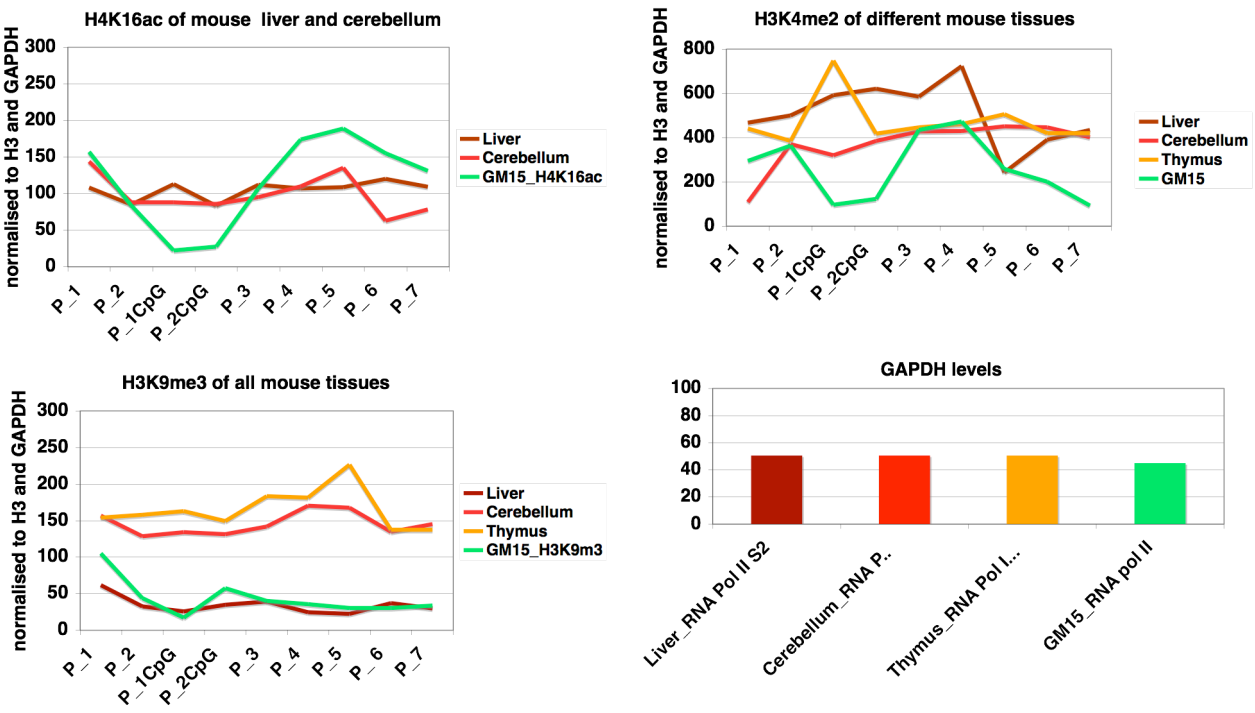

Figure 56: Histone modifications of the human *frataxin* transgene in different mouse tissues. Each value has been normalised to H3 and to GAPDH. The results of GM15 are shown in green for comparison. Primers for *FXN* are the same used for experiments performed on human (Fig. 6). Each tissue seems to posses its own unique histone modification pattern.

The YAC human *frataxin* holds well presented H3K4me2 levels in all tissues investigated, although generally higher than the ones found in the human lymphocytes. However, the thymus (orange graph) displaying the organ closest to the human lymphocytes tested, does not exhibit a similar pattern to the GM15 cell line (green). Moreover, the histone modification H3K4me2 peaks strongly at the RNA pol II pausing site. This peak differs to the pattern obtained for GM15, perhaps indicating a not fully functional element in the mouse thymus. The liver (brown) displays even higher levels of H3K4me2 and additionally lacks the “dip” at the RNA pol II pausing site, which is characteristic for the human *frataxin*. The liver does show a striking drop of the positive mark after the GAA expansion. Furthermore, of all mouse tissues investigated, cerebellum (pink) exhibits the lowest H3K4me2 level,

even though these are still higher than the ones measured for the human lymphocytes. So far, cerebellum is the only mouse tissue investigated displaying a slight “dip” around the pausing site, suggesting an at least partly working RNA pol II pausing element in this tissue.

While investigating the inactive histone mark H3K9me3 within the cerebellum, high levels were found with a minor increase around the GAA expansion site. This increase was not detectable adjacent 5’ and 3’ of the GAA expansion, excluding a spreading of this inactive mark from the GAA repeat into the locus. A similar even more pronounced increase occurred in the thymus, accompanied by a sharp drop after the GAA expansion. Consistent with the finding that the liver expresses *Fxn* mRNA at comparatively high levels (brown) it was found to have a lower level of the H3K9me3 modification which was previously associated with “silent” heterochromatin (Almeida R et al., 2006).

Due to a lack of material the highly active mark H4K16ac was investigated only on liver and cerebellum. Overall the H4K16ac amounts correlate well with the levels obtained from the human GM15 cell line. However, as the amount of the other histone modifications is generally higher in the mouse context than in the human, the actual effect of the H4K16ac modification is presumably less pronounced in the mouse. Moreover, liver shows a small peak where the characteristic “dip” in humans occurs. Furthermore, in this context the GAA repeat does not seem to influence the H4K16ac level positively, most likely because the GAA expansion is not as dramatic as the one occurring in GM15 with over 1090 repeats. However, the cerebellum sample, although lacking the “dip” of H4K16ac at the pausing site, shows a slight increase of H4K16ac around the GAA repeat which is lost further downstream.

ChIP results with DNA binding antibodies

In order to verify if the proteins already found to bind at the first part of the *frataxin* locus in human lymphocytes were also binding at the same site of the human transgene in the mouse, ChIP experiments were performed using antibodies against RNA pol II S2, HP1γ and NELF-E. Each value obtained was normalised to H3 ChIP and then further normalised to murine *GAPDH* in order to account for tissue specific differences.

The results obtained for the antibody against RNA pol II show a peak around the putative RNA pol II pausing site in all tissues investigated. Nevertheless, the peaks obtained for the different mouse tissues are less pronounced than the ones received for the human GM15 and GM14 cell line. The high levels of elongating RNA pol II detected 5' and 3' of exon 1 is in accordance with the high *frataxin* mRNA and protein levels detected by Pook and colleagues (Al-Mahdawi et al., 2004). This result suggests that the human pausing element also accumulates RNA pol II in the mouse context.

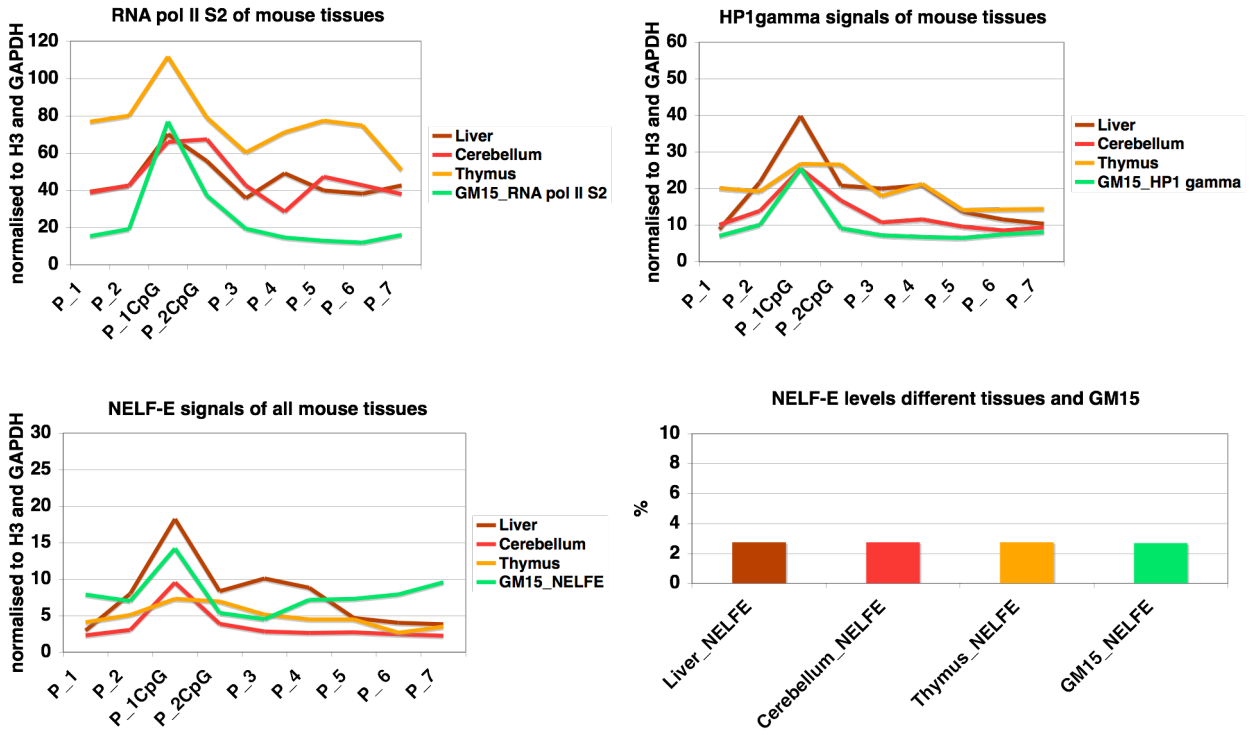

Figure 57: ChIP against RNA pol II, HP1γ and NELF-E. All values displayed are normalised to H3 and GAPDH. Each ChIP has been performed on liver (brown), cerebellum (pink) and thymus (orange). Values obtained from ChIP on GM15 are displayed for comparison. As control the levels of NELF-E at the murine and the human *GAPDH* gene are shown. Primers and their location are shown in figure 6.

The thymus (orange) shows the highest levels of elongating RNA pol II over the area investigated although also having the highest degree of the inactive mark H3K9me3. This clearly indicates the need for discussing histone mark results in the context of other factors, rather than studying the level of one single mark. In the mouse context the RNA pol II is already detected at higher levels even 6000 bp 5' of the human *FXN*

gene UTR, compared to the results obtained in the human cell line. Despite of that, the pausing site seems to arrest the RNA pol II at least partly, as levels drop after the putative pausing site by ~ 40 %. Furthermore, 3' of the GAA expansion, the level of elongating RNA pol II increased in the thymus as well as in the cerebellum. Although liver and cerebellum seem to hold similar RNA pol II levels along the *FXN* gene, the pausing in cerebellum seems to be more pronounced or stronger along the first CpG-island than in the other tissues investigated. Additionally, adjacent to the GAA expansion, liver and cerebellum display an opposite pattern. In the cerebellum the level of RNA pol II 5' of the repeat is lower than for the rest of the gene, with an increase 3' of the repeat. The liver shows similar RNA pol II levels 5' and 3' of the GAA expansion, however, directly 5' of the GAA repeat an increase of RNA pol II is detectable. The control gene *GAPDH* showed similar levels of NELF-E and RNA pol II on all mouse tissues examined (Fig. 56 + 57), suggesting that the detected significant differences in RNA pol II levels might be real.

Interestingly, HP1γ ChIP results present a peak at the RNA pol II pausing site in cerebellum and thymus compared to the human cell lines (GM15 as example). Only liver shows twice the amount of HP1γ. Additionally, the HP1γ peak in thymus is extended across the first CpG-island. All mouse tissues reveal an additional peak 5' of the GAA expansion that is not detectable in human samples.

The mouse ChIP signals obtained for NELF-E exhibit similar levels to the ones detected in humans although each tissue seems to have its particular level. Except for thymus all tissues displayed a sharp peak at the pausing site, whereas liver shows the highest level and cerebellum the lowest. However, thymus shows a relatively low and broad peak around the site of RNA pol II pausing. This experiment might reflect tissue differences in the regulation of *frataxin*, but in order to estimate the influence of the GAA repeat, the control mouse exhibiting the YAC *FXN* with normal repeats is needed.

Primary transcript RNA-FISH on EBV-cells show that GAA expansion slows *frataxin* mRNA expression and reveals additional influencing factors of long GAA repeats (Results beginning 2005).

Patients with different severities but the same GAA repeat expansion may provide an opportunity to identify modifying factors. Therefore, an informative patient combination might be two patients with different severity and onset of the FRDA disease but with the same GAA repeat length. As late onset FRDA patients with long repeats are very rare it was necessary to study EBV-transformed B-lymphocyte cell lines from patients exhibiting a similar repeat length but a different onset and severity of FRDA. In order to investigate if additional factors would influence the transcription process, both patient cell lines and a control cell line were hybridised with the probe shown in Fig**.** 6 recognising the RNA 5' or 3' of the GAA repeat.

For each EBV-transformed B-cell line two independent experiments were performed. For each experiment two slides per cell line were processed and 60 cells per slide were counted. The results presented display the average percentage of all counted slides and the indicated error-bars show the standard deviation.

In order to assess possible differences due to the presence of an expansion of the GAA repeat between healthy and FRDA cell lines on a single cell level, primary transcript RNA-FISH was performed.

These results show that all three different EBV-transformed cell lines hybridised with the probe recognising the primary transcript RNA 5' of the GAA expansion showed a similar *frataxin* signal distribution (Fig. 58). Whereas the bi-allelic expression showed the greatest variation of between 48 % and 55 %, the mono-allelic expression varied between 7 % and 13 % and the cells with no detectable signal showed the smallest variation at 37 %. However, after hybridisation with a probe recognising the RNA 3' of the GAA expansion, a different signal distribution was detectable when compared to the 5' result for each cell line. In cells of the control line the mono-allelic cells increased (19 %) and the bi-allelic expressing cells decreased (46 %), whereas the non-expressing cells stayed more or less the same (Fig. 58). A similar finding was observed 3' of the GAA repeat (even if not expanded) when primary lymphocytes from a normal individual were analysed.

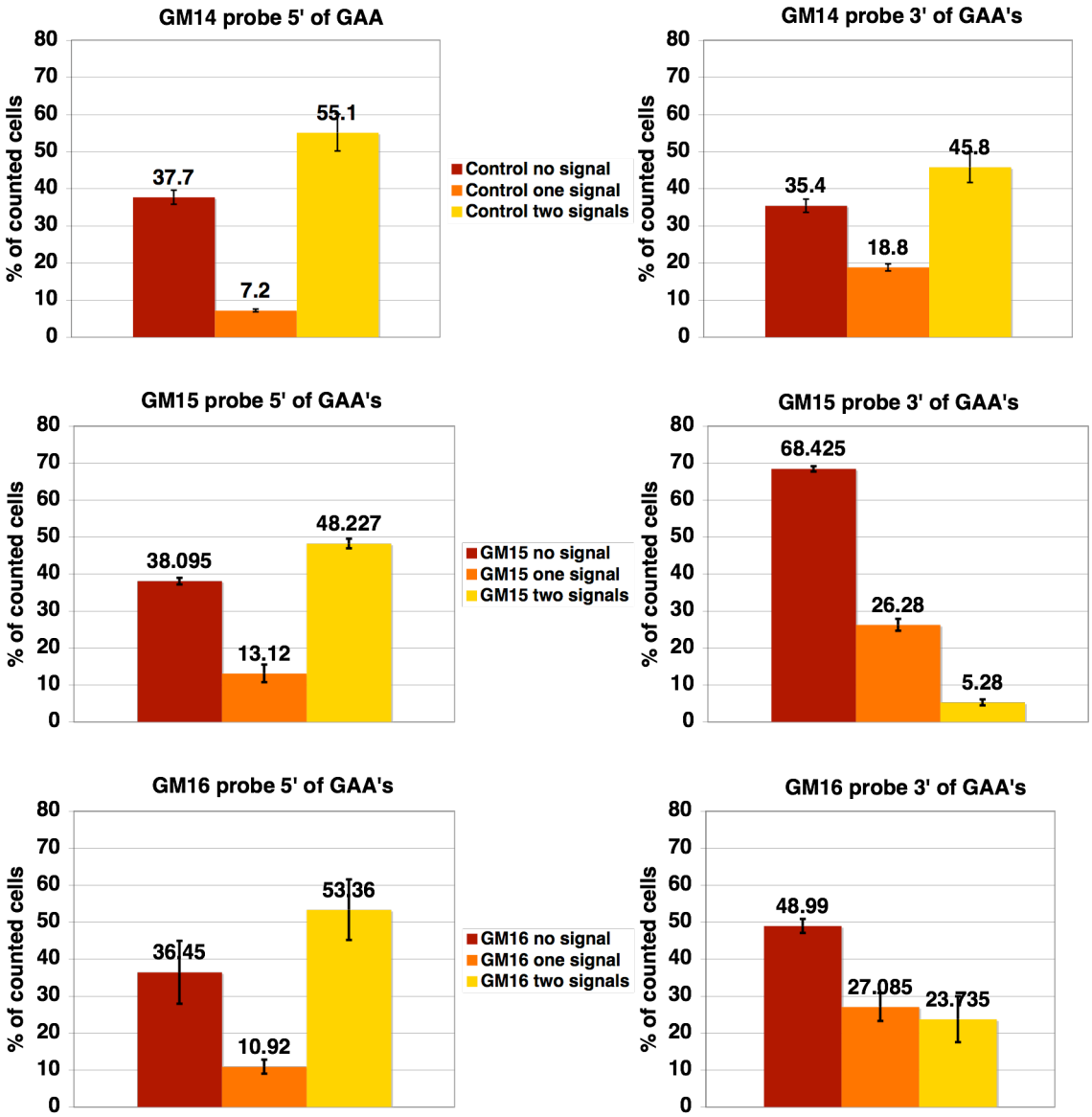

Figure 58: Primary transcript RNA-FISH. One type of cell line is displayed in each row. In each case the left diagram represents results obtained with a probe recognising the RNA 5' of the GAA repeat whereas the right diagram displays results obtained with a probe recognising intron 3 and 4 respectively. The dark brown column shows how frequently a cell with no signal has been counted. The orange column indicates cells with one signal and the yellow column represents cells where two signals for *frataxin* were counted.

Interestingly, when probed 3' of the GAA expansion the early onset GM15 cell line cells, did not show a *frataxin* signal in ~ 68 % of cells, whereas in the late-onset GM16 cell line only 49 % of cells did not reveal a signal compared to the control. Furthermore, the proportion of cells expressing *frataxin* mono-allelic did not differ between the patient cell lines, but the proportion of bi-allelic expressing cells deviated much more. Moreover, cells derived from the early-onset GM15 cell line showed bi-

allelic expression in only 5 % of cells whereas 24 % of cells derived from the late-onset patient GM16 were still able to transcribe *frataxin* bi-allelic (Fig. 58).

References

References

Agazie, Y.M., Burkholder, G.D., and Lee, J.S. (1996). Triplex DNA in the nucleus: direct binding of triplex-specific antibodies and their effect on transcription, replication and cell growth. Biochem J 316 (Pt 2), 461-466.

Aida, M., Chen, Y., Nakajima, K., Yamaguchi, Y., Wada, T., and Handa, H. (2006). Transcriptional pausing caused by NELF plays a dual role in regulating immediate-early expression of the junB gene. Mol Cell Biol 26, 6094-6104.

Al-Mahdawi, S., Pinto, R.M., Ruddle, P., Carroll, C., Webster, Z., and Pook, M. (2004). GAA repeat instability in Friedreich ataxia YAC transgenic mice. Genomics 84, 301-310.

Al-Mahdawi, S., Pinto, R.M., Varshney, D., Lawrence, L., Lowrie, M.B., Hughes, S., Webster, Z., Blake, J., Cooper, J.M., King, R., et al. (2006). GAA repeat expansion mutation mouse models of Friedreich ataxia exhibit oxidative stress leading to progressive neuronal and cardiac pathology. Genomics 88, 580-590.

Allis, C.D., Jenuwein, T., Reinberg, D. and Caparros, ML (2007). “Epigenetics”. Cold Spring Harbor Laboratory Press, Cold Spring Harbor, New York.

Andressoo, J.O., and Hoeijmakers, J.H. (2005). Transcription-coupled repair and premature ageing. Mutat Res 577, 179-194.

Annunziato, A.T., and Hansen, J.C. (2000). Role of histone acetylation in the assembly and modulation of chromatin structures. Gene Expr 9, 37-61.

Ballestar, E., Esteller, M., and Richardson, B.C. (2006). The epigenetic face of systemic lupus erythematosus. J Immunol 176, 7143-7147.

Bannister, A.J., Zegerman, P., Partridge, J.F., Miska, E.A., Thomas, J.O., Allshire, R.C., and Kouzarides, T. (2001). Selective recognition of methylated lysine 9 on histone H3 by the HP1 chromo domain. Nature 410, 120-124.

Bao, L., Zhou, M., and Cui, Y. (2007). CTCFBSDB: a CTCF-binding site database for characterization of vertebrate genomic insulators. Nucleic Acids Res.

Barrett, A., Madsen, B., Copier, J., Lu, P.J., Cooper, L., Scibetta, A.G., Burchell, J., and Taylor-Papadimitriou, J. (2002). PLU-1 nuclear protein, which is upregulated in breast cancer, shows restricted expression in normal human adult tissues: a new cancer/testis antigen? Int J Cancer 101, 581-588.

Barski, A., Cuddapah, S., Cui, K., Roh, T.Y., Schones, D.E., Wang, Z., Wei, G., Chepelev, I., and Zhao, K. (2007). High-resolution profiling of histone methylations in the human genome. Cell 129, 823-837.

Bell, A.C., West, A.G., and Felsenfeld, G. (1999). The protein CTCF is required for the enhancer blocking activity of vertebrate insulators. Cell 98, 387-396.

Belotserkovskii, B.P., De Silva, E., Tornaletti, S., Wang, G., Vasquez, K.M., and Hanawalt, P.C. (2007). A triplex-forming sequence from the human c-MYC promoter interferes with DNA transcription. J Biol Chem 282, 32433-32441.

Berciano, J., Mateo, I., De Pablos, C., Polo, J.M., and Combarros, O. (2002). Friedreich ataxia with minimal GAA expansion presenting as adult-onset spastic ataxia. J Neurol Sci 194, 75-82.

Berger, S.L. (2007). The complex language of chromatin regulation during transcription. Nature 447, 407-412.

Bernstein, B.E., Humphrey, E.L., Erlich, R.L., Schneider, R., Bouman, P., Liu, J.S., Kouzarides, T., and Schreiber, S.L. (2002). Methylation of histone H3 Lys 4 in coding regions of active genes. Proc Natl Acad Sci U S A 99, 8695-8700.

Bernstein, B.E., Kamal, M., Lindblad-Toh, K., Bekiranov, S., Bailey, D.K., Huebert, D.J., McMahon, S., Karlsson, E.K., Kulbokas, E.J., 3rd, Gingeras, T.R., et al. (2005). Genomic maps and comparative analysis of histone modifications in human and mouse. Cell 120, 169-181.

Bestor, T.H., and Ingram, V.M. (1983). Two DNA methyltransferases from murine erythroleukemia cells: purification, sequence specificity, and mode of interaction with DNA. Proc Natl Acad Sci U S A 80, 5559-5563.

Bhidayasiri, R., Perlman, S.L., Pulst, S.M., and Geschwind, D.H. (2005). Late-onset Friedreich ataxia: phenotypic analysis, magnetic resonance imaging findings, and review of the literature. Arch Neurol 62, 1865-1869.

Bi, G., and Jiang, G. (2006). The molecular mechanism of HDAC inhibitors in anticancer effects. Cell Mol Immunol 3, 285-290.

Bidichandani, S.I., Ashizawa, T., and Patel, P.I. (1998). The GAA triplet-repeat expansion in Friedreich ataxia interferes with transcription and may be associated with an unusual DNA structure. Am J Hum Genet 62, 111-121.

Bidichandani, S.I., Garcia, C.A., Patel, P.I., and Dimachkie, M.M. (2000). Very late-onset Friedreich ataxia despite large GAA triplet repeat expansions. Arch Neurol 57, 246-251.

Bidichandani, S.I., Purandare, S.M., Taylor, E.E., Gumin, G., Machkhas, H., Harati, Y., Gibbs, R.A., Ashizawa, T., and Patel, P.I. (1999). Somatic sequence variation at the Friedreich ataxia locus includes complete contraction of the expanded GAA triplet repeat, significant length variation in serially passaged lymphoblasts and enhanced mutagenesis in the flanking sequence. Hum Mol Genet 8, 2425-2436.

Bird, A. (1998). Transcriptional repression by the methyl-CpG-binding protein MeCP2 involves a histone deacetylase complex. Nature 393, 386-389.

Bird, A. (2001). Molecular biology. Methylation talk between histones and DNA. Science 294, 2113-2115.

Bird, A. (2002). DNA methylation patterns and epigenetic memory. Genes Dev 16, 6-21.

Bird, A., Taggart, M., Frommer, M., Miller, O.J., and Macleod, D. (1985). A fraction of the mouse genome that is derived from islands of nonmethylated, CpG-rich DNA. Cell 40, 91-99.

Bird, A.P., and Wolffe, A.P. (1999). Methylation-induced repression--belts, braces, and chromatin. Cell 99, 451-454.

Bitterman, K.J., Anderson, R.M., Cohen, H.Y., Latorre-Esteves, M., and Sinclair, D.A. (2002). Inhibition of silencing and accelerated aging by nicotinamide, a putative negative regulator of yeast sir2 and human SIRT1. J Biol Chem 277, 45099-45107.

Blander, G., and Guarente, L. (2004). The Sir2 family of protein deacetylases. Annu Rev Biochem 73, 417-435.

Boa, S., Coert, C., and Patterton, H.G. (2003). Saccharomyces cerevisiae Set1p is a methyltransferase specific for lysine 4 of histone H3 and is required for efficient gene expression. Yeast 20, 827-835.

Bolden, J.E., Peart, M.J., and Johnstone, R.W. (2006). Anticancer activities of histone deacetylase inhibitors. Nat Rev Drug Discov 5, 769-784.

Brownell, J.E., and Allis, C.D. (1996). Special HATs for special occasions: linking histone acetylation to chromatin assembly and gene activation. Curr Opin Genet Dev 6, 176-184.

Bunse, M., Bit-Avragim, N., Riefflin, A., Perrot, A., Schmidt, O., Kreuz, F.R., Dietz, R., Jung, W.I., and Osterziel, K.J. (2003). Cardiac energetics correlates to myocardial hypertrophy in Friedreich's ataxia. Ann Neurol 53, 121-123.

Burkholder, G.D., Latimer, L.J., and Lee, J.S. (1988). Immunofluorescent staining of mammalian nuclei and chromosomes with a monoclonal antibody to triplex DNA. Chromosoma 97, 185-192.

Burnett, R., Melander, C., Puckett, J.W., Son, L.S., Wells, R.D., Dervan, P.B., and Gottesfeld, J.M. (2006). DNA sequence-specific polyamides alleviate transcription inhibition associated with long GAA.TTC repeats in Friedreich's ataxia. Proc Natl Acad Sci U S A 103, 11497-11502.

Buyse, G., Mertens, L., Di Salvo, G., Matthijs, I., Weidemann, F., Eyskens, B., Goossens, W., Goemans, N., Sutherland, G.R., and Van Hove, J.L. (2003). Idebenone treatment in Friedreich's ataxia: neurological, cardiac, and biochemical monitoring. Neurology 60, 1679-1681.

Campuzano, V., Montermini, L., Lutz, Y., Cova, L., Hindelang, C., Jiralerspong, S., Trottier, Y., Kish, S.J., Faucheux, B., Trouillas, P., et al. (1997). Frataxin is reducedin Friedreich ataxia patients and is associated with mitochondrial membranes. Hum Mol Genet 6, 1771-1780.

Campuzano, V., Montermini, L., Molto, M.D., Pianese, L., Cossee, M., Cavalcanti, F., Monros, E., Rodius, F., Duclos, F., Monticelli, A., et al. (1996). Friedreich's ataxia: autosomal recessive disease caused by an intronic GAA triplet repeat expansion. Science 271, 1423-1427.

Carruthers, L.M., and Hansen, J.C. (2000). The core histone N termini function independently of linker histones during chromatin condensation. J Biol Chem 275, 37285-37290.

Chen, Z., Zang, J., Whetstine, J., Hong, X., Davrazou, F., Kutateladze, T.G., Simpson, M., Mao, Q., Pan, C.H., Dai, S., et al. (2006). Structural insights into histone demethylation by JMJD2 family members. Cell 125, 691-702.

Chernukhin, I., Shamsuddin, S., Kang, S.Y., Bergstrom, R., Kwon, Y.W., Yu, W., Whitehead, J., Mukhopadhyay, R., Docquier, F., Farrar, D., et al. (2007). CTCF interacts with and recruits the largest subunit of RNA polymerase II to CTCF target sites genome-wide. Mol Cell Biol 27, 1631-1648.

Cheung, P., Allis, C.D., and Sassone-Corsi, P. (2000). Signaling to chromatin through histone modifications. Cell 103, 263-271.

Chiani, F., Di Felice, F., and Camilloni, G. (2006). SIR2 modifies histone H4-K16 acetylation and affects superhelicity in the ARS region of plasmid chromatin in Saccharomyces cerevisiae. Nucleic Acids Res 34, 5426-5437.

Chodosh, L.A., Fire, A., Samuels, M., and Sharp, P.A. (1989). 5,6-Dichloro-1-beta-D- ribofuranosylbenzimidazole inhibits transcription elongation by RNA polymerase II in vitro. J Biol Chem 264, 2250-2257.

Christensen, J., Agger, K., Cloos, P.A., Pasini, D., Rose, S., Sennels, L., Rappsilber, J., Hansen, K.H., Salcini, A.E., and Helin, K. (2007). RBP2 belongs to a family of demethylases, specific for tri-and dimethylated lysine 4 on histone 3. Cell 128, 1063- 1076.

Clark, R.M., De Biase, I., Malykhina, A.P., Al-Mahdawi, S., Pook, M., and Bidichandani, S.I. (2007). The GAA triplet-repeat is unstable in the context of the human FXN locus and displays age-dependent expansions in cerebellum and DRG in a transgenic mouse model. Hum Genet 120, 633-640.

Cooper, D.N. (1983). Eukaryotic DNA methylation. Hum Genet 64, 315-333.

Cooper, D.N., Taggart, M.H., and Bird, A.P. (1983). Unmethylated domains in vertebrate DNA. Nucleic Acids Res 11, 647-658.

Coppola, J.A., Field, A.S., and Luse, D.S. (1983). Promoter-proximal pausing by RNA polymerase II in vitro: transcripts shorter than 20 nucleotides are not capped. Proc Natl Acad Sci U S A 80, 1251-1255.

Cossee, M., Puccio, H., Gansmuller, A., Koutnikova, H., Dierich, A., LeMeur, M., Fischbeck, K., Dolle, P., and Koenig, M. (2000). Inactivation of the Friedreich ataxia mouse gene leads to early embryonic lethality without iron accumulation. Hum Mol Genet 9, 1219-1226.

Cossee, M., Schmitt, M., Campuzano, V., Reutenauer, L., Moutou, C., Mandel, J.L., and Koenig, M. (1997). Evolution of the Friedreich's ataxia trinucleotide repeat expansion: founder effect and premutations. Proc Natl Acad Sci U S A 94, 7452-7457.

de Ruijter, A.J., van Gennip, A.H., Caron, H.N., Kemp, S., and van Kuilenburg, A.B. (2003). Histone deacetylases (HDACs): characterization of the classical HDAC family. Biochem J 370, 737-749.

Dervan, P.B., and Edelson, B.S. (2003). Recognition of the DNA minor groove by pyrrole-imidazole polyamides. Curr Opin Struct Biol 13, 284-299.

Dhalluin, C., Carlson, J.E., Zeng, L., He, C., Aggarwal, A.K., and Zhou, M.M. (1999). Structure and ligand of a histone acetyltransferase bromodomain. Nature 399, 491-496.

Di Prospero, N.A., Sumner, C.J., Penzak, S.R., Ravina, B., Fischbeck, K.H., and Taylor, J.P. (2007). Safety, tolerability, and pharmacokinetics of high-dose idebenone in patients with Friedreich ataxia. Arch Neurol 64, 803-808.

Dodge, J.E., Okano, M., Dick, F., Tsujimoto, N., Chen, T., Wang, S., Ueda, Y., Dyson, N., and Li, E. (2005). Inactivation of Dnmt3b in mouse embryonic fibroblasts results in DNA hypomethylation, chromosomal instability, and spontaneous immortalization. J Biol Chem 280, 17986-17991.

Dormann, H.L., Tseng, B.S., Allis, C.D., Funabiki, H., and Fischle, W. (2006). Dynamic regulation of effector protein binding to histone modifications: the biology of HP1 switching. Cell Cycle 5, 2842-2851.

Drewell, R.A., Goddard, C.J., Thomas, J.O., and Surani, M.A. (2002). Methylation-dependent silencing at the H19 imprinting control region by MeCP2. Nucleic Acids Res 30, 1139-1144.

Durr, A., and Brice, A. (1996). Genetics of movement disorders. Curr Opin Neurol 9, 290-297.

Ebralidse, K.K., Hebbes, T.R., Clayton, A.L., Thorne, A.W., and Crane-Robinson, C. (1993). Nucleosomal structure at hyperacetylated loci probed in nuclei by DNA-histone crosslinking. Nucleic Acids Res 21, 4734-4738.

Ehrlich, M., Gama-Sosa, M.A., Huang, L.H., Midgett, R.M., Kuo, K.C., McCune, R.A., and Gehrke, C. (1982). Amount and distribution of 5-methylcytosine in human DNA from different types of tissues of cells. Nucleic Acids Res 10, 2709-2721.

Ehrlich, M., Hopkins, N.E., Jiang, G., Dome, J.S., Yu, M.C., Woods, C.B., Tomlinson, G.E., Chintagumpala, M., Champagne, M., Dillerg, L., et al. (2003). Satellite DNA hypomethylation in karyotyped Wilms tumors. Cancer Genet Cytogenet 141, 97-105.

Eissenberg, J.C., Morris, G.D., Reuter, G., and Hartnett, T. (1992). The heterochromatin-associated protein HP-1 is an essential protein in Drosophila with dosage-dependent effects on position-effect variegation. Genetics 131, 345-352.

Elgin, S.C. (1996). Heterochromatin and gene regulation in Drosophila. Curr Opin Genet Dev 6, 193-202.

Epplen, C., Epplen, J.T., Frank, G., Miterski, B., Santos, E.J., and Schols, L. (1997). Differential stability of the (GAA)n tract in the Friedreich ataxia (STM7) gene. Hum Genet 99, 834-836.

Faragher, J.M. (2005). A Great and Noble Scheme: The Tragic Story of the Expulsion of the French Acadians from their American Homeland. New York: W. W. Norton & Company.

Felsenfeld, G., Burgess-Beusse, B., Farrell, C., Gaszner, M., Ghirlando, R., Huang, S., Jin, C., Litt, M., Magdinier, F., Mutskov, V., et al. (2004). Chromatin boundaries and chromatin domains. Cold Spring Harb Symp Quant Biol 69, 245-250.

Festenstein, R., Sharghi-Namini, S., Fox, M., Roderick, K., Tolaini, M., Norton, T., Saveliev, A., Kioussis, D., and Singh, P. (1999). Heterochromatin protein 1 modifies mammalian PEV in a dose- and chromosomal-context-dependent manner. Nat Genet 23, 457-461.

Filla, A., De Michele, G., Cavalcanti, F., Pianese, L., Monticelli, A., Campanella, G., and Cocozza, S. (1996). The relationship between trinucleotide (GAA) repeat length and clinical features in Friedreich ataxia. Am J Hum Genet 59, 554-560.

Finnin, M.S., Donigian, J.R., Cohen, A., Richon, V.M., Rifkind, R.A., Marks, P.A., Breslow, R., and Pavletich, N.P. (1999). Structures of a histone deacetylase homologue bound to the TSA and SAHA inhibitors. Nature 401, 188-193.

Fischer, A., Hofmann, I., Naumann, K., and Reuter, G. (2006). Heterochromatin proteins and the control of heterochromatic gene silencing in Arabidopsis. J Plant Physiol 163, 358-368.

Fischle, W., Wang, Y., and Allis, C.D. (2003). Histone and chromatin cross-talk. Curr Opin Cell Biol 15, 172-183.

Fivaz, J., Bassi, M.C., Pinaud, S., and Mirkovitch, J. (2000). RNA polymerase II promoter-proximal pausing upregulates c-fos gene expression. Gene 255, 185-194.

Fleming, J., Spinoulas, A., Zheng, M., Cunningham, S.C., Ginn, S.L., McQuilty, R.C., Rowe, P.B., and Alexander, I.E. (2005). Partial correction of sensitivity to oxidant stress in Friedreich ataxia patient fibroblasts by frataxin-encoding adeno- associated virus and lentivirus vectors. Hum Gene Ther 16, 947-956.

Fujita, A., Sato, J.R., Garay-Malpartida, H.M., Yamaguchi, R., Miyano, S., Sogayar, M.C., and Ferreira, C.E. (2007). Modeling gene expression regulatory networks with the sparse vector autoregressive model. BMC Syst Biol 1, 39.

Fuks, F., Hurd, P.J., Wolf, D., Nan, X., Bird, A.P., and Kouzarides, T. (2003). The methyl-CpG-binding protein MeCP2 links DNA methylation to histone methylation. J Biol Chem 278, 4035-4040.

Gomez, M., Clark, R.M., Nath, S.K., Bhatti, S., Sharma, R., Alonso, E., Rasmussen, A., and Bidichandani, S.I. (2004). Genetic admixture of European FRDA genes is the cause of Friedreich ataxia in the Mexican population. Genomics 84, 779-784.

Gomez-Sebastian, S., Gimenez-Cassina, A., Diaz-Nido, J., Lim, F., and Wade-Martins, R. (2007). Infectious delivery and expression of a 135 kb human FRDA genomic DNA locus complements Friedreich's ataxia deficiency in human cells. Mol Ther 15, 248-254.

Gottesfeld, J.M. (2007). Small molecules affecting transcription in Friedreich ataxia. Pharmacol Ther 116, 236-248.

Grabczyk, E., Mancuso, M., and Sammarco, M.C. (2007). A persistent RNA.DNA hybrid formed by transcription of the Friedreich ataxia triplet repeat in live bacteria, and by T7 RNAP in vitro. Nucleic Acids Res 35, 5351-5359.

Grabczyk, E., and Usdin, K. (2000). The GAA*TTC triplet repeat expanded in Friedreich's ataxia impedes transcription elongation by T7 RNA polymerase in a length and supercoil dependent manner. Nucleic Acids Res 28, 2815-2822.

Grant, L., Sun, J., Xu, H., Subramony, S.H., Chaires, J.B., and Hebert, M.D. (2006). Rational selection of small molecules that increase transcription through the GAA repeats found in Friedreich's ataxia. FEBS Lett 580, 5399-5405.

Greene, E., Entezam, A., Kumari, D., and Usdin, K. (2005). Ancient repeated DNA elements and the regulation of the human frataxin promoter. Genomics 85, 221-230.

Greene, E., Mahishi, L., Entezam, A., Kumari, D., and Usdin, K. (2007). Repeat-induced epigenetic changes in intron 1 of the frataxin gene and its consequences in Friedreich ataxia. Nucleic Acids Res 35, 3383-3390.

Gribnau, J., de Boer, E., Trimborn, T., Wijgerde, M., Milot, E., Grosveld, F., and Fraser, P. (1998). Chromatin interaction mechanism of transcriptional control in vivo. Embo J 17, 6020-6027.

Grozinger, C.M., Chao, E.D., Blackwell, H.E., Moazed, D., and Schreiber, S.L. (2001). Identification of a class of small molecule inhibitors of the sirtuin family of NAD-dependent deacetylases by phenotypic screening. J Biol Chem 276, 38837-38843.

Gu, W., Wind, M. and Reines D. (1996). Increased accommodation of nascent RNA in a product site on RNA polymerase II during arrest. PNAS Vol. 93, 6935-6940.

Gui, C.Y., Ngo, L., Xu, W.S., Richon, V.M., and Marks, P.A. (2004). Histone deacetylase (HDAC) inhibitor activation of p21WAF1 involves changes in promoter-associated proteins, including HDAC1. Proc Natl Acad Sci U S A 101, 1241-1246.

Haigis, M.C., and Guarente, L.P. (2006). Mammalian sirtuins--emerging roles in physiology, aging, and calorie restriction. Genes Dev 20, 2913-2921.

Hall, I.M., Shankaranarayana, G.D., Noma, K., Ayoub, N., Cohen, A., and Grewal, S.I. (2002). Establishment and maintenance of a heterochromatin domain. Science 297, 2232-2237.

Hart, P.E., Lodi, R., Rajagopalan, B., Bradley, J.L., Crilley, J.G., Turner, C., Blamire, A.M., Manners, D., Styles, P., Schapira, A.H., et al. (2005). Antioxidant treatment of patients with Friedreich ataxia: four-year follow-up. Arch Neurol 62, 621-626.

Hebert, M.D., and Whittom, A.A. (2007). Gene-based approaches toward Friedreich ataxia therapeutics. Cell Mol Life Sci.

Henikoff, S. (2001). Chromosomes on the move. Trends Genet 17, 689-690.

Herman, D., Jenssen, K., Burnett, R., Soragni, E., Perlman, S.L., and Gottesfeld, J.M. (2006). Histone deacetylase inhibitors reverse gene silencing in Friedreich's ataxia. Nat Chem Biol 2, 551-558.

Hernick, M., and Fierke, C.A. (2005). Zinc hydrolases: the mechanisms of zinc-dependent deacetylases. Arch Biochem Biophys 433, 71-84.

Hewer, R.L. (1968). Study of fatal cases of Friedreich's ataxia. Br Med J 3, 649-652.

Hoff, K.G., Avalos, J.L., Sens, K., and Wolberger, C. (2006). Insights into the sirtuin mechanism from ternary complexes containing NAD+ and acetylated peptide. Structure 14, 1231-1240.

Holliday, R., and Pugh, J.E. (1975). DNA modification mechanisms and gene activity during development. Science 187, 226-232.

Hudson, B.P., Martinez-Yamout, M.A., Dyson, H.J., and Wright, P.E. (2000). Solution structure and acetyl-lysine binding activity of the GCN5 bromodomain. J Mol Biol 304, 355-370.

Ikura, T., and Ogryzko, V.V. (2003). Chromatin dynamics and DNA repair. Front Biosci 8, s149-155.

Iwase, S., Lan, F., Bayliss, P., de la Torre-Ubieta, L., Huarte, M., Qi, H.H., Whetstine, J.R., Bonni, A., Roberts, T.M., and Shi, Y. (2007). The X-linked mental retardation gene SMCX/JARID1C defines a family of histone H3 lysine 4 demethylases. Cell 128, 1077-1088.

Jain, A., Rajeswari, M.R., and Ahmed, F. (2002). Formation and thermodynamic stability of intermolecular (R*R*Y) DNA triplex in GAA/TTC repeats associated with Freidreich's ataxia. J Biomol Struct Dyn 19, 691-699.

Janssen, S., Cuvier, O., Muller, M., and Laemmli, U.K. (2000a). Specific gain- and loss-of-function phenotypes induced by satellite-specific DNA-binding drugs fed to Drosophila melanogaster. Mol Cell 6, 1013-1024.

Janssen, S., Durussel, T., and Laemmli, U.K. (2000b). Chromatin opening of DNA satellites by targeted sequence-specific drugs. Mol Cell 6, 999-1011.

Jauslin, M.L., Meier, T., Smith, R.A., and Murphy, M.P. (2003). Mitochondria-targeted antioxidants protect Friedreich Ataxia fibroblasts from endogenous oxidative stress more effectively than untargeted antioxidants. Faseb J 17, 1972-1974.

Jiralerspong, S., Liu, Y., Montermini, L., Stifani, S., and Pandolfo, M. (1997). Frataxin shows developmentally regulated tissue-specific expression in the mouse embryo. Neurobiol Dis 4, 103-113.

Johansson, A.M., Stenberg, P., Pettersson, F., and Larsson, J. (2007). POF and HP1 Bind Expressed Exons, Suggesting a Balancing Mechanism for Gene Regulation. PLoS Genet 3, e209.

Jones, B.K., Levorse, J., and Tilghman, S.M. (2001). Deletion of a nuclease-sensitive region between the Igf2 and H19 genes leads to Igf2 misregulation and increased adiposity. Hum Mol Genet 10, 807-814. Jones, P.A., and Taylor, S.M. (1980). Cellular differentiation, cytidine analogs and DNA methylation. Cell 20, 85-93.

Kamine, J., Elangovan, B., Subramanian, T., Coleman, D., and Chinnadurai, G. (1996). Identification of a cellular protein that specifically interacts with the essential cysteine region of the HIV-1 Tat transactivator. Virology 216, 357-366.

Kanduri, C., Thakur, N., and Pandey, R.R. (2006). The length of the transcript encoded from the Kcnq1ot1 antisense promoter determines the degree of silencing. Embo J 25, 2096-2106.

Karthikeyan, G., Santos, J.H., Graziewicz, M.A., Copeland, W.C., Isaya, G., Van Houten, B., and Resnick, M.A. (2003). Reduction in frataxin causes progressive accumulation of mitochondrial damage. Hum Mol Genet 12, 3331-3342.

Kelso, G.F., Porteous, C.M., Coulter, C.V., Hughes, G., Porteous, W.K., Ledgerwood, E.C., Smith, R.A., and Murphy, M.P. (2001). Selective targeting of a redox-active ubiquinone to mitochondria within cells: antioxidant and antiapoptotic properties. J Biol Chem 276, 4588-4596.

Keogh, M.C., Podolny, V., and Buratowski, S. (2003). Bur1 kinase is required for efficient transcription elongation by RNA polymerase II. Mol Cell Biol 23, 7005- 7018.

Kimura, A., Umehara, T., and Horikoshi, M. (2002). Chromosomal gradient of histone acetylation established by Sas2p and Sir2p functions as a shield against gene silencing. Nat Genet 32, 370-377.

Kimura, H., and Shiota, K. (2003). Methyl-CpG-binding protein, MeCP2, is a target molecule for maintenance DNA methyltransferase, Dnmt1. J Biol Chem 278, 4806-4812.

Kirmizis, A., Santos-Rosa, H., Penkett, C.J., Singer, M.A., Vermeulen, M., Mann, M., Bahler, J., Green, R.D., and Kouzarides, T. (2007). Arginine methylation at histone H3R2 controls deposition of H3K4 trimethylation. Nature 449, 928-932.

Klose, R.J., Yamane, K., Bae, Y., Zhang, D., Erdjument-Bromage, H., Tempst, P., Wong, J., and Zhang, Y. (2006). The transcriptional repressor JHDM3A demethylates trimethyl histone H3 lysine 9 and lysine 36. Nature 442, 312-316.

Klose, R.J., and Zhang, Y. (2007). Regulation of histone methylation by demethylimination and demethylation. Nat Rev Mol Cell Biol 8, 307-318.

Koutnikova, H., Campuzano, V., Foury, F., Dolle, P., Cazzalini, O., and Koenig, M. (1997). Studies of human, mouse and yeast homologues indicate a mitochondrial function for frataxin. Nat Genet 16, 345-351.

Kouzarides, T. (2000). Acetylation: a regulatory modification to rival phosphorylation? Embo J 19, 1176-1179.

Kouzarides, T. (2007). Chromatin modifications and their function. Cell 128, 693-705.

Krasilnikova, M.M., Kireeva, M.L., Petrovic, V., Knijnikova, N., Kashlev, M., and Mirkin, S.M. (2007). Effects of Friedreich's ataxia (GAA)n*(TTC)n repeats on RNA synthesis and stability. Nucleic Acids Res 35, 1075-1084.

Krasilnikova, M.M., and Mirkin, S.M. (2004). Replication stalling at Friedreich's ataxia (GAA)n repeats in vivo. Mol Cell Biol 24, 2286-2295.

Krumm, A., Hickey, L.B., and Groudine, M. (1995). Promoter-proximal pausing of RNA polymerase II defines a general rate-limiting step after transcription initiation. Genes Dev 9, 559-572.

Kruszewski, M., and Szumiel, I. (2005). Sirtuins (histone deacetylases III) in the cellular response to DNA damage--facts and hypotheses. DNA Repair (Amst) 4, 1306-1313.

Lachner, M., O'Carroll, D., Rea, S., Mechtler, K., and Jenuwein, T. (2001). Methylation of histone H3 lysine 9 creates a binding site for HP1 proteins. Nature 410, 116-120.

Ladik, J., Bende, A., and Bogar, F. (2007). Calculation of the band structure of polyguanilic acid in the presence of water and Na+ ions. J Chem Phys 127, 055102.

Laine, J.P., and Egly, J.M. (2006). Initiation of DNA repair mediated by a stalled RNA polymerase IIO. Embo J 25, 387-397.

Landry, J., Slama, J.T., and Sternglanz, R. (2000a). Role of NAD(+) in the deacetylase activity of the SIR2-like proteins. Biochem Biophys Res Commun 278, 685-690.

Landry, J., Sutton, A., Tafrov, S.T., Heller, R.C., Stebbins, J., Pillus, L., and Sternglanz, R. (2000b). The silencing protein SIR2 and its homologs are NAD-dependent protein deacetylases. Proc Natl Acad Sci U S A 97, 5807-5811.

Lawrence, R.J., Earley, K., Pontes, O., Silva, M., Chen, Z.J., Neves, N., Viegas, W., and Pikaard, C.S. (2004). A concerted DNA methylation/histone methylation switch regulates rRNA gene dosage control and nucleolar dominance. Mol Cell 13, 599-609.

Lee, D.Y., Teyssier, C., Strahl, B.D., and Stallcup, M.R. (2005). Role of protein methylation in regulation of transcription. Endocr Rev 26, 147-170.

Lee, N., Zhang, J., Klose, R.J., Erdjument-Bromage, H., Tempst, P., Jones, R.S., and Zhang, Y. (2007). The trithorax-group protein Lid is a histone H3 trimethyl-Lys4 demethylase. Nat Struct Mol Biol 14, 341-343.

Li, B., Weber, J.A., Chen, Y., Greenleaf, A.L., and Gilmour, D.S. (1996). Analyses of promoter-proximal pausing by RNA polymerase II on the hsp70 heat shock gene promoter in a Drosophila nuclear extract. Mol Cell Biol 16, 5433-5443.

Li, E., Bestor, T.H., and Jaenisch, R. (1992). Targeted mutation of the DNA methyltransferase gene results in embryonic lethality. Cell 69, 915-926.

Liang, G., Klose, R.J., Gardner, K.E., and Zhang, Y. (2007). Yeast Jhd2p is a histone H3 Lys4 trimethyl demethylase. Nat Struct Mol Biol 14, 243-245.

Lim, F., Palomo, G.M., Mauritz, C., Gimenez-Cassina, A., Illana, B., Wandosell, F., and Diaz-Nido, J. (2007). Functional recovery in a Friedreich's ataxia mouse model by frataxin gene transfer using an HSV-1 amplicon vector. Mol Ther 15, 1072-1078.

Litt, M.D., Simpson, M., Recillas-Targa, F., Prioleau, M.N., and Felsenfeld, G. (2001). Transitions in histone acetylation reveal boundaries of three separately regulated neighboring loci. Embo J 20, 2224-2235.

Lodi, R., Hart, P.E., Rajagopalan, B., Taylor, D.J., Crilley, J.G., Bradley, J.L., Blamire, A.M., Manners, D., Styles, P., Schapira, A.H., et al. (2001a). Antioxidant treatment improves in vivo cardiac and skeletal muscle bioenergetics in patients with Friedreich's ataxia. Ann Neurol 49, 590-596.

Lodi, R., Rajagopalan, B., Blamire, A.M., Cooper, J.M., Davies, C.H., Bradley, J.L., Styles, P., and Schapira, A.H. (2001b). Cardiac energetics are abnormal in Friedreich ataxia patients in the absence of cardiac dysfunction and hypertrophy: an in vivo 31P magnetic resonance spectroscopy study. Cardiovasc Res 52, 111-119.

Lodi, R., Taylor, D.J., and Schapira, A.H. (2001c). Mitochondrial dysfunction in Friedreich's ataxia. Biol Signals Recept 10, 263-270.

Lomberk, G., Wallrath, L., and Urrutia, R. (2006). The Heterochromatin Protein 1 family. Genome Biol 7, 228.

Loyola, A., and Almouzni, G. (2007). Marking histone H3 variants: how, when and why? Trends Biochem Sci 32, 425-433.

Lu, P.J., Sundquist, K., Baeckstrom, D., Poulsom, R., Hanby, A., Meier-Ewert, S., Jones, T., Mitchell, M., Pitha-Rowe, P., Freemont, P., et al. (1999). A novel gene (PLU-1) containing highly conserved putative DNA/chromatin binding motifs is specifically up-regulated in breast cancer. J Biol Chem 274, 15633-15645.

Luger, K., Mader, A.W., Richmond, R.K., Sargent, D.F., and Richmond, T.J. (1997). Crystal structure of the nucleosome core particle at 2.8 A resolution. Nature 389, 251- 260.

Mandal, S.S., Chu, C., Wada, T., Handa, H., Shatkin, A.J., and Reinberg, D. (2004). Functional interactions of RNA-capping enzyme with factors that positively and negatively regulate promoter escape by RNA polymerase II. Proc Natl Acad Sci U S A 101, 7572-7577.

Mariappan, S.V., Catasti, P., Silks, L.A., 3rd, Bradbury, E.M., and Gupta, G. (1999). The high-resolution structure of the triplex formed by the GAA/TTC triplet repeat associated with Friedreich's ataxia. J Mol Biol 285, 2035-2052.

Mariotti, C., Solari, A., Torta, D., Marano, L., Fiorentini, C., and Di Donato, S. (2003). Idebenone treatment in Friedreich patients: one-year-long randomized placebo-controlled trial. Neurology 60, 1676-1679.

Marshall, N.F., Peng, J., Xie, Z., and Price, D.H. (1996). Control of RNA polymerase II elongation potential by a novel carboxyl-terminal domain kinase. J Biol Chem 271, 27176-27183.

Martin, C., and Zhang, Y. (2005). The diverse functions of histone lysine methylation. Nat Rev Mol Cell Biol 6, 838-849.

McLeod, J.G. (1971). An electrophysiological and pathological study of peripheral nerves in Friedreich's ataxia. J Neurol Sci 12, 333-349.

Metzger, E., Wissmann, M., Yin, N., Muller, J.M., Schneider, R., Peters, A.H., Gunther, T., Buettner, R., and Schule, R. (2005). LSD1 demethylates repressive histone marks to promote androgen-receptor-dependent transcription. Nature 437, 436-439.

Mikkelsen, T.S., Ku, M., Jaffe, D.B., Issac, B., Lieberman, E., Giannoukos, G., Alvarez, P., Brockman, W., Kim, T.K., Koche, R.P., et al. (2007). Genome-wide maps of chromatin state in pluripotent and lineage-committed cells. Nature 448, 553- 560.

Miranda CJ, S.M., Ohshima K, Smith J, Li L, Cossee M, Koenig M, Sequeiros J, Kaplan J, Pandolfo M. (2002). Frataxin knockin mouse. FEBS Lett 13, 8.

Mirkin, S.M., (2007). Expandable DNA repeats and human disease. Nature 447, 932-940.

Mizzen, C.A., Yang, X.J., Kokubo, T., Brownell, J.E., Bannister, A.J., Owen-Hughes, T., Workman, J., Wang, L., Berger, S.L., Kouzarides, T., et al. (1996). The TAF(II)250 subunit of TFIID has histone acetyltransferase activity. Cell 87, 1261- 1270.

Monros, E., Molto, M.D., Martinez, F., Canizares, J., Blanca, J., Vilchez, J.J., Prieto, F., de Frutos, R., and Palau, F. (1997). Phenotype correlation and intergenerational dynamics of the Friedreich ataxia GAA trinucleotide repeat. Am J Hum Genet 61, 101-110.

Montermini, L., Andermann, E., Labuda, M., Richter, A., Pandolfo, M., Cavalcanti, F., Pianese, L., Iodice, L., Farina, G., Monticelli, A., et al. (1997a). The Friedreich ataxia GAA triplet repeat: premutation and normal alleles. Hum Mol Genet 6, 1261-1266.

Montermini, L., Richter, A., Morgan, K., Justice, C.M., Julien, D., Castellotti, B., Mercier, J., Poirier, J., Capozzoli, F., Bouchard, J.P., et al. (1997b). Phenotypic variability in Friedreich ataxia: role of the associated GAA triplet repeat expansion. Ann Neurol 41, 675-682.

Monticelli, A., Giacchetti, M., De Biase, I., Pianese, L., Turano, M., Pandolfo, M., and Cocozza, S. (2004). New clues on the origin of the Friedreich ataxia expanded alleles from the analysis of new polymorphisms closely linked to the mutation. Hum Genet 114, 458-463.

Mooney, R.A., and Landick, R. (2003). Tethering sigma70 to RNA polymerase reveals high in vivo activity of sigma factors and sigma70-dependent pausing at promoter-distal locations. Genes Dev 17, 2839-2851.

Muller, W.G., Rieder, D., Karpova, T.S., John, S., Trajanoski, Z., and McNally, J.G. (2007). Organization of chromatin and histone modifications at a transcription site. J Cell Biol 177, 957-967.

Murr, R., Loizou, J.I., Yang, Y.G., Cuenin, C., Li, H., Wang, Z.Q., and Herceg, Z. (2006). Histone acetylation by Trrap-Tip60 modulates loading of repair proteins and repair of DNA double-strand breaks. Nat Cell Biol 8, 91-99.

Muse, G.W., Gilchrist, D.A., Nechaev, S., Shah, R., Parker, J.S., Grissom, S.F., Zeitlinger, J., and Adelman, K. (2007). RNA polymerase is poised for activation across the genome. Nat Genet.

Mutskov, V., Gerber, D., Angelov, D., Ausio, J., Workman, J., and Dimitrov, S. (1998). Persistent interactions of core histone tails with nucleosomal DNA following acetylation and transcription factor binding. Mol Cell Biol 18, 6293-6304.

Nagy, Z., and Tora, L. (2007). Distinct GCN5/PCAF-containing complexes function as co-activators and are involved in transcription factor and global histone acetylation. Oncogene 26, 5341-5357.

Nakayama, J., Rice, J.C., Strahl, B.D., Allis, C.D., and Grewal, S.I. (2001). Role of histone H3 lysine 9 methylation in epigenetic control of heterochromatin assembly. Science 292, 110-113.

Nan, X., Campoy, F.J., and Bird, A. (1997). MeCP2 is a transcriptional repressor with abundant binding sites in genomic chromatin. Cell 88, 471-481.

Narlikar, G.J., Fan, H.Y., and Kingston, R.E. (2002). Cooperation between complexes that regulate chromatin structure and transcription. Cell 108, 475-487. Ng, H.H., and Bird, A. (1999). DNA methylation and chromatin modification. Curr Opin Genet Dev 9, 158-163.

Ng, H.H., Robert, F., Young, R.A., and Struhl, K. (2003). Targeted recruitment of Set1 histone methylase by elongating Pol II provides a localized mark and memory of recent transcriptional activity. Mol Cell 11, 709-719.

North, B.J., and Verdin, E. (2004). Sirtuins: Sir2-related NAD-dependent protein deacetylases. Genome Biol 5, 224.

Obuse, C., Iwasaki, O., Kiyomitsu, T., Goshima, G., Toyoda, Y., and Yanagida, M. (2004). A conserved Mis12 centromere complex is linked to heterochromatic HP1 and outer kinetochore protein Zwint-1. Nat Cell Biol 6, 1135-1141.

Ohno, M., Fukagawa, T., Lee, J.S., and Ikemura, T. (2002). Triplex-forming DNAs in the human interphase nucleus visualized in situ by polypurine/polypyrimidine DNA probes and antitriplex antibodies. Chromosoma 111, 201-213.

Ohshima, K., Montermini, L., Wells, R.D., and Pandolfo, M. (1998). Inhibitory effects of expanded GAA.TTC triplet repeats from intron I of the Friedreich ataxia gene on transcription and replication in vivo. J Biol Chem 273, 14588-14595.

Ohshima, K., Sakamoto, N., Labuda, M., Poirier, J., Moseley, M.L., Montermini, L., **Ranum**, L.P., Wells, R.D., and Pandolfo, M. (1999). A nonpathogenic GAAGGA repeat in the Friedreich gene: implications for pathogenesis. Neurology 53, 1854-1857.

Orlando, V., Strutt, H., and Paro, R. (1997). Analysis of chromatin structure by in vivo formaldehyde cross-linking. Methods 11, 205-214.

Owen, D.J., Ornaghi, P., Yang, J.C., Lowe, N., Evans, P.R., Ballario, P., Neuhaus, D., Filetici, P., and Travers, A.A. (2000). The structural basis for the recognition of acetylated histone H4 by the bromodomain of histone acetyltransferase gcn5p. Embo J 19, 6141-6149.

Pandolfo, M. (1998). Molecular genetics and pathogenesis of Friedreich ataxia. Neuromuscul Disord 8, 409-415.

Pandolfo, M. (2006). Friedreich ataxia: Detection of GAA repeat expansions and frataxin point mutations. Methods Mol Med 126, 197-216.

Palangat, M., Meier, T.I., Keene, R.G., and Landick, R. (1998). Transcriptional pausing at +62 of the HIV-1 nascent RNA modulates formation of the TAR RNA structure. Mol Cell 1, 1033-1042.

Panyutin, I.G., and Neumann, R.D. (1994). Sequence-specific DNA double-strand breaks induced by triplex forming 125I labeled oligonucleotides. Nucleic Acids Res 22, 4979-4982.

Panyutin, I.V., Sedelnikova, O.A., Bonner, W.M., Panyutin, I.G., and Neumann, R.D. (2005). DNA damage produced by 125I-triplex-forming oligonucleotides as a measure of their successful delivery into cell nuclei. Ann N Y Acad Sci 1058, 140-150.

Peters, A.H., and Schubeler, D. (2005). Methylation of histones: playing memory with DNA. Curr Opin Cell Biol 17, 230-238.

Pianese, L., Tammaro, A., Turano, M., De Biase, I., Monticelli, A., and Cocozza, S. (2002). Identification of a novel transcript of X25, the human gene involved in Friedreich ataxia. Neurosci Lett 320, 137-140.

Pianese, L., Turano, M., Lo Casale, M.S., De Biase, I., Giacchetti, M., Monticelli, A., Criscuolo, C., Filla, A., and Cocozza, S. (2004). Real time PCR quantification of frataxin mRNA in the peripheral blood leucocytes of Friedreich ataxia patients and carriers. J Neurol Neurosurg Psychiatry 75, 1061-1063.

Ping, Y.H., and Rana, T.M. (2001). DSIF and NELF interact with RNA polymerase II elongation complex and HIV-1 Tat stimulates P-TEFb-mediated phosphorylation of RNA polymerase II and DSIF during transcription elongation. J Biol Chem 276, 12951-12958.

Pokholok, D.K., Harbison, C.T., Levine, S., Cole, M., Hannett, N.M., Lee, T.I., Bell, G.W., Walker, K., Rolfe, P.A., Herbolsheimer, E., et al. (2005). Genome-wide map of nucleosome acetylation and methylation in yeast. Cell 122, 517-527.

Pollard, L.M., Bourn, R.L., and Bidichandani, S.I. (2007a). Repair of DNA double-strand breaks within the (GAA*TTC)n sequence results in frequent deletion of the triplet-repeat sequence. Nucleic Acids Res.

Pollard, L.M., Chutake, Y.K., Rindler, P.M., and Bidichandani, S.I. (2007b). Deficiency of RecA-dependent RecFOR and RecBCD pathways causes increased instability of the (GAA{middle dot}TTC)n sequence when GAA is the lagging strand template. Nucleic Acids Res 35, 6884-6894.

Price, D.H. (2000). P-TEFb, a cyclin-dependent kinase controlling elongation by RNA polymerase II. Mol Cell Biol 20, 2629-2634.

Puccio, H., Simon, D., Cossee, M., Criqui-Filipe, P., Tiziano, F., Melki, J., Hindelang, C., Matyas, R., Rustin, P., and Koenig, M. (2001). Mouse models for Friedreich ataxia exhibit cardiomyopathy, sensory nerve defect and Fe-S enzyme deficiency followed by intramitochondrial iron deposits. Nat Genet 27, 181-186.

Rajeev, K.G., Jadhav, V.R., and Ganesh, K.N. (1997). Triplex formation at physiological pH: comparative studies on DNA triplexes containing 5-Me-dC tethered at N4 with spermine and tetraethyleneoxyamine. Nucleic Acids Res 25, 4187-4193.

Rao, J.N., Neumann, L., Wenzel, S., Schweimer, K., Rosch, P., and Wohrl, B.M. (2006). Structural studies on the RNA-recognition motif of NELF E, a cellular negative transcription elongation factor involved in the regulation of HIV transcription. Biochem J 400, 449-456.

Rea, S., Eisenhaber, F., O'Carroll, D., Strahl, B.D., Sun, Z.W., Schmid, M., Opravil, S., Mechtler, K., Ponting, C.P., Allis, C.D., et al. (2000). Regulation of chromatin structure by site-specific histone H3 methyltransferases. Nature 406, 593-599.

Reuter, G., and Spierer, P. (1992). Position effect variegation and chromatin proteins. Bioessays 14, 605-612.

Ribai, P., Pousset, F., Tanguy, M.L., Rivaud-Pechoux, S., Le Ber, I., Gasparini, F., Charles, P., Beraud, A.S., Schmitt, M., Koenig, M., et al. (2007). Neurological, cardiological, and oculomotor progression in 104 patients with Friedreich ataxia during long-term follow-up. Arch Neurol 64, 558-564.

Richardson, D.R., Mouralian, C., Ponka, P., and Becker, E. (2001). Development of potential iron chelators for the treatment of Friedreich's ataxia: ligands that mobilize mitochondrial iron. Biochim Biophys Acta 1536, 133-140.

Richter, A., Poirier, J., Mercier, J., Julien, D., Morgan, K., Roy, M., Gosselin, F., Bouchard, J.P., and Melancon, S.B. (1996). Friedreich ataxia in Acadian families from eastern Canada: clinical diversity with conserved haplotypes. Am J Med Genet 64, 594-601.

Riggs, A.D. (1975). X inactivation, differentiation, and DNA methylation. Cytogenet Cell Genet 14, 9-25.

Ringrose, L., Ehret, H., and Paro, R. (2004). Distinct contributions of histone H3 lysine 9 and 27 methylation to locus-specific stability of polycomb complexes. Mol Cell 16, 641-653.

Ristow, M., Mulder, H., Pomplun, D., Schulz, T.J., Muller-Schmehl, K., Krause, A., Fex, M., Puccio, H., Muller, J., Isken, F., et al. (2003). Frataxin deficiency in pancreatic islets causes diabetes due to loss of beta cell mass. J Clin Invest 112, 527- 534.

Rosenberg, M.I., and Parkhurst, S.M. (2002). Drosophila Sir2 is required for heterochromatic silencing and by euchromatic Hairy/E(Spl) bHLH repressors in segmentation and sex determination. Cell 109, 447-458.

Rossi, D.J., Londesborough, A., Korsisaari, N., Pihlak, A., Lehtonen, E., Henkemeyer, M., and Makela, T.P. (2001). Inability to enter S phase and defective RNA polymerase II CTD phosphorylation in mice lacking Mat1. Embo J 20, 2844-2856.

Rustin, P., Munnich, A., and Rotig, A. (1999). Quinone analogs prevent enzymes targeted in Friedreich ataxia from iron-induced injury in vitro. Biofactors 9, 247-251.

Sakamoto, N., Akasaka, K., Yamamoto, T., and Shimada, H. (1996). A triplex DNA structure of the polypyrimidine: polypurine stretch in the 5' flanking region of the sea urchin arylsulfatase gene. Zoolog Sci 13, 105-109.

Sakamoto, N., Chastain, P.D., Parniewski, P., Ohshima, K., Pandolfo, M., Griffith, J.D., and Wells, R.D. (1999). Sticky DNA: self-association properties of long GAA.TTC repeats in R.R.Y triplex structures from Friedreich's ataxia. Mol Cell 3, 465-475.

Sakamoto, N., Larson, J.E., Iyer, R.R., Montermini, L., Pandolfo, M., and Wells, R.D. (2001a). GGA*TCC-interrupted triplets in long GAA*TTC repeats inhibit the formation of triplex and sticky DNA structures, alleviate transcription inhibition, and reduce genetic instabilities. J Biol Chem 276, 27178-27187.

Sakamoto, N., Ohshima, K., Montermini, L., Pandolfo, M., and Wells, R.D. (2001b). Sticky DNA, a self-associated complex formed at long GAA*TTC repeats in intron 1 of the frataxin gene, inhibits transcription. J Biol Chem 276, 27171-27177.

Santos-Rosa, H., Schneider, R., Bannister, A.J., Sherriff, J., Bernstein, B.E., Emre, N.C., Schreiber, S.L., Mellor, J., and Kouzarides, T. (2002). Active genes are tri-methylated at K4 of histone H3. Nature 419, 407-411.

Sarsero, J.P., Holloway, T.P., Li, L., McLenachan, S., Fowler, K.J., Bertoncello, I., Voullaire, L., Gazeas, S., and Ioannou, P.A. (2005). Evaluation of an FRDA-EGFP genomic reporter assay in transgenic mice. Mamm Genome 16, 228-241.

Sarsero, J.P., Li, L., Wardan, H., Sitte, K., Williamson, R., and Ioannou, P.A. (2003). Upregulation of expression from the FRDA genomic locus for the therapy of Friedreich ataxia. J Gene Med 5, 72-81.

Saveliev, A., Everett, C., Sharpe, T., Webster, Z., and Festenstein, R. (2003). DNA triplet repeats mediate heterochromatin-protein-1-sensitive variegated gene silencing. Nature 422, 909-913.

Schneider, E.E., Albert, T., Wolf, D.A., and Eick, D. (1999). Regulation of c-myc and immunoglobulin kappa gene transcription by promoter-proximal pausing of RNA polymerase II. Curr Top Microbiol Immunol 246, 225-231.

Schneider, R., Bannister, A.J., Myers, F.A., Thorne, A.W., Crane-Robinson, C., and Kouzarides, T. (2004). Histone H3 lysine 4 methylation patterns in higher eukaryotic genes. Nat Cell Biol 6, 73-77.

Schols, L., Amoiridis, G., Przuntek, H., Frank, G., Epplen, J.T., and Epplen, C. (1997). Friedreich's ataxia. Revision of the phenotype according to molecular genetics. Brain 120 (Pt 12), 2131-2140.

Schubeler, D., MacAlpine, D.M., Scalzo, D., Wirbelauer, C., Kooperberg, C., van Leeuwen, F., Gottschling, D.E., O'Neill, L.P., Turner, B.M., Delrow, J., et al. (2004). The histone modification pattern of active genes revealed through genome-wide chromatin analysis of a higher eukaryote. Genes Dev 18, 1263-1271.

Secombe, J., and Eisenman, R.N. (2007). The function and regulation of the JARID1 family of histone H3 lysine 4 demethylases: the Myc connection. Cell Cycle 6, 1324-1328.

Seznec, H., Simon, D., Bouton, C., Reutenauer, L., Hertzog, A., Golik, P., Procaccio, V., Patel, M., Drapier, J.C., Koenig, M., et al. (2005). Friedreich ataxia: the oxidative stress paradox. Hum Mol Genet 14, 463-474.

Seznec, H., Simon, D., Monassier, L., Criqui-Filipe, P., Gansmuller, A., Rustin, P., Koenig, M., and Puccio, H. (2004). Idebenone delays the onset of cardiac functional alteration without correction of Fe-S enzymes deficit in a mouse model for Friedreich ataxia. Hum Mol Genet 13, 1017-1024.

Shahbazian, M.D., Zhang, K., and Grunstein, M. (2005). Histone H2B ubiquitylation controls processive methylation but not monomethylation by Dot1 and Set1. Mol Cell 19, 271-277.

Shen, L., Ahuja, N., Shen, Y., Habib, N.A., Toyota, M., Rashid, A., and Issa, J.P. (2002). DNA methylation and environmental exposures in human hepatocellular carcinoma. J Natl Cancer Inst 94, 755-761.

Shen, L., Kondo, Y., Guo, Y., Zhang, J., Zhang, L., Ahmed, S., Shu, J., Chen, X., Waterland, R.A., and Issa, J.P. (2007). Genome-wide profiling of DNA methylation reveals a class of normally methylated CpG island promoters. PLoS Genet 3, 2023-2036.

Shi, Y., Lan, F., Matson, C., Mulligan, P., Whetstine, J.R., Cole, P.A., Casero, R.A., and Shi, Y. (2004). Histone demethylation mediated by the nuclear amine oxidase homolog LSD1. Cell 119, 941-953.

Shia, W.J., Pattenden, S.G., and Workman, J.L. (2006). Histone H4 lysine 16 acetylation breaks the genome's silence. Genome Biol 7, 217.

Shogren-Knaak, M., Ishii, H., Sun, J.M., Pazin, M.J., Davie, J.R., and Peterson, C.L. (2006). Histone H4-K16 acetylation controls chromatin structure and protein interactions. Science 311, 844-847.

Simon, D., Seznec, H., Gansmuller, A., Carelle, N., Weber, P., Metzger, D., Rustin, P., Koenig, M., and Puccio, H. (2004). Friedreich ataxia mouse models with progressive cerebellar and sensory ataxia reveal autophagic neurodegeneration in dorsal root ganglia. J Neurosci 24, 1987-1995.

Sims, R.J., 3rd, Chen, C.F., Santos-Rosa, H., Kouzarides, T., Patel, S.S., and Reinberg, D. (2005). Human but not yeast CHD1 binds directly and selectively to histone H3 methylated at lysine 4 via its tandem chromodomains. J Biol Chem 280, 41789-41792.

Smith, R.A., Porteous, C.M., Coulter, C.V., and Murphy, M.P. (1999). Selective targeting of an antioxidant to mitochondria. Eur J Biochem 263, 709-716.

Snowden, A.W., Gregory, P.D., Case, C.C., and Pabo, C.O. (2002). Gene-specific targeting of H3K9 methylation is sufficient for initiating repression in vivo. Curr Biol 12, 2159-2166.

Somoza, J.R., Skene, R.J., Katz, B.A., Mol, C., Ho, J.D., Jennings, A.J., Luong, C., Arvai, A., Buggy, J.J., Chi, E., et al. (2004). Structural snapshots of human HDAC8 provide insights into the class I histone deacetylases. Structure 12, 13251334.

Spies, M., and Kowalczykowski, S.C. (2006). The RecA binding locus of RecBCD is a general domain for recruitment of DNA strand exchange proteins. Mol Cell 21, 573-580.

Squatrito, M., Gorrini, C., and Amati, B. (2006). Tip60 in DNA damage response and growth control: many tricks in one HAT. Trends Cell Biol 16, 433-442.

Stein, R., Razin, A., and Cedar, H. (1982). In vitro methylation of the hamster adenine phosphoribosyltransferase gene inhibits its expression in mouse L cells. Proc Natl Acad Sci U S A 79, 3418-3422.

Sturm, B., Bistrich, U., Schranzhofer, M., Sarsero, J.P., Rauen, U., Scheiber-Mojdehkar, B., de Groot, H., Ioannou, P., and Petrat, F. (2005). Friedreich's ataxia, no changes in mitochondrial labile iron in human lymphoblasts and fibroblasts: a decrease in antioxidative capacity? J Biol Chem 280, 6701-6708.

Suka, N., Luo, K., and Grunstein, M. (2002). Sir2p and Sas2p opposingly regulate acetylation of yeast histone H4 lysine16 and spreading of heterochromatin. Nat Genet 32, 378-383.

Svetlov, V., Belogurov, G.A., Shabrova, E., Vassylyev, D.G., and Artsimovitch, I. (2007). Allosteric control of the RNA polymerase by the elongation factor RfaH. Nucleic Acids Res 35, 5694-5705.

Taipale, M., and Akhtar, A. (2005). Chromatin mechanisms in Drosophila dosage compensation. Prog Mol Subcell Biol 38, 123-149.

Takeuchi, T., Watanabe, Y., Takano-Shimizu, T., and Kondo, S. (2006). Roles of jumonji and jumonji family genes in chromatin regulation and development. Dev Dyn 235, 2449-2459.

Tanny, J.C., Dowd, G.J., Huang, J., Hilz, H., and Moazed, D. (1999). An enzymatic activity in the yeast Sir2 protein that is essential for gene silencing. Cell 99,735-745.

Thomas, T., and Voss, A.K. (2007). The diverse biological roles of MYST histone acetyltransferase family proteins. Cell Cycle 6, 696-704.

Tse, C., Sera, T., Wolffe, A.P., and Hansen, J.C. (1998). Disruption of higher-order folding by core histone acetylation dramatically enhances transcription of nucleosomal arrays by RNA polymerase III. Mol Cell Biol 18, 4629-4638.

Urbach, A.R., and Dervan, P.B. (2001). Toward rules for 1:1 polyamide:DNA recognition. Proc Natl Acad Sci U S A 98, 4343-4348.

van den Boom, V., Jaspers, N.G., and Vermeulen, W. (2002). When machines get stuck--obstructed RNA polymerase II: displacement, degradation or suicide. Bioessays 24, 780-784.

Vannini, A., Volpari, C., Filocamo, G., Casavola, E.C., Brunetti, M., Renzoni, D., Chakravarty, P., Paolini, C., De Francesco, R., Gallinari, P., et al. (2004). Crystal structure of a eukaryotic zinc-dependent histone deacetylase, human HDAC8, complexed with a hydroxamic acid inhibitor. Proc Natl Acad Sci U S A 101, 15064-15069.

Vaquero, A., Scher, M., Lee, D., Erdjument-Bromage, H., Tempst, P., and Reinberg, D. (2004). Human SirT1 interacts with histone H1 and promotes formation of facultative heterochromatin. Mol Cell 16, 93-105.

Vaquero, A., Sternglanz, R., and Reinberg, D. (2007). NAD+-dependent deacetylation of H4 lysine 16 by class III HDACs. Oncogene 26, 5505-5520.

Vetcher, A.A., Napierala, M., Iyer, R.R., Chastain, P.D., Griffith, J.D., and Wells, R.D. (2002). Sticky DNA, a long GAA.GAA.TTC triplex that is formed intramolecularly, in the sequence of intron 1 of the frataxin gene. J Biol Chem 277, 39217-39227.

Warburton, P.E., Waye, J.S., and Willard, H.F. (1993). Nonrandom localization of recombination events in human alpha satellite repeat unit variants: implications for higher-order structural characteristics within centromeric heterochromatin. Mol Cell Biol 13, 6520-6529.

Williams, R.R., Azuara, V., Perry, P., Sauer, S., Dvorkina, M., Jorgensen, H., Roix, J., McQueen, P., Misteli, T., Merkenschlager, M., et al. (2006). Neural induction promotes large-scale chromatin reorganisation of the Mash1 locus. J Cell Sci 119, 132-140.

Wiren, M., Silverstein, R.A., Sinha, I., Walfridsson, J., Lee, H.M., Laurenson, P., Pillus, L., Robyr, D., Grunstein, M., and Ekwall, K. (2005). Genomewide analysis of nucleosome density histone acetylation and HDAC function in fission yeast. Embo J 24, 2906-2918.

Wolffe, A.P. (2001). Transcriptional regulation in the context of chromatin structure. Essays Biochem 37, 45-57.

Wood, J.G., Rogina, B., Lavu, S., Howitz, K., Helfand, S.L., Tatar, M., and Sinclair, D. (2004). Sirtuin activators mimic caloric restriction and delay ageing in metazoans. Nature 430, 686-689.

Wu, C.H., Yamaguchi, Y., Benjamin, L.R., Horvat-Gordon, M., Washinsky, J., Enerly, E., Larsson, J., Lambertsson, A., Handa, H., and Gilmour, D. (2003). NELF and DSIF cause promoter proximal pausing on the hsp70 promoter in Drosophila. Genes Dev 17, 1402-1414.

Wu, J., Wang, S.H., Potter, D., Liu, J.C., Smith, L.T., Wu, Y.Z., Huang, T.H., and Plass, C. (2007). Diverse histone modifications on histone 3 lysine 9 and their relation to DNA methylation in specifying gene silencing. BMC Genomics 8, 131.

Xu, W.S., Parmigiani, R.B., and Marks, P.A. (2007). Histone deacetylase inhibitors: molecular mechanisms of action. Oncogene 26, 5541-5552.

Yamaguchi, Y., Takagi, T., Wada, T., Yano, K., Furuya, A., Sugimoto, S., Hasegawa, J., and Handa, H. (1999). NELF, a multisubunit complex containing RD, cooperates with DSIF to repress RNA polymerase II elongation. Cell 97, 41-51.

Yang, M., Culhane, J.C., Szewczuk, L.M., Jalili, P., Ball, H.L., Machius, M., Cole, P.A., and Yu, H. (2007). Structural basis for the inhibition of the LSD1 histone demethylase by the antidepressant trans-2-phenylcyclopropylamine. Biochemistry 46, 8058-8065.

Yang, X.J. (2004). Lysine acetylation and the bromodomain: a new partnership for signaling. Bioessays 26, 1076-1087.

Yunis, J.J., and Yasmineh, W.G. (1971). Heterochromatin, satellite DNA, and cell function. Structural DNA of eucaryotes may support and protect genes and aid in speciation. Science 174, 1200-1209.

Zeng, L., and Zhou, M.M. (2002). Bromodomain: an acetyl-lysine binding domain. FEBS Lett 513, 124-128.

Zhang, Y., and Reinberg, D. (2001). Transcription regulation by histone methylation: interplay between different covalent modifications of the core histone tails. Genes Dev 15, 2343-2360.

Zhang, Z., Klatt, A., Gilmour, D.S., and Henderson, A.J. (2007). Negative elongation factor NELF represses human immunodeficiency virus transcription by pausing the RNA polymerase II complex. J Biol Chem 282, 16981-16988.

Zhao, K., Harshaw, R., Chai, X., and Marmorstein, R. (2004). Structural basis for nicotinamide cleavage and ADP-ribose transfer by NAD(+)-dependent Sir2 histone/protein deacetylases. Proc Natl Acad Sci U S A 101, 8563-8568.

Ziemba, A., Derosier, L.C., Methvin, R., Song, C.Y., Clary, E., Kahn, W., Milesi, D., Gorn, V., Reed, M., and Ebbinghaus, S. (2001). Repair of triplex-directed DNA alkylation by nucleotide excision repair. Nucleic Acids Res 29, 4257-4263.